CENTRAL RESEARCH LIBRARY
DOCUMENT COLLECTION

MARTIN MARIETTA ENERGY SYSTEMS LIBRARIES
3 4456 0358880 1

ORNL-3605
Volume 1
UC-33 – Propulsion Systems and
Energy Conversion
TID-4500 (34th ed.)

PROCEEDINGS OF 1963 HIGH-TEMPERATURE LIQUID-METAL HEAT TRANSFER TECHNOLOGY MEETING

CENTRAL RESEARCH LIBRARY
DOCUMENT COLLECTION
LIBRARY LOAN COPY
DO NOT TRANSFER TO ANOTHER PERSON
If you wish someone else to see this
document, send in name with document
and the library will arrange a loan.

OAK RIDGE NATIONAL LABORATORY
operated by
UNION CARBIDE CORPORATION
for the
U.S. ATOMIC ENERGY COMMISSION

Printed in USA. Price $7.00. Available from the Clearinghouse for Federal Scientific and Technical Information, National Bureau of Standards, U.S. Department of Commerce, Springfield, Virginia

LEGAL NOTICE

This report was prepared as an account of Government sponsored work. Neither the United States, nor the Commission, nor any person acting on behalf of the Commission:

A. Makes any warranty or representation, expressed or implied, with respect to the accuracy, completeness, or usefulness of the information contained in this report, or that the use of any information, apparatus, method, or process disclosed in this report may not infringe privately owned rights; or

B. Assumes any liabilities with respect to the use of, or for damages resulting from the use of any information, apparatus, method, or process disclosed in this report.

As used in the above, "person acting on behalf of the Commission" includes any employee or contractor of the Commission, or employee of such contractor, to the extent that such employee or contractor of the Commission, or employee of such contractor prepares, disseminates, or provides access to, any information pursuant to his employment or contract with the Commission, or his employment with such contractor.

ORNL-3605
Volume 1

Contract No. W-7405-eng-26

PROCEEDINGS OF 1963
HIGH-TEMPERATURE LIQUID-METAL HEAT TRANSFER
TECHNOLOGY MEETING

SPONSORED BY THE

ENGINEERING DEVELOPMENT BRANCH, DIVISION OF REACTOR DEVELOPMENT

UNITED STATES ATOMIC ENERGY COMMISSION

AT

OAK RIDGE NATIONAL LABORATORY

SEPTEMBER 4–6, 1963

NOVEMBER 1964

OAK RIDGE NATIONAL LABORATORY
Oak Ridge, Tennessee
Operated by
UNION CARBIDE CORPORATION
for the
U. S. ATOMIC ENERGY COMMISSION

MARTIN MARIETTA ENERGY SYSTEMS LIBRARIES

3 4456 0358880 1

This report was printed from the best available material.

CONTENTS

Volume 1

Preface v

The MPRE — A Boiling Potassium Reactor System A. P. FRAAS 1

The Determination of the Latent Heat of Vaporization, Vapor Pressure, Enthalpy, and Density of Liquid Rubidium and Cesium up to 1800°F . . . . . P. Y. ACHENER 3

Thermophysical Properties of Rubidium and Cesium . . . . . F. TEPPER, A. MURCHISON, J. ZELENAK, and F. ROEHLICH 26

Thermophysical Property Measurements of Alkali Liquid Metals . . . . . J. W. COOKE 66

The Thermodynamic and Transport Properties of Potassium . A. W. LEMMON, JR., H. W. DEEM, E. H. HALL, and J. F. WALLING 88

Thermoelectric Potentials of Molten and Refractory Metals . . . . . C. F. BONILLA, R. R. KYI, H. T. DRUE, and D-I. LEE 116

Report on High Temperature Liquid Metal Heat Transfer Research at Geoscience, Ltd. . . . . H. F. POPPENDIEK and N. D. GREENE 139

Lithium-Boiling Potassium Refractory Metal Loop Facility. . J. P. DAVIS, G. M. KIKIN, W. M. PHILLIPS, and L. S. WOLFSON 171

Heat Transfer Coefficients in Liquid Metal Co-Current Flow Double Pipe Heat Exchangers . . . . . R. P. STEIN 194

Natural Convection Heat Transfer Coefficients for Liquid Tin at High Heat Fluxes . . . . . A. F. BRINSMADE and L. G. DESMON 240

The Effect of Surface Conditions on Pool Boiling Heat Transfer of Sodium . . . . . P. J. MARTO and W. M. ROHSENOW 263

Pool Boiling of Potassium . C. F. BONILLA, M. M. WIENER, and H. BILFINGER 286

Superheat Requirements with Boiling Liquid Metals . . . A. I. KRAKOVIAK 310

Recent Experimental Results in ORNL Studies with Boiling Potassium . . . . . H. W. HOFFMAN 334

Boiling Studies with Potassium . . . . . R. E. BALZHISER 351

CONTENTS

Volume 2

An Experimental Investigation of Forced-Convection Vaporization of Potassium . . . . . P. J. BERENSON and J. J. KILLACKEY 1

Summary of Recent Results of Sodium Boiling Studies . . . . . R. C. NOYES 24

A Proposed Mechanism and Method of Correlation for Convective Boiling Heat Transfer with Liquid Metals . . . . . J. C. CHEN 47

Heat Transfer and Pressure Drop Characteristics for Boiling Rubidium in Forced Convection . . . . . C. R. FISHER 64

Alkali Metals Boiling and Condensing Investigations . . . . . R. D. BROOKS and J. LONGO, JR. 86

Potassium-Mercury Amalgam Boiling Heat Transfer, Two-Phase Flow, and Properties Investigation . . . Y. S. TANG, C. R. SMITH, and P. T. ROSS 110

Heat Transfer During Film Condensation of a Liquid Metal Vapor . . . . . S. P. SUKHATME and W. M. ROHSENOW 132

Liquid Metal Jet Condensers . . . . . L. HAYS 153

Fog-Flow Mercury Condensing Pressure Drop Correlation . . . . . A. KOESTEL, M. GUTSTEIN, and R. T. WAINWRIGHT 198

Heat Transfer from a Hot Sodium Spray Impinging on a Vertical Plate . . . . W. H. NURICK, J. D. SEADER, and T. A. COULTAS 235

Measurement of the Pressure Drop of Superheated Cesium Vapor Across a Laminar Flow Device . . . . . W. A. SAMUEL 250

Selected Parameters for Two-Phase Flow of Sodium . . . . . K. GOLDMANN 270

Stability of Parallel-Path Two-Phase Flow . . . . . T. J. VILD and D. E. SILL 293

The Application of Alkali Metal Vapor Systems to MHD Space Power Generators . . . . . B. HOFFMAN and F. SHAIR 316

Analysis of the Acceleration of Lithium in a Two-Phase Nozzle . . . . . B. G. ELLIOTT 353

Meeting Summation . . . . . R. N. LYON 371

List of Attendees 381

PREFACE

The Third High-Temperature Liquid-Metal Heat-Transfer Technology Conference sponsored by the Engineering Development Branch, Division of Reactor Development, U. S. Atomic Energy Commission, was held at the Oak Ridge National Laboratory on September 4-6, 1963. These meetings were initiated in 1961 as a forum for the direct and personal exchange of information between workers actively engaged in the study of the thermal transport characteristics of liquid metals.

The thirty-four papers presented and discussed during the three days of the conference have been collected in these two volumes to provide a convenient reference for all those participating in the conference. Further, this report, in conjunction with those issued following the previous two meetings [AEC Report ANL-6507 (classified), Argonne National Laboratory, and AEC Report BNL-756, Brookhaven National Laboratory] is a record of the current state of liquid-metal heat-transfer technology in the United States. The topics covered include thermophysical properties, two-phase and single-phase flow, boiling heat transfer under pool, natural-convection, and forced-convection conditions, condensing heat transfer, boiling stability, and magnetohydrodynamic applications.

The effectiveness of these conferences in achieving the avowed purpose is attested to both by the steady increase in the number of papers presented and by the character of the discussions which follow each paper. However, with the publication of the bimonthly "High-Temperature Liquid-Metal Technology Review" (O. E. Dwyer, Brookhaven National Laboratory, Editor), the need for annual meetings has been reduced. A biennial cycle is now planned with the next meeting in 1965; the selection of a site has not been made.

To expedite publication and to allow for a wider distribution, two classified papers have been omitted: (1) "Single-Phase Liquid-Metal Component Development Work," R. W. Kelly, Pratt and Whitney Aircraft, Middletown, Connecticut, and (2) "Two-Phase Potassium Experimental Work," D. G. Randall, Pratt and Whitney Aircraft, Middletown, Connecticut. Those desiring copies of these papers and demonstrating proper clearance may

secure such copies by contacting the authors directly. In addition, brief progress reports on studies underway at NASA-Lewis Research Center, Cleveland, Ohio, and at Sunstrand Aviation, Denver, Colorado, have not been included at the request of the authors. Finally, an introductory address by A. P. Fraas, Oak Ridge National Laboratory, describing the ORNL Medium Power Reactor Experiment (MPRE) as typical of the applications requiring heat transfer and fluid dynamic data on the forced-convection boiling of liquid metals was unfortunately not recorded at the time of this meeting. A condensed version has been included as the first paper in these proceedings.

The success of any meeting derives from the efforts of many; and so I would like to acknowledge the support of all those in the ORNL organization who worked in our behalf. Thanks are also due to O. E. Dwyer, Brookhaven National Laboratory, R. P. Stein, Argonne National Laboratory, and J. J. Keyes, Oak Ridge National Laboratory, who served with me as session chairman, and to R. N. Lyon, Oak Ridge National Laboratory, for undertaking and so successfully accomplishing the monumental task of summarizing, immediately upon the conclusion of the final paper, these three days of reports and discussions. Finally, my appreciation goes to all those attending for their contributions to the fulfillment of the purposes of this conference.

Herbert W. Hoffman
General Chairman

THE MPRE — A BOILING POTASSIUM REACTOR SYSTEM

by

Arthur P. Fraas

Reactor Division
Oak Ridge National Laboratory*
Oak Ridge, Tennessee

A study carried out in the latter part of 1958 disclosed that, for a given peak system temperature, a Rankine vapor cycle employing either potassium or rubidium vapor appears to give the minimum size and weight of the radiator and other major components for turbine-generator nuclear space power plants. Reliability studies indicated that only by going to the simplest possible system could we dare hope to achieve the desired reliability. Preliminary system layouts showed that a single-fluid system with the reactor serving as the boiler is attractive in this respect since it minimizes the number of components. Further, it reduces the peak metal temperature required for a given vapor temperature at the turbine inlet since the lowest temperature in the primary loop of a two-fluid system must be higher than the boiling point of the working fluid by 50 to 100°F. To keep the core pressure drop within reasonable limits, the peak temperature in the primary fluid system must be 100 to 200°F above the minimum temperature. Thus for a given turbine inlet temperature the reactor outlet temperature can be reduced between 200 and 300°F by making use of a single-fluid rather than a two-fluid system. The single fluid system makes it possible to obtain a system weight of about 25 lb/kwe in a stainless steel system with potassium boiling in the reactor at 1540°C.

The boiling-potassium reactor system has the advantage that it permits operation in the 1000 to 2000°F range with relatively low system

---

*Operated by Union Carbide Corporation for the U. S. Atomic Energy Commission.

pressures, e.g., 30 psia at 1550°F. Potassium also happens to be both a very good reactor coolant and an excellent thermodynamic-cycle working fluid for the 1000 to 2000°F temperature range. Its strong wetting characteristics not only contribute to its excellence as a heat transfer medium but also are advantageous if it is used as a lubricant, since capillary forces are very effective in drawing it into the close clearances in bearings rather than acting to expel the liquid, as is the case with mercury. While the low viscosity of potassium makes it necessary to design for relatively low bearing unit loads, its load-carrying capacity as a lubricant is far superior to that of gases, and numerous successful gas-bearing applications have been demonstrated. These features make potassium exceptionally well suited to a single-fluid nuclear power plant system in which potassium serves to cool the reactor, carry out the thermodynamic cycle, and lubricate the bearings.

Probably the most serious set of problems that stand in the way of the development of a boiling-potassium reactor are those associated with boiling flow stability. Unfortunately, the development of stable, boiling systems in the past has depended more on empirical development work than upon analytical design. Analytical approaches to the boiling flow stability problem have received much attention at ORNL during the past three years, and what is believed to be the first general analytical solution for a simplified system containing a boiler, a turbine, a condenser, and a feed pump with associated connecting plumbing has been worked out. More complex systems are under study with the analog computer and with experimental test rigs that, from the hydraulic standpoint, closely simulate full-scale power plant proportions.

AGN-TP-71

"THE DETERMINATION OF THE LATENT HEAT OF VAPORIZATION, VAPOR PRESSURE, ENTHALPY AND DENSITY OF LIQUID RUBIDIUM AND CESIUM UP TO 1800°F"

by

P. Y. Achener

AEROJET-GENERAL NUCLEONICS
San Ramon, California

To be presented at the Third Annual Meeting on
High Temperature Liquid-Metal Heat Transfer
Technology Held at Oak Ridge National Laboratory
September 4-6, 1963.

ABSTRACT

Apparatuses for the measurement of latent heats of vaporization, vapor pressures, enthalpies and densities of rubidium and cesium have been designed and operated. Experimental determination of these properties were obtained.

The latent heats of vaporization of rubidium and cesium were measured from 970° to $1805^{\circ}F$ and 1002° to $1596^{\circ}F$, respectively, in a system in which the saturation temperature was controlled by the pressure of the argon cover gas.

The following equations were obtained for the latent heats of vaporization:

$$h_{fg} = 414.8 - 0.0513T \text{ for rubidium}$$

$$h_{fg} = 257.4 - 0.0362T \text{ for cesium,}$$

where

$$h_{fg} = \text{Btu/lb}$$

$$T = {}^{\circ}F.$$

In the same apparatus the vapor pressures were also measured. The following equations were obtained:

$$\log_{10}P = 5.20071 - \frac{6994.68}{T + 459.7} \quad \text{for rubidium}$$

$$\log_{10}P = 5.09475 - \frac{6680.185}{T + 459.7} \quad \text{for cesium,}$$

where

$$P = \text{psia}$$

$$T = {}^{\circ}F.$$

These equations give values of the normal boiling point of $1274.4^{\circ}F$ and $1241.1^{\circ}F$ for rubidium and cesium, respectively.

The enthalpies of rubidium and cesium were measured in a Bunsen ice calorimeter in the temperature range of 150° to $1650^{\circ}F$. The data obtained fits the following equations:

$$H_T^{\circ} - H_{32^{\circ}F}^{\circ} = 9.012 + 0.09915T - 1.553 \times 10^{-5}\,T^2 + 4.329 \times 10^{-9}T^3 \text{ for rubidium}$$

$$H_T^{\circ} - H_{32^{\circ}F}^{\circ} = 2.711 + 0.08543T - 4.803 \times 10^{-5}\,T^2 + 1.995 \times 10^{-8}T^3 \text{ for cesium}$$

$$H = \text{Btu/lb}$$

$$T = {}^{\circ}F.$$

From these equations the specific heats were obtained:

$$Cp = 0.09915 - 3.106 \times 10^{-5}T + 1.299 \times 10^{-8}T^2 \text{ for rubidium}$$

$$Cp = 0.08543 - 9.605 \times 10^{-5}T + 5.985 \times 10^{-8}T^2 \text{ for cesium}$$

$$Cp = \text{Btu/lb-}^{o}\text{F}.$$

The density of liquid rubidium and cesium was measured by the pycnometer method. The following equations were obtained for the density of rubidium and cesium:

$$d = \frac{1.472}{1 + 1.3309 \times 10^{-4}\ (T-102) + 5.2106 \times 10^{-8}\ (T-102)^2} \quad \text{for rubidium}$$

$$d = \frac{1.84}{1 + 1.1755 \times 10^{-4}\ (T-82.4) + 7.656 \times 10^{-8}\ (T-82.4)^2} \quad \text{for cesium}$$

where $d = gr/cm^3$

$T = {}^{o}F.$

The work was performed under contract to the U. S. Atomic Energy Commission under Contract AT(04-3)-368, P. A. No. 1.

1. INTRODUCTION

Experimental studies have been conducted by Aerojet-General Nucleonics, to determine thermodynamic properties of Rb and Cs as a part of an overall Rb and Cs evaluation program. To date, the latent heat of vaporization from 1000° to 1800°F for Rb, from 1000° to 1600°F for Cs, the enthalpy and specific heat from 160° to 1650°F for both Rb and Cs, and the density of the saturated liquid have been determined experimentally. Work is now underway to measure the PVT relationships for the superheated vapors of Rb and Cs up to 2000°F. Additional work is also planned for the following year (1965) to obtain data on viscosity of the liquid and vapor and specific heat and thermal diffusivity of the vapor.

Prior to the inception of the present program, very few thermodynamic property data were available in the temperature range up to 1800°F. These are of interest to the designer of space electric power and propulsion systems. Compilations and theoretical calculations have been done for most alkali metals and are found in the works of Weatherford, et. al.,[1] Evans, et. al.,[2] and Stull and Sinke[3].

Mine Safety Appliances Company has measured the enthalpy of Rb by the copper block drop calorimeter, the density of Rb using a dilatometer and the vapor pressure of Rb in a boiler against a pressure of argon measured with a mercury manometer.[4] The vapor pressures of Rb and Cs were also measured by C. Bonilla.[5] However, no direct measurements of latent heat of vaporization have been done for the alkali metals.

The Rb and Cs used during this program were purchased from Penn Rare Metals, Inc., and before use were gettered with a mixture of 50% zirconium chips and 50% titanium chips at 1200°F and filtered through a stainless steel sintered filter. The analysis of the metals before loading in the apparatus will be given in the topical report[6].

LATENT HEAT AND VAPOR PRESSURE

1. INTRODUCTION

In the past, the latent heat of vaporization of liquid metals has been obtained by calculation, generally using the Clapeyron equation and the vapor pressure data. In these calculations it is assumed that the vapor follows the ideal gas law and the effect of dimerization as a function of temperature is accounted for, using a calculated value for the equilibrium constant of dimerization. It was therefore of interest to measure experimentally the latent heat of vaporization.

The approach consisted of boiling the liquid metal in an internally heated pressure vessel. The vapor was condensed in a series of vertical heat exchangers and the condensate flowed into a vessel of calibrated volume maintained at a known temperature slightly above the melting point. The mass of condensate was then obtained by calculation based on the density at this temperature. An argon pressurization system controlled the boiling temperature and provided the means to return the condensate back to the boiler. Figure 1 shows the schematic arrangement of the apparatus.

2. DESCRIPTION OF THE APPARATUS

Only a brief description of the apparatus will be given below; more details can be found in Reference 6.

The latent heat apparatus consisted of five major components: boiler, heat exchanger, volumeter, system pressurization and controls and electrical instrumentation and controls.

The boiler, Figure 2, was a pressure vessel made of two Haynes-25 hemispherical heads 6 inches inside diameter, welded together. A 900-watt, molybdenum heater, sheathed with Inconel, was positioned within the lower head. Also in the lower part of the vessel was the vapor outlet tube which protruded inside above the liquid metal level. Five calibrated chromel-alumel thermocouples penetrated through the upper head and monitored the liquid and vapor temperatures.

To minimize heat losses, a radiant shield assembly made of 14 concentric cylinders, surrounded the boiler vessel. Ten of these shields were made of molybdenum, three of rhodium-plated nickel and the last one of aluminum. A closely wound 2000-watt guard heater was located between the third and fourth shield, starting at the inside and completely surrounding the boiler on all sides.

The heat exchanger assembly placed below the boiler began with a nitrogen-cooled condenser, followed by a nitrogen-cooled subcooler. Then a water-cooled unit was used for the final adjustment of the condensate temperature before it entered the volumeter.

All components described so far were located inside a vacuum chamber to minimize heat losses by convection and conduction and to prevent oxidation at high temperatures.

Upon leaving the water-cooled subcooler, the condensate line left the vacuum chamber and was connected to the volumeter assembly (Figure 3). The volumeter was a slender vertical tube fitted with electrical level probes and a thermocouple. The volume between the probes was calibrated within an accuracy of $\pm$ 0.03%. Below the volumeter was a storage vessel which received the liquid condensate until steady state conditions were reached. After this, the condensate was forced to flow into the volumeter by closing the pneumatic Valve No. 1. The two probes inside the volumeter were connected electrically to a timer which started when the first probe was touched by the rising liquid metal and stopped when the second probe was contacted.

Argon was used in the system as a cover gas and the boiling temperature was adjusted by regulating the argon pressure. Sensitive pressure regulators and accurate pressure gauges were provided for the ranges of 0 to 800 mm Hg (vacuum range) and 0 to 300 psig. The argon pressure was also used as a means of returning the liquid metal back to the boiler when the storage vessel was full.

The electrical instrumentation consisted of temperature measuring instruments and controllers. The power input to the boiler was set manually and read on a $\pm$ 1/4% accurate wattmeter. The power input to the guard heater was controlled by an automatic controller which received its signal from a differential thermocouple having one junction against the guard heater and the other against the outside wall of the boiler.

3. PRINCIPLE OF OPERATION

The method of operation was a modification of that used by Henning[7] for his measurements of the latent heat of vaporization of water in 1906.

The method of controlling boiler temperature involved using argon as a cover gas to establish the boiling pressure, thereby establishing the boiling temperature. The heat input to the boiler can then be set manually to any given value. This method has the advantage of allowing several measurements to be made at the same temperature, but with different power inputs. While it is extremely difficult to completely eliminate the heat losses even when using elaborate shielding and guard heaters, it will be seen that the method of operation provides a means of analytically eliminating the heat losses from the results. This is important, since a change of a few degrees in the temperature differences between boiler and guard heater results in relatively large heat losses either in or out of the boiler.

Consider two consecutive experiments performed at the same temperature but at different power inputs, P_1 and P_2. Let q_1 and q_2 be the rates of heat losses in or out of the boiler in each experiment; m_1 and m_2 the masses of condensate collected during times t_1 and t_2, and h_{fg} the latent heat of vaporization at that temperature. We have the relations:

$$P_1 t_1 = m_1 h_{fg} + q_1 t_1 \tag{1}$$

$$P_2 t_2 = m_2 h_{fg} + q_2 t_2 \tag{2}$$

from which:

$$h_{fg} = \frac{P_1 t_1}{m_1} - \frac{q_1 t_1}{m_1} = \frac{P_2 t_2}{m_2} - \frac{q_2 t_2}{m_2} \tag{3}$$

If both experiments are made under identical conditions of temperature and temperature-difference, ΔT, between boiler and guard heater and if this ΔT is such that the heat losses are small compared to the heat that goes to vaporization, it can be assumed that $q_1 = q_2$ and Equations (1) and (2) give:

$$h_{fg} = \frac{P_1 - P_2}{\frac{m_1}{t_1} - \frac{m_2}{t_2}} \tag{4}$$

However, this is strictly true only at the value of ΔT for which there are no heat losses. Therefore the method of operation has consisted in making a number of test runs at different ΔT, at the two power inputs P_1 and P_2, in order to determine the value of ΔT which corresponds to zero heat losses. The value of:

$$\frac{Pt}{m} = h_{fg} + \frac{qt}{m} \tag{5}$$

was plotted as a function of ΔT at P_1 and P_2.

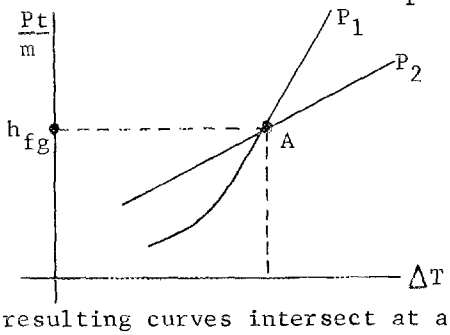

The two resulting curves intersect at a point of equal ΔT and equal value of Pt/m. Therefore:

$$\frac{P_1 t_1}{m_1} = \frac{P_2 t_2}{m_2} \tag{6}$$

Hence from Equation (3):

$$\frac{q_1 t_1}{m_1} = \frac{q_2 t_2}{m_2} \tag{7}$$

But since $m_1 \cong m_2 \cong$ constant, and $t_1 \neq t_2$ we must have $q_1 = q_2 = 0$ at the intersection point in order to satisfy Equation (7). Therefore we have:

$$h_{fg} = \left[\frac{P_1 t_1}{m_1}\right]_A = \left[\frac{P_2 t_2}{m_2}\right]_A \tag{8}$$

From the foregoing it is seen that two approaches were possible: one consists of first determining the value of ΔT for which the quantity Pt/m is the same at high and low power levels, and then making several more runs at this value of ΔT. Pairs of data which fulfill these conditions can then be combined according to Equation (4) to obtain h_{fg}. In the second approach the variation of the quantity Pt/m is determined over a wide range of ΔT values for both the high and low power levels. Equations can then be fitted to the two sets of data points and solved for their common value which gives the latent heat.

4. RESULTS

The first method was used for the rubidium and the second for the cesium runs. Figure 4 shows the results for cesium at 1400°F. A total of 206 data points were obtained for rubidium from 970 to 1805°F and 143 points for cesium from 1000° to 1600°F. Figure 5 shows the latent heat results for rubidium.

The following linear equations were obtained for the latent heat of vaporization:

$$h_{fg} = 414.8 - 0.05137T \text{ Btu/lb for rubidium} \tag{9}$$

$$h_{fg} = 257.4 - 0.0362T \text{ Btu/lb for cesium,} \tag{10}$$

where

$T = {}^{\circ}F.$

The accuracy of these equations is estimated to be $\pm$ 1% and the probable error of the distribution of the data was $\pm$ 0.2% and $\pm$ 0.5% for rubidium and cesium, respectively.

Also measured in the latent heat apparatus were the vapor pressures of Rb and Cs from 881° to 1808°F and from 843° to 1600°F, respectively. The equations obtained from the data are as follows:

$$\log_{10}P = 5.20071 - \frac{6994.68}{T + 459.7} \quad \text{for rubidium} \tag{11}$$

$$\log_{10}P = 5.09475 - \frac{6680.185}{T + 459.7} \quad \text{for cesium,} \tag{12}$$

where

P = psia

$T = {}^{\circ}F.$

Equations (11) and (12) give value of normal boiling temperatures of 1274.4°F and 1241.1°F, respectively. The estimated uncertainty of the pressure values given by these equations is ± 1.3%. The vapor pressure curves are shown in Figures 6 and 7.

ENTHALPY OF THE LIQUID

1. DESCRIPTION OF THE APPARATUS

The enthalpies of rubidium and cesium were measured in a stainless steel Bunsen ice calorimeter designed along the lines of the calorimeter of Deem and Lucks.[8] The ice calorimeter was chosen because of the ease of maintaining an adiabatic enclosure, the relative simplicity of its construction, and the accuracy obtainable with the instrument.[8,9,10]

In this device, the heat to be measured is allowed to melt ice which is in thermal equilibrium with water in a closed system, and the resulting decrease in volume is determined by means of mercury drawn into the system. The calibration factor, K, of the ice calorimeter (i.e., the ratio of heat input to mass of mercury intake) is a function only of accurately known physical constants; the heat of fusion of ice L, the specific volume of ice V_i, the specific volume of water V_W, and the density of mercury d_m are related by the equation:

$$K = \frac{L}{(V_i - V_W) d_m} \tag{13}$$

For properly designed calorimeters it has been determined that this calibration factor was equal to 0.25647 ± 0.00006 Btu/gr Hg.[10]

The calorimeter designed at AGN is shown in Figures 8 and 9. The sample container was made of tantalum-10% tungsten sheet selected because of its high strength at elevated temperatures.

The furnace situated above the calorimeter was of the cylindrical split-type and had three separately controlled heating zones to provide a uniform temperature distribution along the axis. The furnace was mounted on a vertical stand which allowed it to be swung out of the way after the capsule had been dropped into the calorimeter. The beaker of mercury which was used to supply the inside inventory, was permanently placed on one of the pans of a laboratory torsion balance. This had the advantage of enabling the operator to follow the experiment as it progressed and to determine when the sample had reached a thermal equilibrium with the calorimeter. The calibration of the calorimeter was checked by first using pure sapphire and next a block of 316 stainless steel. In each case the result was in agreement with the reported value within 1%.[9,11,12] Special care was taken to form a gas-free ice mantle at the beginning of the experiments.

2. RESULTS

Thirty six runs were made with rubidium between the temperatures of 147° and 1650°F. Of these, 11 data points were rejected because of inconsistency with the rest of the data. These variations were due in part to accidental slow down of the capsule during the drop which resulted in a low value of the enthalpy and, in some cases, were due to air leaks in the mercury system.

Of the 26 runs made with cesium, 23 were retained. The data was fitted by least squares analysis to polynominal equations of the third degree; the following equations were obtained for the enthalpies.

$$H_T^o - H_{32^oF}^o = 9.012 + 0.09915T - 1.553 \times 10^{-5}T^2 + 4.329 \times 10^{-9}T^3 \text{ for rubidium} \quad (14)$$

$$H_T^o - H_{32^oF}^o = 2.711 + 0.08543T - 4.803 \times 10^{-5}T^2 + 1.995 \times 10^{-8}T^3 \text{ for cesium} \quad (15)$$

where

H^o = Btu/lb

T = °F.

The probable errors were 0.75 Btu/lb and 0.53 Btu/lb for Rb and Cs, respectively or 0.88% at the 50% level for both Rb and Cs.

From the enthalpy equation, the specific heats were calculated by differentiation:

$$Cp = 0.09915 - 3.106 \times 10^{-5}T + 1.299 \times 10^{-8}T^2 \text{ Btu/lb-}^oF \text{ for rubidium} \quad (16)$$

$$Cp = 0.08543 - 9.605 \times 10^{-5}T + 5.985 \times 10^{-8}T^2 \text{ Btu/lb-}^oF \text{ for cesium} \quad (17)$$

Figures 10 and 11 show the enthalpy results. It is seen that the specific heat curves go through a minimum which is typical of alkali metals.

LIQUID DENSITY MEASUREMENTS

The densities of rubidium and cesium were measured over the temperature ranges of 1407° to 1670°F and 1207° to 1670°F, respectively, as a continuation of the measurements begun under the previous program in the temperature range of 102° to 1345°F for rubidium and 83° to 1300°F for cesium. The approach has consisted of using the pycnometer method in which the liquid metal is allowed to expand and overflow out of a calibrated capsule as the temperature is increased (Figure 12). The only measurement necessary is the weighing of the capsule after each heating to determine the amount of liquid metal left in it. Four pycnometers, made of 316 stainless steel, were used and were contained in a Haynes-25 vessel pressurized with argon.

One problem which had limited the usefulness of the method during the previous program was the flashing over of the liquid metal during the cooling of the capsule. This resulted in a loss of liquid metal from the pycnometer

and an erroneous density value. To overcome this difficulty a check valve was incorporated in the overflow tube of the pycnometer. It simply consisted of a 3/16 inch diameter tungsten carbide ball resting by gravity on a ground tapered seat provided within the overflow tube. During heating, the expanding liquid raised the ball and overflowed through the slots cut on the side of the tube. During the cooling, the ball rested on the seat. An overpressure of argon prevented boiling of the liquid and the formation of vapor bubbles. Two platinum-platinum 10% rhodium calibrated thermocouples protruding through the cover were used. In the analysis of the results, the expansion of the pycnometers was accounted for using the values of the expansion coefficient given by Deem and Lucks[12].

The following equations were obtained for the density of rubidium and cesium vs temperature:

$$d = \frac{1.472}{1 + 1.3309 \times 10^{-4} (T-102) + 5.2106 \times 10^{-8} (T-102)^2} \quad \text{for rubidium} \quad (18)$$

$$d = \frac{1.84}{1 + 1.1755 \times 10^{-4} (T-82.4) + 7.656 \times 10^{-8} (T-82.4)^2} \quad \text{for cesium} \quad (19)$$

where $d = gr/cm^3$
$T = {}^{o}F.$

ACKNOWLEDGEMENT

The assistance of Mr. T. Conlon in the design and operation of the apparatus used during this program and of Mr. D. Miramontes in the laboratory operations and tests is hereby gratefully acknowledged. Acknowledgement is also due Mr. R. Fischer who helped with the tests and the data reduction.

LIST OF REFERENCES

1 W. D. Weatherford, Jr., et. al., Properties of Inorganic Energy-Conversion and Heat-Transfer Fluids for Space Applications, WADD-TR 61-96, SRI (1961).

2 W. H. Evans, et. al., "Thermodynamic Properties of the Alkali Metals", J. of Res. NBS, 55:83 (1955).

3 D. R. Stull and G. C. Sinke, "Thermodynamic Properties of the Elements", American Chemical Society, Washington, D. C. (1956).

4 F. Tepper, et. al., Thermophysical Properties of Rubidium, TDR No. ASD-TDR-63-133, MSA Research Corporation, (1963).

5 C. F. Bonilla, et. al., Vapor Pressure of Alkali Metals - III. Rubidium, Cesium, and Sodium-Potassium Alloys (NaK) up to 100 Pounds per Square Inch, High-Temperature Liquid-Metal Heat-Transfer Technology Meeting, Brookhaven, May 1962.

6 AGN-8090, The Determination of Latent Heat of Vaporization, Vapor Pressure, Enthalpy and Density of Liquid Rubidium and Cesium up to 1800°F, Topical Report, 1963.

7 J. K. Roberts and A. R. Miller, Heat and Thermodynamics, Interscience Publishers, Inc., Fifth Ed., New York, 1960.

8 H. W. Deem and C. F. Lucks, "An Improved All-Metal Bunsen-Type Ice Calorimeter", Instruments Society of America, PPT-4-58-1, (1958).

9 D. C. Ginnings and R. J. Corruccini, "Enthalpy, Specific Heat, and Entropy of Aluminum Oxide from 0° to 900°C", J. of Res. NBS, 38:593, (1947).

10 D. C. Ginnings and R. J. Corruccini, "An Improved Ice Calorimeter - The Determination of Its Calibration Factor and The Density of Ice at 0°C", J. of Res. NBS, 38:583, (1947).

11 G. T. Furukawa, et. al., "Thermal Properties of Aluminum Oxide from 0° to 1200°F", J. of Res. NBS, 57:67 (1956).

12 H. W. Deem and C. F. Lucks, Thermal Properties of Thirteen Metals, ASTM Special Publication No. 227 (1958).

AGN TP-71

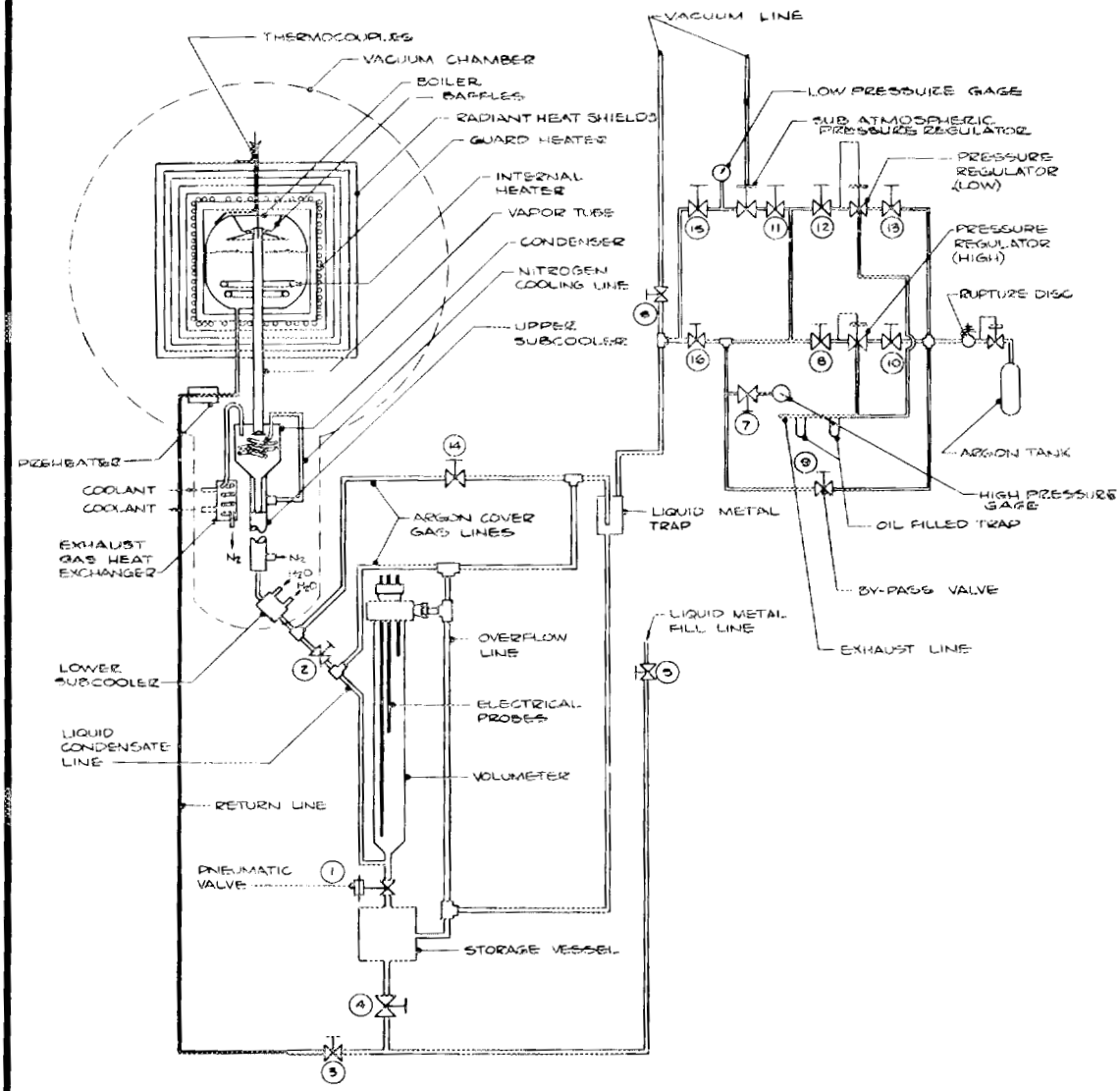

FIGURE 1. SCHEMATIC DIAGRAM OF LATENT HEAT APPARATUS

13.6-63-2993

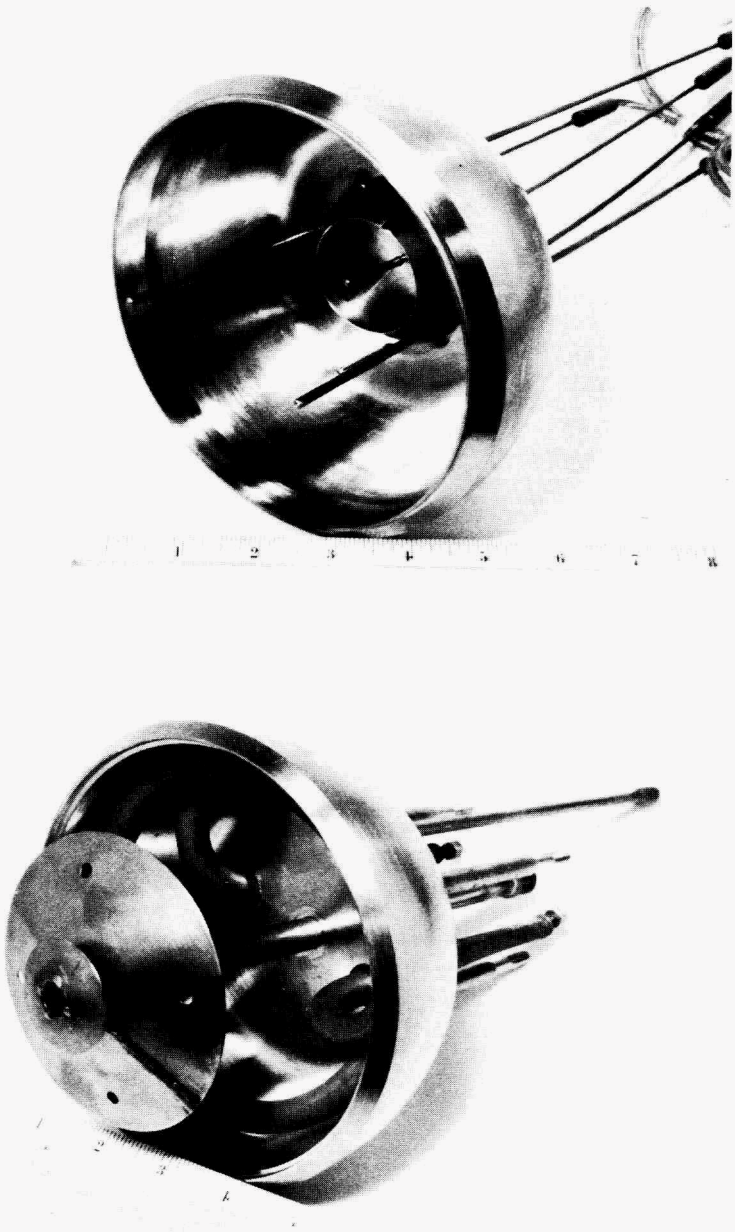

FIGURE 2. LATENT HEAT BOILER

AGN TP-71

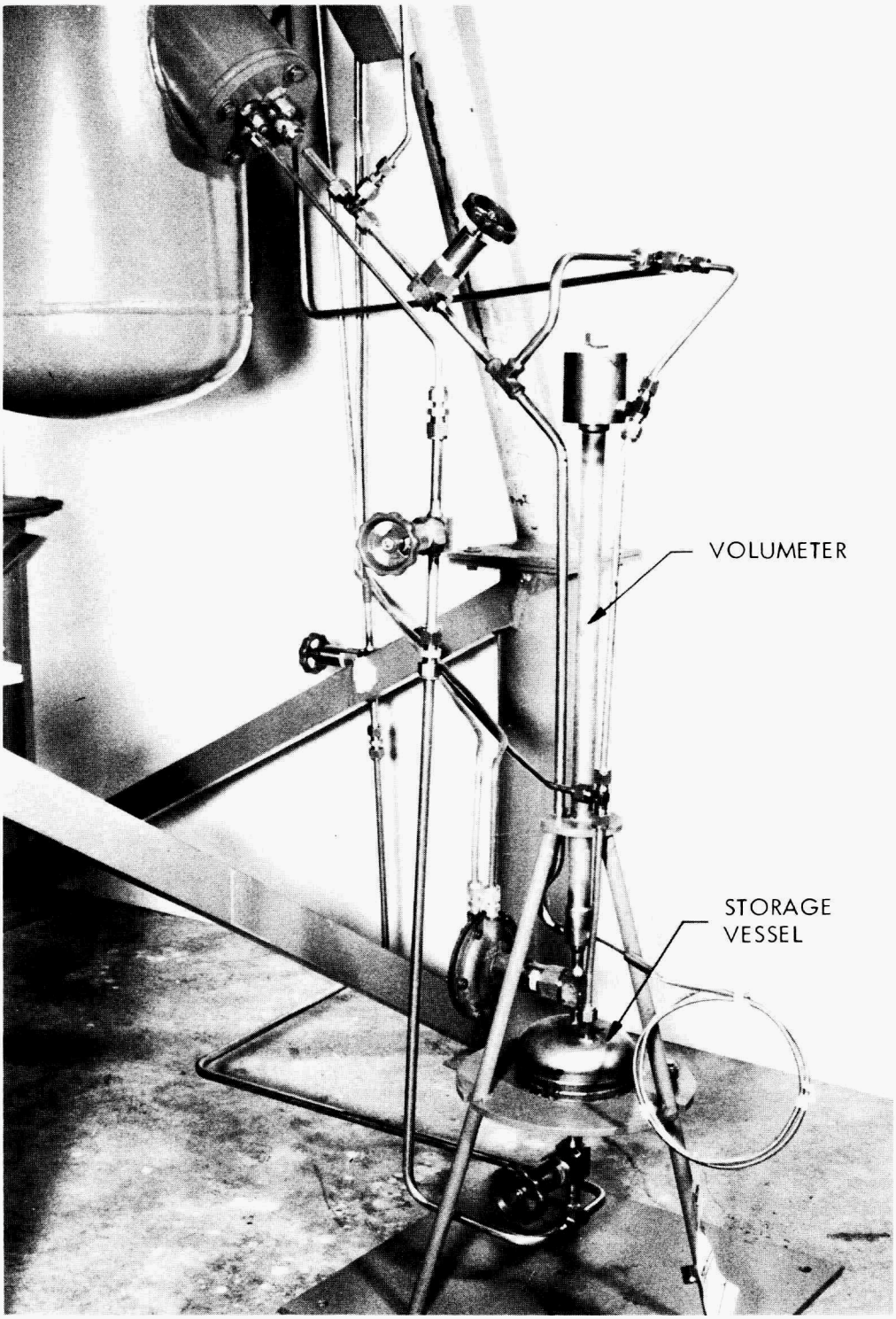

FIGURE 3. LATENT HEAT VOLUMETER

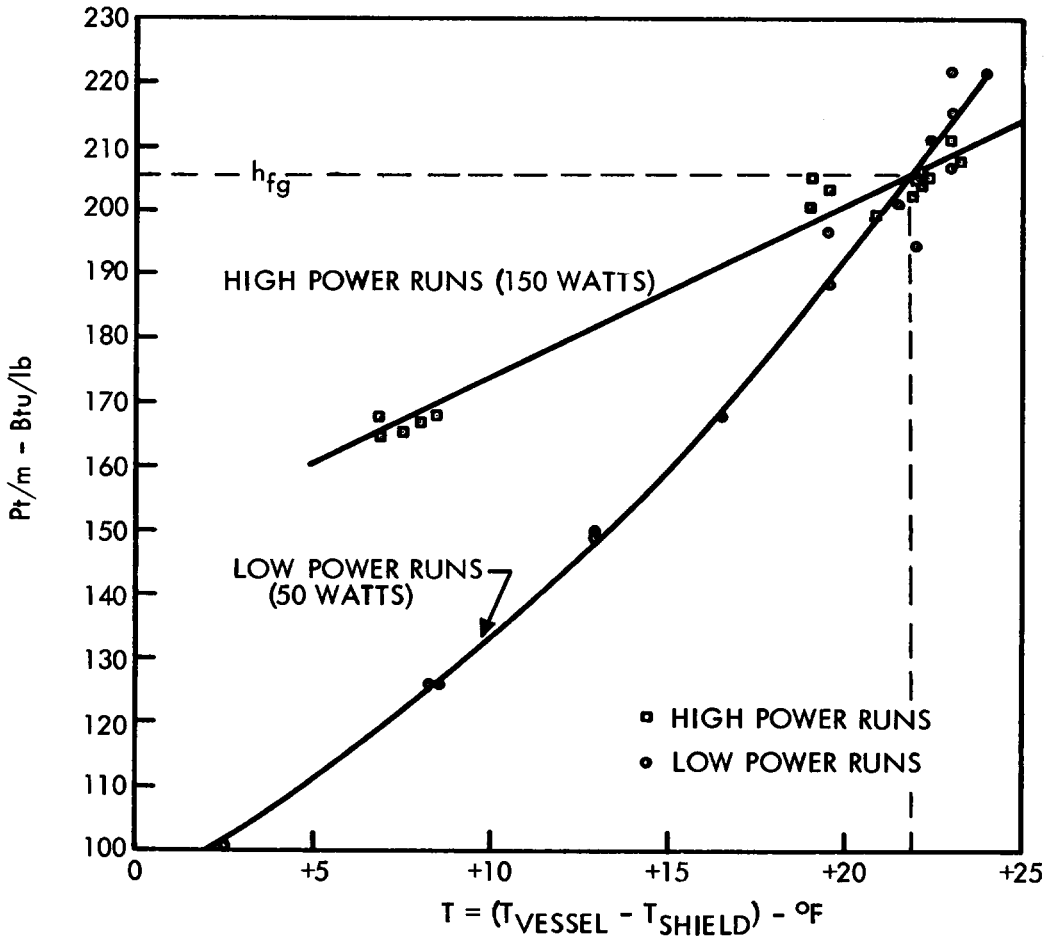

FIGURE 4. LATENT HEAT OF CESIUM AT 1400°F

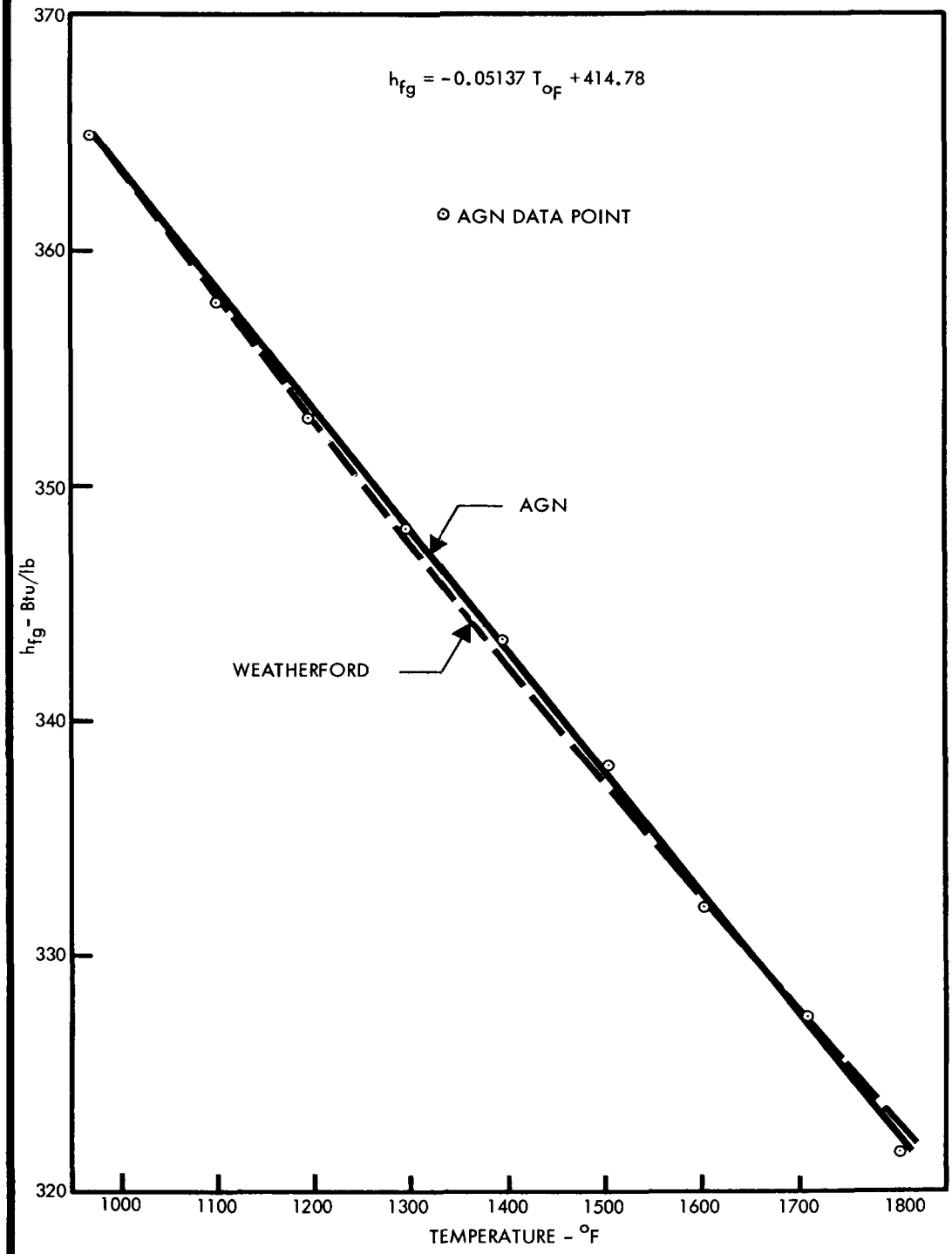

FIGURE 5. LATENT HEAT OF RUBIDIUM

13.6-63-2988

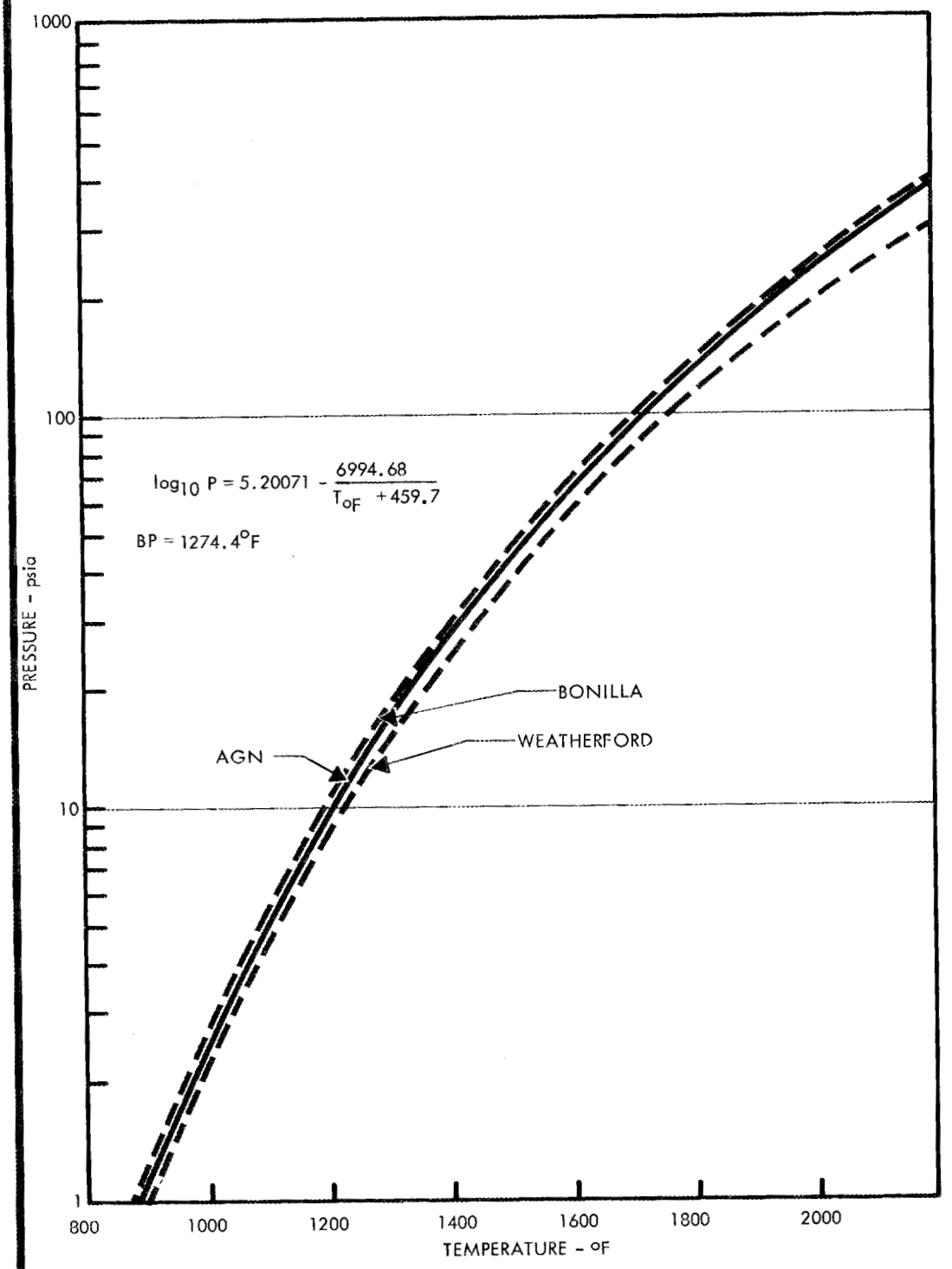

FIGURE 6. VAPOR PRESSURE OF RUBIDIUM

13.6-63-2990

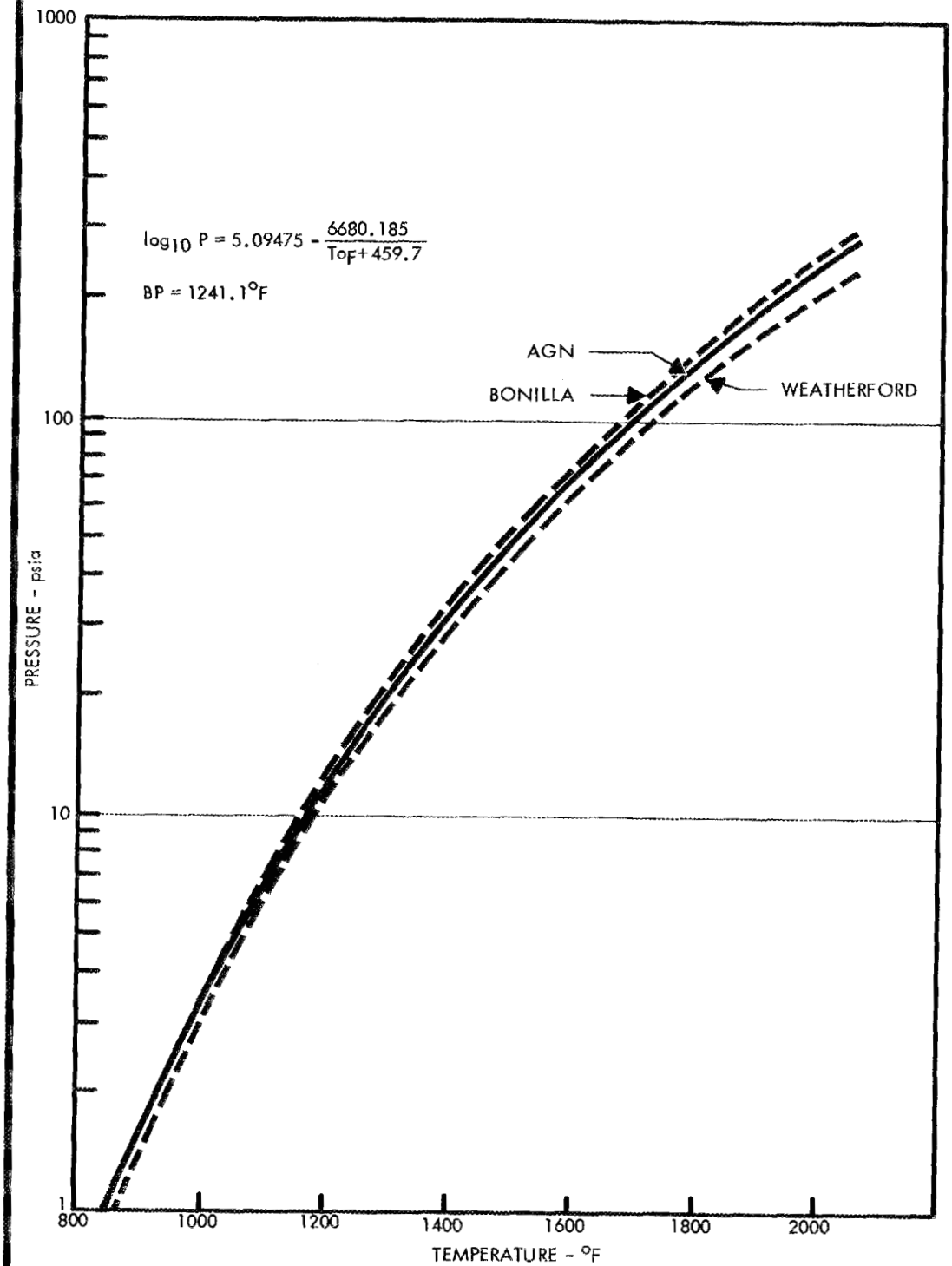

FIGURE 7. VAPOR PRESSURE OF CESIUM

136-63-2991

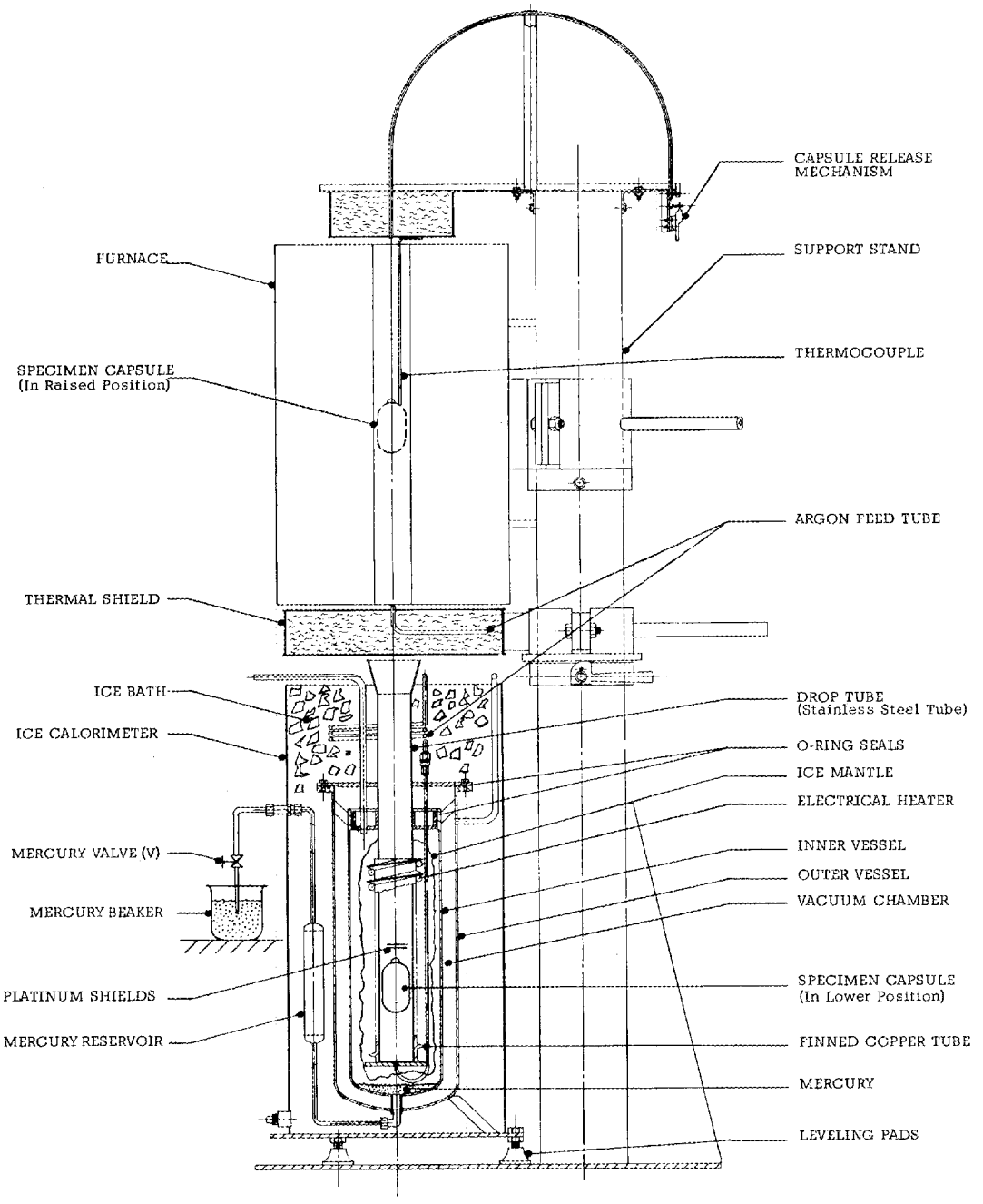

FIGURE 8. SPECIFIC HEAT APPARATUS WITH ICE CALORIMETER

13-6-65-2995

AGN PT-71

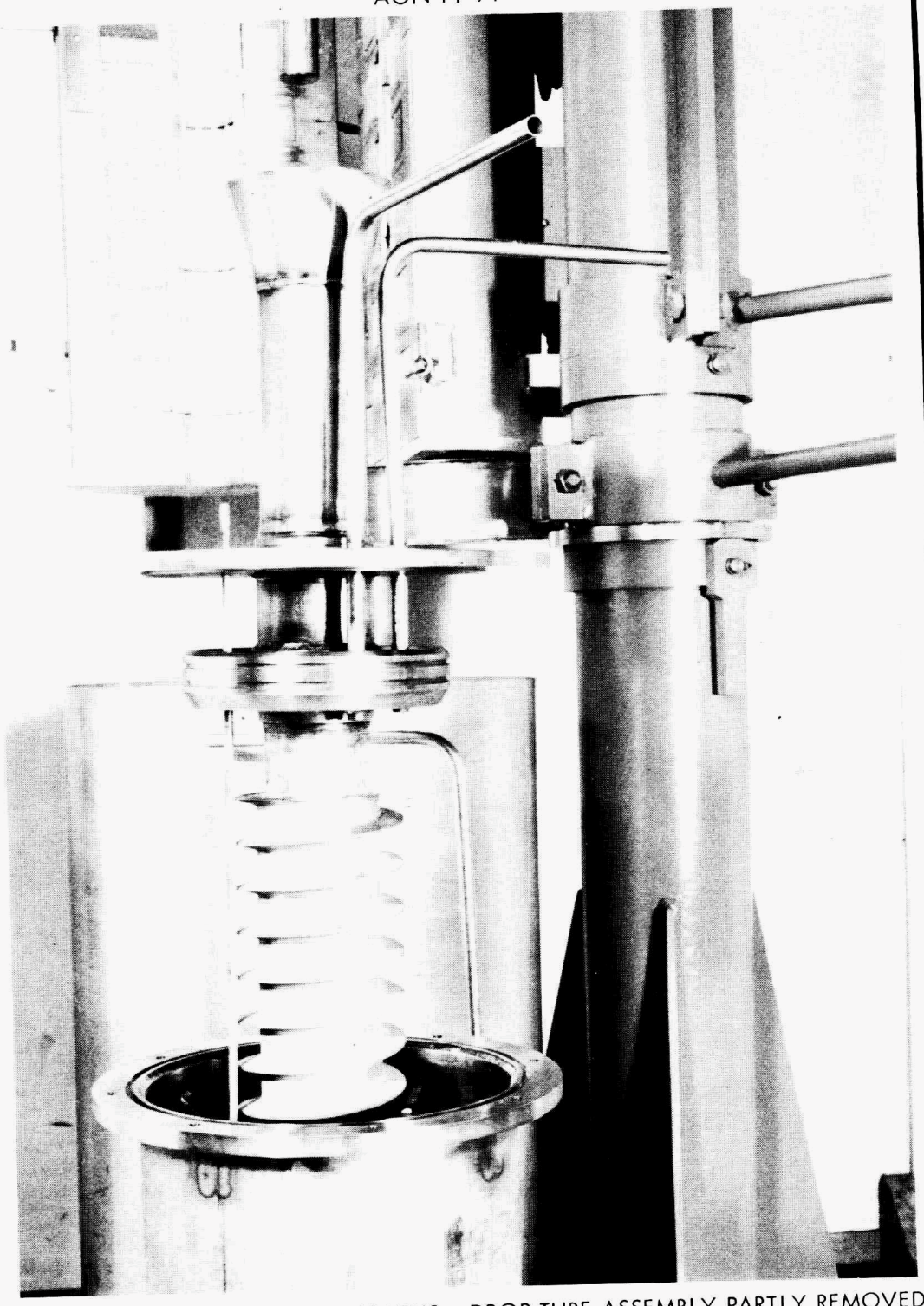

FIGURE 9. SPECIFIC HEAT APPARATUS - DROP TUBE ASSEMBLY PARTLY REMOVED

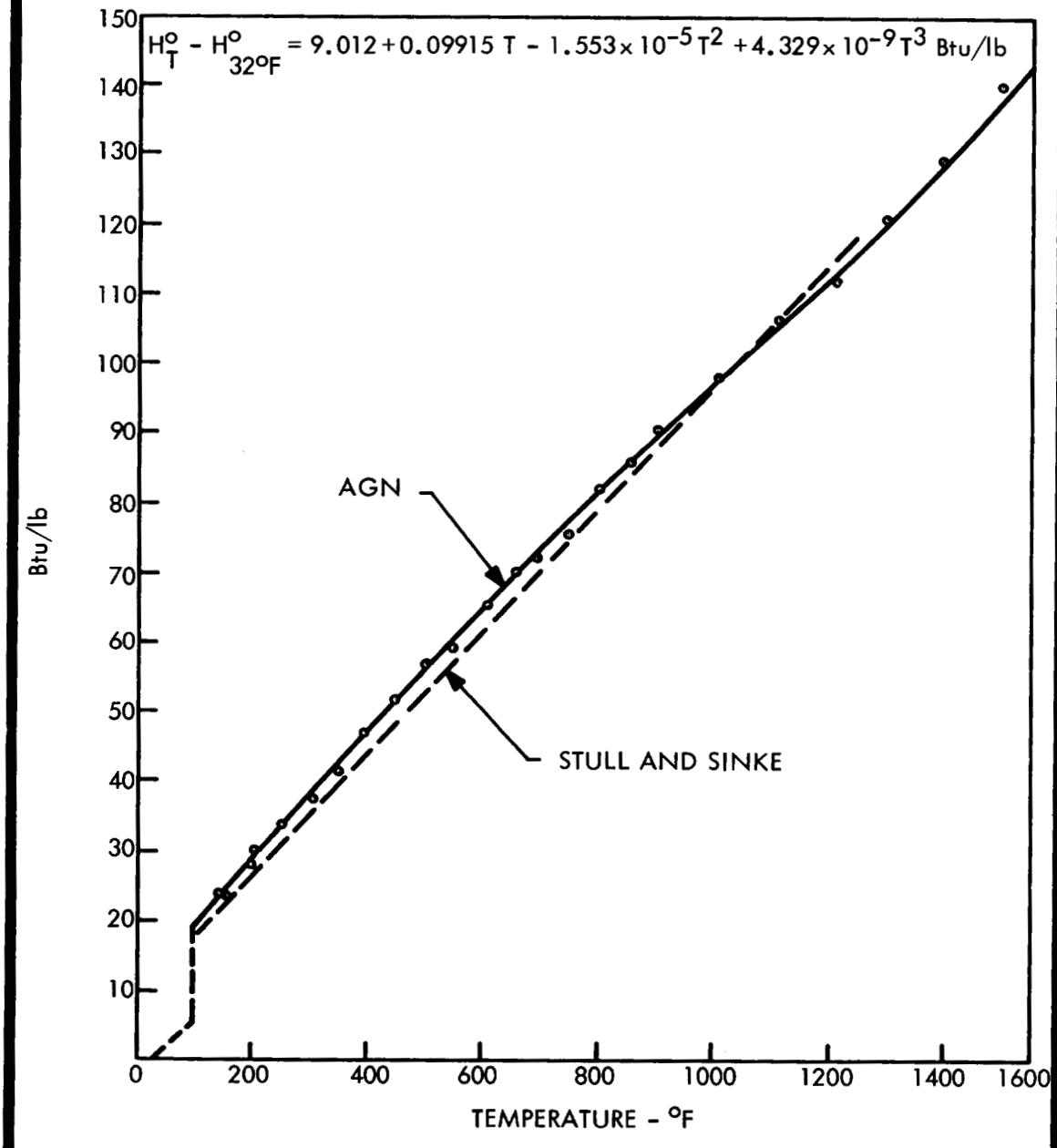

FIGURE 10. ENTHALPY OF RUBIDIUM

136-63-5015

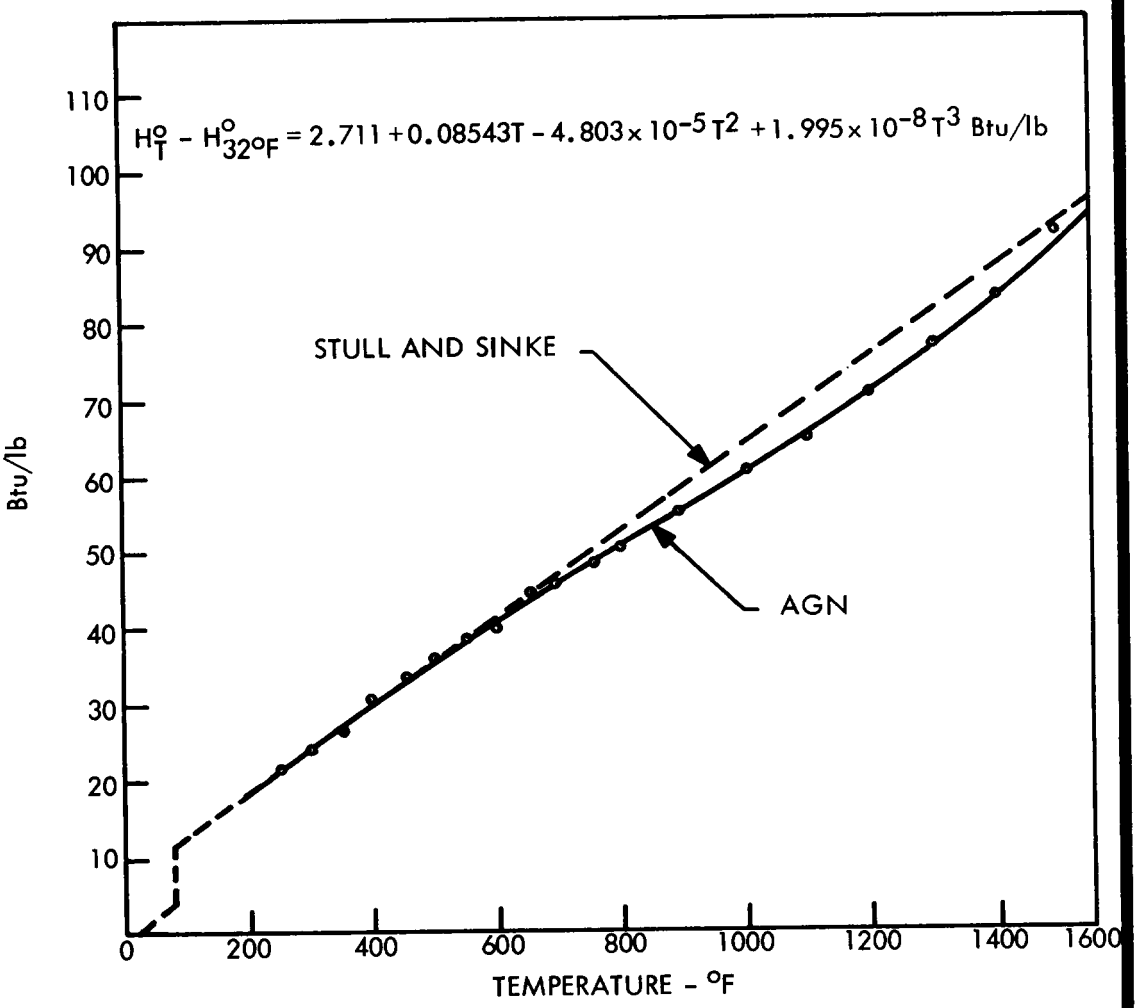

FIGURE 11. ENTHALPY OF CESIUM

1320-69-3016

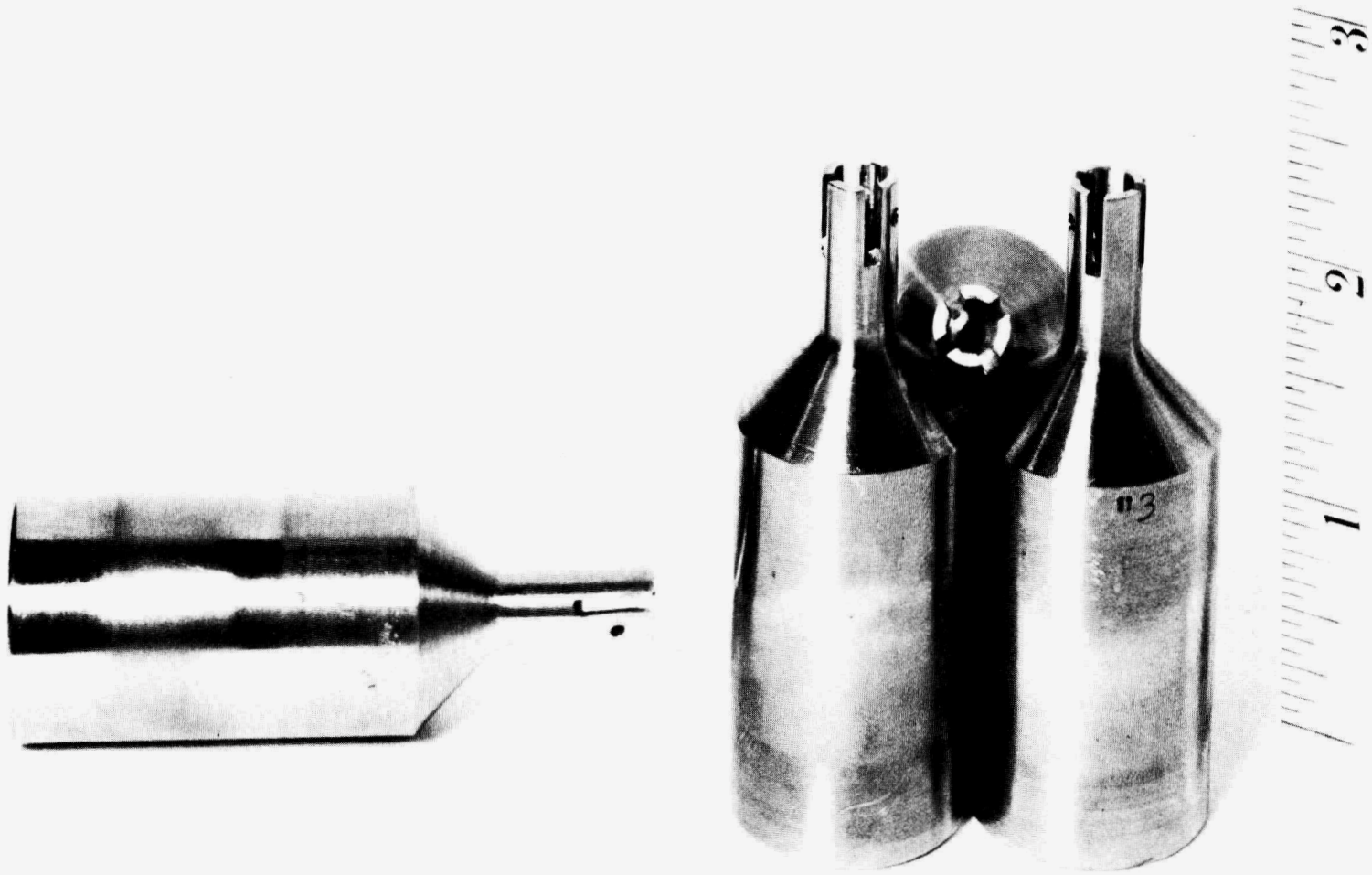

FIGURE 12. PYCNOMETERS

THERMOPHYSICAL PROPERTIES OF RUBIDIUM AND CESIUM

by

F. Tepper, A. Murchison, J. Zelenak and F. Roehlich

INTRODUCTION

Alkali metals appear to be particularly suitable for use as working fluids in Rankine cycle engines. Unfortunately, many of the properties of alkali metals are not known with sufficient certainty in the high temperature region to permit optimization of design criteria for developing maximum efficiency systems.

A program, sponsored by the USAF, was undertaken at MSAR to determine the thermophysical properties of rubidium metal. Recently, determination of the properties of cesium was included in the program. The specific properties to be measured to 2000°F are:

1. Vapor pressure
2. Density of the liquid
3. Specific heat of the liquid
4. PVT of the vapor
5. Viscosity of the liquid
6. Thermal conductivity of the liquid
7. Specific heat of the vapor
8. Thermal conductivity of the vapor
9. Viscosity of the vapor

A large part of the program has been directed towards development of techniques for the analysis of trace impurities in the alkali metals.

As of this writing, the completed determinations include the vapor pressure of rubidium and of cesium, the density and electrical resistivity of liquid rubidium and the specific heat of liquid rubidium and of liquid cesium. The density of liquid cesium has been determined to 708°F.

ALKALI METAL ANALYSIS

A considerable part of the effort associated with the program has been directed towards the development of techniques for analysis of alkali metals employed for physical property determinations.

The rubidium employed in the study was produced at MSAR and was analyzed for foreign alkali metals using flame spectrophotometric and emission spectroscopic techniques. The sodium, potassium and cesium contents were respectively 0.003, 0.21 and 0.37 weight per cent. Other metallic impurities totalled less than 100 parts per million. The sodium, potassium and rubidium contents of MSAR produced cesium to be employed in this study were respectively 10, 15 and 70 ppm.

Investigation of analytical methods for oxygen, carbon and nitrogen impurity contents was required. Nitrogen, as rubidium nitride, was determined via a modified Kjehldahl method, by converting the nitride to ammonia in a caustic solution and measuring the ammonia with Nessler's reagent. The lower limit of detection with this method is 2 ppm with a sensitivity of $\pm$ 2 ppm. A two gram rubidium sample was removed from a stainless steel sampling container and reacted with methanol. An argon sweep was used to transport released ammonia from the reaction flask to a receiver where the ammonia was collected in HCl. Nessler's reagent was added to the solution and the intensity of the color was measured with a Klett Summerson colorimeter. Results indicated a nitrogen concentration of 2.1 ppm. The analysis was repeated under nitrogen cover gas and 4.6 ppm nitrogen was found. Analysis of as-produced cesium via the above described method resulted in values less than 2 ppm.

A method for the analysis of carbon in sodium had been developed at MSAR prior to initiation of this program. The carbon in sodium is converted to CO_2 and the CO_2 is measured with an infrared spectrophotometer. The minimum detection limit for carbon in sodium is 10 ppm with a sensitivity of $\pm$ 10 ppm. Carbon analysis of rubidium resulted in a value of 28 ppm, while analysis in triplicate of cesium resulted in values of 90, 91 and 58 ppm carbon. A single analysis of this cesium charge after hot-trapping with zirconium turnings resulted in a value of 31 ppm carbon. Further analytical work for carbon in rubidium and cesium is necessary to establish the sensitivity and precision of this technique for carbon in these elements

The amalgamation method was evaluated as a technique for analyzing oxygen in rubidium and cesium. Samples of rubidium extracted from a reactor equipped with a cold leg were analyzed via the standard amalgamation procedure. Oxygen values of 122, 139, 122 and

138 ppm resulted, with an average value of 130. After two days of cold trapping with the hot leg at 600°F and a frozen rubidium cold leg, values of 32, 49 and 56 ppm oxygen resulted, suggesting the possibility of cold-trapping as a means of reducing the oxygen level.

Oxygen analyses of as-produced cesium via the amalgamation procedure resulted in an average value of 14 ppm. After oxygen has been added to the charge, which should have increased the oxygen level to approximately 65 ppm, the average of experimental values was only 8.6 ppm. It was apparent that the amalgamation procedure is not a reliable method, possibly due to solution or reaction of cesium oxide in mercury.

A program has been initiated to determine oxygen content in cesium by thermal arrest of the freezing curve. Initial results are promising and work is continuing.

VAPOR PRESSURE OF RUBIDIUM

Recent work by Bonilla[1] and Cochran[2] gives the vapor pressure of rubidium to 7.5 atm. abs. and 10 atm. abs., respectively. Other data exist for lower pressures.[3-9] This study covers the range 0.04 to 14.59 atm. abs.

A. Rubidium Purity

The rubidium was distilled to high purity and gettered with zirconium chips to remove oxygen. Analysis of the rubidium gave Cs, 0.37%; K, 0.21%; Na, trace; O, 50 ppm; N(as nitride), <2 ppm; C, ~ 28 ppm. Several grams of zirconium chips were added to the boiler and the rubidium was gettered throughout the experiment.

B. Apparatus

The apparatus consists of a boiler and an air condenser which is attached to a manifold connecting a source of pure argon and appropriate pressure measuring devices.

The boiler consists of a vertical cylinder (1 inch ID by 4.5 inches with 0.125 inch wall) with a thermocouple well extending horizontally into the center of the boiler 0.75 inches from the top. Welded to the top of the boiler is the condenser which consists of a 30 inch section of tubing (0.56 inches ID with 0.09 inch wall). A piece of 0.25 inch OD tubing is located axially within the condenser along its entire length and serves as a thermocouple well.

The top of the condenser is welded to a stainless steel tee. One end of the tee leads to a ball valve, used for charging the apparatus, the other end to the manifold.

The boiler is separated by asbestos paper from a 1.5 inch OD stainless steel tube designed to fit snugly into the furnace. The tubing helps to integrate the temperature over the height of the boiler and prevents stray emfs from the Kanthal heating elements (AC resistance heated) from interfering with the thermocouple reading.

The turnings which were added to the boiler ameliorated the problem of bumping encountered by other investigators at low pressures.[10]

The apparatus closely follows, in principle, that of Makansi which was applied to sodium,[11] potassium,[12] cesium[1] and rubidium[1]. In practice, the apparatus was simplified considerably by using Haynes No. 25 alloy as the material of construction. It was not necessary to balance with an external pressure and yet, the apparatus could be used with rubidium several hundred degrees fahrenheit higher than the balanced one made of Inconel, with no detectable deformation. A simpler thermocouple arrangement was employed and, based on the careful study of Bonilla[1] of the temperature gradient above and below the surface of the liquid metal, it appeared to be suitable. A Pt-Pt-10% Rh thermocouple was mounted in the boiler well and three chromel-alumel thermocouples were located along the condenser.

C. Procedure

The procedure of Bonilla and Makansi[1] was followed closely in all but unimportant details. Setting the argon pressure at the desired value, the power to the furnace was adjusted until boiling occurred at the desired rate as determined by the height of the boiling ring. The height of the ring was followed by the chromel-alumel thermocouples mounted within the condenser thermocouple well. After 5 minutes or more of equilibrium, marred only by minor pressure surges, the temperature of the boiler thermocouple and the pressure of the argon in the manifold were recorded.

D. Results and Discussion

In Table 1 fifty six data points are listed along with regression line values at the same temperatures and the per cent deviation of each point from the regression line.

All data were fitted to the following equations which are valid from 800°F to 2000°F.

$$\log_{10} P = \frac{-7,005.20}{T} + 4.04369 \qquad (1)$$

TABLE 1 - VAPOR PRESSURE DATA FOR RUBIDIUM

Run No.	Temperature °R	Experimental Pressure mm	Experimental Pressure Atm.abs	Regression Line mm	Per cent deviation from regression line
1	1289.3	30.50	0.04013	30.99	-1.61
2	1298.9	35.05	0.04611	33.99	+3.02
3	1317.7	39.95	0.05256	40.58	-1.55
4	1343.8	50.80	0.06684	51.47	-1.30
5	1351.4	54.50	0.07171	55.06	-1.02
6	1364.1	60.95	0.08019	61.53	- .94
7	1381.9	71.10	0.09355	71.66	- .78
8	1396.0	80.10	0.1054	80.62	- .65
9	1411.6	90.75	0.1194	91.61	- .94
10	1426.5	101.8	0.1339	103.2	-1.36
11	1425.2	102.2	0.1345	102.2	0
12	1449.7	124.0	0.1632	123.7	+ .24
13	1492.9	170.3	0.2241	170.7	- .23
14	1492.9	170.5	0.2243	170.7	- .12
15	1521.5	208.2	0.2739	209.1	- .43
16	1541.8	243.4	0.3203	240.5	+1.21
17	1542.7	244.0	0.3211	241.9	+ .87
18	1546.8	250.7	0.3299	248.7	+ .80
19	1548.1	251.1	0.3304	250.9	+ .08
20	1576.3	303.7	0.3996	302.3	+ .46
21	1594.2	343.0	0.4513	339.1	+1.15
22	1617.7	395.2	0.5200	392.8	+ .61
23	1616.7	395.7	0.5207	390.4	+1.31
24	1623.0	407.3	0.5359	405.8	+ .37
25	1648.7	481.7	0.6338	473.8	+1.67
26	1650.7	481.8	0.6339	479.5	+ .61
27	1655.9	500.2	0.6582	494.4	+1.17
28	1674.7	559.0	0.7355	551.5	+1.36
29	1689.5	608.2	0.8003	600.1	+1.35
30	1716.3	704.1	0.9264	696.6	+1.08
31	1729.7	758.3	0.9978	749.2	+1.21
32	1731.3	764.8	1.0063	755.6	+1.22
33	1741.4	805.4	1.0597	797.6	+ .98
34	1773.0	926.0	1.218	940.8	-1.57
35	1844.2	1347	1.772	1337	+ .75
36	1866.0	1425	1.875	1480	-3.72
37	1893.4	1659	2.183	1677	-1.07
38	1947.2	2075	2.730	2123	-2.26
39	1952.5	2179	2.867	2171	+ .37
40	1966.8	2220	2.921	2306	-3.73
41	2018.4	2866	3.771	2844	+ .77
42	2019.7	2867	3.772	2858	+ .31
43	2066.0	3435	4.520	3419	+ .47
44	2088.0	3730	4.908	3712	+ .48
45	2111.6	4076	5.363	4046	+ .74
46	2147.3	4629	6.091	4594	+ .76
47	2170.2	4978	6.550	4973	+ .10
48	2184	5246	6.903	5212	+ .65
49	2224.2	5961	7.843	5957	+ .07
50	2274.9	6998	9.208	7002	- .06
51	2277.2	7005	9.217	7052	- .67
52	2277.1	7026	9.245	7050	- .34
53	2320.7	8024	10.56	8053	- .34
54	2362.4	9060	11.92	9105	- .49
55	2410.9	10,374	13.65	10,440	- .63
56	2435.3	11,090	14.59	11,170	- .72

$$\log_{10} P = \frac{-7,110.53}{T} - 0.140579 \log_{10} T + 4.50749 \qquad (2)$$

$$\log_{10} P = \frac{-7,071.61}{T} - 0.0000217774T + 4.121014 \qquad (3)$$

for P in atm. abs. and T in °R.

These data are well represented by the regression line (equation 1) which has a standard deviation of 1.24%. The three term correlating expressions have standard deviations of 1.20%. The Kirchhoff equation (2) is recommended because of its widespread use and probable superiority in a calculation of latent heat of vaporization.

The linearity of the data shown by equation (1) is unusual over the range studied. Gray,[13] however, discussed the general problem and concludes that theoretical justifications for linearity exist.

A comparison of results with available high pressure data is given in Table 2. Regression line values are listed at 100° intervals over the range 1300°R to 2400°R for these data and for the correlating equations of Bonilla[1] and Cochran.[2]

Also in Table 2 are the calculated results of Shapiro and Meisl[14] (as reported by Weatherford[15]). These workers adjusted experimental values to yield consistent thermodynamic data; iterating vapor pressure until the ratio of the heat of vaporization to temperature equalled the entropy of vaporization. Their calculation extended to about 20 atms. abs.

Bonilla's data are about 3% higher than MSAR data, Cochran's results are about 6% lower and the calculated results are about 13% lower. Bonilla's correlating expression has a standard error of 1.26% and Cochran reports an estimated accuracy of ± 2 per cent.

A comparison of the present data for the normal boiling point of rubidium with the results obtained by other investigators is given in Table 3. Normal boiling points were computed by extrapolation of the low pressure data obtained by Moore[3], Battelle[3], Kelley[4], Ditchburn[5-8] and Johanssen[9]. None of the low pressure data could be applied to pressures higher than 1 atmosphere with any confidence.

VAPOR PRESSURE OF CESIUM

The vapor pressure of cesium has been determined in the range 850°F to 1950°F (0.07 to 13.7 atm abs) in the same apparatus which was used for rubidium. Experimental data and the percent de-

TABLE 2 - COMPARISON OF VAPOR PRESSURE RESULTS FOR RUBIDIUM

T°R	T°K	MSAR[a] P atm.	Bonilla[b] P atm.	% Deviation From MSAR	AGN[c] P atm.	% Deviation From MSAR	Weatherford[d] P atm.	% Deviation From MSAR
1300	722.2	0.04519	.04722	+4.5	.03692	-18.3	.03921	-13.3
1400	777.8	0.1097	.1142	+4.1	.09491	-13.5	.09642	-12.1
1500	833.3	0.2364	.2457	+3.8	.2133	- 9.8	.2093	-12.6
1600	888.9	0.4629	.4801	+3.7	.4309	- 6.9	.4111	-11.2
1700	944.4	0.8375	.8669	+3.5	.7961	- 4.9	.7437	-11.2
1800	1000.0	1.419	1.466	+3.3	1.368	- 3.6	1.255	-11.5
1900	1055.5	2.274	2.347	+3.2	2.211	- 2.8	1.994	-12.3
2000	1111.1	3.476	3.583	+3.0	3.396	- 2.3	3.023	-13.0
2100	1167.7	5.104	5.254	+2.9	4.974	- 2.5	4.409	-13.6
2200	1222.2	7.236	7.442	+2.8	7.027	- 2.9	6.192	-14.4
2300	1277.8	9.953	(10.227)	+2.7	9.599	- 3.5	8.410	-15.5
2400	1333.3	13.33	(13.68)	+2.6	(12.75)	- 4.3	11.09	-16.8
		Sd = 1.24%	Sd = 1.26%	Avg = +3.3%		Avg = -6.3%		Avg = -13.1%

(a) $\log_{10} P \text{ atm} = \frac{-7,005.200}{T°R} + 4.04369$ Standard deviation = 1.24 per cent

(b) $\log_{10} P \text{ atm} = \frac{-6,983.036}{T°R} + 4.04573$ Standard error = 1.26 per cent

(c) $\log_{10} P \text{ atm} = \frac{-4,640.4}{T°K} - 1.5283 \log_{10} T°K + 9.3615$ Estimated accuracy = ± 2 per cent

(d) calculated results

TABLE 3 - COMPARISON WITH LOW PRESSURE DATA (Rb)

Source of Data	Boiling Point (°F)
MSAR	1272
Bonilla[1] (Columbia Univ)	1266
Cochran[2] (AGN)	1279
Moore[3] (ORNL)	1261*
Battelle[3]	1269*
Kelley[4] (a compilation)	1254*
Ditchburn[5,6,7,8] (a compilation)	1271*
Johanssen[9]	>1280*

*extrapolated

viation of each point from the regression line are listed in Table 4. The regression line of the 23 data points is given by

$$\log_{10} P_{atm\ abs} = \frac{-6,631.74}{T^{\circ}R} + 3.90111$$

with a standard deviation of 0.72 percent.

No further statistical analysis of the data will be made because of the satisfactory straight line correlation.

A comparison of MSAR results with those of Bonilla[1], AGN[2] and Shapiro and Meisl[14] is made in Table 5.

The normal boiling point was found to be 1240°F. Bonilla obtained a boiling point of 1231°F, AGN - 1274°F, Hultgren's compilation - 1259°F, Shapiro and Meisl (also reported by Weatherford) - 1260°F.

DENSITY OF LIQUID RUBIDIUM

The density of rubidium has been determined to 1300°F by AGN[2], to 750°F by ORNL[3] and has been calculated from the densities of potassium and sodium (reported by Weatherford[15]). The AGN results were obtained dilatometrically and those of ORNL by an Archimedean method. This study covers the range 150° to 2000°F using a dilatometer device.

A. Rubidium Purity

The rubidium was taken from the same batch as that used in the vapor pressure work. While it was gettered prior to charging the apparatus there were no zirconium chips in the apparatus.

B. Apparatus

A dilatometer is a device which measures the volume of a given weight of liquid. It has the important advantage of enabling a range of densities to be determined from a single charge; in our case, a span of up to 150°F could be covered. Dilatometers are frequently beset with the problem of bubble formation.

The dilatometer which was used consists of a cylinder 4 inches by 1 inch ID with a 0.125 inch wall, having a thermocouple well projecting to the center of the volume from below. The top of the cylinder is tapered to minimize bubble formation and is attached to a 10 inch length of tubing which has a volume of 0.180 ml per inch of length. The top of the tubing is connected to a ball valve and to a source of pure argon. Three protuberances were welded onto the tubing to serve as base points and to facilitate interpretation of the x-ray photographs which were used to determine the meniscus level.

TABLE 4 - CESIUM VAPOR PRESSURE DATA

Pressure (mm Hg)	Temperature (°R)	Calculated Pressure* (mm/Hg)	% deviation of regression line from data
53.3	1312.4	53.55	+0.47
73.0	1348.2	72.94	-0.08
92.0	1377.5	92.81	+0.87
111.7	1402.2	112.8	+0.98
144.2	1435.7	145.5	+0.89
186.9	1470.6	187.2	+0.16
233.6	1502.6	233.6	0
310.3	1544.8	308.3	-0.65
395.5	1583.8	393.3	-0.56
476.3	1613.3	469.1	-1.53
589.0	1653.1	589.1	+0.02
695.2	1681.2	687.5	-0.97
808.6	1711.1	805.8	-0.35
1300	1807.5	1296	-0.31
2001	1902.1	1974	-1.37
2499	1958.6	2489	-0.40
3286	2032.0	3298	+0.36
3911	2078.1	3897	-0.36
4916	2145.6	4910	-0.12
5956	2205.5	5957	+0.02
7470	2282.9	7532	+0.82
9016	2349.5	9105	+0.98
10370	2401.4	10480	+1.05

SD = 0.72%

$$* \log_{10} P = \frac{-6,631.74}{T} + 6.78192$$

for P in mm Hg and T in °R

TABLE 5 - CESIUM VAPOR PRESSURE - COMPARISON OF RESULTS

Temperature °R	Temperature °K	MSAR(1) P (atm)	Bonilla(2) P (atm)	AGN(3) P (atm)	Weatherford(4) P (atm)
1300	722.2	0.0631	--	--	0.0545
1400	777.8	0.1459	0.1522	--	0.1288
1500	833.3	0.3020	0.3155	0.1861	0.2689
1600	888.9	0.5624	0.5967	0.4146	0.5084
1700	944.4	1.0002	1.049	0.8166	0.8932
1800	1000.0	1.647	1.733	1.455	1.474
1900	1055.6	2.575	2.713	2.397	2.286
2000	1111.1	3.847	4.064	3.658	3.383
2100	1166.7	5.536	5.857	5.296	4.820
2200	1222.2	7.704	--	7.253	6.639
2300	1277.8	10.417	--	--	8.886
2400	1333.3	13.737	--	--	11.558
Deviation from MSAR			~+5%	~-15%	~-12%

(1) $\log_{10} P = \frac{-6,631.74}{T} + 3.90111$ standard deviation = 0.72%

for P in atm, T in °R.

(2) $\log_{10} P = \frac{-6,665.302}{T} + 5.10876$ standard error = 1.44%

for P in PSIA and T in °R.

(3) $\log_{10} P = \frac{-7,474.39}{T} - 7.59618 \log_{10} T + 30.4259$ estimated accuracy = ±2%

for P in atm and T in °K.

(4) Calculated results, Shapiro and Meisl.

The apparatus was calibrated with mercury at room temperature and a value of 49.2 ml was obtained at the lowest protuberance. As it is necessary to know the change in volume of the cylinder with temperature a calculation was made based on the published data of the Haynes Stellite Company which lists the coefficient of linear expansion for Haynes No. 25 to 3 places at 200° increments from 70° to 2000°F. A detailed calculation of the change in volume with temperature was made and applied to the data as a correction. At 2000°F the volume increased 5.92% compared to that at 70°F. Uncertainties due to cross-sectional variations in the capillary tubing would result in an error in computation of volume estimated to be less than 0.1%, since the total internal volume of the rubidium in the capillary was generally less than one percent of the total volume of the charge.

Determination of the height of the rubidium meniscus in the tube could be made to within 1 mm with no difficulty. This corresponds to a truly negligible error of the order of 1 part in 7000.

C. Procedure

The apparatus was charged with a known quantity of rubidium and the temperature raised so that the meniscus was located in the tubing. The volume-temperature relationship was then determined along the tubing. Removing or adding a known quantity of rubidium enabled higher or lower temperatures to be investigated.

It was necessary to apply an argon pressure somewhat in excess of the boiling point at the temperature of interest. The degree of excess was of no significance as demonstrated by the addition of 7 atmospheres argon pressure to an experiment at 1650°F with no detectable change in density.

At temperatures in excess of 1500°F some difficulty was encountered with bubble formation. This problem was ameliorated by the following precautions:

1. Decreasing the temperature gradient along the tubing by use of insulation and nichrome heating wire.

2. Using only the lower portion of the tubing (i.e. 4 inches).

3. Pressurizing with argon while slightly below the temperature of interest and concurrently heating the tubing, then proceeding to temperature and recording data.

D. Results and Discussion

All 60 data points, in the range 150°F to 2000°F, are listed in Table 6 in the order of increasing temperature. Table 6 also indicates which points were obtained at identical charges (i.e. a set of results) and when the apparatus was cleaned and recharged. Recalibration of the volume of the bomb after both charges showed an increase in volume of less than 0.2%.

All data were analyzed statistically for 8 functional forms. These 8 equations are listed in Table 7, along with standard deviations, in chronological order. The precision of the data seemed to warrant extensive analysis.

The straight line (equation 1) is probably suitable for most applications, as it has a standard deviation of 0.0063 g/cc. Equation 4 is recommended because it is the simplest expression achieving a standard deviation of 0.0035 g/cc, which is equivalent to a precision of about 0.3%. Equations 5, 7 and 8, which are more complex, also have standard deviations of 0.0035 g/cc; this figure apparently being a true measure of the precision of the data. Equation 2 was rejected because of an obviously poor fit and equation 6 because of an inflection point in the range of interest.

In Figure 1 these data are compared graphically with those of Cochran[2] and ORNL[3]. The results of ORNL are in fair agreement, particularly at low temperatures. The archimedean method which was used by ORNL could be expected to give trouble at higher temperatures, as the rubidium is contained in an open vessel in a dry box under 1 atmosphere of argon and the rate of vaporization increases with temperature. The AGN data are best represented by a curve

$$d = 1.497 - 2.530 \times 10^{-4}\, t + 4.08 \times 10^{-8}\, t^2$$

which is assigned an estimated accuracy of $\pm$ 0.005 g/cc to 1300°F and $\pm$ 0.01 g/cc from 1300 to 1800°F by Cochran. Marked differences exist between AGN data and those of MSAR.

The calculated results appearing in Weatherford's compilation, and not reported here, are about 0.1 g/cc higher than the MSAR data at 1500°F.

The lack of effect of an overpressure of 7 atmospheres of argon upon the density of rubidium at 1650°F shows that the liquid is not compressible under these conditions. A change of only 1 mm in the height of the rubidium would have been observed and that change is equivalent to 1 part in 7000 of the volume.

TABLE 6 - RUBIDIUM DENSITY DATA

No.	Temperature	Density	Set No.
1	157.9	1.477	12
2	167.4	1.475	12
3	193.2	1.471	12
4	197.8	1.469	12
5	224.3	1.466	12
6	401.0	1.440	1
7	429.4	1.434	1
8	430.4	1.433	1
9	454.4	1.429	1
10	556.8	1.395	2
11	596.3	1.385	2
12	644.4	1.374	2
13	667.5	1.368	2
14	698.7	1.361	2
15	817.8	1.329	3
16	827.9	1.319	13
17	858.0	1.319	3
18	890.9	1.305	13
19	898.9	1.310	3
20	939.3	1.301	3
21	955.9	1.294	4
22	986.6	1.287	4
23	1016.6	1.281	4
24	1060.9	1.271	4
25	1080.5	1.264	5
26	1094.1	1.264	4
27	1113.0	1.255	5
28	1141.6	1.247	5
29	1183.7	1.239	5
30	1204.3	1.230	6
31	1209.3	1.235	5
32	1242.9	1.223	6
33	1281.9	1.215	6
34	1313.6	1.207	6
35	1322.1	1.206	6
36	1332.8	1.200	7
37	1377.3	1.190	7
38	1425.0	1.181	7
39	1457.0	1.166	8
40	1479.0	1.162	8
41	1522.5	1.148	8
42	1602.1	1.127	9
43	1602.1	1.127	9
44	1623.9	1.122	9
45	1629.7	1.120	10
46	1639.8	1.118	9
47	1646.0	1.118	10
48	1667.1	1.114	10
49	1723.6	1.092	11
50	1737.2	1.091	11
51	1746.6	1.087	11
52	1771.9	1.081	11
53	1909.8	1.045	14
54	1923.4	1.043	14
55	1933.6	1.039	14
56	1937.9	1.034	14
57	1973.6	1.033	15
58	1989.4	1.021	15
59	1993.9	1.028	15
60	1994.9	1.028	15

The apparatus was charged with rubidium prior to sets 1, 12 and 15. Between sets (for a particular charge) a portion of the rubidium was removed from the apparatus.

TABLE 7 - STATISTICAL ANALYSIS OF RUBIDIUM DENSITY DATA

No.	Equation	Standard Deviation (g/cc)	a	b	c	d	Remarks
1	$\rho = a + bZ$	0.0063	1.53383	-0.252996	---	---	
2	$\rho = a + \frac{b}{Z}$	0.0907	1.13250	0.0774922	---	---	Poor fit
3	$\rho = a + bZ + cZ^2$	0.0045	1.51933	-0.218683	-0.0154436	---	
4	$\rho = a + bZ + \frac{c}{Z}$	0.0035	1.55643	-0.265111	-0.00626779	---	Best curve
5	$\rho = a + bZ + \frac{c}{Z^2}$	0.0035	1.54614	-0.260982	-0.000816322	---	
6	$\rho = a + bZ + cZ^2 + dZ^3$	0.0041	1.51055	-0.178605	-0.0591314	0.0133070	Inflects at 1481°F
7	$\rho = a + bZ + cZ^2 + \frac{d}{Z}$	0.0035	1.55458	-0.262526	-0.000929390	-0.00599877	
8	$\rho = a + bZ + cZ^2 + \frac{d}{Z^2}$	0.0035	1.53975	-0.249735	-0.00440185	-0.000666378	

$Z = t/1000$
ρ = g/cc
t = degrees F
a, b, c, d = constants

Data consists of 60 points in the range 150°F to 2000°F, with density varying from about 1.5 to about 1.0.

DENSITY OF LIQUID CESIUM

The density of cesium has been obtained to 708°F in the same apparatus used for rubidium. Data are listed in Table 8.

Work is continuing and it is anticipated that cesium density will be obtained to 2000°F in the near future.

PVT OF THE VAPOR

The pressure-volume-temperature relationship of rubidium and of cesium from the saturated vapor line to over 1900°F is currently being investigated.

The apparatus, shown schematically in Figure 2, consists of two Haynes-25 cylinders, which are separated by a Haynes-25 diaphragm of 2.2 mil thickness. Temperature is measured with three Pt-Pt-10% Rh thermocouples, which had been calibrated at the National Bureau of Standards. Isothermality is approached by power adjustment of three cylindrical heater elements. A 2°F gradient is commonly achieved along the 6 1/2" long chamber which is to contain the alkali metal vapor.

Known weights of alkali metal are added to the lower cylinder in the form of stainless steel ampoules, which rupture upon heating in the bomb. The bomb is evacuated and sealed off with a pinch-off device. The pressure in the alkali metal filled cylinder is measured by balancing the diaphragm in a null position with a known pressure of argon. The null pressure is defined as that pressure necessary to break electrical contact of the diaphragm with the probe. The balancing argon pressure is measured with a U-tube manometer to 1000 mm Hg and with a Bourdon tube gauge (accuracy ± 0.05 psi) for pressures between 1000 mm Hg and 215 psia.

Initial PVT data for rubidium are shown in Figures 3 and 4. The volume of the lower cylinder is redetermined with mercury prior to each charge. Volume corrections with temperature are computed from linear expansion coefficients for Haynes-25 alloy and are shown in Figure 5. Pressure-temperature data in the saturated region agrees closely with earlier vapor pressure data. Reproducibility of pressure readings in the unsaturated region was approximately ±0.1 psi below 1600°F and slightly greater at higher temperatures.

TABLE 8 - DENSITY OF LIQUID CESIUM

Temperature (°F)	Density (g/cc)
104.7	1.840
190.1	1.811
212.1	1.806
215.7	1.805
228.8	1.801
230.1	1.801
234.0	1.800
259.3	1.792
515.9	1.714
519.6	1.711
540.4	1.706
553.4	1.702
573.8	1.694
587.0	1.691
596.5	1.688
629.6	1.678
641.7	1.673
670.9	1.665
708.1	1.655

The pressure-temperature relationship of three different rubidium charges have been measured. Analysis of the rubidium present in the bomb after the first run suggested an error in the weight of rubidium added to the bomb prior to the first run. The rubidium weights in Runs 2 and 3 were respectively 96.5 and 239 milligrams. The apparent molecular weight in each of the last two charges is about 101. The difference between this value and the atomic weight of rubidium (85.5) is attributed to the combined effect of polymerization and compressibility. No attempt will be made to reduce the data to equations of state until a significant number of runs have been performed.

SPECIFIC HEAT OF LIQUID RUBIDIUM

Kelley[33] gives a value of 0.0913 cal/g-°C for the heat capacity of liquid rubidium from 39°C to 126°C. Rengade[34] reports the equation

$$cp = 0.0921 - 0.00026T°C$$

from which the value at the melting point (39°C) is 0.0899 cal/g-°C. Stull and Sinke[35] estimated 0.0877 cal/g-°C at the boiling point. There are no experimental data for the specific heat of rubidium at elevated temperature.

The standard method of obtaining specific heat at elevated temperature is to heat the sample to be measured to a determined temperature and then drop the sample into a calorimeter of known heat capacity.

The ice calorimeter initially was chosen for this work because it requires no temperature or electrical measuring instruments and possesses a very high sensitivity.

Ginnings, et al[36] describe in detail a thoroughly refined apparatus and procedure which were used as models for this program. The principal source of error in this work lies in the determination of the temperature of the sample as it hangs in the furnace, with lack of isothermality the probable major cause of difficulty.

Prolonged equilibration times were encountered in the ice calorimeter, and it was decided to perform the determinations using a copper block calorimeter, which existed at the facility. Heat content measurements on rubidium have been made over most of the temperature range of interest utilizing a copper block calorimeter. Heat content values have been used to derive a preliminary set of thermodynamic functions for solid and liquid rubidium. These thermodynamic functions have been used in conjunction with the measured vapor pressures to obtain heats of vaporization by the "Third Law" method.

Experimental

The calorimeter used for the heat content measurements was a copper block drop calorimeter based on the design of Southard[37] as modified by Kelley and Naylor.[38] The calorimeter design is shown schematically in Fig 6. The sample, A, is suspended in the furnace, B, by means of a wire attached to the drop tube plunger, C. The plunger is controlled by a brake mechanism which controls the rate of fall of the sample. When the sample has reached thermal equilibrium in the furnace, as measured by a Pt-Pt-10%Rh thermocouple, the drop plunger is released, the gates, D, at the bottom of the furnace and at the copper block are opened to allow passage of the capsule. As the capsule enters the calorimeter, the brake mechanism brings the sample to a stop, in good thermal contact with the copper block. After the drop, which takes 2 to 3 seconds, the gates are closed. Both gates are provided with narrow slots to allow the suspension wire to pass through them when closed.

The calorimeter proper, E, is a gold-plated copper cylinder resting on knife-edge supports in a brass case. The case is immersed in a large oil bath thermostatted at 25.00 ± 0.01°C. The sample, in the form of a slightly tapered cylinder, drops into the calorimeter receiving well, also slightly tapered to assure good thermal contact between the sample and the calorimeter. The temperature of the copper block is followed by means of a calorimetric platinum resistance thermometer inserted in a well parallel to the sample receiving well and midway between the receiving well and the outside surface of the block. The heat capacity of the copper block is obtained by electrical calibration using a Manganin heater wound on the tapered plug which contains the receiving well.

The furnace consists of an electrical heating element and two layers of insulation. A cooling water jacket surrounds the whole assembly. The heated zone is within a one inch inside diameter porcelain tube on which the heating element is wound. The windings are held in place by a high temperature cement and a second

porcelain tube fits over the windings as a protective cover. Platinum-10 percent rhodium wire (B and S gage No. 22) is wound with 4 1/2 turns per inch for 12 inches at the center of the tube and at 6 turns per inch for 1 1/2 inches on each end.

The insulation is a 5 inch layer of -28 mesh zirconia followed by a 2 inch layer of cast Firecrete refractory. Cooling water circulating through the jacket minimizes heat transfer to the calorimeter.

The rubidium sample, 1.9335 grams, was contained in a cylindrical Haynes Alloy No. 25 capsule having a coaxial thermocouple well. A similar Haynes capsule was used for the heat content measurements of the empty container.

All of the energy measurements are made in terms of the defined thermochemical calorie equal to 4.184 (exactly) absolute joules. The ice point of the absolute temperature scale was 273.15°K.

Heat Content and Derived Properties

The experimental heat content data, corrected for the contribution of the capsule, are given in chronological order in Table 9. Vaporization corrections were calculated and found to be negligibly small.

Over the temperature range from 500° to 1400°K, the heat content data for the empty capsule were fitted by least squares to the expression

$$H_T^\circ - H_{298}^\circ (\text{cal/g}) = 52.28 + 0.021686T + 4.0315\times10^{-6}T^2 + 5.79244\times10^3/T.$$

At each data point for the filled capsule, the heat content of the capsule was calculated from the above expression and substracted from the total enthalpy change.

The raw data for the rubidium sample were fitted by least squares to the linear expression

$$H_T^\circ - H_{298}^\circ \ (\text{cal/mole}) = 7.53T - 1624.$$

The standard deviation over the range from 500°K to 1300°K is of the order of ± 2%. Using the low temperature data of Dauphinee and Martin[39], as compiled by Stull and Sinke[40], a consistent table of thermodynamic functions were derived for solid and liquid rubidium.

TABLE 9 - RUBIDIUM HEAT CONTENT DATA

Temperature (°K)	$H_T - H_{298.15}$ cal/mole
504.4	2227
622.5	3047
737.6	4028
853.6	4626
946.7	5239
991.5	5953
1017.5	6203
1172.0	7186
1205.0	7528
1268.0	7888

The high temperature data were extrapolated below 500°K and the heat of fusion (reported[40] as 540 cal/mole) was adjusted upward to 615 cal/mole to bring the two sets of data into agreement. The smoothed heat content and derived thermodynamic functions are tabulated in Table 10.

SPECIFIC HEAT OF CESIUM

Heat content measurements were made on a sample of cesium from 170°F to 1770°F. Plastic failure of the thermocouple well in the Haynes container due to too thin a wall (not corrosion) at about 1860°F prevented completion of the measurements to the planned upper limit of 2000°F.

The data are listed in Table 11 and are shown graphically in Fig 7. Also in Fig 7 are the data obtained previously for rubidium and, for comparison, the calculated results of Stull and Sinke as reported by Weatherford for both metals. Inspection of the figure shows close agreement between experimental and calculated results with regard to both magnitude and slope (heat capacity).

Above 620°F the data were fitted by least squares to the linear relation

$$H_T - H_{298} = -1506 + 7.25\ T°C$$

where $H_T - H_{298}$ is the heat content in cal g-atom^{-1} and T is the temperature in °K. This yields a constant heat capacity of 7.25 cal deg^{-1} g-atom^{-1}.

Below 620°F an anomaly was observed in heat content. These data were not included in the derivation of the analytical expression for heat content. The deviation from the straight-line portion of the curve is real, as attested by the order in which points were taken. Initial runs were in the order of 800, 512, 854, to 1520°F, then back to the region 170-530°F in random order, then repeating the 850-1770°F range. No further investigation of the anomalous range was done. Since our work covers the range of 500 to 2000°F we do not propose to reinvestigate at this time, having acceptable results in the range of interest.

The standard deviation of the data above 620°F from the linear expression is ± 1.5%. It is believed that this expression can be extended from 1770°F to 2000°F with a 2 percent uncertainty. This extrapolation is uncomplicated due to the straight line correlation.

TABLE 10 - DERIVED THERMODYNAMIC FUNCTIONS FOR SOLID AND LIQUID RUBIDIUM

Temp. (°K)	$H^\circ_T - H^\circ_{298}$ cal/mole	S°_T cal/deg mole	$\left(\frac{F^\circ_T - H^\circ_{298}}{T}\right)$ cal/deg mole	Cp cal/deg mole
298.15	0	18.22	18.22	7.50
300	15	18.27	18.22	7.55
312 (c)	105	18.57	18.23	7.57
312 (b)	720	20.54	18.23	7.56
400	1385	22.41	18.95	7.55
500	2141	24.09	19.81	7.53
600	2894	25.46	20.64	7.53
700	3647	26.62	21.41	7.53
800	4400	27.63	22.13	7.53
900	5153	28.52	22.79	7.53
1000	5906	29.31	23.40	7.53
1100	6659	30.03	23.98	7.53
1200	7412	30.69	24.51	7.53
1300	8165	31.29	25.01	7.53
1400	8918	31.85	25.48	7.53

TABLE 11 - HEAT CONTENT DATA FOR CESIUM

T (°K)	$H_T - H_{298}$ cal g-atom^{-1}	T (°K)	$H_T - H_{298}$ cal g-atom^{-1}
351.1	1115	691.1	3460
376.5	1427	721.5	3797
389.7	1548	737.1	3743
399.9	1628	855.0	4810
420.8	1924	879.7	4957
454.2	2451	916.8	5087
506.1	2850	970.0	5485
513.1	2772	1027.1	5932
533.0	2930	1116.0	6581
534.8	2939	1190.0	7087
545.0	2880	1238.0	7465
689.6	3455		

It is not planned to extend the data to 2000°F because of the high probable validity of the short extrapolation and the agreement with calculated results.

VISCOSITY OF THE LIQUID

A literature survey has been performed on existing viscosity data for rubidium and for cesium and on methods of determining the viscosity of liquid metals. Experimental data are scarce for alkali metals and, except for recently completed work on potassium,[19] do not exist above 700°C. Data have been obtained for sodium, potassium and NaK alloys to 700°C[20-24] and for lithium, rubidium and cesium from their respective melting points to about 350°C.[25]

It has been decided to use a method based on the damping of an oscillating cylinder by the movement of contained liquid. The method has been used recently for potassium[20] and both method and theory are presented in detail by Shvidkovskiy[26] and by Hopkins and Toye.[27]

At the time of writing, inertia of the empty system has been determined and calibration is in progress.

VISCOSITY OF VAPOR

A preliminary literature search has shown that no existing method of vapor viscosity determination is applicable in all detail to alkali metal vapors. A transpiration method utilizing a modified capillary-flow type viscometer has been chosen as the most feasible approach for determination of the vapor viscosity of rubidium and cesium.

The principle of the transpiration method involving laminar flow through a capillary is described by Poiseuille's Law:

$$V = \frac{R^4 \pi \Delta P}{8 \mu L}$$

where $\Delta P = P_1 - P_2$ is the pressure drop over the capillary
R = radius of the capillary
μ = absolute viscosity
L = length of the capillary
V = volumetric flow rate

Measurement of ΔP and V permits computation of absolute viscosity.

The viscometer is shown schematically in Fig 8. It consists of a boiler, superheater, test section containing capillary tube and pressure sensing devices, and condensate collector.

The boiler will be charged with a sufficient amount of metal to assure several hours of vapor transpiration. After gettering the metal in the boiler and allowing the test section, superheater, and condenser to equilibrate to their desired respective temperatures, the boiler temperature will be raised to approximately 1200°F to establish a rubidium driving pressure.

The vapor will pass through a demister to assure entrapment of any liquid droplets and then to the superheater which will provide the necessary amount of superheat (1400°-2000°F). Viscosity will be determined at various degrees of superheat to evaluate the effect of total pressure on viscosity.

The pressure drop over the capillary will be measured by two null-point pressure-sensing devices. The balance of the system pressure drop will be reduced by a throttling valve. After passing through the throttling valve, the vapor will be condensed and cooled sufficiently to permit utilization of a glass collection tube for measuring the rate of liquid metal condensed. The mass flow rate which can be computed from liquid density will permit calculation of volumetric flow rate.

Following a series of runs, the metal will be recycled to the boiler by means of inert gas pressure.

Corrections for kinetic energy and curved pipe flow should not represent more than 1-2% of the viscosity value while the slip correction has been proven to be negligible. Since the apparatus will be operated at very low Reynold's numbers, no transition to turbulence is expected.

THERMAL CONDUCTIVITY OF THE LIQUID

A literature survey has been performed on existing thermal conductivity data for the alkali metals and on methods used for the determinations. Most investigators have favored the use of the guard ring or longitudinal heat flow method for directly determining liquid thermal conductivity.[19,23,24,28-30]

In unsteady state determinations, thermal diffusivity is actually measured.[24] This type of measurement is easier to obtain, less accurate and has been applied to higher temperatures than steady state determinations which measure thermal conductivity.

In general, thermal conductivity measurements are difficult, require elaborate apparatus and have not yet been successfully performed for liquids to 2000°F.

Thermal conductivity is related to electrical conductivity (the reciprocal of electrical resistivity) by the Lorenz number, as follows:

$$L = \frac{K}{\sigma T} = \frac{2\pi}{3} \frac{k^2}{e}$$

where L = Lorenz number
K = thermal conductivity
σ = electrical conductivity
T = absolute temperature
k = Bolzmann's constant
e = electron charge

For most metals at temperatures in excess of about 200°K there is good agreement between the experimental Lorenz number (calculated from K, σ and T) and the theoretical Lorenz number (2.72×10^{-13} esu, 2.44×10^{-8} volt^2/degree^2 calculated from the right hand term above). The average deviation for the experimental Lorenz number of 13 metals at 273°K is less than 5% from the theoretical. For sodium and for two grades of NaK the average experimental Lorenz number was within 4.5%, 1.2% and 4.1%, respectively, of the calculated value from 100 to 500°C.[31]

Alloying of metals would cause no problem and the liquid state is advantageous as it would minimize lattice effects and the possibility of isotropism. High temperature could be expected to increase the validity of the Lorenz relationship. In view of these circumstances, it was decided to measure electrical resistivity and translate these results by the Weidemann-Franz-Lorenz law.

The resistivity of liquid rubidium was determined by measurement of the total resistivity of a 0.500 in. diameter Haynes-25 tube (0.063 in. wall) filled with liquid rubidium. The Haynes-25 container which was 22 inches long, was mounted inside of a cylindrical stainless steel heating block with an outside diameter of 3.5 inches and an inside diameter of 2.0 inches. Three Kanthal wound tube elements, with separate controls on each element served to heat the block to experimental temperature, and maintain an isothermal zone over the central 14 in. section of the Haynes-25 container.

Temperature measurements were made with three U.S. Bureau of Standards calibrated Pt-Pt/10% Rh thermocouples and a L&N, K-3 potentiometer. Resistance measurements were made with a four probe double ratio Kelvin Bridge (Honeywell #1622) and a sensitive galvanometer. Direct current was supplied from a 6-volt lead storage battery converted to 2-volt operation and equipped with a current reversing switch. Electrical contacts were welded onto the container tube and filed down to achieve point contact. A purified argon supply was used to suppress boiling of the rubidium.

The experimental procedure consisted of first determining the resistance of the Haynes No. 25 alloy container tube, then filling it with rubidium and measuring the resistance of the filled tube at various temperatures throughout the range. Calibration resistance measurements of the evacuated containment tube were taken from 80°F to 2000°F and are presented in Fig 9. From these results it is apparent that a constant temperature-resistance profile has been established for the Haynes No. 25 alloy tube. Temperature and resistance measurements were made with the furnace element current off in order to minimize any induced emfs. The tube was charged, under vacuum, with approximately 60 grams of rubidium metal. An over-pressure of NaK purified argon was then applied through a stainless steel tube protruding from the top of the container. Resistance measurements on the filled container were then made. All measurements were made in several groups or heating runs. The apparatus was allowed to cool to room temperature after each run.

The resistance of the liquid metal sample was calculated from the formula for parallel resistors:

$$R_1 = \frac{R_3 R_2}{R_2 - R_3}$$

where R_1 = resistance of the liquid metal
R_2 = calibrated resistance of Haynes No. 25 alloy container tube
R_3 = resistance of tube filled with liquid metal

The resistivity of the liquid metal is computed from the equation:

$$\rho = (R_1)\frac{A}{l}$$

where A = cross sectional area of the liquid metal (cm^2)
l = length of the liquid metal column (cm $\pm$ 0.002 cm)

It was evident that heating the empty container tube to any temperature below 1850°F had negligible effect on subsequent resistance readings at temperatures below 1850°F. The changes in resistance which occurred after heating the cylinder over 1950°F may possibly be attributed to changes of phase within the Haynes-25. The temperature gradient along the 14 inch filled tube section between the Kelvin Bridge potential lead-terminals was held to about ±2°F. Two resistance measurements were made at each reading (one for each direction of bridge current) and the average taken as the true resistance value. This ΔR is due to the thermoelectric effect and to thermal emfs of the thermocouples. A large bridge current ($\sim$3 amps) held this difference to a minimum.

Resistivity determinations have been completed for rubidium to 2000°F and are presented in Fig 10. The results agree with previous determinations which were made to 1380°F.[32]

SPECIFIC HEAT AND THERMAL CONDUCTIVITY OF VAPOR

Determination of specific heat and thermal conductivity will be performed after much of the data discussed in preceding sections has been obtained. As yet, no methods have been chosen.

BIBLIOGRAPHY

1. Bonilla, Sawhney and Makansi, "Vapor Pressure of Alkali Metals, III", Second Annual High Temperature Liquid Metal Heat Transfer Technology Meeting, May 1962.

2. Cochran, "Rubidium-Cesium Evaluation Program Thermodynamic Property Measurements", Ibid.

3. Whitman and Stockton, AEC Report CF-55-6-49 (Pt I) 1954.

4. Kelley, U.S. Bur. Mines Bull. No. 383, 1935.

5. Ditchburn and Gilmour, Revs. Modern Physics 13 310, 1941.

6. "Liquid Metals Handbook", Lyon, U.S. Govt. Printing Office, 2d Edition, 1952.

7. Hackspill, Compt. Rend. 154 878, 1912.

8. Killian, Phys. Rev. 27 578, 1926.

9. Johanssen and Ruff, Ber., 38 3601, 1905.

10. Bonilla, Private Communication.

11. Makansi, Muendel and Selke, J.Phys. Chem. 59 40, 1955.

12. Makansi, Selke and Bonilla, J. Phys. Chem. 60, 128, 1956.

13. Gray, 2nd Symposium on Thermophysical Properties (Princeton, N.J.) A.S.M.E. January, 1962.

14. Shapiro and Meisl, General Electric Co., R 60 FPD 358-A, November, 1960.

15. WADD TR 96 (1961).

16. Rodenbush and Walters, JACS 52 2654 (1930).

17. Ann. Phys. 26 833, 1908.

18. Ewing, et al, NRL Problem CO5-15, NASA order number NTF-92, 1962.

19. Lemmon, Engineering Properties of Potassium, Battelle Memorial Inst., June, 1962.

BIBLIOGRAPHY (Continued)

20. Chiong, Proc. Roy. Soc. A157, 264-77, 1936.

21. Ewing, et al, J. Phys. Chem. 57 1086, 1954.

22. Ewing, et al JACS 73, 1168, 1951.

23. Ewing, et al JACS 74, 11, 1952.

24. Novikov, J. Nucl. Eng. 4 387, 1957.

25. Andrade and Dobbs, Proc. Roy. Soc. A211 12.

26. Shvidkovskiy, Viscosity of Fused Metals, NASA Technical Translation F-88, March 1962.

27. Hopkins and Toye, Proc. Phys. Soc. B63 733, 1950.

28. Yaggee and Untermeyer, ANL 4458.

29. Hall, Phys. Rev. 53 1004-9, 1938.

30. Powell and Tye, Proc. Joint Conference on Thermodynamic and Transport Properties of Fluids, London, pp 182-7, 1958.

31. Rahiser, Mine Safety Appliances Technical Report 24, 1953.

32. Kapelner and Bratton, Electrical Resistivity of Na, K, Rb and Cs in the Liquid State, PWAC-376, 1962.

33. Kelley, U.S. Bur. Mines Bull. No. 476, 1949.

34. Rengade, Bull. Soc. Chem. France, 15, 130, 1914.

35. Stull and Sinke, Thermodynamic Properties of the Elements, Washington, ACS, 1956.

36. Ginnings et al, NBS RP 2694, Vol 57, 1956.

37. Southard, JACS 63 3142 (1941).

38. Kelley, Naylor and Shomate, U.S. Bur. of Mines Tech. Paper 83 (1955) RP 2608.

39. Dauphinee, et al, Proc. Roy. Soc., Series A, 233 (1955).

40. Stull and Sinke, Thermodynamic Properties of the Elements, Washington, ACS (1956).

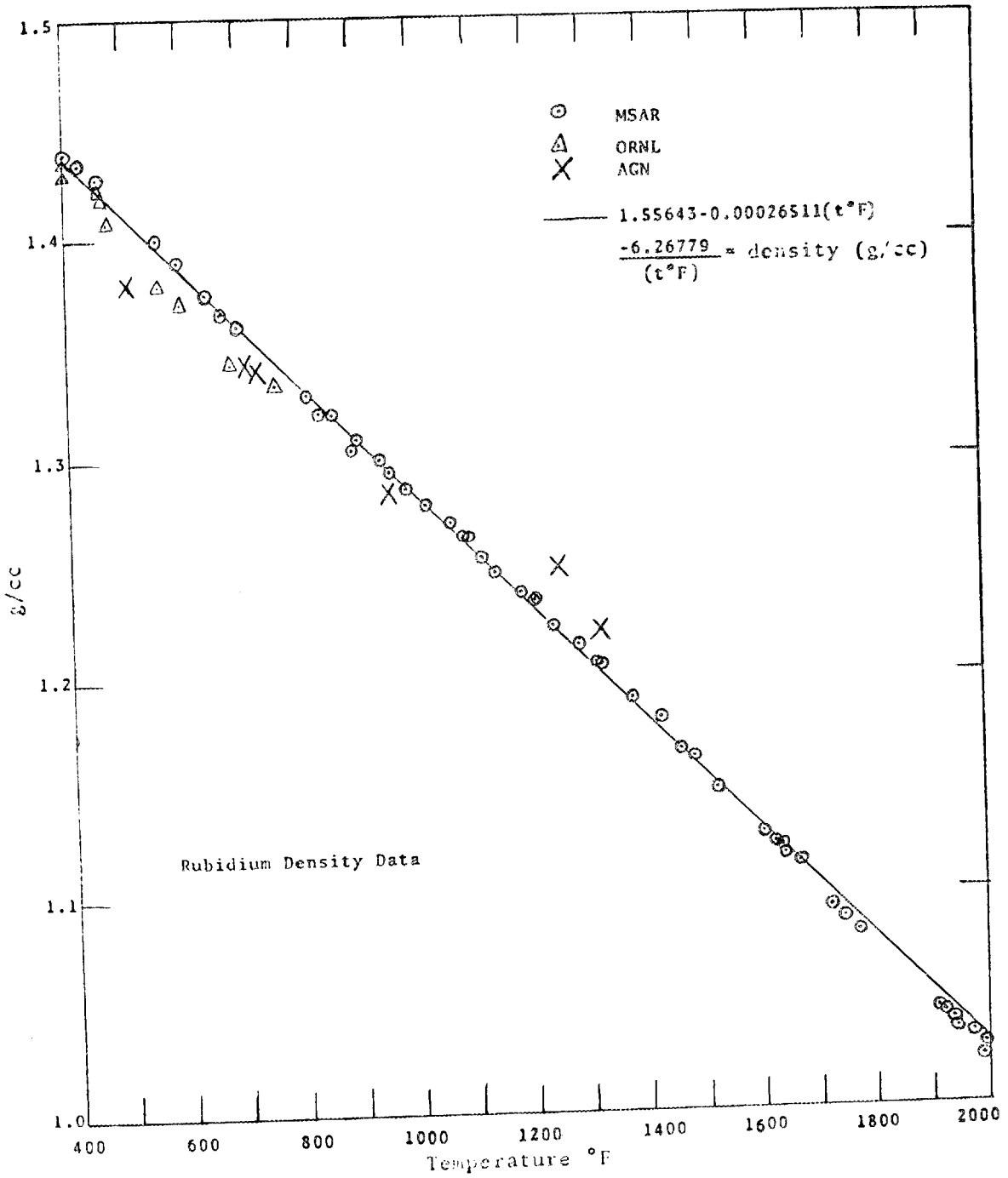

FIG 1 - RUBIDIUM DENSITY DATA

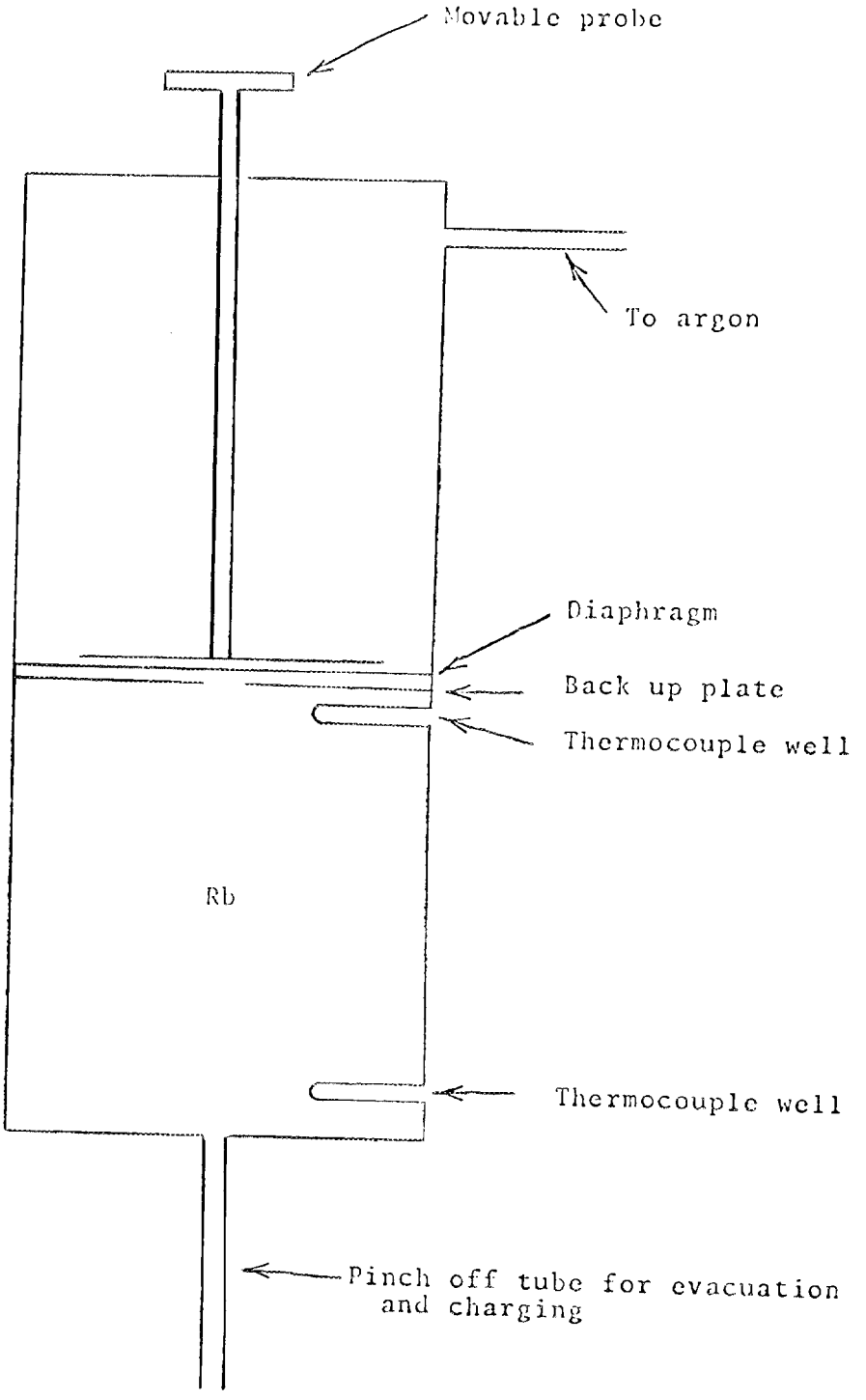

FIG 2 - PVT APPARATUS

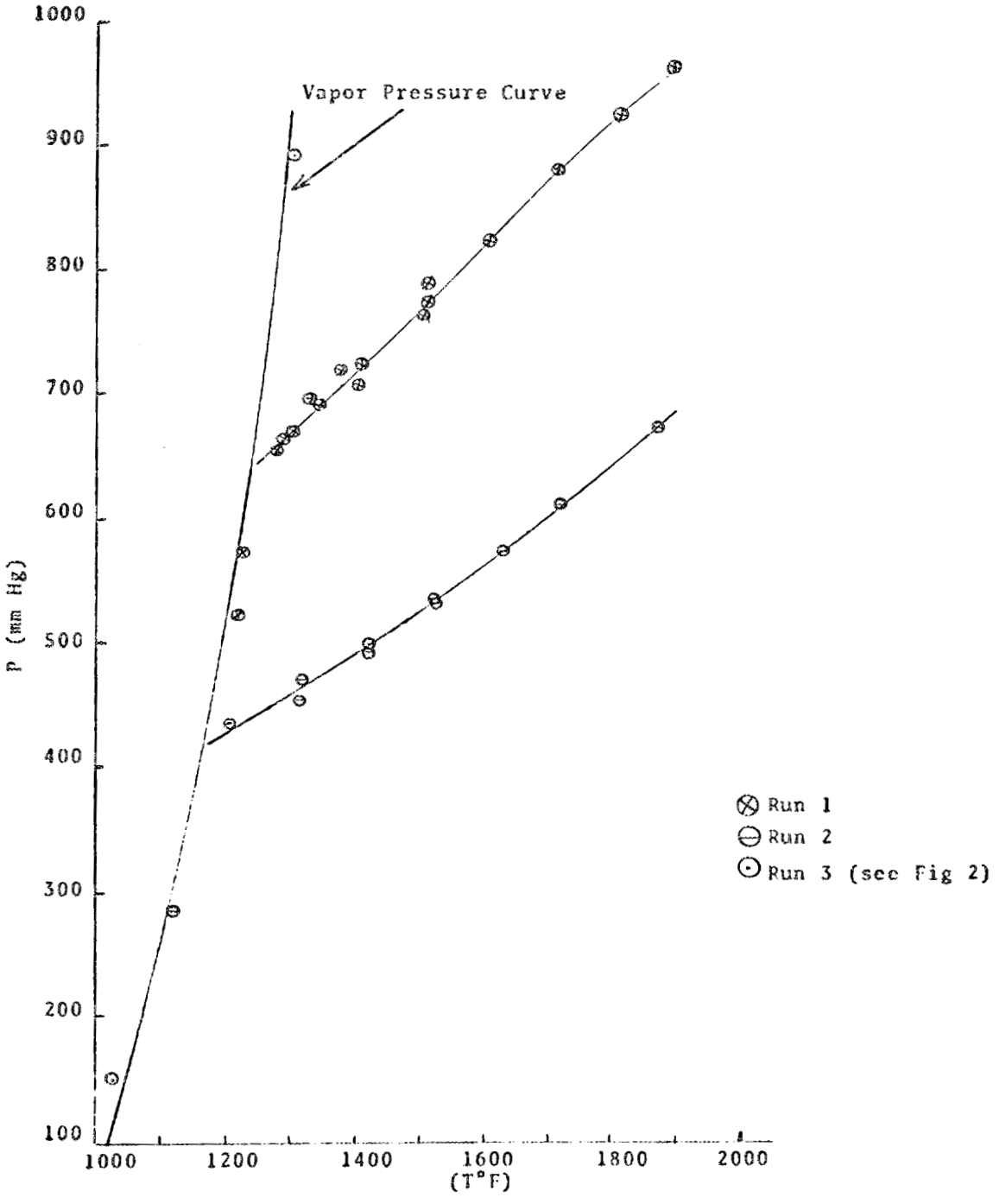

FIG 3 - RUBIDIUM PVT DATA

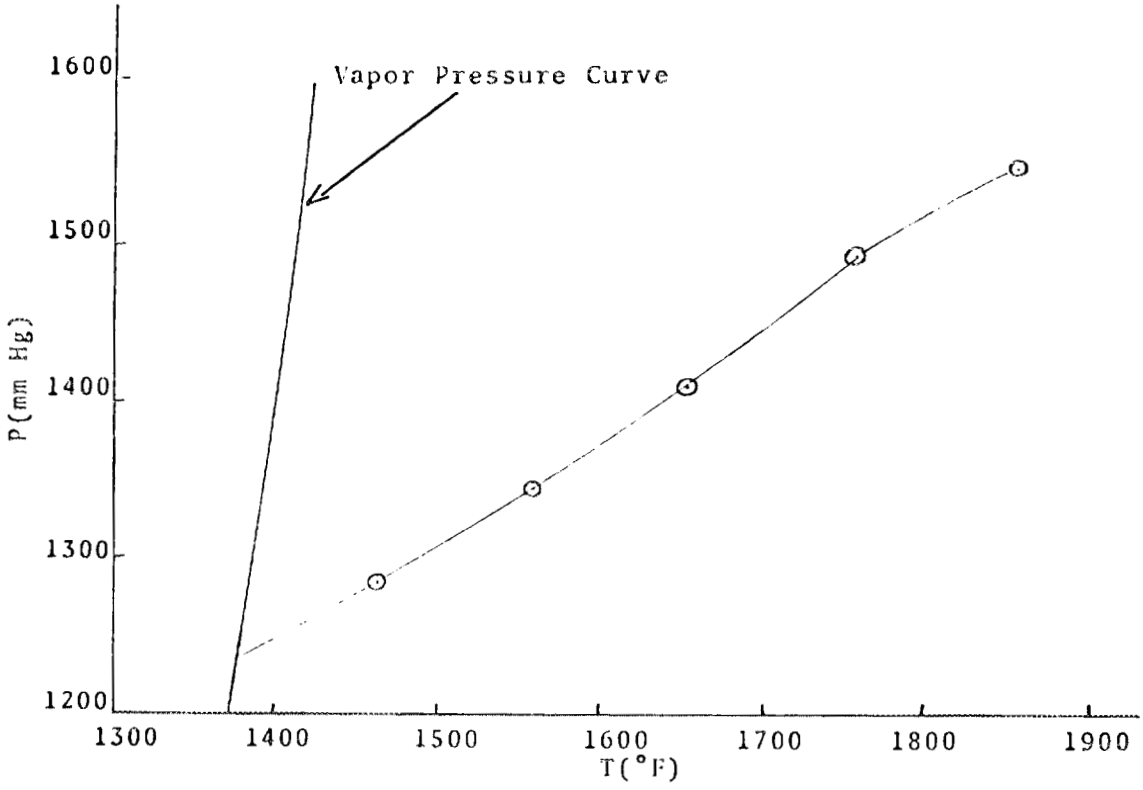

FIG 4 - RUBIDIUM PVT DATA

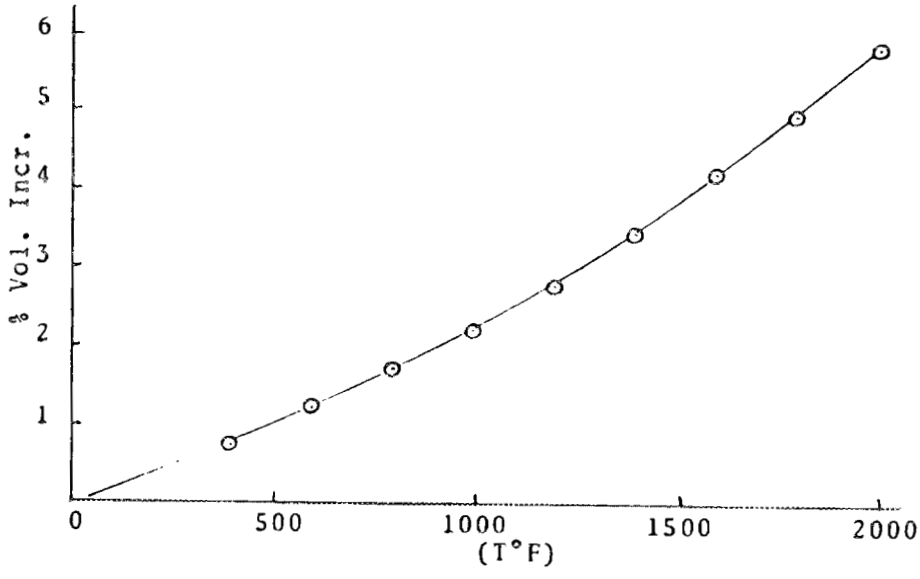

FIG 5 - EXPANSION OF HAYNES CONTAINER

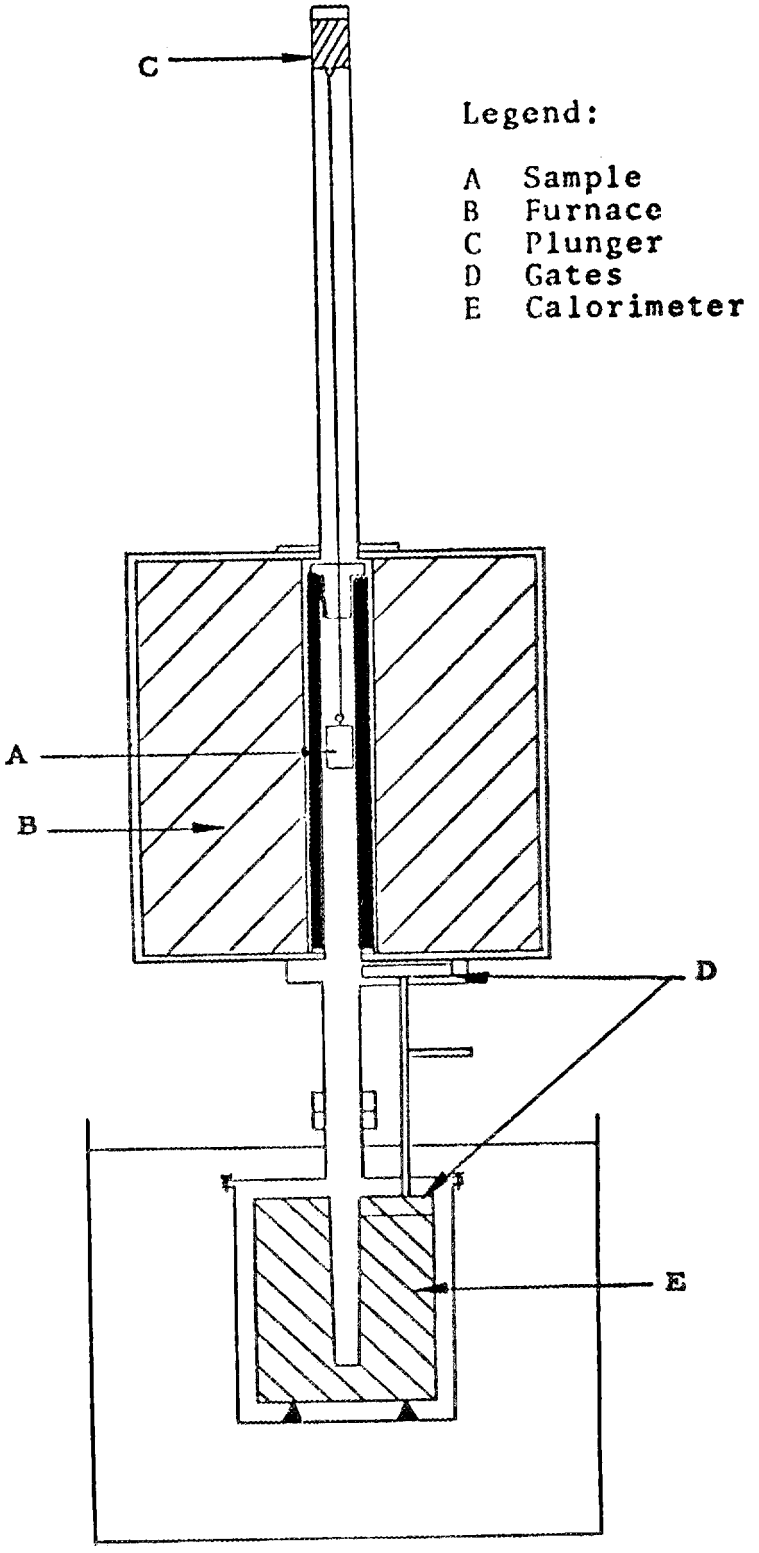

FIG 6 - COPPER BLOCK CALORIMETER

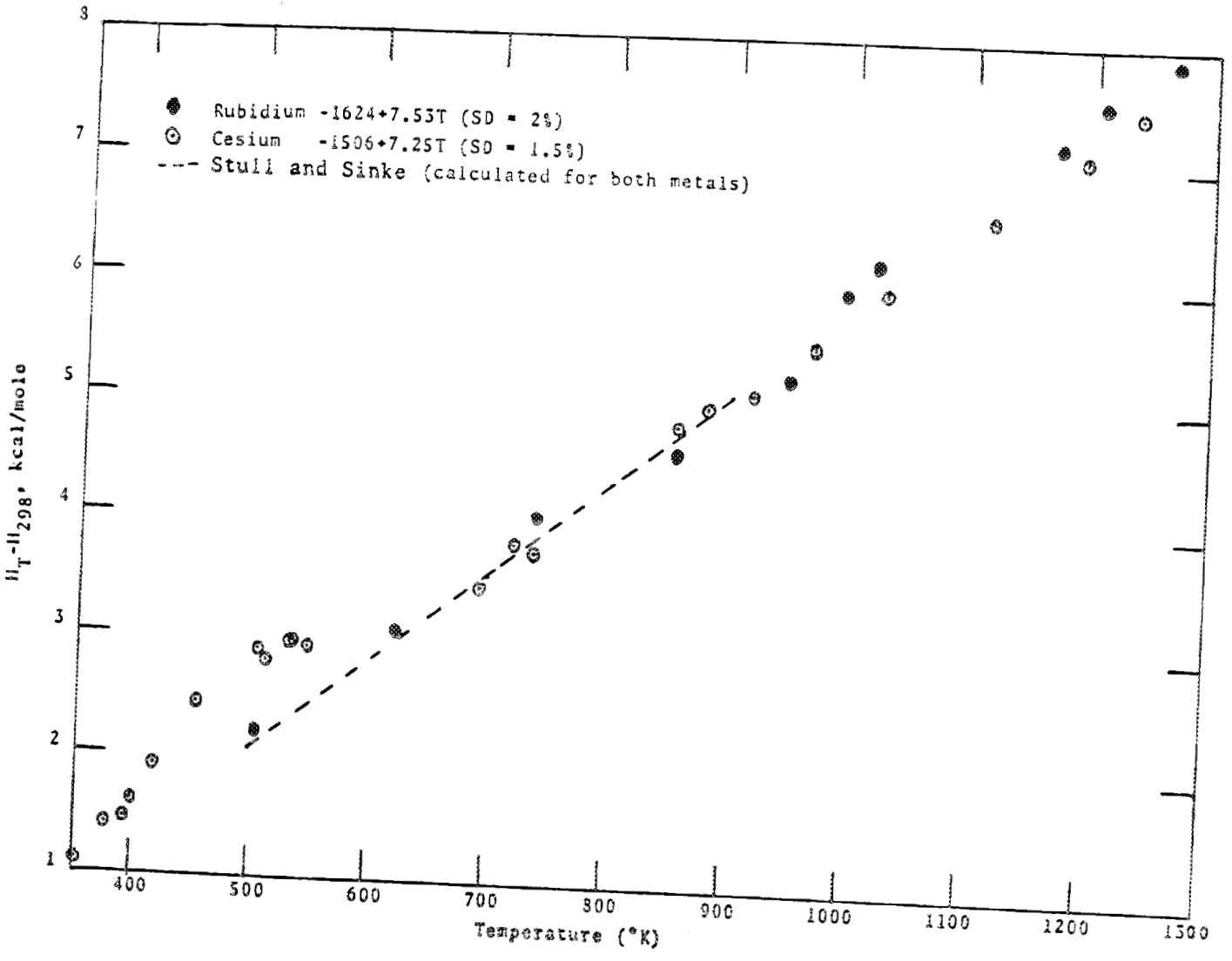

FIG 7 - HEAT CONTENT DATA

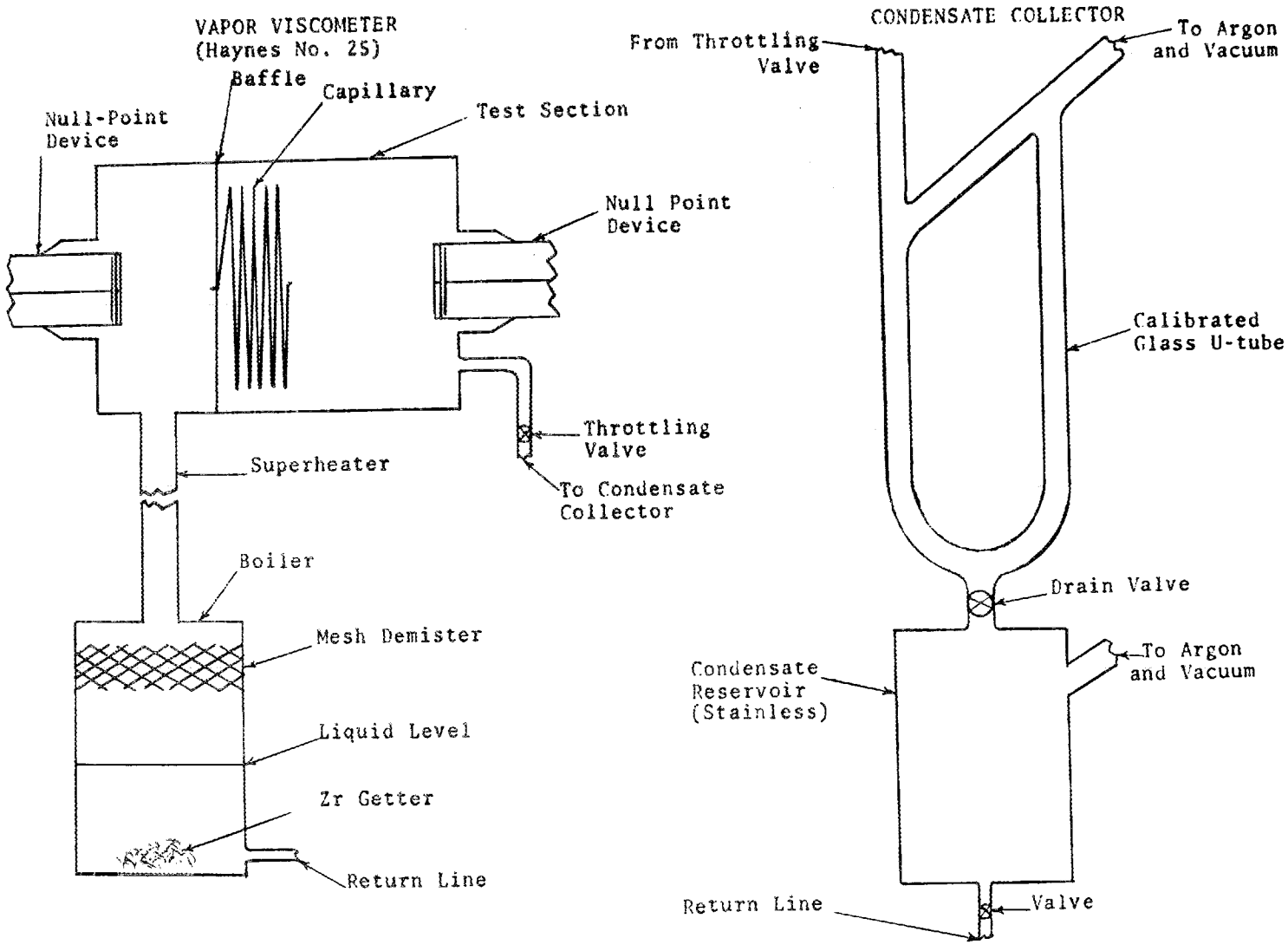

FIG 8 - VAPOR VISCOMETER AND CONDENSATE COLLECTOR

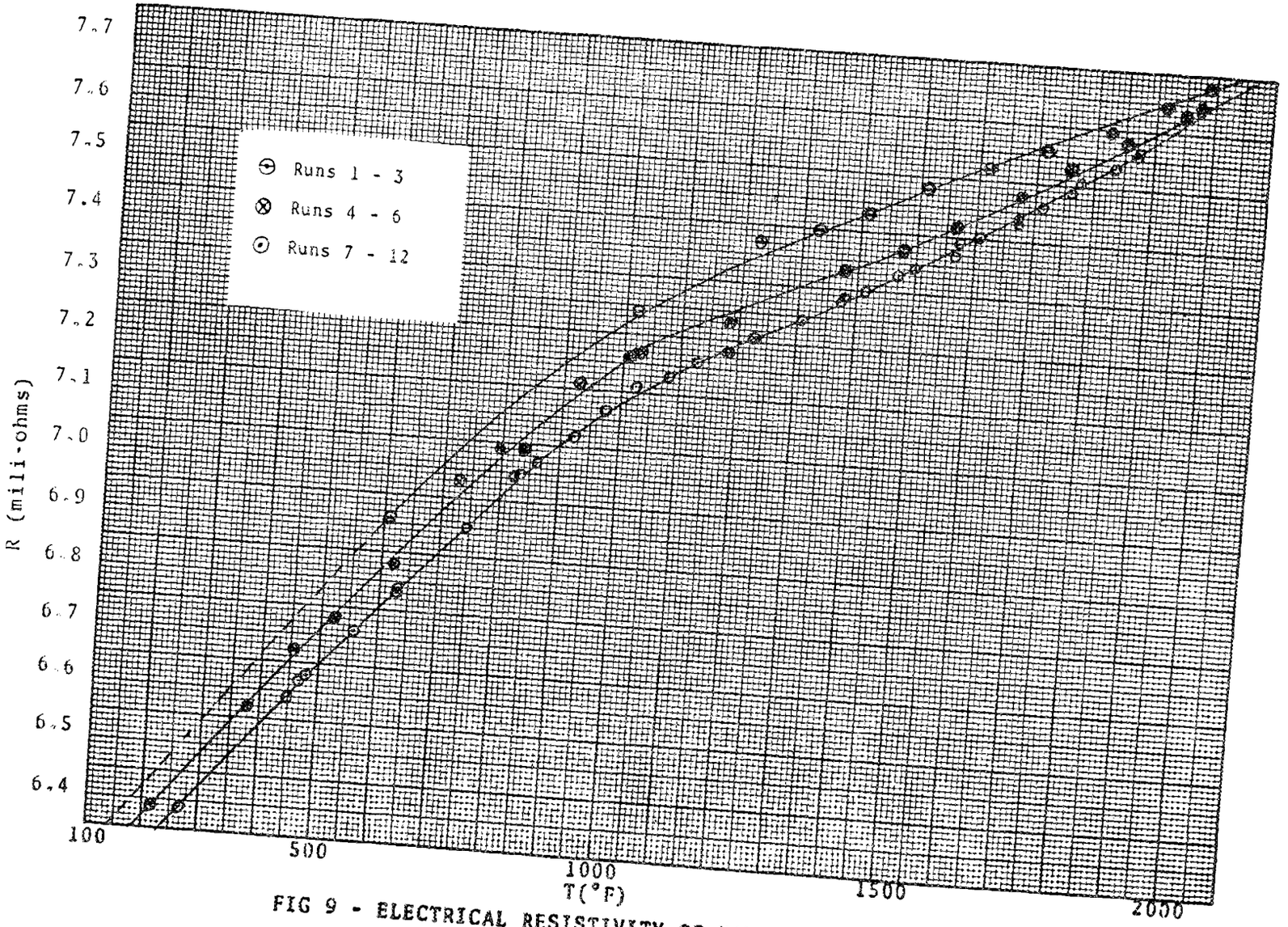

FIG 9 - ELECTRICAL RESISTIVITY OF HAYNES CONTAINER

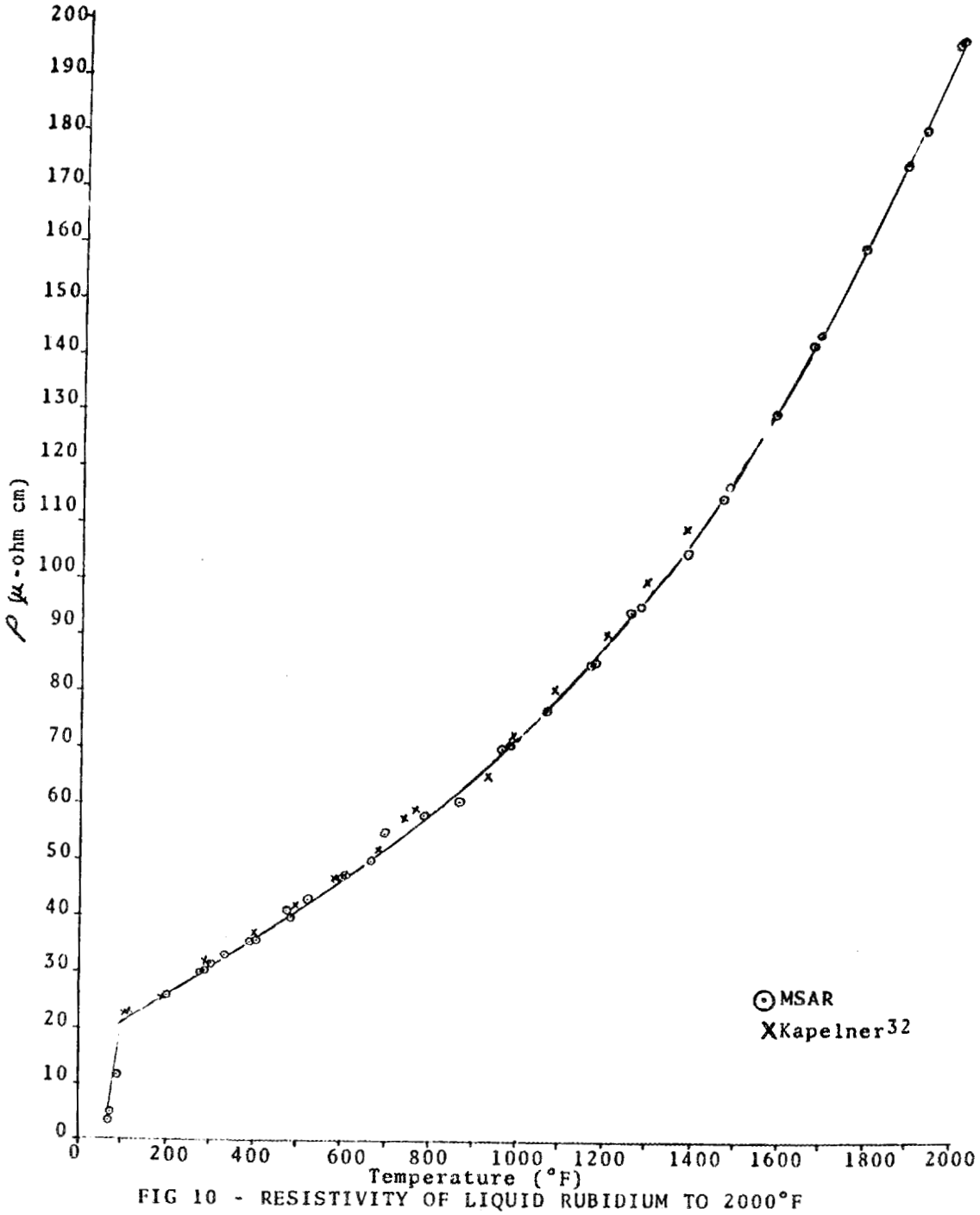

FIG 10 - RESISTIVITY OF LIQUID RUBIDIUM TO 2000°F

THERMOPHYSICAL PROPERTY MEASUREMENTS OF ALKALI LIQUID METALS

J. W. Cooke
Oak Ridge National Laboratory
Oak Ridge, Tennessee

ABSTRACT

The final results of the experimental determination of the thermal conductivity of 99.8+ wt % molten lithium from 320 to 830°C are reported in this paper. The preliminary results just obtained for the surface tension of 99.97 wt % molten potassium from 70 to 713°C using a maximum bubble-pressure apparatus are also given in this paper.

PART I. THERMAL CONDUCTIVITY OF MOLTEN LITHIUM

Introduction

Molten lithium has long appeared attractive as a high-temperature, high-efficiency heat-transfer medium. As more knowledge is gained of its compatability with various container materials, molten lithium seems certain to find application as a coolant for space power reactors and other high-performance reactor systems. However, knowledge of its thermophysical properties, particularly thermal conductivity, is still limited with regard to temperature range and agreement of experimental data. For example, the five investigations[1-5] previously available for the thermal conductivity of molten lithium disagree by as much as 80% in absolute magnitude. In an attempt to resolve these disagreements and to extend the data to higher temperatures, an apparatus was developed to determine the thermal conductivity of molten lithium from 320 to 830° C. The final results of this investiation are given in this paper.

Apparatus

A comparative, axial-heat-flow thermal conductivity apparatus utilizing compensating guard heating was developed for the investigation and is shown in Fig. 1. The central part of the apparatus, the test piece, consisted of an expansion tank, main heater, upper heat meter, sample container, and lower heat meter. Heat from the main heater flowed down the test piece and into the water-cooled sink. Surrounding the test piece were a coaxial guard tube and an alumina cylinder which supported the guard heaters. Heat flow in the radial direction was minimized by maintaining with the guard heaters an axial temperature profile in the guard tube which matched the axial temperature profile of the test piece.

The heat meters and sample cavity were all 1.5 in. in diameter and ~3 in. long. The wall of the sample cavity was 0.0625 in. For temperature measurements along the test piece, 15 thermocouples made from 30-gauge Pt vs Pt-10% Rh wires were placed in 0.055-in.-diam radial thermowells which extended to the centerline of the test piece: one thermocouple in each of four planes spaced 0.5 in. apart in the upper heat meter, one thermocouple in each of three planes spaced 0.75 in. apart in the lithium sample, and two thermocouples in each of four planes spaced 0.5 in. apart in the lower heat meter. Eleven thermocouples were placed in corresponding planes in the guard tube.

The apparatus was situated in a furnace which maintained the surrounding at an adequate temperature level to further reduce any radial heat flow and to assist in calibrating the thermocouples in place. Fiberfrax insulation was carefully placed in all void regions within the furnace. The entire system was maintained in a high vacuum (3 to 8 $\times 10^{-5}$ torr) to minimize the convective, conductive, and corrosive effects of an atmosphere.

Operating Procedure

Initial filling difficulties caused by the high-surface tension, large heat of fusion, and low density of the lithium were overcome and the sample cavity was successfully filled with a void-free sample of lithium metal whose spectrochemical analysis is given in Table 1.

The Pt vs Pt-10% Rh thermocouples used in the investigation were calibrated by very lightly spot-welding eight thermocouples at a time to the junctions of a 24-gauge NBS Pt vs Pt-10% Rh thermocouple. The standard and attached thermocouples were placed in the center of a 24-in.-long horizontal furnace for calibration. Thus, eight thermocouples at a time were calibrated

Table 1. Spectrochemical Analyses of the Lithium Sample Before and After Thermal Conductivity Determinations

Impurity	Weight Per Cent	
	Before	After
Na	0.015	0.015[a]
K	0.060	0.060[a]
Ca	0.0001	0.0001[a]
Al	0.0005	0.0005[a]
Si	0.001	0.0058
Cl	0.04	0.04[a]
N	0.012	0.012[a]
Ni	<0.0015	0.0022
Cr	<0.0015	<0.001
Ti	<0.0010	<0.0010[a]
N_2	0.0063	0.0063[a]
O_2	0.0003	0.0003[a]
Mn		<0.002
Fe	0.0027	0.0024
Other (estimated)	0.025	0.025[a]
Li (by difference)	99.82	99.81

[a]These values were assumed to remain unchanged.

relative to each other and to the standard, reducing the calibration error in the Δt measurements to an estimated ±0.20°C. An electrically guarded and shielded I&N K-3 potentiometer and μv amplifier system was used to measure the thermocouple emfs. Considerable care was taken to minimize extraneous thermal emfs.

After the assembly of the apparatus was completed, the system pressure was reduced to 3×10^{-5} torr and the furnace heat gradually increased over a period of a week. When the apparatus reached 345°C, an axial temperature gradient was established in the test piece, and the guard heaters were adjusted to obtain a matching axial temperature gradient in the guard tube. To match the two gradients within acceptable limits usually required 8 to 10 hr, and to insure steady state this condition was maintained another 6 to 10 hr before a set of data was taken. During operation a check for induced emf was made by reading each thermocouple during a momentary shutoff of all electrical supply to the system.

The conductivity was calculated from a heat balance at the interface between the upper heat meter and sample and also at the interface between the lower heat meter and sample using the equation:

$$k_{Li} = \frac{(k\ A\ dt/dx)_H}{(A\ dt/dx)_{Li}} - k_H \left(\frac{A_W}{A_{Li}} \right) , \qquad (1)$$

where k, A, x, and t refer to conductivity, cross-sectional area, axial length, and temperature, and the subscripts H, W, and Li refer to the heat meter, sample container wall, and lithium sample. The temperature gradients at the interfaces were calculated from an equation of the form:

$$t = ax^2 + bx + c \quad , \qquad (2)$$

which was least-squares fitted to the temperature data of the three respective regions of the test piece (e.g., the sample and two heat meter regions).

Results

Determinations from the temperature gradients in both the upper and lower heat meters for each of 13 runs (26 determinations in all) were made of the conductivity of molten lithium from 320 to 830°C. These results can be represented to within ±2.2% rms deviation by the least-squares equation:

$$k\ (\text{watt/cm}\cdot{}^\circ\text{C}) = 0.345\ [1 + 9.058 \times 10^{-4}\ t\ (^\circ\text{C})]\ , \qquad (3)$$

and are shown plotted versus temperature in Fig. 2. The two values from run 9 appeared to be excessively high and were not included in determining the linear least-squares line shown as a solid line in Fig. 2. The average deviation of the 26 values, <u>including</u> those from run 9, about the least-squares line was +3.9% and -1.2%.

The average deviation of the 16 values of conductivity from 320 to 500°C about the least-squares line was +0.8% and -0.7%. Above 550°C all three of the sample-region thermocouples became erratic, and it became necessary to obtain the lithium temperature gradient from the interfacial temperatures extrapolated from the two heat-meter regions. The average deviation of the ten points above 550°C about the least-squares line was +4.8% and -3.5%.

A typical axial temperature profile along the test piece and guard tube is shown in Fig. 3 for run 8. (Because of the compressed scale, the slight curvature in the profile is not shown in Fig. 3.) The agreement of temperature and gradient between the test piece and guard tube for both the heat meter and sample regions can be seen from this typical profile to be quite good. The two interfacial temperature drops were always in the direction of heat flow and for the first eight runs averaged 0.8°C.

After the determinations had been completed, an in-place relative calibration of the thermocouples was made by operating the system isothermally at 595°C. The mean deviation of the test piece thermocouples about their averaged value was ±0.30°C. This was approximately 50% more than the error estimated for the initial Δt measurements, indicating that the thermocouple emf had drifted from the initial calibrations.

Discussion of Results

From consideration of many possible sources of errors, the total uncertainty in the results was conservatively estimated to be less than ±8 to ±15% from the lower to the higher temperatures. That the actual uncertainty was probably less than the total uncertainty is evidenced by (a) the good agreement between the two independent axial-heat-flow measurements [the difference varying from 0.1 to 3.8%], (b) the modest amount of radial heat exchange [always $\leq$ 1.0% of the axial-heat flow], and (c) the consistency of the axial temperature profiles.

Extrapolations to the melting point of the present data, previous results, and values predicted by the Wiedemann-Franz relationship [using electrical resistivity data from ref. 6] agree to within ±7% [see Fig. 2]; whereas above 550°C, the present results compare well only with predicted values, particularly in temperature dependency. The temperature dependency of the present results is positive, which is contrary to the data for either molten sodium or potassium, but is consistent with the volumetric coefficient of thermal expansion of molten lithium being almost half that of either molten sodium or potassium.

From a broad extrapolation of the present data to the calculated critical conductivity, the conductivity of the molten lithim appears to reach

a maximum of 0.78 watt/cm·°C at 1700°C. This will require further investigation at high temperatures for verification. By substituting a niobium alloy for the stainless steel, the present apparatus could be used to extend the conductivity data to the normal boiling point (1317°C).

PART II. SURFACE TENSION OF MOLTEN POTASSIUM

Introduction

An important factor in the correlation and evaluation of boiling and condensing data for molten potassium is the interfacial tension between the liquid and vapor phases. Only values near the melting point have been reported in the literature for the surface tension of molten potassium.[7] To extend the data to near the boiling point, an investigation was initiated using a maximum bubble pressure apparatus. The preliminary results of this investigation are given in this paper.

Apparatus

The maximum bubble-pressure apparatus used for the determinations is shown schematically in Fig. 4. High-purity helium was supplied at very low flow to a capillary tube whose end was immersed to various depths in the liquid potassium. The maximum pressure attained within the slowly growing bubble before disengagement from the capillary tip was measured with a micromanometer (sensitivity ±0.01 mm). The water-filled micromanometer was separated from the molten potassium with liquid nitrogen-cooled molecular sieve traps. The immersion depth was measured with a dial indicator (sensitivity ±0.025 mm) which was zeroed at the point of electrical contact of the capillary tube with the liquid surface. The apparatus was contained in a vacuum dry box.

Several Inconel capillary tubes of various inside diameters (1.53568 to 1.66370 mm) and outside diameters (2.39522 to 3.17508 mm) were used for the determinations. The diameters were measured with a Moore Universal Measuring Machine (sensitivity $\pm 5 \times 10^{-4}$ mm) using a 40 power microscope. The tubes were also calibrated from surface tension determinations of triply distilled, doubly deionized water. The molten potassium sample was heated in a Variac controlled exterior furnace. The sample temperatures were measured with three Chromel-Alumel thermocouples — one just above the surface and two in the liquid.

Operating Procedure

The vacuum dry box was evacuated to and maintained at 2×10^{-5} torr until the pressure buildup (with the diffusion pump off) was less than 3×10^{-3} torr/hr. After filling the dry box with high-purity helium (99.999+ wt %), the container of potassium, whose spectrochemical analysis before and after the determinations is given in Table 2, was opened and inserted in the furnace. After heating the potassium to the desired temperature, the micromanometer was zeroed, and the capillary tube zeroed at the point of electrical contact with the molten potassium. The tube was then lowered to various depths, and the maximum pressure recorded at each depth. The helium flow through the capillary tube was regulated to form one to two bubbles a minute. For this particular system, a bubble formation rate greater than two per minute gave lower pressures due to pressure losses through the pressure measuring system. The capillary tube was then raised out of the liquid, and the zero level was rechecked. The temperature was raised to another level and the above procedure repeated.

Table 2. Spectrochemical Analysis of Potassium Batch No. 1 Before and After Surface Tension Determinations

Element	Before, ppm	After, ppm
Oxygen	26;35	–
Iron	<5	3.3
Chromium	<1	<1
Nickel	6.7	2.2
Lithium	<1	<1
Sodium	60[a]	110[b]
Rubidium	132	47
Cesium	20	22
Aluminum	<10	<10
Magnesium	<2	<2
Copper	<1	–
Cobalt	<5	<5
Calcium	11	3
Molybdenum	<3	–
Boron	10	–
Lead	<5	–
Titanium	<5	–
Silver	<1	–
Zirconium	<10	–
Potassium (by difference)	99.97 wt %	

[a]Sample taken in polyethylene bottle.

[b]Sample taken in glass bottle.

Results

Two hundred and two determinations were made of the surface tension of molten potassium relative to a mixture of helium and potassium vapor from 70 to 713°C for both increasing and decreasing temperatures,

using two different batches of potassium and four different capillary tubes. The preliminary results were calculated using Schroedinger's equation,[8]

$$\sigma = \frac{pr}{2}\left[1 - \frac{2}{3}\frac{r}{h} - \frac{1}{6}\left(\frac{r}{h}\right)^2\right], \tag{4}$$

where σ = surface tension (dynes/cm),

p = surface tension component of maximum pressure (dynes/cm^2),

h = surface tension component of maximum pressure (cm of fluid),

r = capillary tube radius (cm).

The results are shown plotted as a function of temperature in Fig. 5 and can be expressed by the least-squares equation:

$$\sigma = 115.51 - 0.0653\ t\ (°C) \tag{5}$$

from 70 to 710°C with a mean square deviation of ±0.64 dynes/cm. Several of the values around 200°C were not included in the least-squares analysis for reasons to be discussed later.

The results are considered preliminary for the following reasons:

1. Corrections have yet to be made for the thermal expansion of the capillary tube and the fluid volume displaced by the capillary tube.

2. Redetermination of the capillary tube radii and recalibrations of the tubes using water after the investigation have not been completed.

3. An analysis for the impurities in the second batch of potassium after the determinations has not been completed.

4. Schroedinger's equation was used for the calculations instead of the more precise, but involved, iterative procedure of Sugden[9] (spot checks indicate a difference of less than one per cent between the two methods for this investigation).

As a calibration check of the apparatus, the surface tension relative to helium of triply distilled, doubly deionized water was determined at 28°C using capillary tube No. 1 and found to be 2% below the value reported by Dorsey[10] for pure water relative to air. A large part of this difference can be attributed to the substitution of helium for air, as pointed out by Gambill.[11] Calibrations of the other tips have not been completed.

The density of potassium was also calculated from the data using the equation:

$$\rho_K = \frac{(H_1 - H_2)\ \rho_{H_2O}\ [1 - (d/D)^2]}{(I_1 - I_2)\ [1 + \alpha\ (t - t_o)]}\ , \qquad (6)$$

where ρ = density (g/cm^3),

d = outside diameter of capillary tube (cm),

H = manometer reading (cm of H_2O),

D = inside diameter of potassium container (cm),

I = depth of capillary tube below surface (cm),

α = coefficient of linear thermal expansion of Inconel ($°C^{-1}$),

t = potassium temperature (°C),

t_o = room temperature (°C),

and where the subscripts:

K = potassium,

H_2O = water,

$1,2$ = two different depths.

The results are plotted as a function of temperature in Fig. 6.

Discussion of Results

The major sources of error in the surface tension determinations and the estimated maximum uncertainties are shown in Table 3.

Table 3. Uncertainties in the Surface Tension Determinations

Source	Uncertainty
Density of manometer fluid	±0.0-%
Density of potassium	±0.7
Tube diameter	±0.6
Immersion depth	±0.7
Maximum pressure determination	±0.3
Total	±2.3%

Additional uncertainties amounting up to ±1% are probably present in the preliminary surface tension results because the corrections, mentioned previously, have not yet been applied.

Some surface tension values around 200°C are as much as 5% below the least-squares line (see Fig. 5). All of these lower values were recorded within 10 to 20 minutes after a new capillary tube had been installed. Thus, although still debatable, the present feeling is that these lower values resulted from poor wetting of the capillary tube by the potassium.

The only investigation of the surface tension of potassium that has thus far been found in the literature was by Quarterman and Primak[7] in 1949 using the capillary rise method. Their results fall ~20% below the present values (see Fig. 5). In their own opinion, their results could be 15% too low due to a possible contact angle between the potassium and the glass capillary tube and to the difficulties in measuring the capillary

height between the two concave menisci.

The composite of three investigations of the density of molten potassium obtained from the Liquid Metals Handbook[12] is compared with the present results in Fig. 6. The agreement is quite good with the present results averaging 0.4% higher. Such agreement is a good indication of the consistency and precision of the surface tension values obtained in this investigation.

After the preliminary surface tension results for molten potassium have been completely evaluated, the investigation will be continued to obtain the surface tension and density of the other alkali metals to near their boiling points. Upon completion of these determinations, a study will be made of the contact angles of alkali metal droplets on various sample surfaces.

Acknowledgment

The author wishes to acknowledge the guidance of H. W. Hoffman during the early stages of these investigations, the valuable assistance of S. J. Claiborne in constructing and operating the apparatus, and the conscientious typing of this paper by Dolores Eden.

References

1. F. Y. Yaggee and S. Untermyer, "The Relative Thermal Conductivities of Lithium, Sodium, Eutectic Nak, and Heat Capacity of Lithium," USAEC Report ANL-4458, Argonne National Laboratory, April 21, 1950.

2. H. A. Webber, D. Goldstein, and R. C Fellinger, "Determinations of the Thermal Conductivity of Molten Lithium," Trans. ASME, 77: 97–102 (1955).

3. C. T. Ewing, Naval Research Laboratory, personal communication to J. W. Cooke, Oak Ridge National Laboratory, Aug. 5, 1960.

4. M. A. Mikheev, ed., Problems in Heat Transfer, pp. 1–11, Publishing House of the Academy of Sciences, USSR, Moscow, 1959; translated by U. S Joint Publications Research Service, New York [AEC-tr-4511 (January 1962)].

5. I. I. Rudnev, V. S. Lyashenko, and M. D. Abramovich, "Diffusivity of Sodium and Lithium," Atomic Energy, 3: 877–880 (1962).

6. S. N. Kapelner, "The Electrical Resistivity of Lithium and Sodium-Potassium Alloy," Report PWAC-349, Pratt and Whitney Aircraft Company, June 30, 1961.

7. L. A. Quarterman and W. L. Primak, "The Capillary Rise, Contact Angle, and Surface Tension of Potassium," J. Am. Chem. Soc., 72: 3035 (1950).

8. E. Schroedinger, "Note on the Capillary Pressure in Gas Bubbles," Ann. Physik, 46: 413 (1915).

9. S. Sugden, "The Determination of Surface Tension from Maximum Pressure in Bubbles," J. Chem. Soc., 1: 858 (1922).

10. N. E. Dorsey, Properties of Ordinary Water Substance, Reinhold Publishing Corp., New York, 1940.

11. W. R. Gambill, "Surface Tension of Pure Liquids," Chem. Engrg., 56: 146 (April 1958).

12. R. N. Lyon, ed., Liquid Metals Handbook, 2nd ed., p. 42, U. S. Government Printing Office, Washington, D. C., 1952.

UNCLASSIFIED
ORNL-LR-DWG 58254A

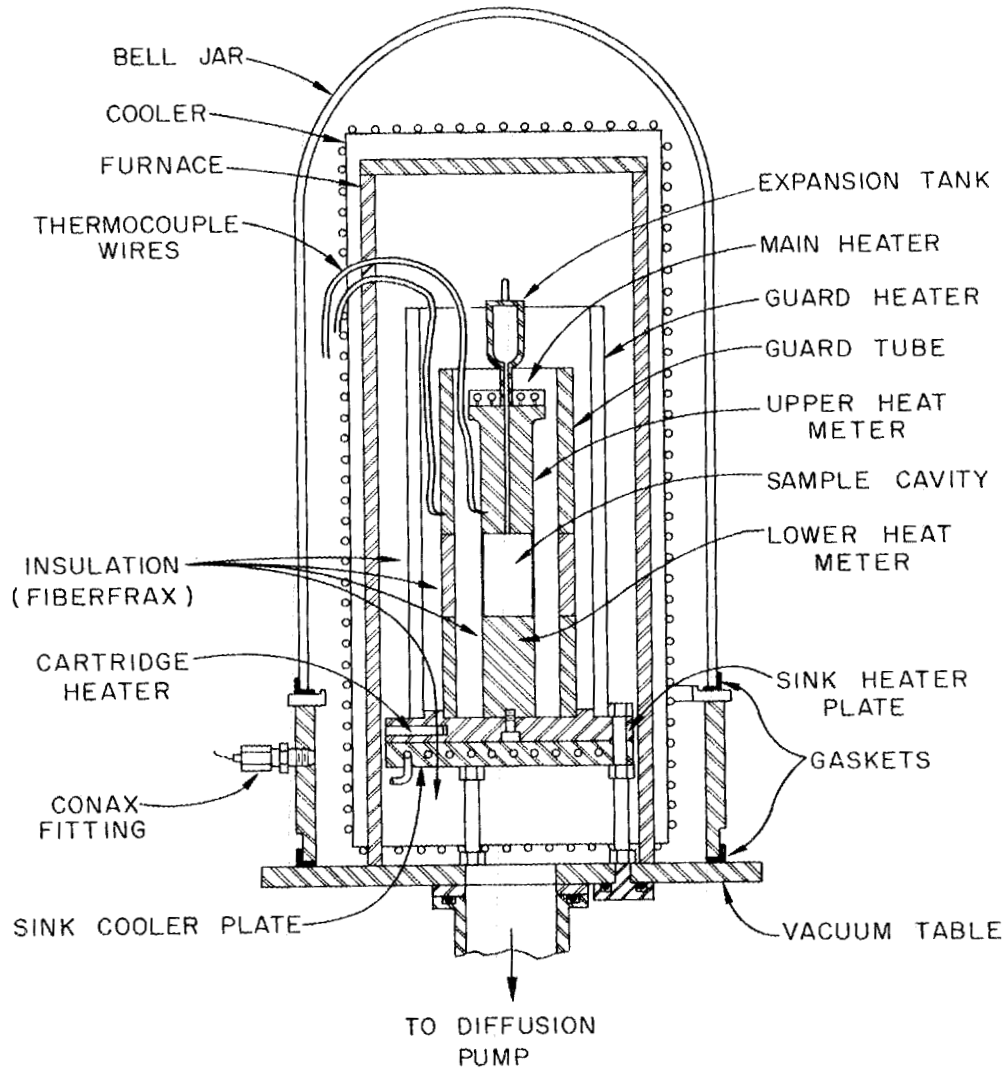

Fig. 1. Cross-Sectional View of Assembled Axial-Heat-Flow Thermal Conductivity Apparatus for Liquid Metals.

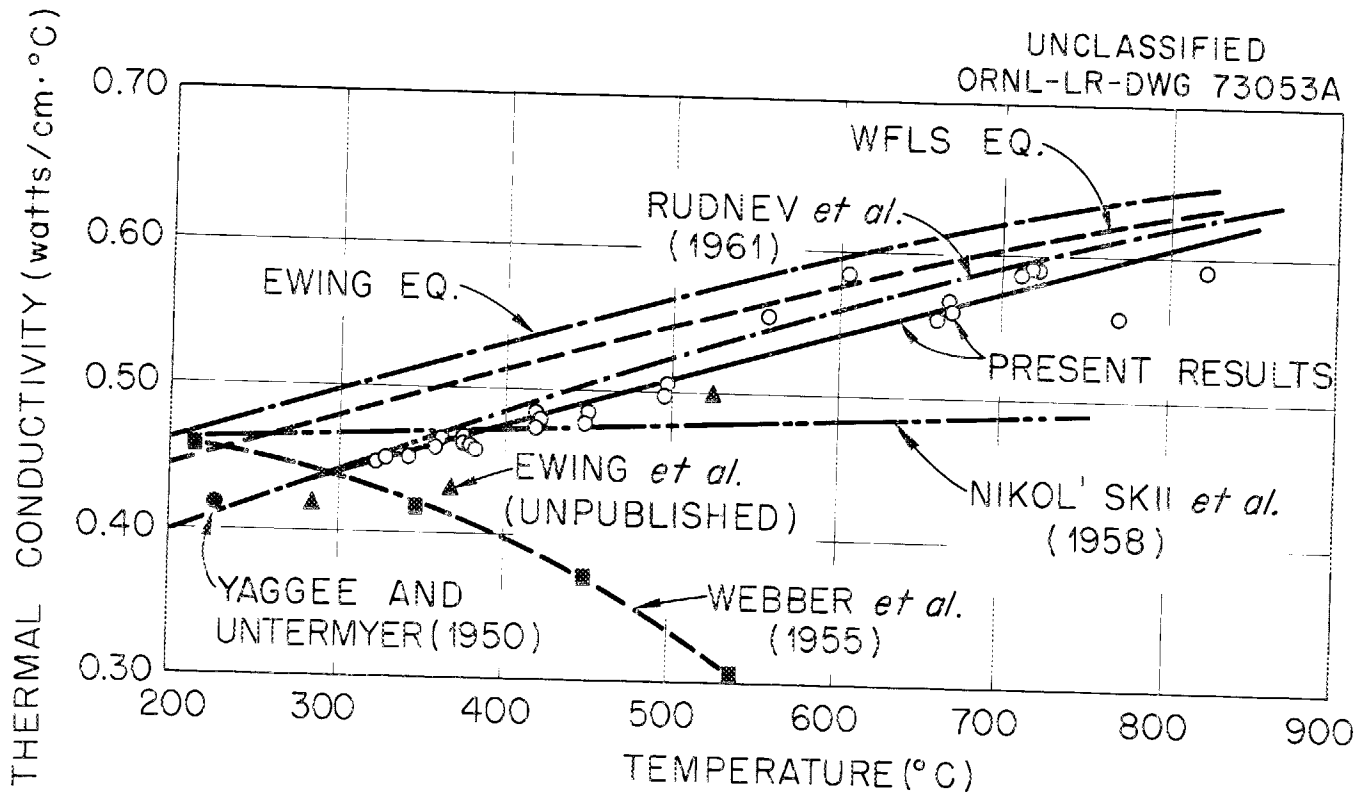

Fig. 2. Thermal Conductivity of Molten Lithium – Present, Previous, and Predicted Values.

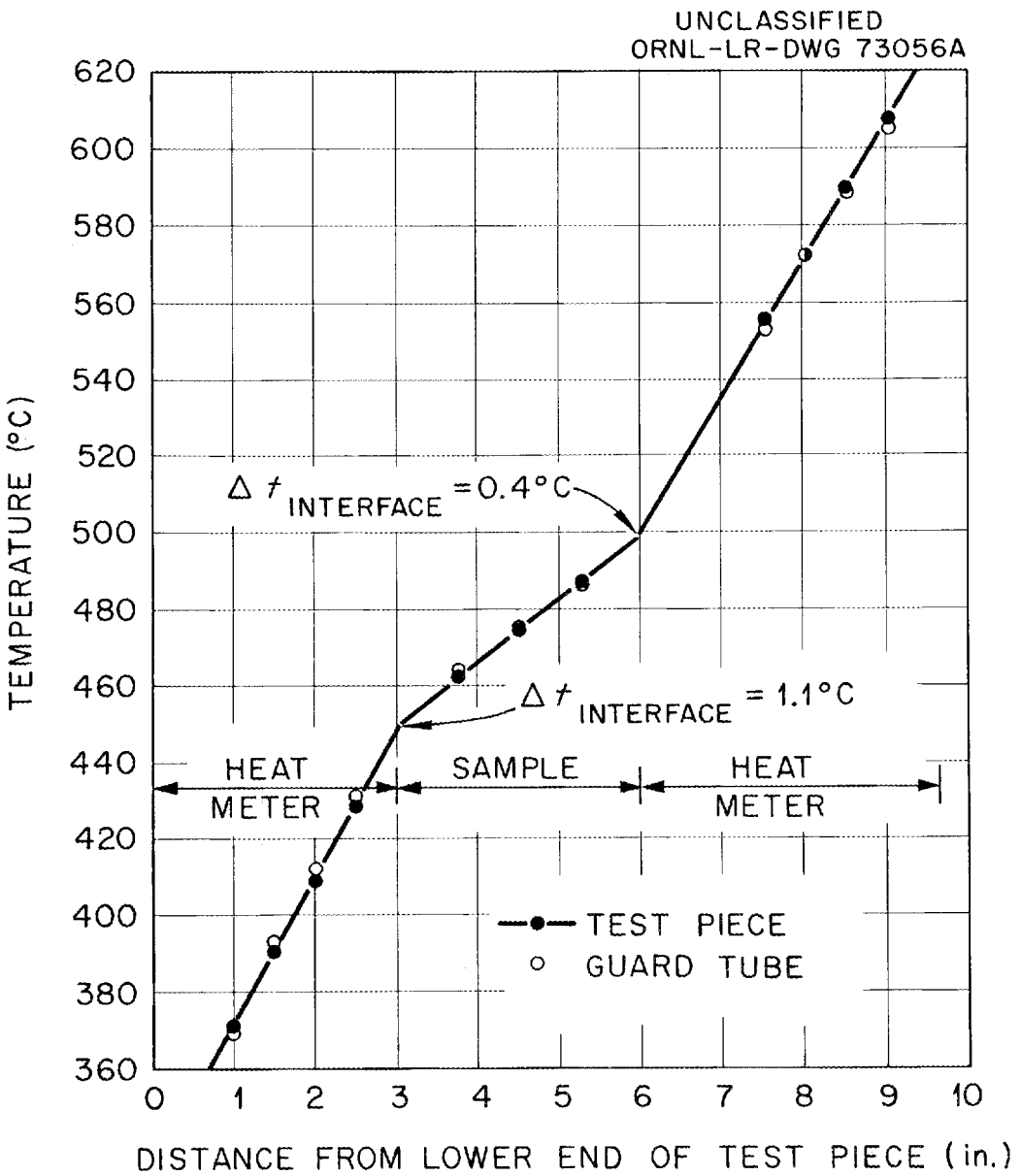

Fig. 3. Typical Axial Themperature Profiles Along Test Piece and Guard Tube – Run No. 8.

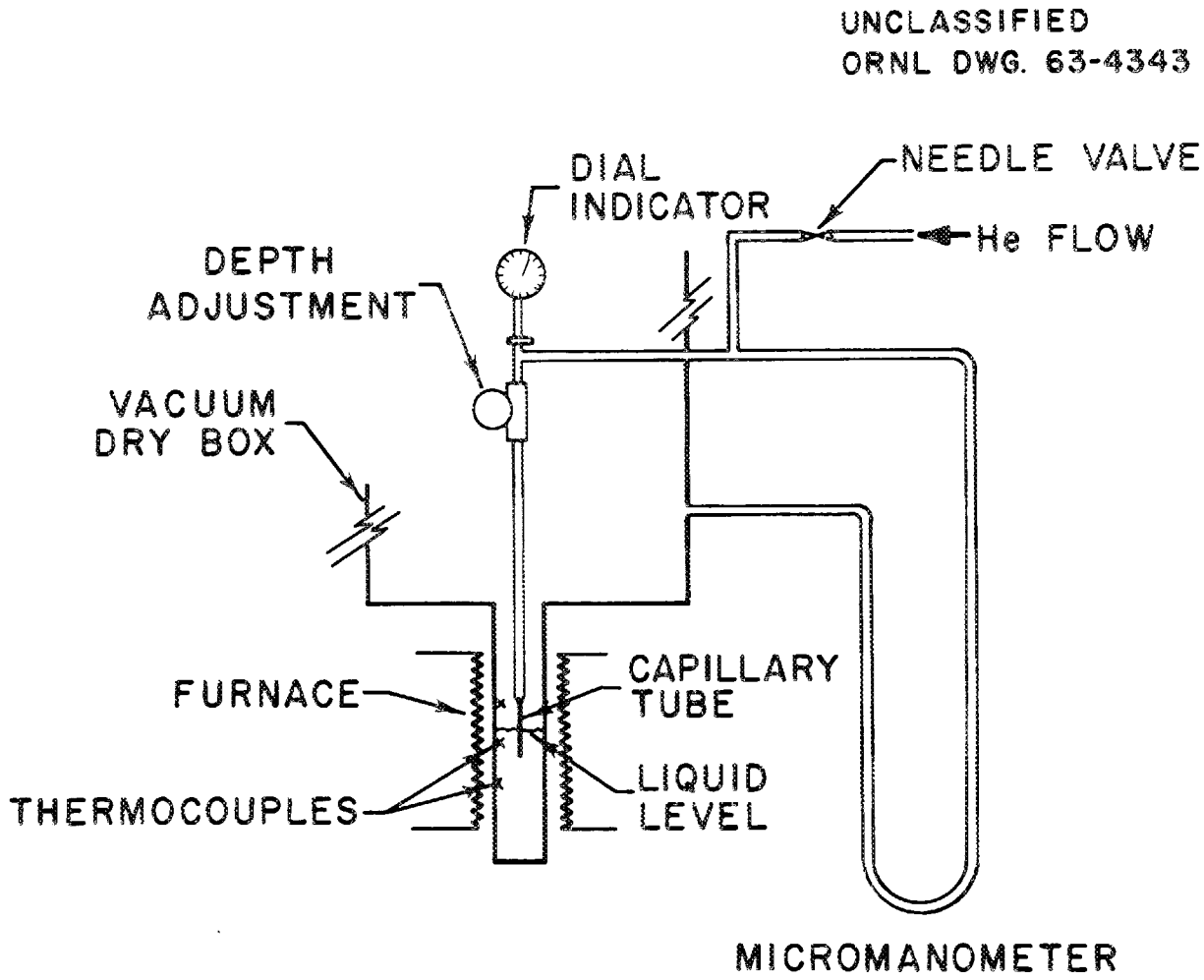

Fig. 4. Maximum Bubble-Pressure Apparatus for Surface Tension Determinations with Liquid Metals.

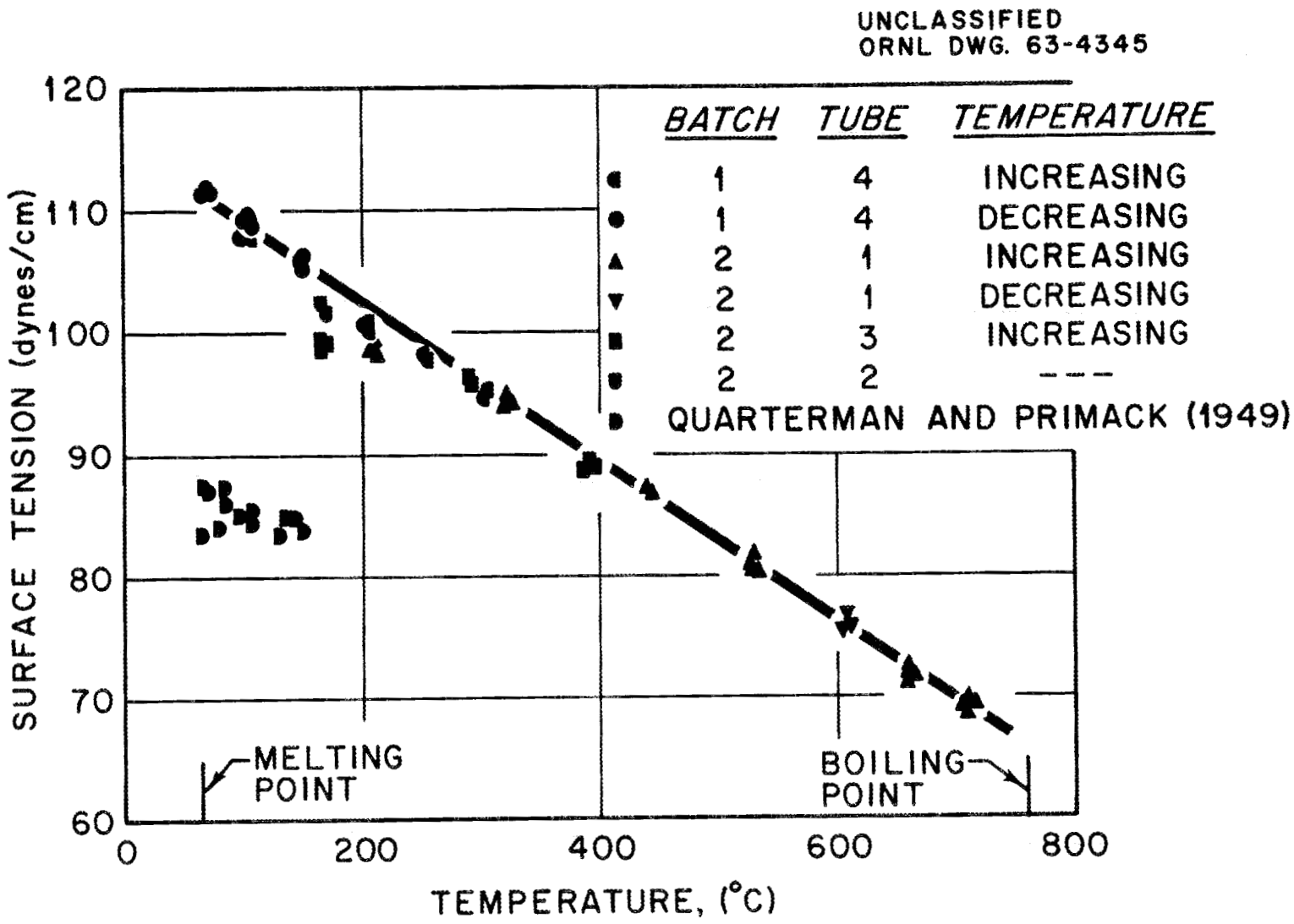

Fig. 5. Surface Tension of Molten Potassium as a Function of Temperature.

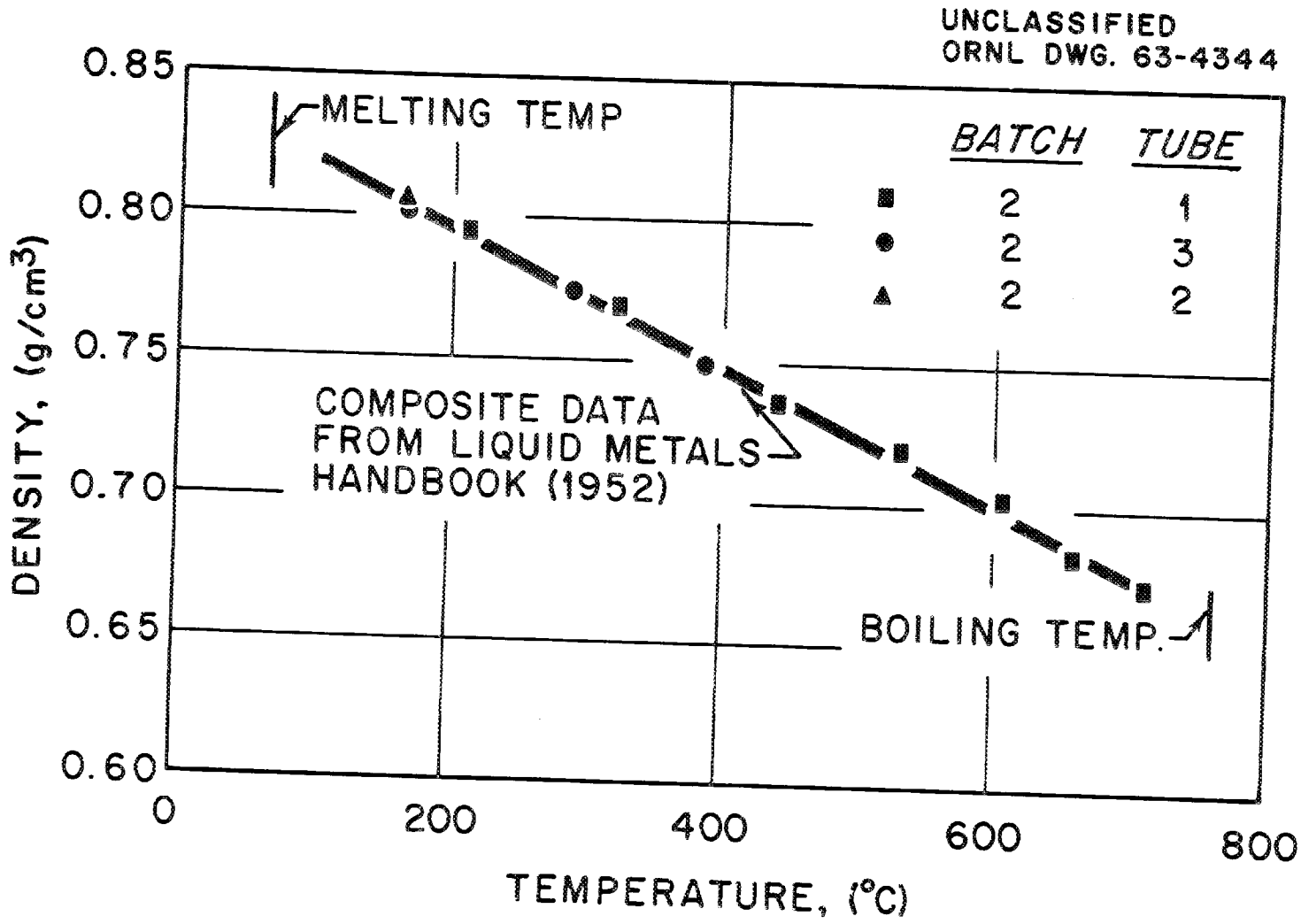

Fig. 6. Density of Molten Potassium Obtained by Maximum Bubble-Pressure Method.

DISCUSSION

MR. FISHER: Do you plan to measure the surface tension of rubidium or cesium?

MR. COOKE: Yes; we plan to begin those measurements quite soon.

MR. BONILLA: An article by Temple Institute does have surface tension values for potassium apart from those you reference. I believe these have been quoted by Weatherford et al.

MR. COOKE: Thank you; I will look at those.

THE THERMODYNAMIC AND TRANSPORT PROPERTIES OF POTASSIUM

A. W. Lemmon, Jr., H. W. Deem,
E. H. Hall, and J. F. Walling*

SUMMARY

Experimental thermodynamic measurements of liquid enthalpy, vapor pressure, and gas compressibility of potassium at temperatures up to 2100 F (1150 C) are described, and the results are reported. These data were used to derive values for solid, liquid, and vapor specific heat, heat of fusion, and heat of vaporization, and to construct an enthalpy-entropy diagram. Transport-property measurements were made of the liquid viscosity, the liquid thermal conductivity, and the liquid electrical conductivity. These results are also reported to 2100 F (1150 C). For all results, comparisons are made with previous information when such was available.

* All of Battelle Memorial Institute, 505 King Avenue, Columbus, Ohio 43201

INTRODUCTION

In the search for an optimum heat-transfer and working fluid for Rankine power cycles to be operated in space, recent consideration has been given to the various alkali metals. Of these metals, potassium appears to be advantageous in some applications. Consequently, research programs have been undertaken to study its potential.

As these studies began, it was immediately recognized that the basic data available for potassium were inadequate. A few values were available for the thermodynamic and transport properties, but even these did not extend into the temperature range of maximum interest, up to 2100 F (1150 C).

A program was begun at Battelle Memorial Institute in September, 1960, to obtain the needed basic data. The properties of potassium investigated experimentally have been enthalpy of the solid and liquid, vapor pressure, P-V-T characteristics, liquid and vapor viscosity, and liquid and vapor thermal conductivity. The experimental results of these studies are reported with the exception of the vapor viscosity and the vapor thermal conductivity. These latter measurements have not yet been successfully concluded.

In addition to the experimental results, computed results for the specific heats, enthalpy, and entropy are also reported.

THERMODYNAMIC PROPERTIES

Specific Heat and Heat of Fusion

Enthalpy measurements were made in a Bunsen ice calorimeter. Figure 1 is a sectional sketch of the calorimeter well. The ice calorimeter is a closed system in which heat from the specimen melts ice that is in equilibrium with water. The resulting volume change in the ice-water system is determined by weighing the

mercury displaced as the ratio of ice to water changes. The specimen to be measured is encapsulated; an empty capsule of similar size and weight is used to measure the heat content of the capsule material. The calorimeter is periodically checked by dropping properly encapsulated National Bureau of Standards Al_2O_3. Its accuracy is such that the enthalpy of the Al_2O_3 is generally found to be within a fraction of 1 per cent of the National Bureau of Standards values.

This calorimeter has been used to measure specific heats of many materials over a number of years and has been thoroughly proven. It was considered superior to other types for this research because there is no temperature change in the calorimeter since all heat transfer occurs at the ice point.

Nb-1Zr alloy was used as the capsule material. Because the first capsule failed, subsequent lots of the Nb-1Zr alloy were carefully selected, subjected to a metallographic examination, and annealed in a vacuum for 1 hour at 1200 C. Capsules made from a second lot of Nb-1Zr alloy proved satisfactory.

The specimen capsules, empty capsule, and Al_2O_3-containing capsule were dropped at a number of temperatures between 0 and 1150 C. At each specimen drop, adjustments in observed enthalpy were made where necessary to allow for (1) the enthalpy of the capsule material, (2) the heat of vaporization of the potassium vapor in the capsule above the specimen, and (3) capsule oxidation. The maximum adjustments made for the heat of vaporization of the vapor and for oxidation of the capsules were approximately 0.1 and 0.3 per cent, respectively.

Equations for the enthalpy of solid and liquid potassium were obtained by least squares. Instantaneous specific heats in the solid and liquid ranges were calculated at interpolated temperatures, using the first derivative of the least-squares equation. The heat of fusion of potassium was calculated at 63.2 C, the melting temperature of potassium, using the enthalpy equations for the solid and liquid ranges.

TABLE 1. SPECIFIC HEAT OF POTASSIUM

Temperature, t, C	Specific Heat, C_s, cal g^{-1} C^{-1}		
	Battelle (Present Work)	Douglas, et al.[9]	Difference, Present Work Minus Douglas, et al., per cent
		Solid	
0	0.170_5	0.169_7	+0.4
25	0.181_0	0.182_1	-0.6
50	0.191_5	0.194_5	-1.5
		Liquid	
75	0.194_4	0.195_6	-0.6
100	0.192_7	0.194_0	-0.7
200	0.187_2	0.188_7	-0.8
300	0.184_0	0.184_9	-0.5
400	0.182_9	0.182_6	+0.2
500	0.183_9	0.181_8	+1.2
600	0.187_2	0.182_5	+2.6
700	0.192_8	0.184_6	+4.4
800	0.200_4	0.188_3	+6.4
900	0.210_3	--	--
1000	0.222_3	--	--
1100	0.236_6	--	--
1150	0.244_6	--	--

The equation for the specific heat of solid potassium is

$$C_s \text{ (solid)} = 0.1705 + 0.4190 \times 10^{-3} t \text{ (0 to 63.2 C)} \quad . \qquad (1)$$

The equation for the specific heat of liquid potassium is

$$C_s \text{ (liquid)} = 0.2004 - 0.8777 \times 10^{-4} t + 1.0970 \times 10^{-7} t^2 \text{ (63.2 to 1150 C)} \quad , \qquad (2)$$

where

C_s = specific heat, cal $g^{-1}C^{-1}$

t = temperature, C.

The heat of fusion of potassium at the melting point is 14.3_0 cal g^{-1}.

Errors for the specific heats are estimated to be $\pm$ 2 per cent for solid potassium, $\pm$ 2 per cent for liquid potassium to 500 C, and $\pm$ 5 per cent for liquid potassium from 500 to 1150 C.

Table 1 shows specific heats at interpolated temperatures for solid and liquid potassium. Also included in Table 1 are data from Douglas, et al.[1] Table 2 shows the heat of fusion of potassium as measured in this investigation compared with values from four other investigators.

TABLE 2. HEAT OF FUSION OF POTASSIUM

Source	Heat of Fusion, cal g^{-1}
This investigation	14.3_0
Douglas, et al.[1]	14.2_6
Carpenter and Steward[2]	14.5_2
Bridgman[3]	12.8_0
Evans, et al.[4]	14.1_7

Containment difficulties pose the greatest problem in making high-temperature enthalpy measurements of potassium. The Nb-1Zr alloy used in the present work was not completely satisfactory for use to 1150 C because of oxide

formation and difficulties in containing the potassium.

Vapor Pressure

The vapor pressure of liquid potassium was measured at a number of temperatures between 900 and 2100 F. Although many techniques exist for measurement of vapor pressures, each has its limitations; frequently this is the pressure. Because of its applicability over the entire pressure range and the physical simplicity of its apparatus, a modified boiling-point technique was selected for this work.

A small sample of potassium was contained in a stainless steel or Nb-1Zr test tube, and the pressure over it was fixed at various levels of interest with purified helium. Stainless steel was used for most measurements below about 1500 F, and Nb-1Zr for all measurements above this temperature. The temperature rise of the slowly heated sample was measured by a calibrated sheathed thermocouple immersed in the liquid. The boiling temperature was determined by estimating the temperature at which a change occurred in the rate of climb of the sample temperature with time. Pressures below 2 atmospheres were measured with a manometer. Above this pressure, dead-weight-calibrated, Bourdon-type gages were employed. The data are summarized in Figure 2.

In order to assess the thermodynamic agreement between these vapor-pressure data and data obtained by other types of measurements, a conventional third-law treatment was applied to the data using free-energy functions and second virial coefficients recently published by Thorn and Winslow[5]. Results of the calculation of apparent third-law heats of sublimation at absolute zero (ΔH_o^o) are summarized in Figure 3. The decrease in values of this function above about 1150 K was ascribed not to faulty data but to the omission of third virial effects from the equation used to calculate ΔH_o^o. Therefore, using data below about 1150 K, a value

for ΔH_0^o of 21,710 cal/mole was obtained. This agrees well with other investigations. The data above 1150 K were then used to estimate third virial corrections.

The data between 758 and 1430 K are summarized by the following equation with a standard deviation of log P of $\pm$ 0.0097.*

$$\log P = \frac{-4794.3}{T} - 1.97108 \log T + 4.9800\times10^{-4}T - 1.0659\times10^{-7}T^2 + 10.1451 + \frac{1915.4}{T} \exp \frac{-4338.9}{T} + \frac{7.40\times10^4}{T} \exp \frac{-1.056\times10^4}{T}$$

The last term is the third virial correction. Its credibility and interpretation are discussed in some detail elsewhere[6].

These data agree quite well with the more limited data collected at Oak Ridge but privately transmitted to and reported by Thorn and Winslow[5]. Agreement with the data of Makansi, Madsen, Selke, and Bonilla, using the refined treatment of Thorn and Winslow[5] is poorer than with the Oak Ridge work. However, the large discrepancy between all of these data and those of recent Russian work[7] indicates that the latter are certainly in error. This conclusion is re-enforced by the third-law test applied to the Battelle data, since this indicates the concordance of these data and other calorimetric and spectroscopic information.

P-V-T Values

The extent of gas nonideality is most succinctly summarized in compressibility factors. The interpretation of these factors and their use in thermodynamic

* The simpler relation

$$\log P_{atm} = 4.185 - \frac{4332}{T}$$

will yield values for pressure related to the more complex equation as follows:

at 758 K	the same
at 900 K	about 0.5% low
at 1100 K	about 0.5% low
at 1200 K	about 1.5% low
at 1300 K	about 1.5% low
at 1400 K	about 2% low

calculations is most straightforward when they are expressed as a virial expansion,

$$\frac{PV}{nRT} = 1 + B' P + C' P^2$$

Values for the second and third virial coefficients were obtained from spectroscopic and vapor-pressure information. The experimental P-V-T work can not be reported adequately here; its main value was to suggest an increase of about 25 per cent in the value of the third virial coefficient over that estimated from the vapor-pressure measurements. This is within the error limits of that estimation. It was, therefore, concluded that the most reliable values of the compressibility for potassium gas can be calculated from the virial equation, where

$$\log |B| = 8.9912 + \frac{1.471 \times 10^3}{T} - 2.212 \log T$$

$$B' = \frac{-|B|}{82.057T}$$

$$\log |C'| = -6.315 + 4.670 \times 10^3/T$$

$$C < 0$$

Enthalpy, Entropy, and Vapor Specific Heat

The measurements obtained from the ice calorimeter and boiling-point measurements have been used in calculations of the enthalpy and entropy of potassium liquid, vapor, and two-phase systems.

The direct measurement of the enthalpy of the liquid at its vapor pressure and the determination of the heat capacity of the liquid have been discussed earlier. Thus, the liquid enthalpy at the vapor pressure was measured directly, and the integration of the heat capacity to give entropy is straightforward.

Heats and entropies of vaporization were calculated from the Clapeyron equation using the vapor-pressure relation, liquid-density data, and vapor-compressibility information.

The heat and entropy of the gas at any pressure can be calculated from the following equations:

$$H_{gas} - H_o^o = H_{liq} - H_o^o + \Delta H_{vap} + \int_{P_{vap}}^{P} \left(\frac{\partial H}{\partial P}\right)_T dP$$

$$S_{gas} = S_{liq} + \Delta S_{vap} + \int_{P_{vap}}^{P} \left(\frac{\partial S}{\partial P}\right)_T dP \ ,$$

where

$$\int_{P_{vap}}^{P} \left(\frac{\partial H}{\partial P}\right)_T dP = \left(B - T\frac{dB}{dT}\right)\left(P - P_{vap}\right) + \left(C - T\frac{dC}{dT}\right)\left(\frac{P^2 - P_{vap}^2}{2}\right)$$

$$\int_{P_{vap}}^{P} \left(\frac{\partial S}{\partial P}\right)_T dP = - R \ln P/P_{vap} - \frac{dB}{dT}(P - P_{vap}) - \frac{dC}{dT}\left(\frac{P^2 - P_{vap}^2}{2}\right)$$

By means of a digital computer, heats and entropies of (1) the gas at various pressures and temperatures, (2) the liquid at its vapor pressure at various temperatures, and (3) two-phase systems at the vapor pressure and various fractions of liquid and vapor were computed. These results are summarized in Figure 4.

Figure 5 summarizes values for the heat capacity of the gas at several selected pressures. The values were obtained by evaluation of the standard relation

$$C_p = C_p^o - T\left[\frac{d^2B}{dT^2}P + \frac{d^2C}{dT^2}\frac{P^2}{2}\right] \quad .$$

Agreement between the values for enthalpy, entropy, and heat capacity and previous estimates[8] is reasonably good at low pressures, as might be anticipated. Pronounced divergence is apparent at the higher temperatures and

pressures owing mainly to third virial corrections which are included here for the first time.

TRANSPORT PROPERTIES

Liquid Viscosity

The viscosity of liquid potassium has been studied by various workers; however, the agreement among the several sets of data was, in general, outside of the indicated precision of the individual sets. In addition, the temperature range covered was generally rather narrow, only one worker having gone as high as 700 C. In order to clarify the areas of disagreement and to extend the range of measurement to 1150 C, the viscosity of liquid potassium was measured.

A number of methods for the measurement of the viscosity of liquids have been reported. Among these are capillary-flow, oscillating-cylinder (or sphere), oscillating-bob, rotating-cylinder, ultrasonic, X-ray, and polarographic methods. Eight references[9-16] list typical applications of each of these methods.

After consideration of all the factors, the oscillating-cylinder method was selected as the one most readily adaptable to liquid potassium. A closed hollow cylinder containing the liquid was suspended from a torsion wire and permitted to oscillate about the axis of the suspension. Observation of the damping of the cylinder's oscillation by the liquid permitted calculation of the viscosity. The apparatus (shown schematically in Figure 6) consisted of a cylinder, containing the potassium sealed under vacuum, that was connected through a suspension system to a 0.009-inch-diameter hardened-steel torsion wire. The cylinder was heated by an electrical-resistance furnace, and the chamber containing the cylinder and suspension was evacuated to less than 10^{-5} torr. The amplitude of the oscillation was measured by means of an electromechanical position-sensing transducer which did not require constant attention during the 50 to 75 swings necessary for a good measurement of

the damping. The transducer also provided a permanent record for future reference. The temperature of the cylinder was measured by a calibrated Chromel-Alumel thermocouple placed in a well in the top of the cylinder. The leads passed up through the center of the support tube and were so arranged that they were free during the determination of the damping. When it was desired to read the output of this thermocouple, externally operated probes were brought into contact with the leads.

The procedure followed was, first, to equilibrate the liquid overnight for temperatures up to 700 C, and for 3 or 4 hours for higher temperatures. After equilibration, the oscillation was then initiated. After 8 to 10 swings, the next 70 swings were timed with a stopwatch while the recorder traced the oscillations. The amplitude was built up again and the process was repeated. When possible, 8 to 10 sets of 70 swings were recorded at each equilibrium temperature.

The amplitudes were measured on the recorder chart and the logarithmic decrement calculated for each set of 70 swings. The decrements obtained for each set of swings at a given temperature were then averaged. The viscosity was calculated from the logarithmic decrement by the use of the absolute equation given by Shvidkovsky[11]:

$$\nu = \frac{1}{\pi}\left(\frac{I}{MR}\right)^2 \frac{\left(\delta - \frac{\tau}{\tau_o}\delta_o\right)^2}{\tau\sigma^2}, \qquad (1)$$

where

ν = kinematic viscosity

I = moment of inertia of empty system

M = mass of liquid

R = radius of the cylinder

δ, δ_o = logarithmic decrement of filled and empty system

τ, τ_o = period of oscillation of filled and empty system.

The end effect correction, σ, is

$$\sigma = 1 - (3/2)\,x - (3/8)x^2 - a + \frac{R}{H}(b-cx)\,, \qquad (2)$$

where

$x = \frac{\delta}{2\pi}$

$H = 1/2$ the depth of the liquid

a, b, and c are available as tabulated functions of $Y = \frac{2\pi R^2}{\tau\nu^*}$

ν^* is an approximate value of the kinematic viscosity.

In order to minimize the time required to carry out the calculations and to insure accurate solutions, a computer program was written that performs the necessary iterations and takes into account the thermal-expansion effects.

The viscosity data are presented graphically as ν versus t in Figure 7 and η versus t in Figure 8. Figure 7 also shows points read from the curve presented by Novikov[12]. The agreement is satisfactory at 100 and 700 C, but Novikov's results are up to 5 per cent higher in the region between. The results of several other workers are also plotted in Figure 8 for comparison. The values obtained in this work are seen to be in good agreement with those of Sauerwald[17] and Gering and Sauerwald[18], who used the capillary method. Chiong's values[19], obtained by means of a glass oscillating sphere, are about 6 per cent lower at 70 C and cross over at about 240 C. The capillary data of Ewing, et al.,[9, 10] are lower throughout the range covered, the deviation from the values obtained in this work being 10 per cent at 350 C.

The results can be expressed by the following equations:

341 to 643 K (68 to 370 C):

$$\log\eta = \frac{287.1}{T} - 3.0911,$$

with a standard deviation of $\pm$ 0.005 in $\log\eta$.

643 to 1423 K (370 to 1150 C):

$$\log\eta = \frac{409.7}{T} - 3.2817,$$

with a standard deviation of $\pm$ 0.012 in $\log\eta$.

Viscosity, η, is in poise and T is in degrees K. The maximum error is estimated to be about 5 per cent and the probable error is thought to be not greater than 2.5 per cent.

Liquid Thermal Conductivity

Consideration was given to several methods for making thermal-conductivity measurements of liquid potassium. In general, the steady-state method seemed preferable to transient methods because it yields the thermal conductivity directly. Two steady-state, longitudinal-heat-flow, comparative methods were considered. One was the variable-gap method which uses a disk-shaped specimen, and the other was a longitudinal heat-flow method which uses a cylindrically shaped specimen. Of the two methods, the one that uses the cylindrically shaped specimen was selected because of the relatively high thermal conductivity of potassium and the larger temperature gradients between adjacent thermocouples with the cylindrical specimen than with the thin disk specimen.

The apparatus consisted of a specimen container approximately 1 inch in diameter and about 6 inches long, hollowed out of a rod of Nb-1Zr alloy about 13 inches long. Part of the rod was left solid to serve as the reference material for the measurements. Figure 9 is a sketch of the apparatus. A heater placed near the top of the specimen container provided heat which flowed downward through the specimen, reference material, and into a heat sink. Thermal guarding was accomplished by an encircling guard cylinder in which temperatures were adjusted to equal, as nearly as possible, the temperatures in the specimen chamber-reference section assembly at corresponding elevations. This temperature balancing, coupled with the bubbled-alumina thermal insulation between the specimen container and the guard cylinder, minimized radial heat flows. The entire apparatus was contained in a pressure vessel in which an atmosphere of purified argon at pressures up to

500 psi could be maintained. This external pressure on the thin-walled specimen container was adjusted to equal the vapor pressure of the contained potassium.

Thermal-conductivity measurements were made by establishing a thermal equilibrium and then measuring temperatures at three places in the reference material and at seven locations along the thin-walled specimen container. (The thermal conductivity of Nb-1Zr alloy in a solid rod form was measured in another apparatus.) The quantity of heat flowing in the specimen assembly at each thermal equilibrium was calculated from the temperature drop in the reference section and from the physical dimensions of that section. The heat flowing in each section of the thin wall of the specimen container was also calculated, using the measured thermal conductivity of the Nb-1Zr alloy, the wall cross-sectional area, and the temperature drops over measured lengths of the wall. This heat, when subtracted from the total heat flowing, gave the heat flowing through the potassium. From this, the conductivity of each section of the potassium specimen was calculated for its mean temperature, which was the average of the two bounding thermocouples for the section.

Table 3 shows interpolated thermal-conductivity values for potassium and the Nb-1Zr alloy used to contain the specimen. Uncertainties in achieving thermal equilibrium above 800 C preclude reporting data to higher temperatures. Also shown in Table 3 are literature values for the thermal conductivity of potassium.

Over the temperature range 100 to 800 C, the Wiedemann-Franz-Lorenz number for liquid potassium, calculated from the data, averages $2.14 \times 10^{-8} \frac{\text{watt ohm}}{\text{C K}}$. The theoretical value is about $2.45 \times 10^{-8} \frac{\text{watt ohm}}{\text{C K}}$ where C = temperature Celsius

K = temperature Kelvin

TABLE 3. INTERPOLATED THERMAL CONDUCTIVITY OF LIQUID POTASSIUM, PRESENT WORK AND LITERATURE VALUES, AND THE INTERPOLATED THERMAL CONDUCTIVITY OF Nb-1Zr ALLOY

Temperature, C	Thermal Conductivity, watt $cm^{-2}cm\ C^{-1}$ For Potassium				For Nb-1Zr Alloy
	Battelle (Present Work)	Ewing,[20] et al.	Novikov[21]	Mikheev[22]	
100	0.51_0	--	0.60_0	0.46_5	0.47_4
200	0.47_7	0.44_9	0.52_2	0.46_5	0.49_5
300	0.44_4	0.42_4	0.46_8	0.43_4	0.51_4
400	0.41_0	0.40_0	0.42_7	0.39_5	0.53_0
500	0.37_7	0.37_6	0.39_5	0.34_9	0.54_6
600	0.34_4	0.35_4	0.37_5	0.30_3	0.56_0
700	0.31_0	--	--	0.26_2	0.57_4
750	0.29_4	--	--	0.25_6	--
800	0.27_7	--	--	--	0.58_8
900	--	--	--	--	0.60_1
1000	--	--	--	--	0.61_4
1100	--	--	--	--	0.62_7
1150	--	--	--	--	0.63_4

Table 4 shows electrical-resistivity values for liquid potassium and Nb-1Zr alloy obtained from experimental measurements but interpolated to selected temperatures.

TABLE 4. INTERPOLATED ELECTRICAL RESISTIVITY OF LIQUID POTASSIUM AND Nb-1Zr ALLOY

Temperature, C	Electrical Resistivity, microhm cm	
	Liquid Potassium	Nb-1Zr Alloy
100	15.4	19.5
200	21.5	23.7
300	28.4	27.7
400	35.8	31.4
500	44.4	35.1
600	54.7	38.7
700	66.4	42.1
800	79.5	45.4
900	93.8	
1000	110	
1100	131	
1150	145	
1175	153	

CONCLUSIONS AND RECOMMENDATIONS

Reliable values for many of the basic thermodynamic and transport properties of potassium have been measured or derived. The work has led, as well, to the development of some new experimental techniques but has also pointed out the extreme difficulties which can be encountered when work at such high temperatures is necessary. Not the least of the problems was finding an adequate material for containment of potassium and protecting it from attack by the normal atmospheric environment.

Despite the reasonable success achieved, further work is deemed necessary. Additional data points, particularly at high temperatures, would improve the confidence in the results. In some cases, the use of alternative experimental methods would be valuable in this regard.

ACKNOWLEDGMENT

The sponsoring agency for this program has been the National Aeronautics and Space Administration. Technical management has been performed by the Space Electric Power Office at the Lewis Research Center with supporting funds being provided under Contract NAS 5-584.

REFERENCES

(1) Douglas, T. B., Ball, A. F., Ginnings, D. C., and Davis, W. D., "Heat Capacity of Potassium and Three Sodium-Potassium Alloys Between 0 and 800 C, the Triple Point and Heat of Fusion of Potassium", J. Am. Chem. Soc., 74, 2472-2478 (1952).

(2) Carpenter, L. G., and Steward, C. J., "The Atomic Heat of Potassium", Phil. Mag., 27, 551-564 (1939).

(3) Bridgman, P. W., "Change of Phase Under Pressure", Phys. Rev., 3, 153-203 (1914).

(4) Evans, W. H., Jacobson, R., Munson, T. R., and Wagman, D. D., "Thermodynamic Properties of the Alkali Metals", J. Res. Nat. Bur. Stds., 55, 83-96 (1955).

(5) Thorn, R. J., and Winslow, G. F., "Correction of the Potassium Vapor Pressure Equation by Use of the Second Virial Coefficient", J. Phys. Chem., 65, 1297 (1961).

(6) Walling, J. F., "The Third Virial Coefficient of Potassium as Estimated from Its Vapor Pressure", J. Phys. Chem., 67, 1380 (1963).

(7) Grachev, N. S., and Kirilov, P. L., "Experimental Determination of Potassium Vapor Pressure in the Temperature Range 550 to 1280 C", Inzhenerno-Fizicheskiy Zhurnal, 3 [6], 62 (1960).

(8) Weatherford, W. D., Tyler, J. C., and Ku, P. M., "Properties of Inorganic Energy-Conversion and Heat-Transfer Fluids for Space Applications", WADD Technical Reports 61-96, November 1961.

(9) Ewing, C. T., Grand, J. A., and Miller, R. R., "Viscosity of the Sodium-Potassium System", J. Am. Chem. Soc., 73, 1168 (1951).

(10) Ewing, C. T., Grand, J. A., and Miller, R. R., "Viscosity of the Sodium-Potassium System", J. Phys. Chem., 58, 1086 (1954).

(11) Shvidkovsky, E. C., The Viscosity of Liquid Metals, Gostekhizdat, Moscow (1955), English Translation, NASA Technical Translation F-88 (March, 1962).

(12) Novikov, I. I., et al., "The Heat-Transfer and High Temperature Properties of Liquid Alkali Metals", J. Nuclear Energy, 4, 387 (1957). In English.

(13) Jones, W. R. D., Bartlet, W. D., "The Viscosity of Aluminum", J. Inst. Metals, 145 (1952).

(14) Roth, W., and Rich, S. R., "A New Method for Continuous Viscosity Measurement. General Theory of the Ultra-Viscoson", J. Appl. Physics, 24, 940 (1953).

(15) Goroshko, V. D., and Gupalo, U. P., "X-Ray Determination of Viscosity", Zavodskaya Lab., 27, No. 1, 38 (1961).

REFERENCES (Continued)

(16) Elgort, V. M., "Determination of the Viscosity of Liquids by a Polarographic Method", Uzbek. Khim. Zhur., 2, 34 (1961).

(17) Sauerwald, F., "The Measurement of the Viscosity of the Alkali Metals in Vacuum", Z. Fuer Metallkunde, 26, 259 (1934).

(18) Gering, K., and Sauerwald, F., "The Viscosity of Pb, Cd, Zn, Ag, Sn, K and Na", Z. fuer Anorg. Allgem. Chem., 223, 204 (1935).

(19) Chiong, Y. S., "Viscosity of Liquid Sodium and Potassium", Proc. Royal Soc., A-157, 264 (1936).

(20) Ewing, C. T., Grand, J. A., and Miller, R. R., "Thermal Conductivity of Liquid Sodium and Potassium", J. Am. Chem. Soc., 74, 11-14 (January 1952).

(21) Novikov, I. I., et al., "The Heat Transfer and High-Temperature Properties of Liquid Alkali Metals", J. Nuclear Energy II, 4, 387-408 (1957).

(22) Mikheev, M. A., Editor, "Problems in Heat Transfer", Publishing House of the Academy of Sciences, USSR, Moscow, (1959); Translated by U. S. Joint Pub. Res. Service, New York, AEC-TR-4511, pp 1-11 (January 1962) (Nikol'skii, Author).

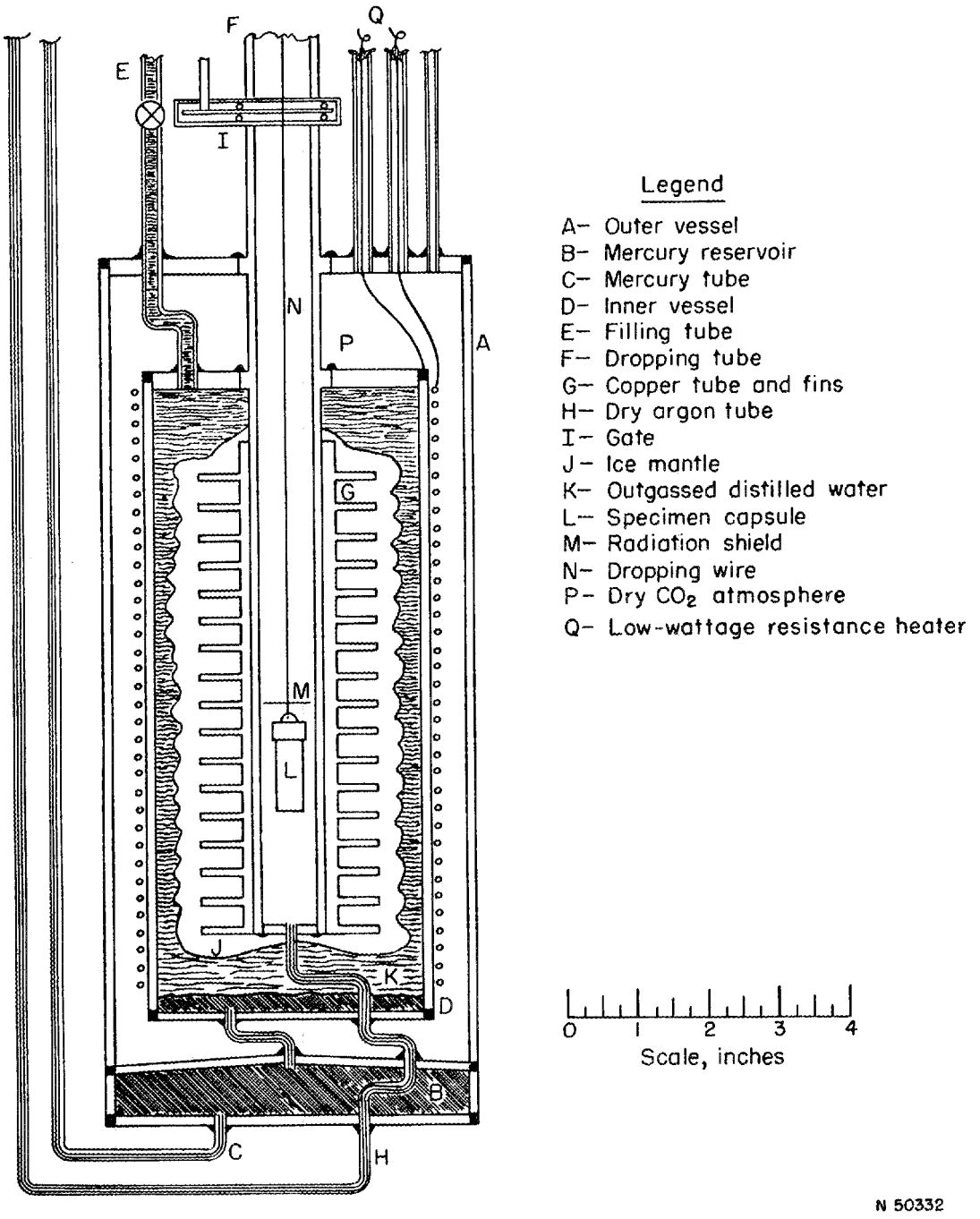

FIGURE 1. STAINLESS STEEL ICE CALORIMETER

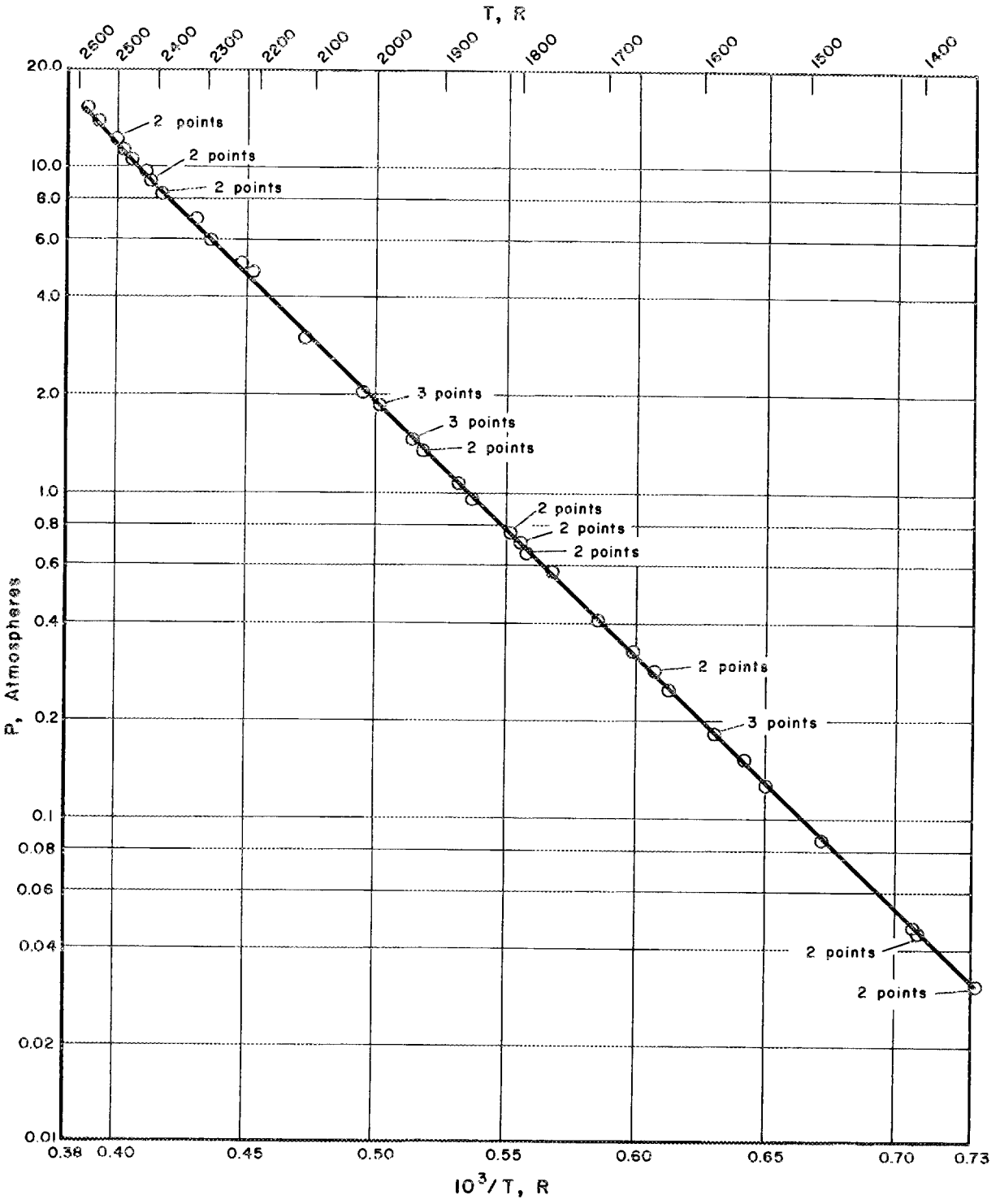

FIGURE 2. THE VAPOR PRESSURE OF POTASSIUM

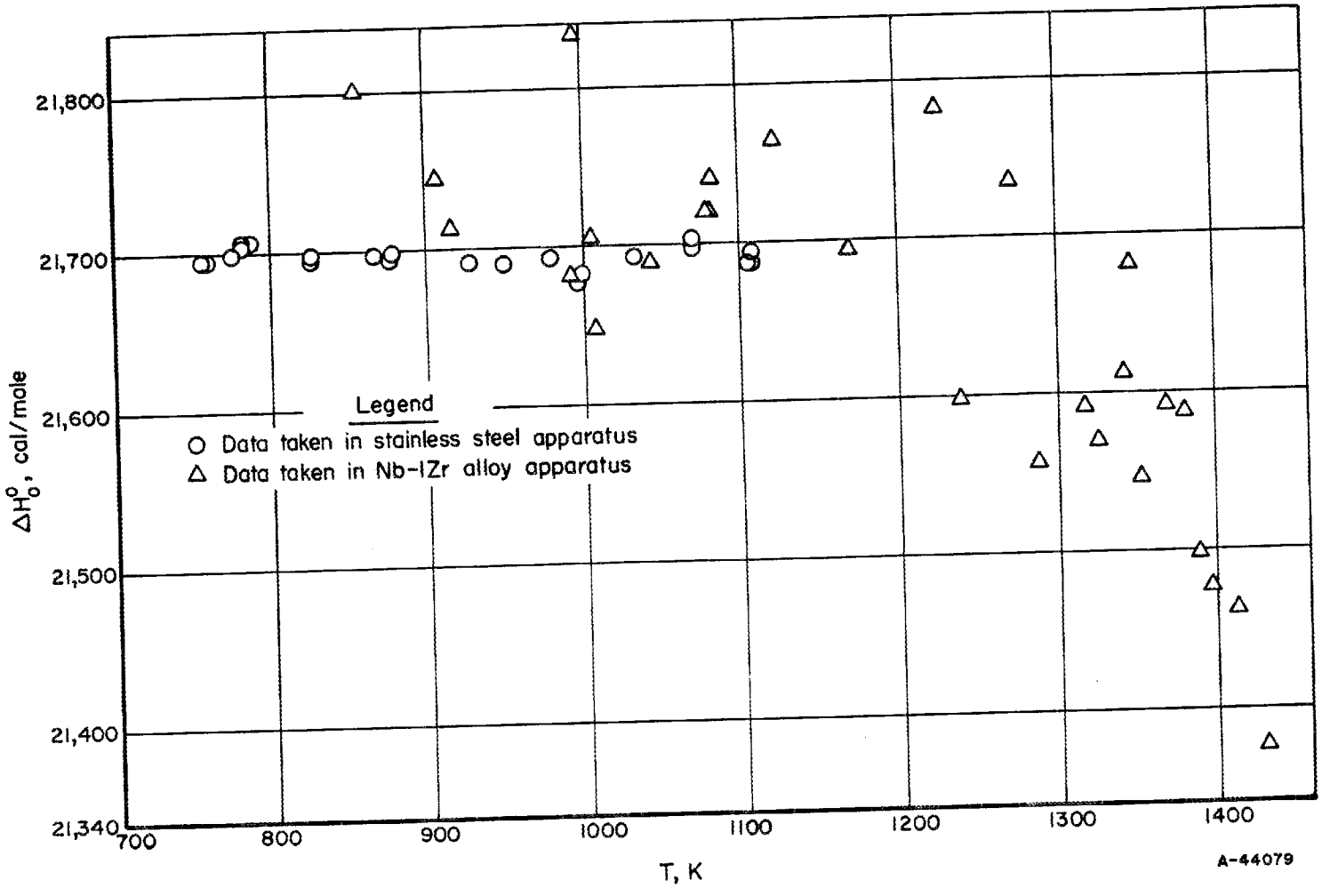

FIGURE 3. APPARENT HEAT OF SUBLIMATION OF MONOMERIC POTASSIUM AT ABSOLUTE ZERO

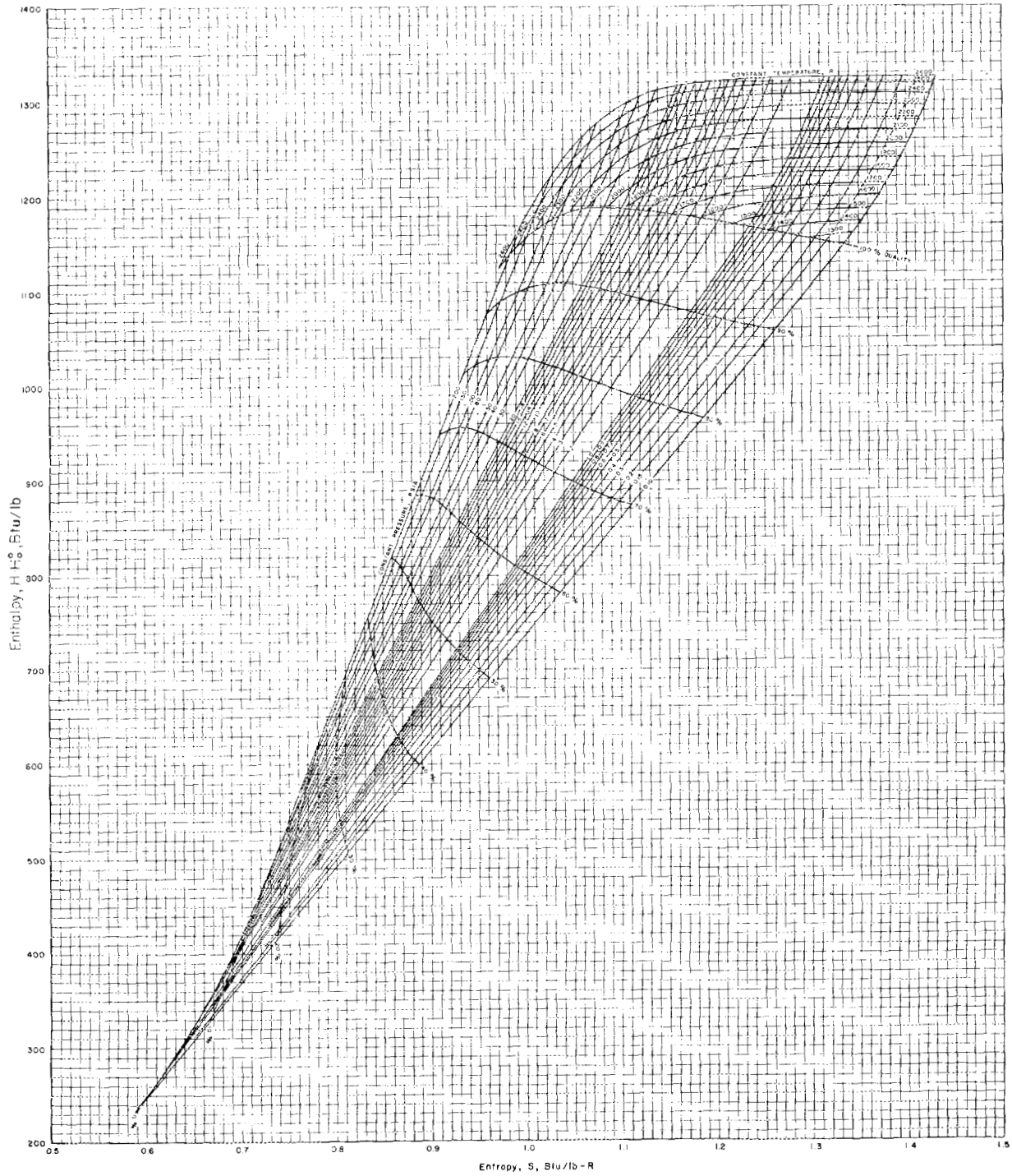

FIGURE 4. ENTHALPY-ENTROPY DIAGRAM FOR POTASSIUM

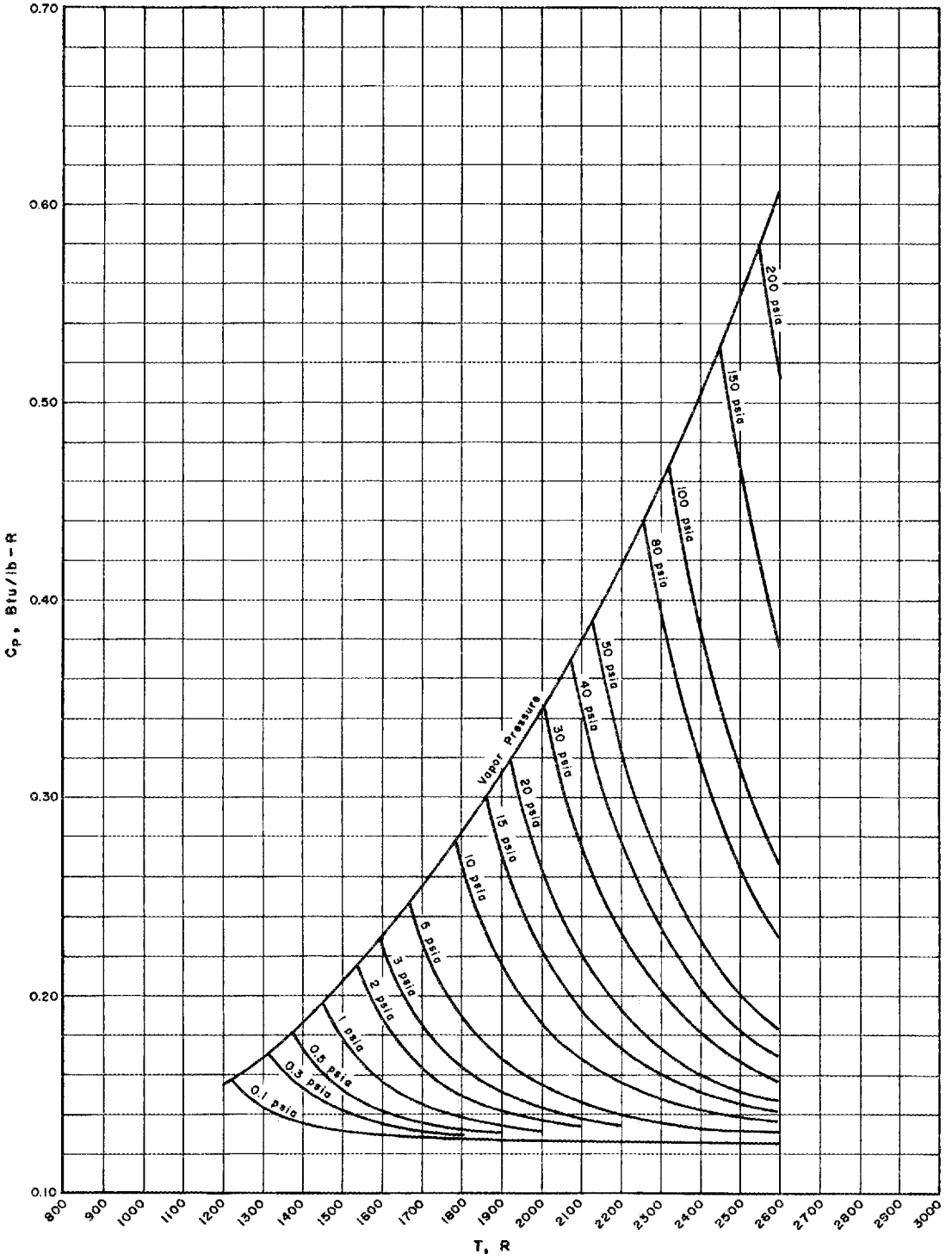

FIGURE 5. HEAT CAPACITY OF GASEOUS POTASSIUM

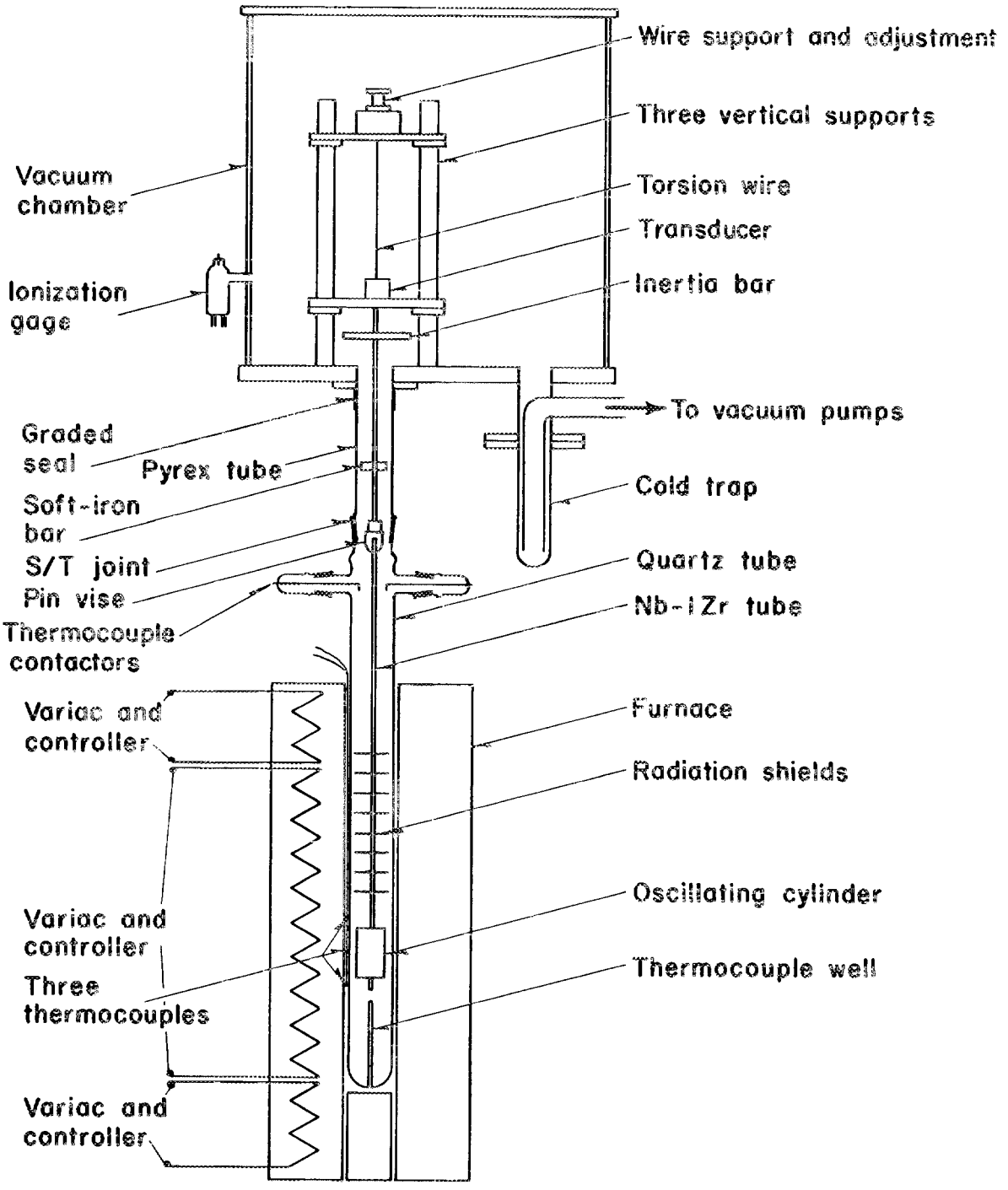

FIGURE 6. SCHEMATIC DIAGRAM OF LIQUID-POTASSIUM VISCOMETER

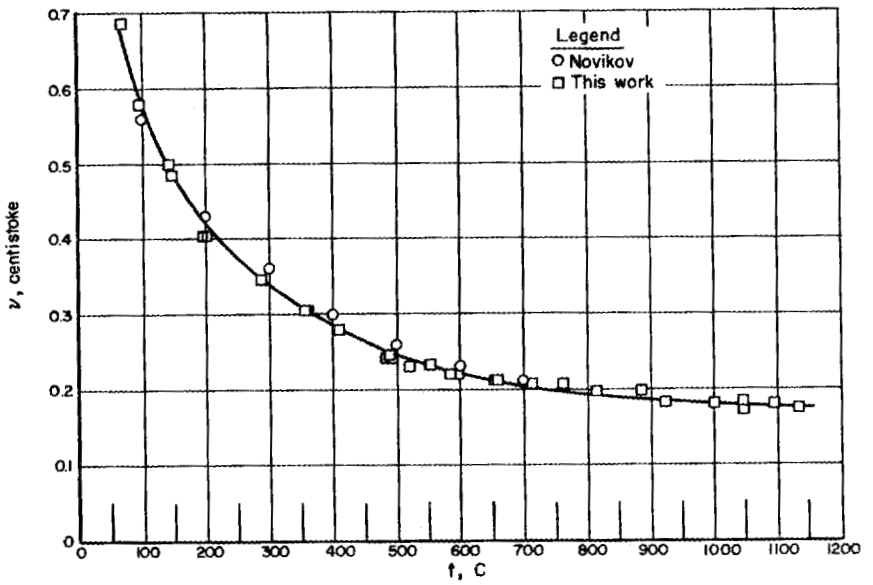

FIGURE 7. KINEMATIC VISCOSITY OF LIQUID POTASSIUM

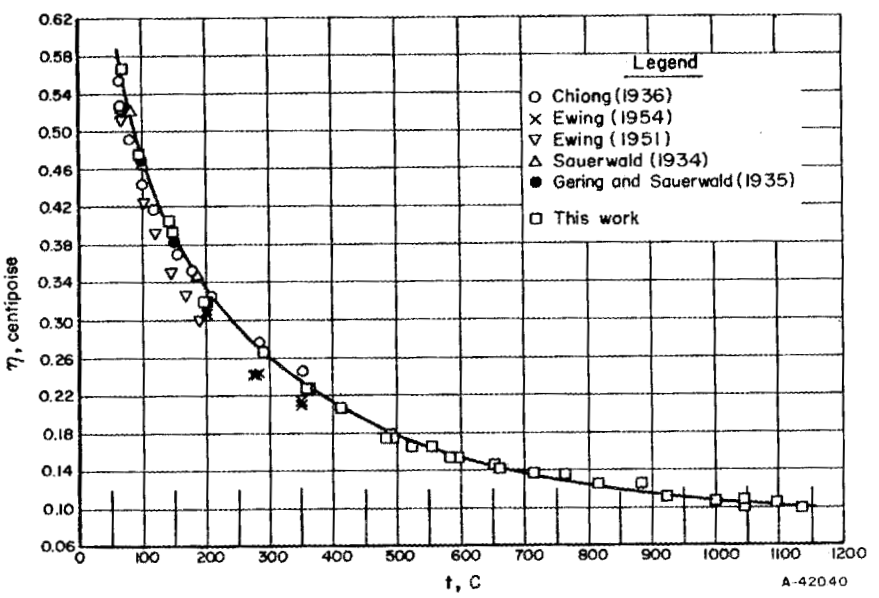

FIGURE 8. ABSOLUTE VISCOSITY OF LIQUID POTASSIUM

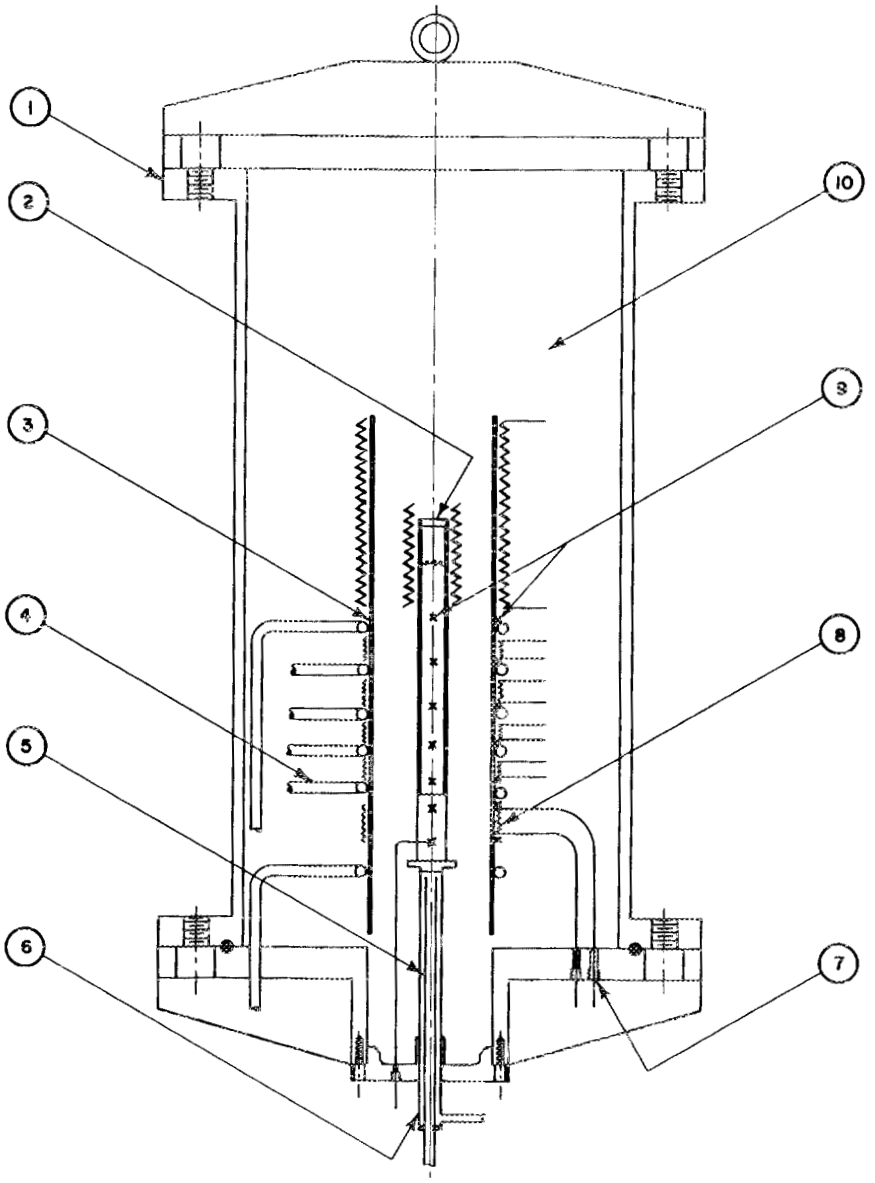

FIGURE 9. SCHEMATIC SKETCH OF THE LIQUID-THERMAL-CONDUCTIVITY APPARATUS

1. Pressure container
2. Specimen assembly
3. Guard assembly
4. Guard cooling coils
5. Specimen sink assembly
6. Sink inlet and outlet
7. Hermetic seals for heater leads and thermocouples
8. Heaters
9. Thermocouples
10. Insulation

DISCUSSION

MR. BERENSON: What were the major areas of disagreement in your H-S diagram relative to the Weatherford (1961) Report?

MR. LEMMON: Referring back to Figure 4, Weatherford's line for 100 per cent vapor did not have a decrease in enthalpy values at the higher temperatures as does the present plot. Also, the lines for other qualities do not curve down correspondingly.

MR. BERENSON: At what pressure does it start its major deviation?

MR. LEMMON: There are differences in all regions, but the major deviation starts at about 800°C, that is, at a pressure of about 1 atmosphere absolute.

MR. BERENSON: Is this figure available in a wall-sized chart?

MR. LEMMON: Yes; the original has a grid size of 12 by 20 inches.

MR. BERENSON: Are copies available?

MR. LEMMON: Yes. There will be a slightly larger chart in our topical report and, if you want one of the 12-by-20-inch size, please let me know.

MR. DAVIS: In the thermal conductivity measurements, are the thermal convection effects negligible?

MR. LEMMON: Yes; they are. If you refer to Figure 9, you will see that the cell containing the potassium had the heat introduced at the top and removed at the bottom. This technique eliminates any tendency for natural convection. Also, in the literature, there is much evidence, established by varying the geometry of the cell, that this technique gives reliable values not effected by thermal convection.

THERMOELECTRIC POTENTIALS OF MOLTEN AND REFRACTORY METALS.

I. Seebeck Potentials of Sodium, Potassium, Rubidium, Cesium, and Mercury vs. Platinum and other Metals.

by

Charles F. Bonilla
Roland R. Kyi
Howard T. Drue*
Do-Ik Lee

Liquid Metal Research Laboratory
Department of Chemical Engineering
Columbia University
New York, N. Y. 10027

*Present address:
Hydrocarbon Research, Inc., New York, N. Y.

INTRODUCTION

Though it is not generally recognized, all electrical conductors show thermoelectric effects. For instance, $NiSO_4$ solutions with nickel leads have a thermal EMF of about 0.89 millivolts per ^{o}C (1). Also, electrical insulators such as MgO show a thermal EMF when hot enough to conduct electricity (2). Even gases have thermoelectric properties when ionized; cesium plasma in direct conversion processes shows approximately 1.3 millivolts per ^{o}C (3).

APPLICATIONS OF LIQUID METAL THERMOELECTRICITY

It is obvious that liquid metals, which have an electrical conductivity close to that of the solid phase, must also have thermoelectric properties. In fact, instances have already been described in which liquid metal thermoelectricity has been used, or has been presumed, or would be useful.

The simplest applications are to quiescent bodies of molten metal. For instance, thermal contact resistance of mercury was measured in a vertical cylindrical plastic cell with a heated steel top plate and a cooled bottom plate (4). The temperature gradient in the mercury, and thus the heat velocity, were calculated from the thermal EMF measured between tiny iron wires passing through the side wall into the mercury, knowing the Hg/Fe thermoelectric power.

Thermoelectricity has also been utilized with flowing liquid metals. Natural convection flow paths in mercury enclosed between parallel vertical planes and heated at the bottom and cooled at the top have been traced with a fixed grid of closely spaced iron contacts (5), and turbulent temperature fluctuations in a pool of boiling mercury have been measured by movable sheathed probe wires (6). Also the radial Δt across an annular stream of sodium can be measured by sheathed wires connected to the annulus walls, to give the temperature of the inner wall from that of the outer wall, separately measured by a standard external thermocouple (7).

Another field is the direct measurement of film heat transfer temperature difference. A mercury-filled capillary touching mercury condensing on a steel pipe, and with steel wire leads to the vapor end of the mercury in the capillary and to the pipe directly, gave the mercury condensing film Δt (8). Stainless steel wires attached to the outside of a heated stainless steel boiling surface and to adjacent unheated surface gave the nucleate boiling Δt of NaK in a loop (9) and that of Rb and K in pool boilers (10).

A number of practical applications have also been proposed. Substantial thermal EMFs can, of course, be observed across liquid metal heat exchangers in operation (11). Such voltages could be used, after calibration, for flow or temperature indi-

cation or control. Since the internal resistance would be very low, heavy external currents can be drawn, and direct-conversion liquid-metal-cooled nuclear reactors of this type have been proposed (12). Also, the heavy internal circulating currents in liquid metals in heat exchangers or nuclear reactors, when combined with an external magnetic field, have been considered as a self-driving EM pump (13), and even simultaneously as a control to develop uniform coolant outlet temperature (14). A boiling indicator for liquid-metal-cooled reactors, based on the increase in thermoelectric noise when boiling initiates, has also been described (15, 16).

It should also be pointed out that when heavy direct current is deliberately passed through a solid/liquid metal interface, as in some heat transfer experiments (17), the resultant Peltier localized heating or cooling of the interface might affect nearby thermocouples, more so the higher the current and thus the lower the voltage. The Thomsen heating or cooling due to current flowing along a temperature gradient in a single metal (18) might also cause an appreciable error in the calculated heating at low voltages.

In spite of the many applications of liquid metal thermoelectricity potential, no thermal EMF data could be located in the open literature, apart from several early studies on mercury (19) and on other liquid metals (20) at relatively low tem-

peratures. In addition, the early work disagrees considerably with the present results based on current commercially pure metals, since evidently such purities were not abailable then. In view of the expanding applicability of such data in this and other laboratories, a continuing program in this direction has been carried out on mercury (21) and on the alkali metals (22, 23).

THERMOELECTRIC POTENTIAL AND THERMOELECTRIC POWER

The total thermal EMF, thermo EMF or thermoelectric potential of a thermocouple employing metals A and B is designated E_{AB}. A positive sign indicates that the (positive) current generated would flow from A to B through the cold junction, and a negative sign indicates the reverse direction. Unless otherwise stated, the cold junction temperature, t_0, is taken as $0^{\circ}C$. E_{AB} is known as the Seebeck EMF, and when measured with a potentiometer and plotted vs. the hot junction temperature, t, constitutes the calibration curve, which serves to give t in the usual manner from the observed E_{AB}.

The slope of E_{AB} vs. t, $d(E_{AB})/dt$, is known as the "Seebeck coefficient" or the "thermoelectric power" of the thermocouple, also designated ϵ_{AB}. Knowing ϵ_{AB} as a point function of t facilitates the direct conversion of small observed differential thermocouple voltages ΔE_{AB} to the temperature differences causing them. The use of differential thermocouples and their interpretation in this manner is particularly convenient in liquid metal heat transfer, due to the small temperature differences attainable, and

specially so if the liquid metal can be used as the intermediate metal, since then the errors or uncertainties of hot junction location are avoided, or at least minimized.

THERMAL EMF OF SOLID METALS

A Pt/Pt, 10% Rh thermocouple was employed for measuring all hot junction temperatures. It showed a deviation of 0.14 to 0.26% from a Bureau of Standards calibrated thermocouple; 0.20% was applied as a correction.

Annealed wires of several alloys used in the fabrication of liquid metal loops were also connected thermally and electrically to the hot junction, to provide thermoelectric data for converting liquid metal calibrations from one solid metal to another. An ice bath was employed for the cold junction, and the voltage was read on a L. and N. Portable Precision Potentiometer. Experimental points were obtained up to about 800°C. They were then plotted, for greater accuracy, as E/t vs. t, interpolated at even temperatures, and multiplied by t to obtain E. Table I gives the voltages obtained vs. platinum, with extrapolations to 900°C. Considering that these metals are available from many manufacturers, and not made to extremely precise compositions or tempers, these calibrations will probably not be exactly duplicated by other samples, and should best be verified in each case, at least at one hot junction temperature. However, for most of the alloys, they would be expected to hold within possibly 1 or 2%, as no critical factor in composition

would be anticipated due to its large difference from any pure component. This is seen by comparing the thermal EMFs of 304 and 316 stainless steels, which differ by less than 8% at any temperature, in spite of a composition difference of some 4% in Ni and 2% in Mo. Also, the thermal EMFs tabulated by Weber (24) for "18-8 Stainless Steel" are fairly close to the 304 values at 300^0C and higher. The thermal EMFs of Chromel P, Alumel, and some other alloys vs. platinum are also available (24, 25).

TABLE I

THERMOELECTRIC POTENTIALS OF SOLID METALS IN MILLIVOLTS WITH RESPECT TO PLATINUM (23)

Temp. (°C)	Pt/Ni* (low C)	Pt/Ni ("A")	304 SS/Pt	316** SS/Pt	L-605*** /Pt	Fe/Pt (25)	Mo/Pt ****
25	.390	.378	.095	.093	.176	0.444	.218
50	.729	.749	.196	.200	.365	0.885	.529
75	1.088	1.098	.320	.326	.580	1.323	.862
100	1.480	1.435	.455	.464	.814	1.754	1.203
125	1.875	1.768	.595	.615	1.063	2.174	1.581
150	2.283	2.089	.746	.774	1.328	2.579	1.985
175	2.695	2.407	.901	.945	1.612	2.972	2.422
200	3.105	2.714	1.066	1.124	1.910	3.346	2.892
225	3.508	3.015	1.238	1.310	2.216	3.697	3.404
250	3.905	3.305	1.420	1.500	2.525	4.033	3.945
275	4.276	3.595	1.603	1.702	2.888	4.352	4.491
300	4.620	3.873	1.797	1.914	3.210	4.656	5.046
325	4.911	4.144	1.999	2.132	3.569	4.943	5.642
350	5.145	4.417	2.198	2.359	3.938	5.219	6.251
375	5.318	4.677	2.411	2.599	4.316	5.479	6.926
400	5.472	4.924	2.636	2.844	4.708	5.720	7.616
425	5.640	5.168	2.865	3.094	5.100	5.950	8.279
450	5.796	5.404	3.101	3.362	5.504	6.183	8.973
475	5.971	5.639	3.339	3.634	5.914	6.422	9.680
500	6.150	5.855	3.595	3.915	6.340	6.655	10.435
525	6.342	6.075	3.848	4.205	6.778	6.904	11.109
550	6.523	6.281	4.114	4.505	7.227	7.161	12.023
575	6.705	6.481	4.387	4.813	7.682	7.429	12.857
600	6.882	6.672	4.668	5.118	8.154	7.710	13.722
625	7.100	6.847	4.966	5.444	8.625	8.000	14.569
650	7.319	7.020	5.265	5.779	9.113	8.333	15.431
675	7.540	7.176	5.582	6.122	9.605	8.687	16.321
700	7.784	7.315	5.915	6.482	10.115	9.058	17.220
725	8.02	7.439	6.264	6.851	10.621	9.454	18.116
750	8.25	7.560	6.615	7.230	11.138	9.870	19.008
775	8.48	7.673	6.975	7.626	11.672	10.292	20.079
800	8.72	7.768	7.352	8.008	12.216	10.744	21.064
825	8.97	7.854	7.739	8.415	12.771	11.220	22.075
850	9.23	7.922	8.143	8.832	13.345	11.662	23.070
875	9.48	7.989	8.549	9.258	13.913	12.084	24.138
900	9.72	8.037	8.973	9.693	14.490	12.483	25.218

Notes: Cold junction is at 0°C. First-named metal is positive at the cold junction when EMFs are listed as positive.

*High-purity low-carbon nickel (Ni 99.8% min, C 0.03% max).

**Cr 17.91, Ni 12.8, Mo 2.4, Mn 1.91, Si 0.46, C 0.05, P 0.014, S 0.009.

***L-605 is also known as Haynes-25. ****Standard pure Mo(99.9+%).

It should be noted that all solid metals are not necessarily desirable as thermocouple elements over their full temperature ranges. For instance, the phase changes of iron above 775°C (20), and of nickel and its alloys near 300°C, can cause some variability in the Seebeck potential, and large changes in the thermoelectric power over certain ranges. Also, some of them show a "neutral temperature" range over which dE/dt approaches zero, and they are useless (e.g., Fe/304SS from 300 to 700°C and Cs/316SS from 100 to 300°C). However, the use of such metals in thermocouples with liquid or other solid metals may be unavoidable. In general, fair accuracy can be obtained, and high accuracy over tested ranges, making such thermocouples preferable in many applications to the insertion of standard but extraneous thermocouples.

The thermoelectric powers dE/dt of the thermocouples in Table I have not been tabulated, but can be calculated with adequate accuracy for most cases by differencing successive values of E in the table.

THERMAL EMF OF MERCURY

For measuring the small temperature differences in the mercury wetting and heat transfer studies previously mentioned (4, 5, 8), the thermoelectric power of mercury vs. iron, nickel, and 304 stainless steel was required. The published data of Oosterhius vs. iron (19) only reach 283°C. Furthermore, a rough check showed

these thermal EMFs are too low for presently employed materials. For these reasons a mercury thermal EMF program was carried out.

Initially it was attempted to measure ΔE directly for small temperature differentials. A wide, 2 mm. I.D. fused-quartz U-tube was installed with each leg rising through a vertical tube-furnace. The U-tube was filled to the middle of each furnace with virgin triple-distilled mercury (99.95% average purity), and a thermocouple-grade iron wire was passed down each leg to the mercury surface. However, it proved difficult to obtain and to measure small temperature differences between the furnaces, and to obtain consistent thermal EMFs. In the final apparatus, one of the furnaces was replaced by an ice bath and the other by a boiling chamber and reflux condenser. In the boiling chamber, the following liquids (with their normal boiling points) were employed: water (100°C), naphthalene (217.96°C), benzophenone (305.9°C), and mercury (353.36°C). The barometric pressure was noted during each test and the appropriate boiling point correction applied. The data obtained are given in Table II.

A power equation of the form: $E = at + bt^2 + ct^3$ was fitted to the four points by Least Squares, employing multiple regression of (E/t) against t and t^2. The following equation was obtained:

$$E = 0.019948t - 1.525 \times 10^{-5}t^2 + 4.88 \times 10^{-9}t^3 \qquad (1)$$

for E in millivolts and t in °C, with the cold junction at 0°C, and Fe+. This equation lies about 10% above Oosterhius' data (v.

Table II). Calculated values are listed in Table III.

Published data on the thermal EMF of his iron wire vs. platinum (26) disagree considerably with Table I, and it must be presumed that iron wire of present purity was not then available. But the Fe/Pt disagreement is greater than the Hg/Fe thermal EMF disagreement between his and present results. Thus it would seem that, in addition, his mercury did not match the present normal purity.

To compute the thermoelectric EMF of mercury with respect to other metals, their EMFs vs. platinum and that of iron vs. platinum from Table I, etc. can be combined algebraically, e.g.,

$$E_{Hg/304} = E_{Hg/Fe} + E_{Fe/Pt} + E_{Pt/304} \quad . \qquad (2)$$

For instance, at 300°C,

$$E_{Hg/304} = -4.744 + 4.850 - 1.797 = -1.691 \text{ mv}$$

(the negative sign indicates that the mercury is negative at the cold junction).

In addition, the thermal EMF of sodium amalgam of 0.058 weight % Na was measured to 375°C vs. iron. The EMF values average some 2% below the Hg/Fe values of Table II, the deviation agreeing roughly per unit contained Na with published thermal EMFs for several times higher Na concentrations (20). Evidently small traces of wetting agents added to mercury will not greatly affect the thermal EMF, and can be calibrated if desired.

TABLE II

THERMOELECTRIC POTENTIAL OF MERCURY-IRON WITH COLD JUNCTION AT $0^{\circ}C$ (21,22)

Liquid	Corrected Boiling Pt.	Observed Potential	Calculated (Equation 1)	Deviation, % lower	Oosterhius Equation(19)	Oosterhius, % lower
	($^{\circ}C$)	(mv.)	(mv.)	(vs. obs'd)	(mv.)	(vs. obs'd)
Water	99.78	1.842	1.8434	-0.08	1.620	12.0
Naphthalene	216.86	3.672	3.6586	+0.37	3.287	10.5
Benzophenone	305.63	4.781	4.8117	-0.64	4.336	9.3
Mercury	353.36	5.379	5.3602	+0.35	4.805	10.7

THERMAL EMF OF ALKALI METALS

Procedure

In view of the reduction of silica by alkali metals, particularly at the higher temperatures of interest, a different type of cell was employed than with mercury. A thin-walled 316 stainless steel tube was sealed shut at one end. Then a slightly shorter, open-ended fairly well-fitting liner of fused quartz or alumina (G.E. Lumalox) was inserted. The tube was then approximately 3/4 filled under argon with the desired alkali metal, which rose both inside and outside of the sleeve, but not to the top. The tube was then sealed off with a rubber stopper varnished in place with Glyptal. Annealed 316 SS wire to serve as one of the thermocouple leads entered through thestopper and dipped slightly into the alkali metal. Another identical wire was bound to the bottom of the SS tube, along with the hot junction of a calibrated Pt-Pt 10 Rh thermocouple.

In operation, the bottom end of the tube was placed near the center of a vertical tubular furnace and the top end rose through an ice bath. The stainless steel wires went to standard ice-cold junctions and thence via copper leads to a potentiometer, where the thermal EMF was read. Although the upper end was the colder one, no voltage fluctuations, such as would be caused by the instabilities of natural convection, were ever observed, no doubt due to suppression of convection by the relatively small diameter (large L/D).

When a Lucalox liner was employed, the hot end could be taken to high temperatures without significant corrosion, as shown by

subsequent falling thermal EMFs agreeing with the initial rising thermal EMFs. However, with SiO_2 liners the maximum temperature employed was 350°C, as corrosion of the liner and thermal EMF deviations were anticipated at higher temperatures.

When higher temperatures were required, an additional 316 stainless steel tube of the same size and gauge, but without insulating liner, was also prepared, and 3/4 filled, as before, with the alkali metal. In this case, however, the top of the tube was pinched and welded shut, instead of using a rubber stopper. The two stainless-steel wires were attached on the outside at the bottom, as before, and just below the liquid level near the top.

Thermal EMFs obtained with an insulating liner were generally plotted as (E/t) vs. t, as before, and values of (E/t), thence E, interpolated at 25°C intervals. However, E values for cesium reached a maximum and reversed, so that direct plotting of E vs. t was preferable, and was used. The results are given in Table III, after correction to platinum with the E for 316 SS vs. Pt from Table I.

When an insulating liner was not used to the maximum temperature, E for the unlined tube was obtained by interpolation of E or (E/t), as above. Then in addition, the ratio of the EMF with the liner divided by the EMF without the liner was plotted against temperature and extrapolated to the desired maximum temperature. This "short-circuiting ratio" was found to be sufficiently independent of temperature, as anticipated, that little error would be

TABLE III

THERMOELECTRIC POTENTIALS OF LIQUID METALS IN MILLIVOLTS WITH RESPECT TO PLATINUM (23)

Temp. (°C)	Pt/Hg*	Pt/Na	Pt/K	Pt/Cs	Pt/Rb
25	0.045	0.029	0.183	0.183	0.061
50	0.079	0.053	0.368	0.382	0.110
75	0.089	0.070	0.563	0.598	0.146
100	0.093	0.084	0.736	0.825	0.179
125	0.091	0.094	0.926	1.063	0.214
150	0.087	0.109	1.124	1.298	0.264
175	0.078	0.122	1.327	1.517	0.324
200	0.073	0.136	1.536	1.720	0.396
225	0.075	0.153	1.753	1.906	0.479
250	0.077	0.175	1.988	2.005	0.575
275	0.082	0.202	2.221	2.198	0.683
300	0.088	0.226	2.466	2.342	0.816
325	0.097	0.263	2.727	2.478	0.972
350	0.104	0.301	3.028	2.593	1.138
375	0.115	0.341	3.337	2.694	1.310
400	0.132	0.390	3.666	2.764	1.494
425	0.148	0.446	4.008	2.819	1.684
450	0.151	0.497	4.360	2.857	1.868
475	0.136	0.551	4.717	2.872	2.066
500	0.117	0.615	5.075	2.871	2.285
525		0.699	5.439	2.866	2.505
550		0.789	5.824	2.854	2.735
575		0.888	6.204	2.839	2.962
600		0.996	6.624	2.818	3.207
625		1.110	7.031	2.805	3.456
650		1.225	7.455	2.801	3.711
675		1.350	7.884	2.803	3.968
700		1.470	8.316	2.822	4.238
725		1.591	8.758	2.850	4.519
750		1.731	9.218	2.885	4.805
775		1.856	9.672		
800		2.016	10.168		
825		2.173	10.643		
850		2.316	11.143		
875		2.461	11.637		
900		2.629	12.150		

Notes: Cold junction is at 0°C. Platinum is positive at the cold junction in all cases.

*Equation 1 minus $E_{Fe/Pt}$ from Table I.

expected in its extrapolation. E interpolated for the unlined tube at any high temperature, multiplied by the extrapolated short-circuiting ratio at that t, gave the corrected or true E.

Potassium: Triple-distilled potassium was run from 372° to 807°C in a SS 316 tube with a 0.21 in. ID Lucalox liner, then from 339° down to 138°C. (E/t) plotted straight against t above 460°C, and the ascending and descending portions below 460° merged well, though not entirely straight. Thus, there is no evidence of corrosion of the Al_2O_3 at these temperatures.

In addition, earlier tests were run (23) on MSA Research commercial 98+% potassium (v. Table IV) to 300°C in a 56 inch x 0.5 inch OD x 0.035 inch wall 316 SS tube with a 53 inch x 10 mm OD x 1 mm wall quartz liner, and to 800°C in a similar empty 316 SS tube. The short-circuiting ratio up to 300°C was substantially constant at 3.94 (average deviation 0.015). The unlined tube data when multiplied by this ratio gave SS 316/K thermal EMFs that averaged well within 1% of the Lucalox data over their whole range, evidently verifying the latter, as well as indicating that normal impurities in commercially pure potassium don't affect the thermal EMF significantly.

The prior published data of Bidwell (20) extend only to 300°C, and are not claimed to be reliable at low temperatures (presumably below the melting point). For differential couples Pt/K/Pt at 200/100°C and 300/100°C they showed the correct polarity, but only about 2/3 of the magnitude from Table III. They were reported in 1914-1924, and purity of the materials seems doubtful.

Table IV

METALLIC IMPURITIES IN PPM IN ALKALI METALS EMPLOYED (23)

Impurity	Potassium (MSAR)	Cesium (Dow)	Rubidium (MSAR)
Ba	10	8	
Si	10	29	
Ca	5	10	
Fe	1	6	
Cr	1	2	
Mn	1	2	
Mg	5	2	
Pb	4	2	
Al	2	5	
Be	1		
Mo	1		
Sn	1		
V	2		
Cu	3	2	
Ag	1		
Ti	10		
Co	5		
Ni	2	2	
N	1		
Cs		(99.5+%)	7000
K	(98+%)	16	1000
Na		16	100
Li		16	70
Rb		116	(99%)
B		16	
Tl		2	
Sr		2	

Rubidium: MSA Research commercial 99% rubidium (v. Table IV) was run (23) to 356°C in a 56 inch x 0.5 inch OD x 0.035 inch wall 316 SS tube with a 53 inch x 10 mm OD x 1 mm wall silica liner and to 732°C in a similar unlined tube. The unlined tube (E/t) plotted vs. t with a maximum deviation of 1% from a straight line having a slight bend at about 500°C. The short-circuiting ratio showed a minimum value at 1.271, rising apparently assymptotically to 1.303 at 400°C. The higher temperature unlined tube data were thus multiplied by 1.303.

The Bidwell equation (20) yields the same polarity, but very close to 3 times the magnitude for the differential EMF of Pt/Rb/Pt at 200/100 and 300/100°C.

Cesium: Dow commercial 99.5+% cesium (v. Table IV) was run to 329°C in a 36 inch x 0.3125 inch OD x 0.020 inch wall 316 SS tube with a 6 mm OD x 1 mm wall SiO_2 sleeve 34 inch long (23). The intermediate temperature runs (136 to 219°C) were carried out afte r the lowest and highest temperatures had been run, and gave full agreement, showing that no significant corrosion of the SiO_2 had occurred. A similar unlined tube was run up to 622°C, then back down. Higher temperatures were not employed because they caused boiling, presumably due to insufficient pressurization with argon before sealing.

The short-circuiting ratio rose close to linearly from 1.129 at 200°C to 1.147 at 350°C. However, it was fairly constant at about 1.200 from 50 to 150°C. Thus, the average figure of 1.17

was employed as the multiplier for the unlined tube data.

Cs/SS 316 shows a thermal EMF maximum at about 210°C, dropping off to zero at 389°C and reversing thereafter. Accordingly, (E/t) plots were not employed. The Bidwell equations (20) yielded differential Pt/Cs/Pt thermal EMFs some 7% low at 200/100°C, and 23% low at 300/100°C, for the best agreement of any alkali metal.

Sodium: Subsequent to the work with the other liquid metals (21-23), triple-distilled Sodium was run in a SS 316 tube with a 0.21 in. ID Lucalox liner from room temperature up to 699°C. Temperatures from 100 to 272°C were then repeated, showing close agreement with the earlier low temperature points, and lack of corrosion of the Al_2O_3 by the Na. The thermal EMFs in Table III up through 700°C were obtained by (E/t) interpolation of these data. Another SS 316 tube without a liner was carried to 879°C and (E/t) similarly obtained to 900°C at 25°C intervals. The short-circuiting ratio from 450 to 700°C plotted smoothly from 1.037 to 1.065 and was extrapolated to 1.076 at 900°C, yielding with the unlined tube data the higher values in Table III.

Bidwell's equation (20) shows an incorrect polarity for the Pt/Na/Pt differential couple at 200/100°C, and correct polarity but 40% too high a value at 300/100°C.

ACKNOWLEDGEMENT

The work here-in described was carried out, as needed for other programs, over the period of 1951-1962. Assistance was

provided under AEC contracts AT(30-1)-1042 and AT(30-1)-2660 and under subcontract RD24-490 with Thompson-Ramo-Wooldridge, Inc. under U.S.Air Force contract AF 33(616)-7368.

The vitreous alumina "Lucalox" liner tubes were kindly provided by the General Electric Company, Lamp Glass Department, Cleveland, Ohio. The triple-distilled sodium and potassium were provided by Dr. L.F. Epstein of General Electric Company from Knolls Atomic Power Laboratory.

BIBLIOGRAPHY

(1) Carr, D.S. and Bonilla, C.F. J. Electrochem. Soc. 99, 475-482 (1952).

(2) Mansfield, R. Proc. Phys. Soc. 66B, 612-614 (1953).

(3) Pidd, R.W. et al. J. Appl. Phys. 30, 1861-1865 (1959).

(4) Bonilla, C.F. and Wang, S.J. U.S. Atomic Energy Comm. NYO-3091 (1952).

(5) Bonilla, C.F. and Wang, S.J. Unpublished report to Knolls Atomic Power Laboratory. "Natural Convection Heat Transfer in Narrow Vertical Liquid Metal Annuli" (Aug. 26, 1954).

(6) Wolkoff, J. Argonne National Laboratory. Internal memorandum ANL-LB-SL-2099 (Jan. 26, 1962).

(7) General Electric Co., Space Power and Propulsion Section, MSD. Quarterly Report No. 1, NASA contract NAS3-2528, p. 18 (July-Sept. 1962).

(8) Misra, B. and Bonilla, C.F. Chem. Engr. Prog. Symp. Ser. 52, No. 18, 7-21 (1956).

(9) Bonilla, C.F., Carreira, M., Gruet, I., and Luis, P. ANL-6507.

(10) Bonilla, C.F., Engelbrecht, J.C. ASD Technical Report 61-697 (1962); Engelbrecht, J.C., M.S. Thesis in Chemical Engineering, Columbia Univ. (1961).

(11) Brooks, R.D. Alplaus Project, Knolls Atomic Power Lab., General Electric Co. Personal communication (1954).

(12) Voorhees, B.G. Knolls Atomic Power Laboratory. Personal communication.

(13) Osterle, J.F. and Angrist, S.W. Amer.Soc.Mech.Engrs. Paper No. 63-HT-24 (Boston, 1963).

(14) Luebke, E.A. and Vandenberg, L.F. Proc. 1955 Conf. on Nuclear Engr., p. A-106. Univ. Cal. Los Angeles.

(15) Bonilla, C.F. and Madsen, N. Atomic Energy Comm. Patent Disclosure No.S-15,922 (May 24, 1957).

(16) Madsen, N. and Bonilla, C.F. Chem.Engr.Prog.Symp.Ser. 30 251-259 (1960).

(17) Noyes, R.C. "An Experimental Study of Pool Boiling of Sodium". Atomics International (Aug. 15, 1961).

(18) English, D. and Barrett, T. AERE E/R 547 (June 1950).

(19) Oosterhius, E. Arch.Neerland.Sci. IIIA. 2, 27-31 (1912).

(20) Caswell, A.E. International Critical Tables 6, 213-229. McGraw-Hill Book Co. (1929); Bradley, C.C., PhilMag. 7, 1337-47 (1962).

(21) Bonilla, C.F., Busch, J.S., Drue, H.T., and Misra, R. U.S. Atomic Energy Comm. NYO-3148 (1952).

(22) Drue, H.T., Bonilla, C.F. Unpublished study ;of thermal EMF of mercury, sodium and sodium amalgams. Dept.of Chem.Engg., Columbia University (1951-53).

(23) Kyi, Roland R.K. M.S. Thesis in Chemical Engineering, Columbia University (1962).

(24) Weber, R.L. "Heat and Temperature Measurement", 396-7. Prentice Hall (1950).

(25) Caldwell, F.R. "Temperature, Its Measurement and Control". 2nd Ed., Vol. 3, part 2, pp. 108,112. Reinhold Pub.Co. (1962).

(26) Alderink, M. Arch.Neerland.Sci. II, 15, 321 (1910).

DISCUSSION

MR. LYON: The fixed ratio which you got between the insulated and uninsulated tube, and the fact that that remained constant over a range of temperature, does that imply natural circulation effects were not a problem?

MR. BONILLA: I believe so, particularly since the internal diameters of the two tubes were different, and natural convection would have been expected to show up at different temperatures in the two tubes. But in addition, substantial lengths at each end would be isothermal, more or less, and might be expected to minimize the thermoelectric effect of a natural circulation that did occur; at least we obtained perfectly steady readings with the cold end on top. We tried it the other way, with the hot end on top, which we could use with the sealed cell; but we frequently obtained steadier readings with the cold end up, possibly related to freezing and shrinking of the alkali metal. Naturally, when you use ice, you have a liquid-to-solid interface in there somewhere. Also, boiling and its instability are less likely when the hot end is below, as the liquid head raises the boiling point.

MR. TEPPER: Dr. Bonilla, there is apparently a real inversion in the 316/cesium. Do you have any reason to suspect what caused this?

MR. BONILLA: It must merely be the nature of the beast! There is a very peculiar double inversion in the iron/stainless steel system, and over a region from about 300 to 700 centigrade you cannot use iron vs. stainless steel, because the potential is always about the same. We haven't gone into the theory of these thermal EMFs, but you do have to be careful with some of the metal pairs.

The 316 stainless/cesium one is interesting. The EMF rises to a maximum, then comes down and goes through zero, reversing in sign. However, with care it can still be used, except at the maximum. Near the point of zero voltage, you have to note the polarity, otherwise you don't know which temperature you have. Just off of the maximum, the direction of change of EMF with temperature would need to be determined, such as by briefly dropping the power.

MR. FISHER: Does your experience indicate how much the varying composition of stainless steel alloys from heat to heat will affect the cumulative potentials?

MR. BONILLA: We didn't make an exhaustive study of that, but we have had it in mind. There is certainly some effect. Weber lists 18-8 vs. platinum, without describing the 18-8. It deviates by several % from our own data on 304 stainless vs. platinum, though probably the difference in composition is small.

On the other hand, the 304 and the 316 data that we obtained deviate throughout by less than 10%, even though there are substantial changes in composition. So our general belief is that it is not appropriate to attach high reproducibility to results with these alloys, because both the composition and the temper are not necessary controlled. On the other hand, one could rely on these tables for approximate results with any alloys of the same general composition. Tiny traces of impurities in a pure material seem to be much more important than substantial variations in principal ingredients of alloys.

Comparing our mercury results with those of Oosterhius, it seems that tiny traces of impurities in the mercury must have made a large difference in thermal EMF. The thermal EMF of Oosterhius' iron versus platinum is quite different from that of present thermocouple iron, but after applying that correction, there is still a big difference between his and our Hg/Fe EMFs. It must be in the mercury.

REPORT ON HIGH TEMPERATURE LIQUID METAL HEAT TRANSFER RESEARCH AT GEOSCIENCE LTD.

By H. F. Poppendiek and N. D. Greene

INTRODUCTION

The high temperature liquid metal heat transfer research at Geoscience Ltd. is being conducted for the Atomic Energy Commission. The studies consist of analytical and experimental liquid metal boiling and condensing with emphasis on high gravity or rotational flow. Both mercury and potassium are being investigated. From the research results, design correlations and criteria are being developed so that nuclear reactor and heat exchanger performance can be predicted. The associated problems of the influence of coolant void perturbations on neutron and heat flux as well as the effect of boiler tube wall temperature fluctuations on metal fatigue are also being considered. F. R. MacDonald, C. M. Sabin, A. S. Thompson and R. K. Livett are also participating in the research program.

During the past year, 1) boiling and condensing heat and momentum transfer models have been analyzed, 2) a liquid metal heat transfer facility has been fabricated, 3) two supplementary heat transfer apparatuses have been constructed, 4) experimental boiling and condensing measurements have been made and, 5) experimental results are being compared to predictions.

RESEARCH PROGRAM

There are a number of different forced flow boiling regimes depending upon such parameters as quantity, mass flow rate and gravity field. One regime of interest is that of slug flow. An investigation of this type of boiling process has yielded information on the temperature fluctuations in the wall of a boiler tube as alternate slugs of vapor and liquid flow through it. It is postulated that the boiler tube has thermal capacity, zero thermal resistance in the radial direction and infinite thermal resistance in the axial direction. The thermal resistance of the fluid is cyclic (see Figure 1), and the mixed-mean fluid temperature is postulated to be a constant saturation temperature. The differential and boundary equations which define the transient heat transfer at a given station along the tube are,

$$q_s = C \frac{dt}{d\theta} + \frac{t}{R_1} \quad \text{for } 0 < \theta < \theta_1, \tag{1}$$

$$q_s = C \frac{dt}{d\theta} + \frac{t}{R_2} \quad \text{for } \theta_1 < \theta < \theta_2 . \tag{2}$$

$$t\ (\theta = 0) = t(\theta = \theta_2) \tag{3}$$

$$q_s\ \theta_2 = \int_0^{\theta_1} \frac{t(\theta)}{R_1}\, d\theta + \int_{\theta_1}^{\theta_2} \frac{t(\theta)}{R_2}\, d\theta \tag{4}$$

The solutions for the boiler tube wall temperature at the beginning of the cycle and the mean wall temperature during the cycle have been derived (reference 1). The difference between these two temperatures is the amplitude of the wall temperature fluctuation. This solution has been used to calculate wall temperature fluctuations in boiler tubes under representative slug flow conditions. The temperature fluctuations were found to be significant only in the low quality region where vapor and liquid slug

lengths were equal or nearly equal. In the other regions, that is, at the entrance of the boiler or downstream in the higher quality regions, heat transfer is controlled by one or the other of the two phases thus yielding very small temperature fluctuations.

A number of researchers have considered heat transfer to drops and in fog flow (see for example, references 2 and 3). Droplet and fog flow heat transfer models which can be used to establish the important parameters and mechanisms are being studied (reference 4). Consider the case of a droplet evaporating from a hot surface. For simplicity, it is postulated that the drop shape is a disk (see Figure 2). The wall temperature is uniform and the droplet temperature is equal to the saturation temperature. Heat is added to the droplet by conduction through the issuing vapor film between the droplet and the boiler tube wall. The vapor film thickness and mass flow rate are unknowns. The use of several physical relations are required to obtain a solution to the problem. Evaporative heat transfer is equated to heat conduction through the film. The weight of the drop is set equal to the integral of the pressure and area under the drop. The pressure under the drop is obtained from the conventional pressure drop equation; however, a variable vapor velocity with radial distance under the drop (as a result of mass addition with radius) is included in the analysis. Simultaneous solutions of these equations yield expressions for the vapor film thickness and mass flow rate. Further, upon equating the mass flow rate to the derivative of the drop weight with respect to time, one can obtain an expression for the droplet vaporization lifetime. The equations describing vapor film thickness and vapor lifetime are

$$\frac{\bar{\delta}}{r_d} = \left(\frac{\zeta}{80}\right)^{1/5} \left(\frac{k_v(t_w - t_s)}{\delta_d^{1/2}\, r_d\, L\, \rho_v^{1/2}\, \rho_\ell^{1/2}\, a^{3/2}}\right)^{2/5} \tag{5}$$

$$\theta_\ell = \frac{30\ \zeta^{1/5}}{7(160)^{1/5}}\ \frac{\gamma_\ell^{4/5}\ L^{3/5}\ r_{d_o}^{7/5}}{\gamma_v^{1/5}(t_w - t_s)^{3/5}\ k_v^{3/5}\ a^{1/5}} \tag{6}$$

Note that as the gravitational field increases, both the film thickness and drop lifetime decreases thereby increasing the heat transfer to the drop. As the gravitational field increases, the droplet population increases at the wall and the total heat transfer is further increased. Figure 3 shows a comparison of experimental lifetimes of water droplets with predicted values. The experimental data were obtained by observing droplet vaporization on a hot plate containing an embedded thermocouple. The experimental water data fall approximately 25% above predicted values. Only limited droplet lifetime measurements for mercury have been made. However, these experimental lifetimes appear to be falling approximately 20% below the predicted values.

Some researchers have suggested that as a drop collides with the heat transfer surface in a boiler tube, the drop is completely vaporized and this process is the prime heat transfer mechanism. After observing many liquid droplets evaporating on a hot plate, it is thought that total vaporization on impact is not completely dominant. It seems probable that droplet evaporation takes place at all radial positions in the fluid; there is no doubt, however, that evaporation is greater near the wall than in the core region of the fluid. Therefore, heat transfer in fog flow can be thought of as forced convection with a volume heat sink. The equations that define the model are,

$$u \frac{\partial t}{\partial x} = \frac{\partial}{\partial r}\left[(a + \epsilon)\, r \frac{\partial t}{\partial r}\right] - \frac{Sr}{\gamma c_p} \tag{7}$$

$$\frac{dq}{dA}(r = r_o) = \left(\frac{dq}{dA}\right)_o \tag{8}$$

$$t_d = t_m \tag{9}$$

where,

$$S = \frac{3 \gamma c_p \epsilon (t - t_s)}{r_o^2 \left(\frac{r_c}{r_o}\right)^3 \left(\frac{r_o}{r_d} - \frac{r_o}{r_c}\right)} \tag{10}$$

The heat sink, S, is defined by a number of postulates. A droplet is surrounded by a region of influence called a cell. Within the cell heat is transferred from the superheated gas at the outer region of the cell to the saturated liquid drop; heat is transferred by an eddy transport process when the cell is located in the turbulent core of the pipe and by conduction when the cell is located near the heat transfer wall. Simultaneous with the heat transfer process, mass is transferred from the droplet surface to the outer regions of the cell by diffusion. A heat transfer analysis of this idealized energy transfer process yields an expression for the heat sink given in Equation 10. The quantity r_d is the drop radius, r_c is the cell radius and r_o is the pipe radius. Note that the heat sink is proportional to an eddy diffusivity and the local superheat and inversely proportional to the cube of the ratio of cell radius to pipe radius and the first power of the ratio of the pipe radius to the drop radius. Figure 4 shows calculated wall and centerline temperature differences as a function of quality for specific conditions shown in the graph; a uniform volume heat sink with radius was postulated. Note the rapid increase in the radial temperature differences in the quality region 0.8 to 1.0. The radial temperature difference at a quality of unity is the gaseous convection value. The droplet radii used in these calculations are uniquely determined by the relation between quality and the liquid-vapor fraction. Figure 5 depicts some experimental boiling heat transfer measurements in Geoscience's high quality boiling heat transfer apparatus for the case of boiling water in linear flow. Note that the functional relation between quality and wall-fluid temperature difference is similar to that predicted in the previous example.

Figure 6 shows a photograph of atomized water droplets in air simulating the case of high quality linear fog flow. The Tyndall effect was used in obtaining the photographs. Figure 6 indicates uniform droplet distribution with radius. The photograph in Figure 7 shows helical fog flow (pitch diameter ratio of 2); the gravitation field has forced the droplets into an annulus contiguous to the tube wall. The consequence of this process is to increase the droplet population in the fluid layers contiguous to the wall thereby increasing the heat sink and the fog flow heat transfer. The result of this effect is demonstrated in a later Figure depicting experimental boiling heat transfer under rotational flow conditions.

The velocity decay of thin, unconstrained, rotating, liquid layers in a stationary tube has been studied. Figure 8 depicts the rotational flow decay model. A turbulent liquid layer is separated from the wall by a viscous vapor film. A momentum transfer analysis has been made which yields a solution for the normalized tangential Reynolds number of the liquid layer as a function of dimensionless decay time, ϕ, and a new parameter C which is a function of the liquid and vapor thicknesses and viscosities. The results of the analysis are shown in Figure 9. Note that as the vapor film thicknesses develop, the decay times increase. It is felt that the results of this analysis will be useful in designing rotational flow guide vanes for high quality regions of boiler tubes.

Calculations have been made of the changes in neutron and heat flux in local regions of idealized nuclear reactors as a result of local coolant density perturbations. Details of this work can be found in reference (4).

Geoscience has constructed and operated two experimental, liquid metal systems to obtain heat and momentum transfer data in both linear and rotational flow boiling. To date, both systems have been used to obtain boiling mercury and water heat transfer data which permit preliminary comparisons to be drawn between linear and rotational flow boiling in both the high and low vapor quality regions.

The system in which the low vapor quality boiling mercury measurements have been made is constructed entirely of tantalum and is capable of operating at 300 psig. The system has been designed to operate a maximum power input of 25 kw. It is also estimated that several hundred degrees of potassium vapor superheat could be attained in this system. A schematic diagram of the tantalum system is shown in Figure 10. The liquid metal flow is accomplished by pressurizing a tantalum-lined reservoir with argon gas. The mercury coolant is forced successively through a vacuum containment vessel, a resistance heated preheater, a boiler section whose walls are instrumented with thermocouples, a separator in which the vapor is removed from the unvaporized fraction, a subcooler with tank, and a condenser having a similar tank.

Presented in Figure 11 is a partial view of the assembled, tantalum heat transfer system. The high temperature components such as the preheater, boiler and vapor separator are enclosed in the containment chamber shown in the center of the photograph.

The load cell instrumentation, from which the tanks are suspended, yields the weight-time variation of mercury.

The thick wall boiler is schematically pictured in Figure 12. In the first series of experiments, this test section was used to obtain low vapor quality boiling mercury heat transfer conductances. The tantalum sheathed thermocouples are embedded longitudinally in the tubular heating surface to negate possible radial conduction errors. To insure uniform circumferential wall temperatures, the boiler tube was constructed by plasma-spraying with tantalum to a depth of about 0.30 inches. Approximately 0.01 inches of plasma-sprayed alumina provided both electrical insulation for the heating elements and a thermal bond as shown.

Subsequent to the final system assembly and prior to cleaning, a series of measurements of heat transfer conductances to ordinary water were conducted. The results of a typical measurement at a Reynolds number of 25,600 are shown in Figure 13 (reference 1). The experimental Nusselt numbers were found to be in good agreement with the literature values. These measurements were made to obtain additional verification of system accuracy, response and integrity.

Some typical low vapor quality, linear flow, boiling mercury heat transfer data are shown in Figure 14. The sudden wall temperature rise which occurred during a small increase in heat flux may be attributed to the transition from nucleate boiling to film boiling.

Figure 15 indicates some representative heat transfer results for helically flowing, boiling mercury. The coolant flow rates and heat fluxes are approximately similar to the data in Figure 14, but it is now noted that the peak wall temperatures are materially lower. The differences between minimum and maximum wall temperatures for the helical flow experiments are less than half the corresponding values measured in linear flow.

A comparison is made in Figure 16 between one linear flow and two helical flow wall temperature distributions for similar conditions of heat flux and flow rate. The ΔT (°F) denotes the difference between the wall and saturation temperatures. It is of interest, particularly, to compare wall temperatures in run No. 43 at a total flow rate

of 60 lb/hr with corresponding values in run No. 22, where the flow rate was 50% greater and the quality was about 50% less.

The auxiliary system in which boiling mercury heat and momentum transfer data were obtained was essentially constructed of a single, 25 ft section of 3/8 inch stainless steel tubing. Three feet of the exit end were instrumented with wall thermocouples and pressure taps, and the boiler was heated by passing an electrical current through the tube wall. The system was gravity fed from a 12-foot standpipe containing the mercury reservoir. The heated components of the system were heavily insulated and heat loss corrections were determined from the equilibrium power input over the desired temperature range with no fluid flow. Pressure levels of about 30 psia were obtained at wall temperatures of about 1850°F. It was ascertained that, at vapor qualities from approximately 20 to 100 per cent in the film boiling and fog flow regimes, no measurable power was generated within the working fluid. This condition was established from the measured linear potential distribution along the boiler length for the above vapor quality range.

Shown in Figure 17 are some typical boiler wall temperature distributions for both linear and helical flow. The last two wall temperature stations which were located far beyond the heated section represent the mixed mean fluid temperatures. It may be noted that although the heat flux in the helical, or rotational flow case was about twice the linear flow value, the wall temperatures were comparable. Vapor qualities were 27% and 74% for linear and helical flow, respectively. Coolant flow rates were again comparable.

Pressure drop data at a constant flow rate of about 65 lb/hr were obtained in both linear and helical flow. Vapor qualities ranged from approximately 27 to 100%. In Figure 18 the results of the pressure drop measurements are presented versus mercury vapor quality. The pressure drop measurements for helical flow fall only a little above the values for linear flow. The flow cross section was identical in both cases.

Helical and linear boiling heat transfer conductances are compared as a function of vapor quality in Figure 19. The data have been normalized on the basis of the linear

flow conductances. It may be noted that the conductances in helical flow boiling remain constant until very high vapor qualities are attained, then fall rapidly to the predicted value for single-phase helical flow. It is also noted that conductance values for helical flow are nearly four fold higher than the corresponding values in linear boiling over the quality and mean flow rate ranges studied. Linear flow conductance data beyond a quality of 90 per cent were not obtained in this series of experiments. Current experiments will yield more detailed information on boiling heat transfer and fluid friction over a broader range of variables.

NOMENCLATURE

a	acceleration of gravity or thermal diffusivity
c_p	heat capacity
C	thermal capacitance
dq/dA	radial heat flux
k_v	thermal conductivity of vapor
L	latent heat of vaporization
q_s	heat flow from reactor fuel to boiler tube wall
r	radial distance
r_c	cell radius
r_d	drop radius
r_{d_o}	drop radius at $\theta = 0$
r_o	boiler tube radius
R_1, R_2	fluid thermal resistances
S	volume heat sink
t	boiler tube wall temperature in excess of the mixed mean fluid temperature or the local vapor temperature
t_d	a datum or reference temperature
t_m	mixed mean fluid temperature
t_w	wall temperature
t_s	saturation temperature
u	local fluid velocity
x	axial distance
$\bar{\delta}$	average vapor film thickness
δ_d	drop thickness or height
ϵ	eddy diffusivity

γ	weight density
γ_ℓ	liquid weight density
γ_v	vapor weight density
ρ_ℓ	liquid mass density
ρ_v	vapor mass density
θ	time
θ_ℓ	droplet vaporization time
ζ	Weisbach friction factor

REFERENCES

1. Poppendiek, H. F., Greene, N. D., MacDonald, F. R., Sabin, C.M. and Livett, R. K., "Quarterly Technical Report on High Acceleration Field Heat Transfer for Auxiliary Space Nuclear Power Systems," (AEC Contract No. (04-3)-409), Period March 1, 1963 to May 31, 1963. GLR-14.

2. Gido, R. G., and Koestel, A., "Mercury Wetting and Nonwetting Condensing Research," TRW Contract NAS 3-2159, Progress Report ER-5214, January 1963.

3. Goldmann, K., et al., "Burnout in Turbulent Flow - A Droplet Diffusion Model," Trans. ASME, J. Heat Trans. Vol. 83, Series C. No. 2, May 1961.

4. Poppendiek, H. F., Greene, N. D., MacDonald, F. R., Sabin, C. M. and Livett, R. K. "Annual Technical Report on High Acceleration Field Heat Transfer for Auxiliary Space Nuclear Power Systems," (AEC Contract No. (04-3)-409), Period September 1, 1962 through August 31, 1963. GLR-15.

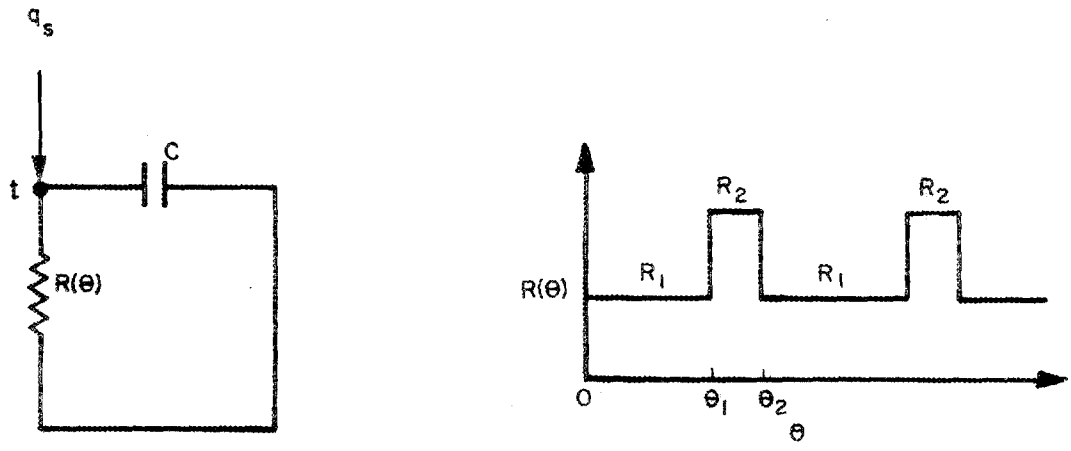

Figure 1. Thermal circuit and square wave conductance function for slug flow model.

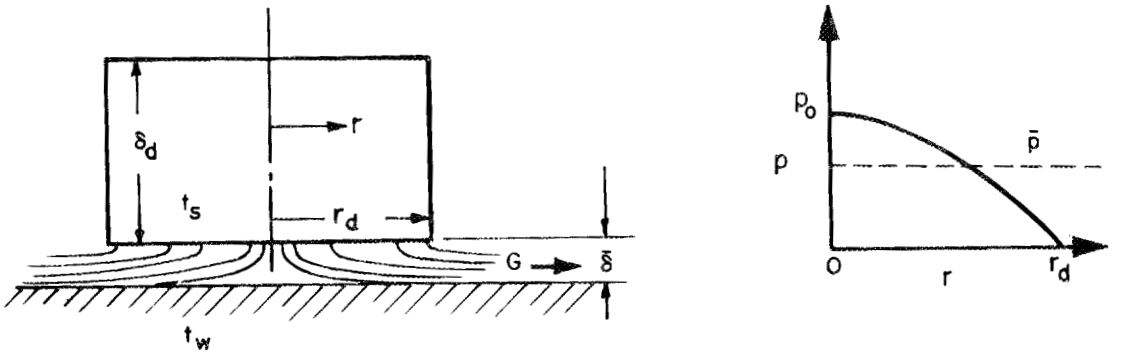

Figure 2. Geometry and pressure field for droplet model.

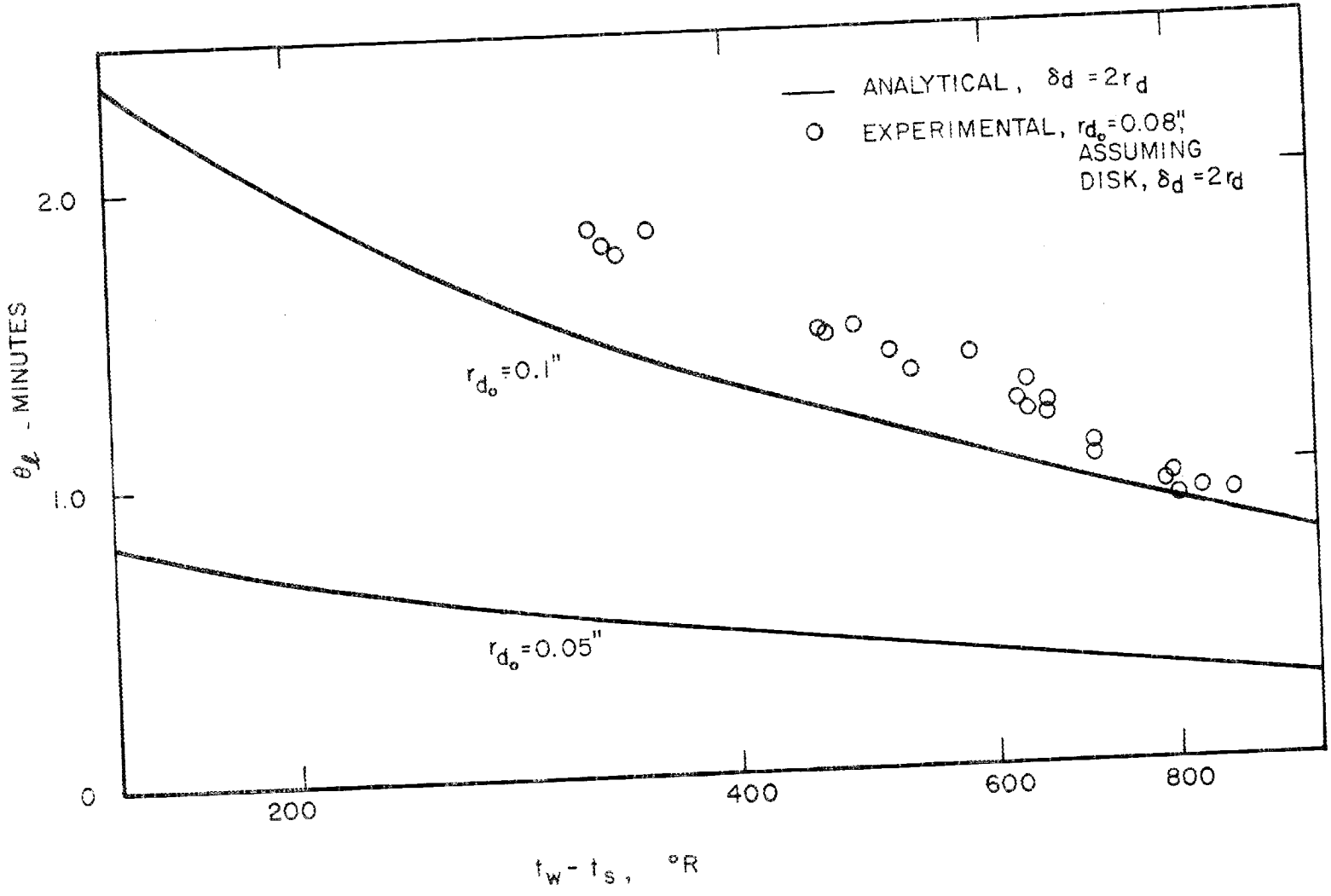

Figure 3. Water droplet lifetimes.

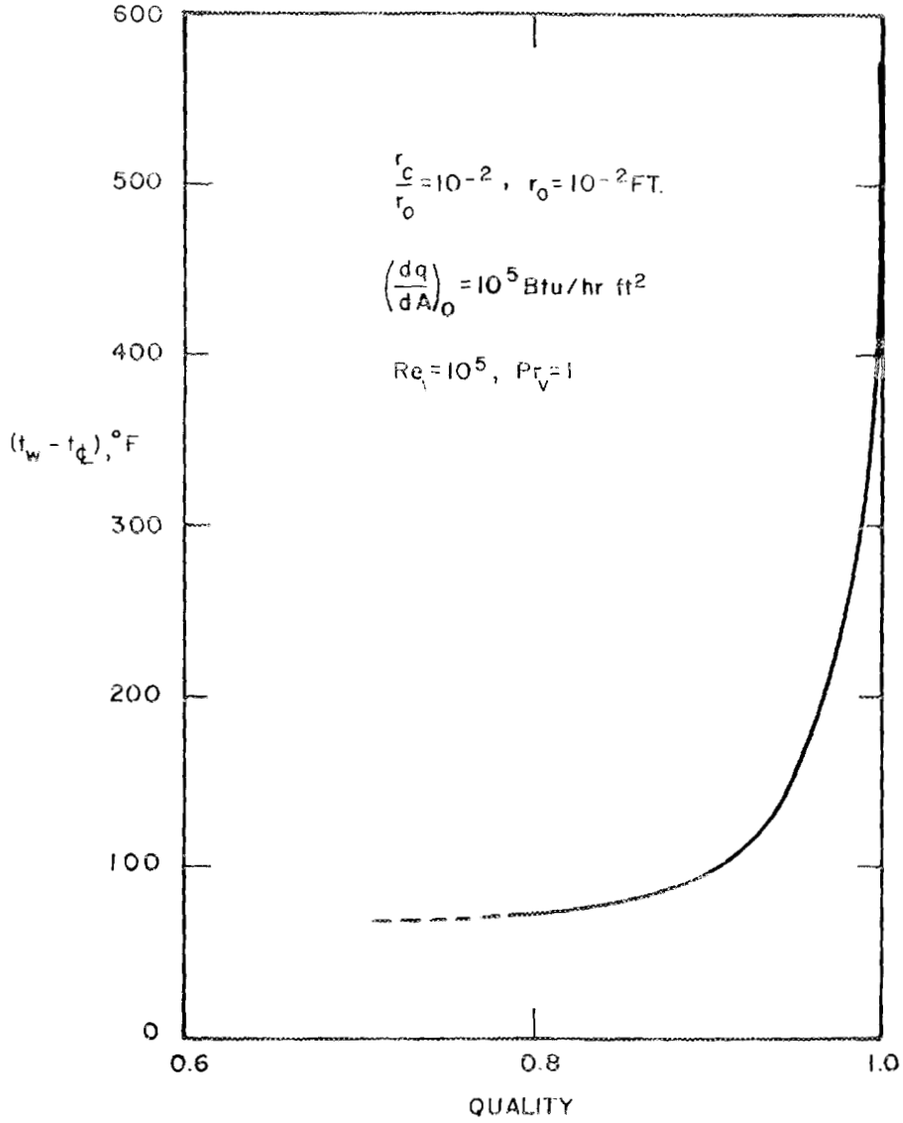

Figure 4. Typical graph of $(t_w - t_{\mathbb{C}})$ for water boiling in the high quality region using the fog heat transfer model.

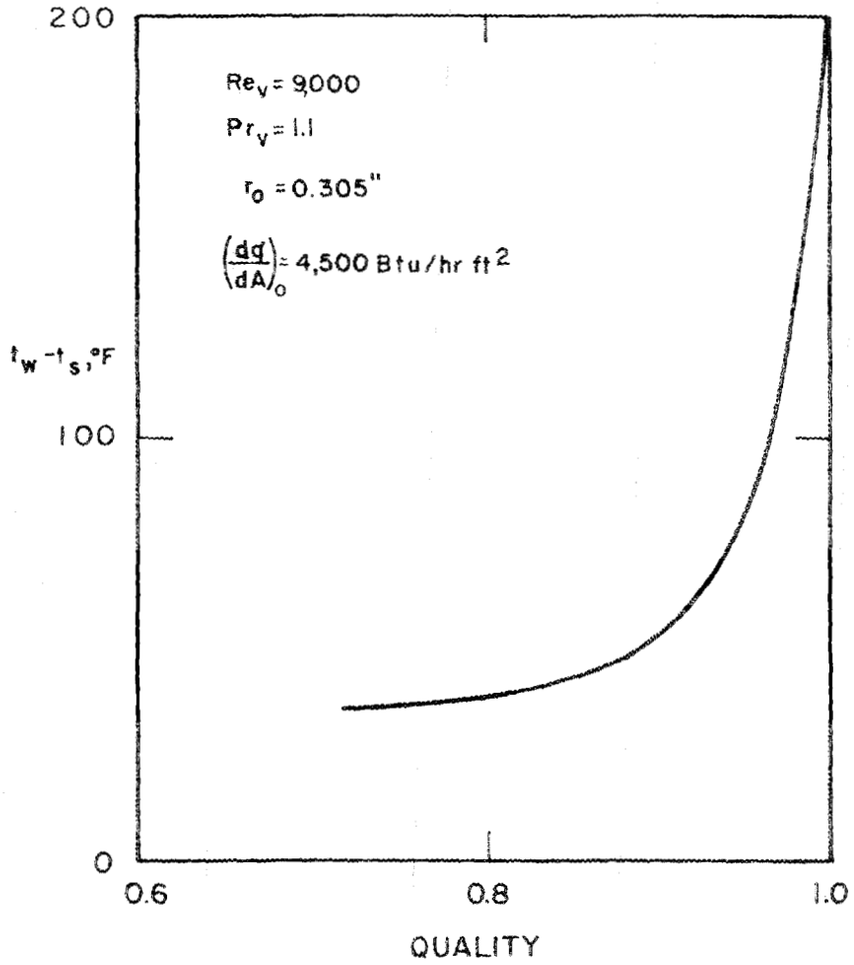

Figure 5. Experimental water boiling data in the high quality region (linear flow).

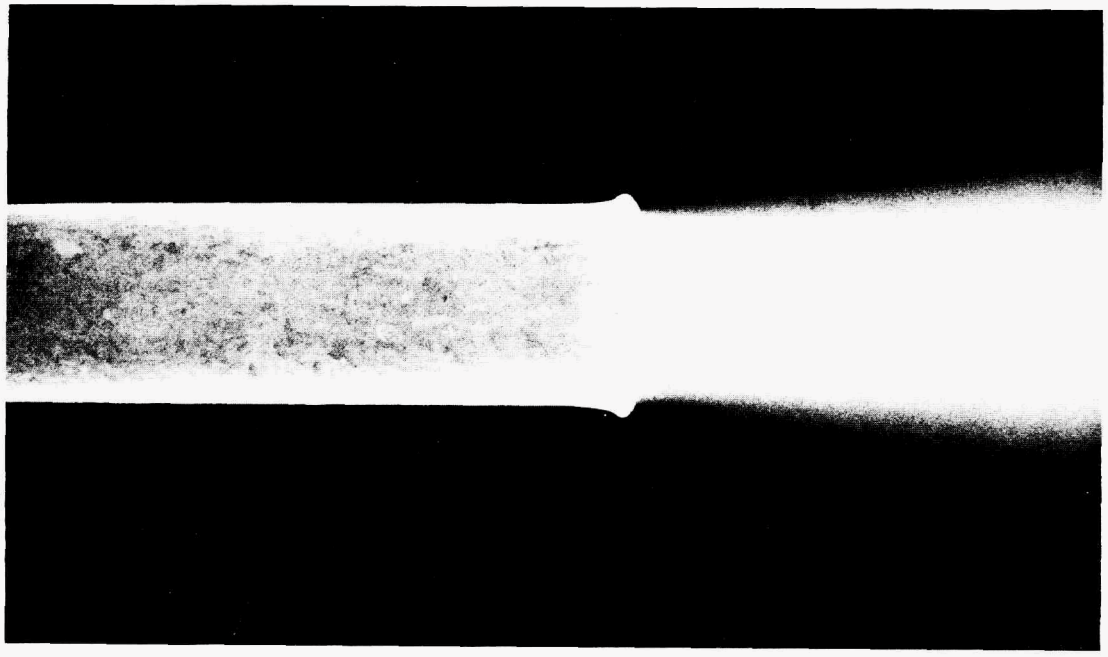

Figure 6. Linear fog flow.

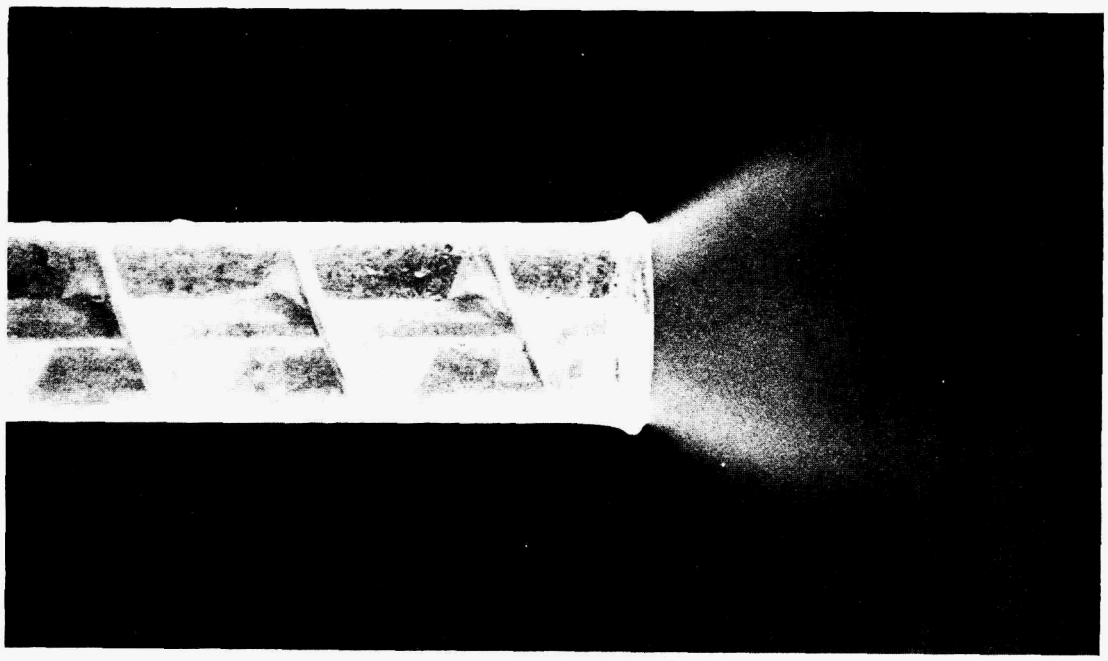

Figure 7. Helical fog flow (P/D = 1).

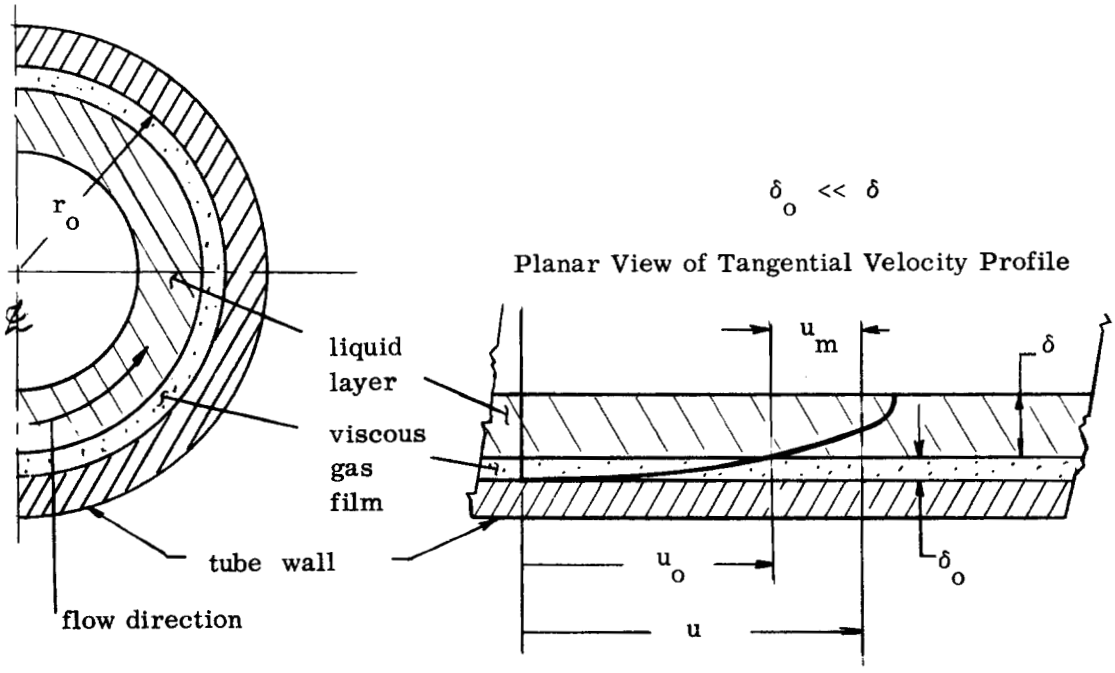

Figure 8. Two-phase flow decay model

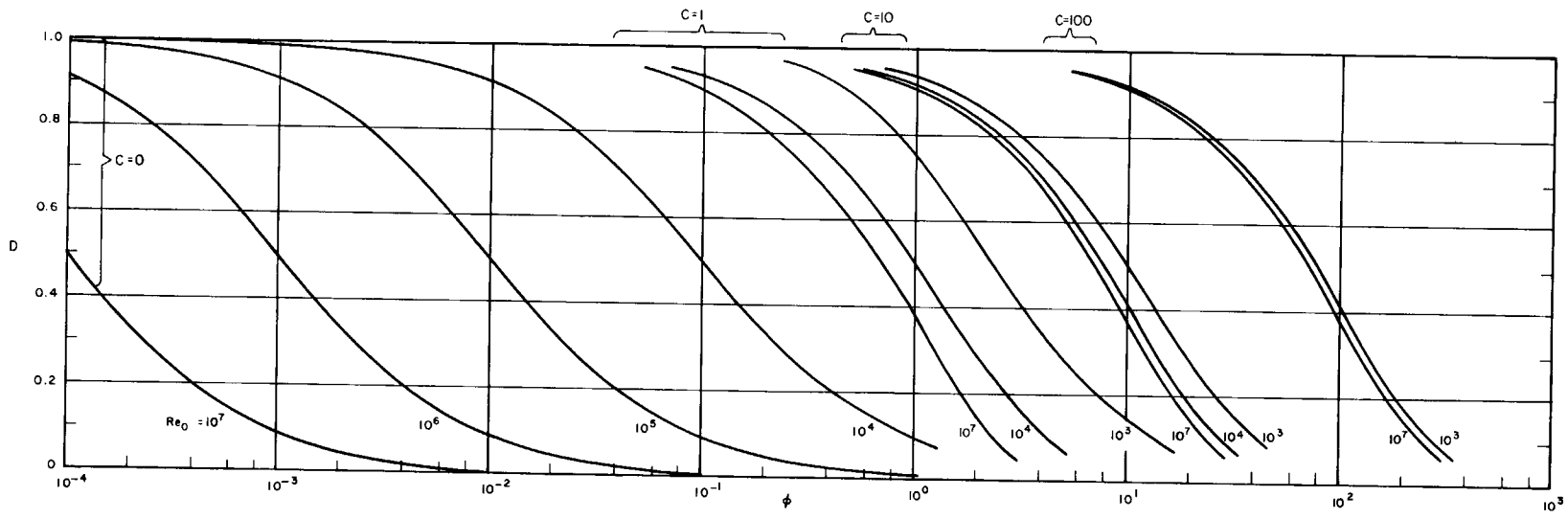

Figure 9. Re/Re_o vs. ϕ for various values of C and Re_o.

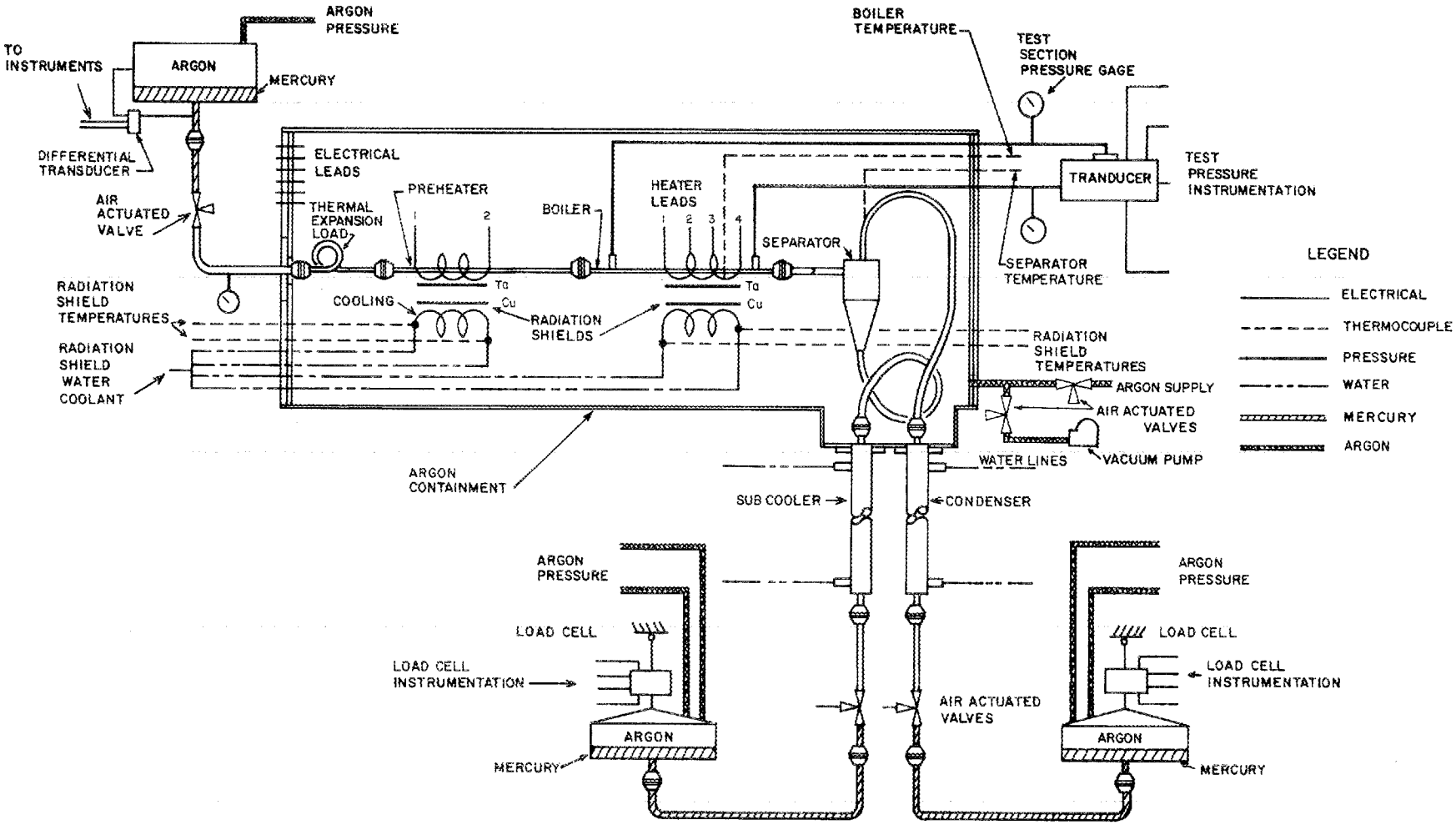

Figure 10. Experimental mercury heat transfer system.

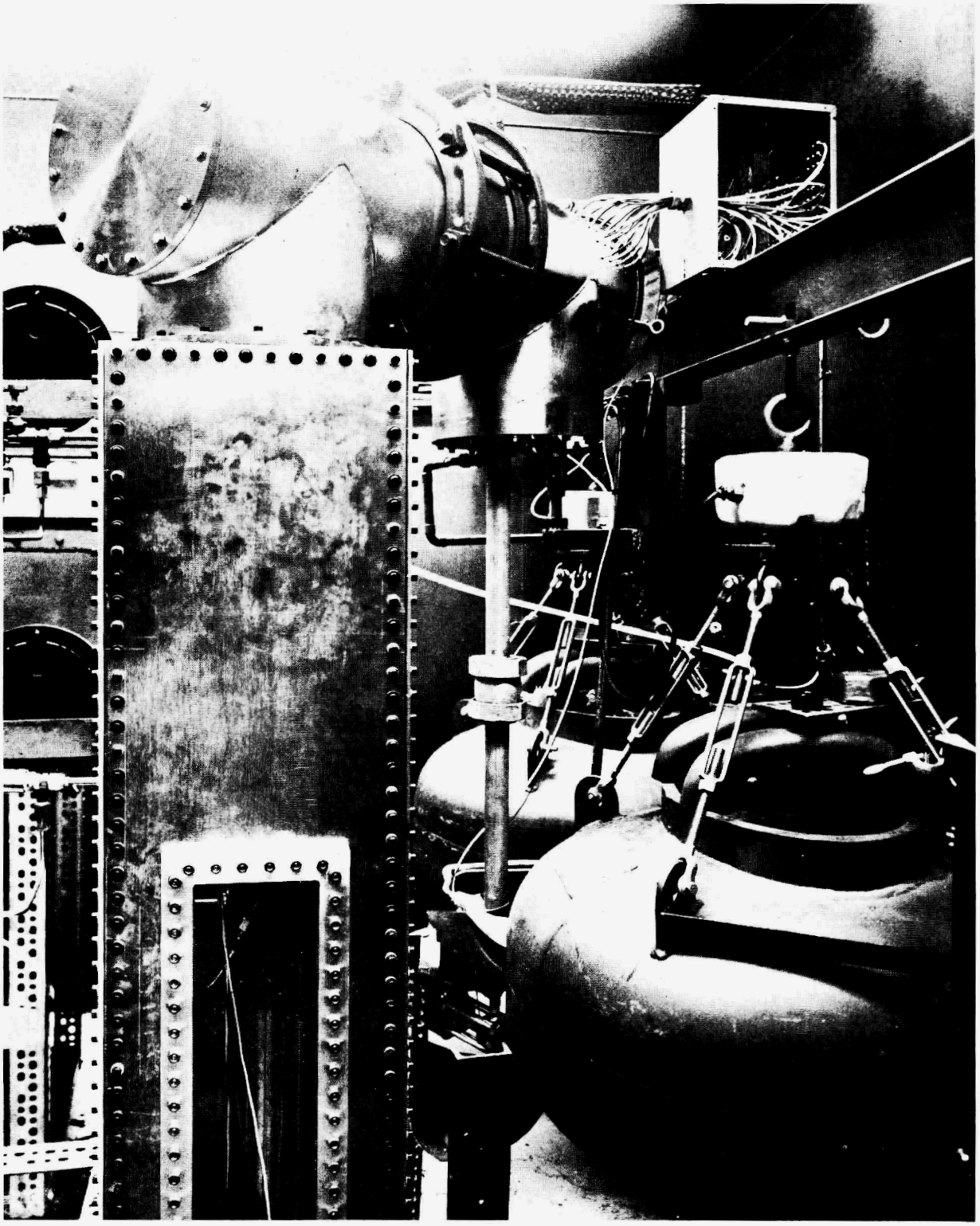

Figure 11. View of completed heat transfer system.

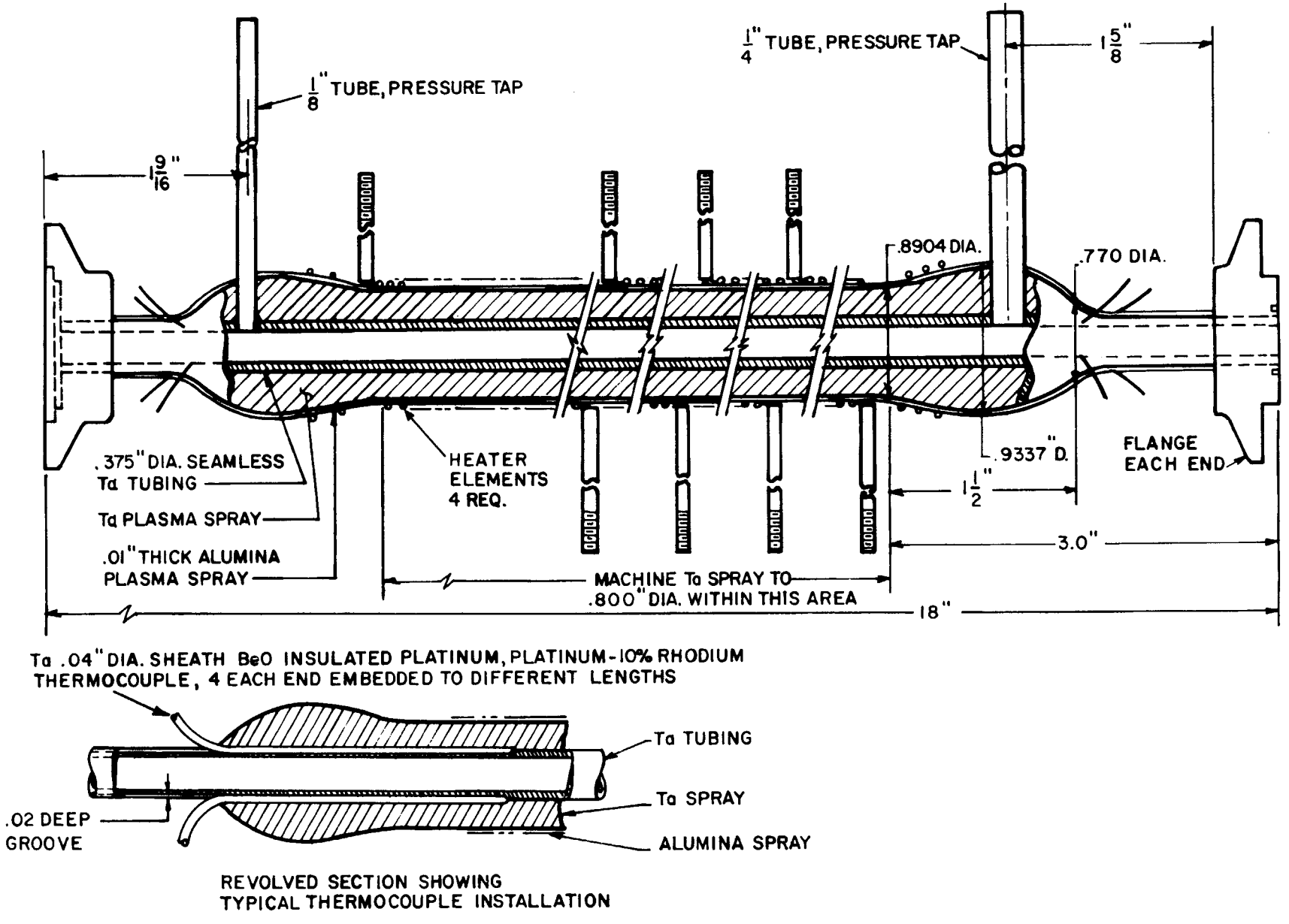

Figure 12. Thickwall boiler design.

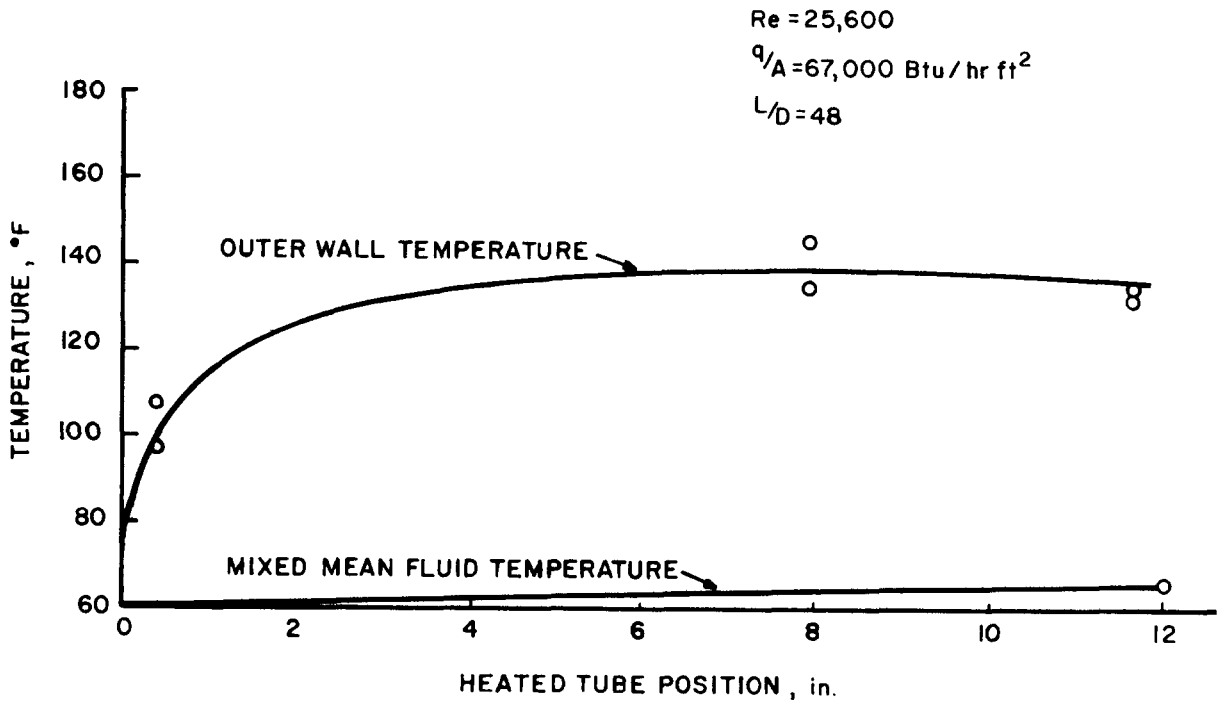

Figure 13. Typical outer wall and mixed-mean fluid temperatures for the heated boiler with forced water flow.

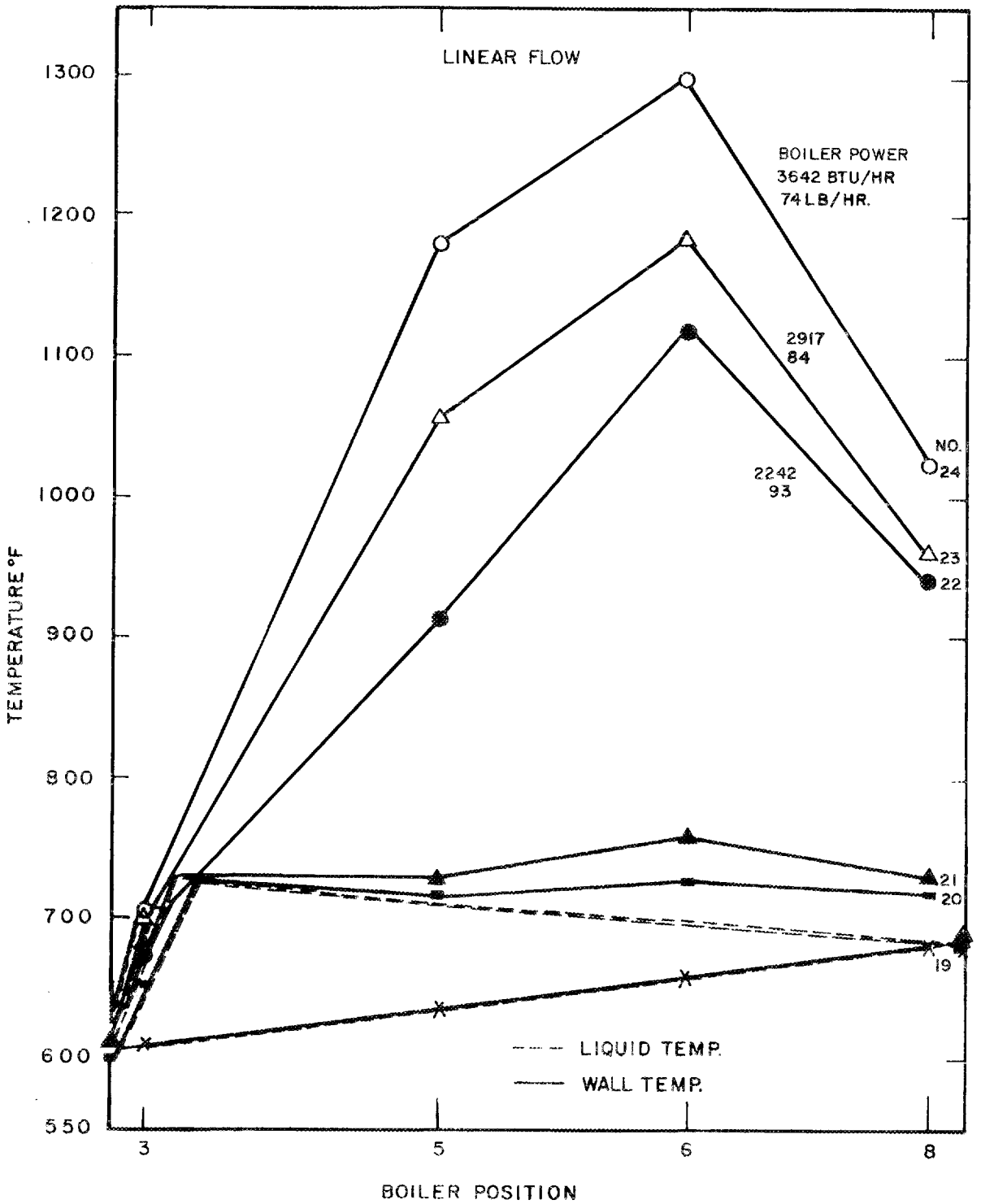

Figure 14. Linear flow boiler wall temperature distributions.

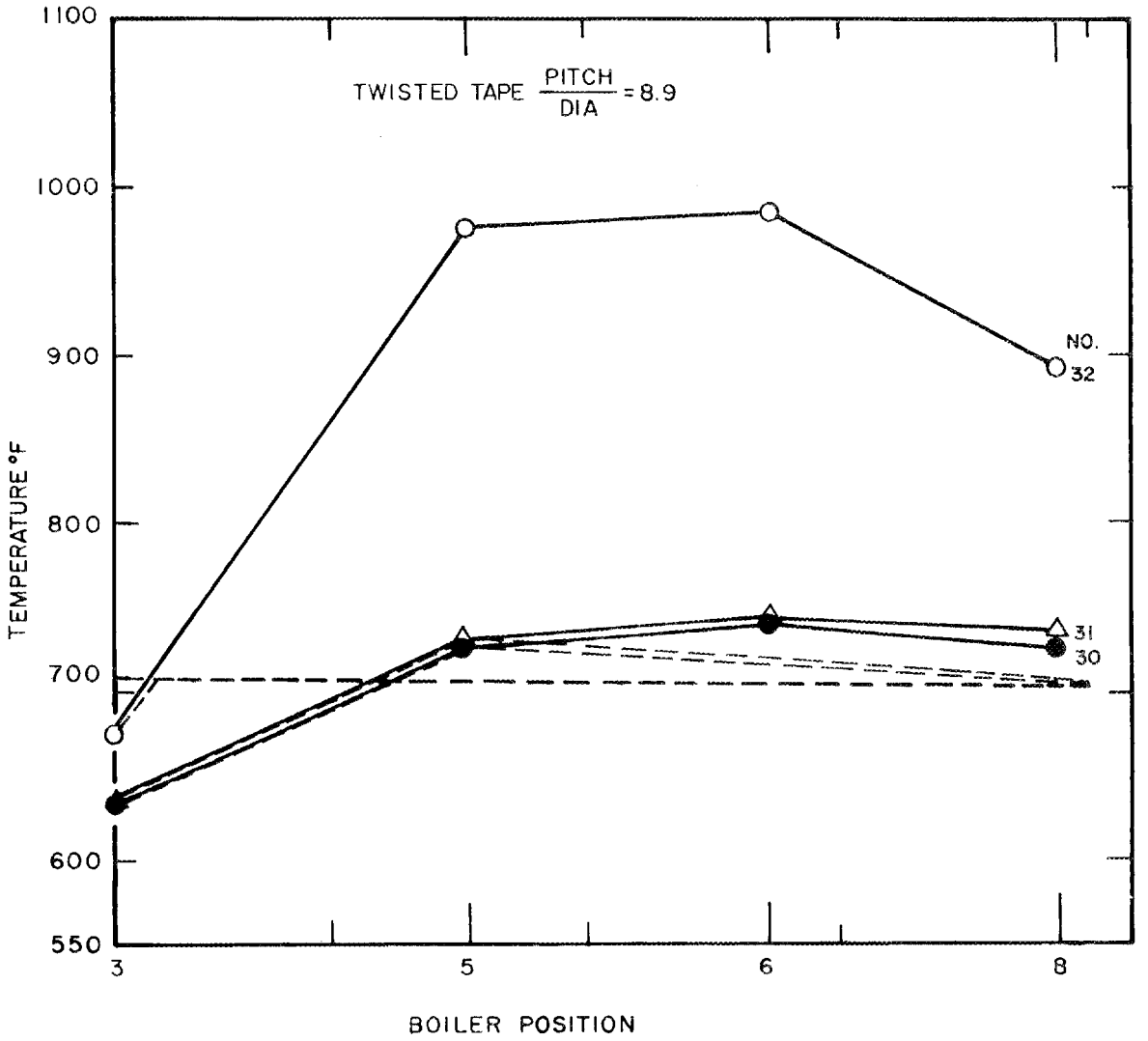

Figure 15. Helical flow boiler wall temperature distributions.

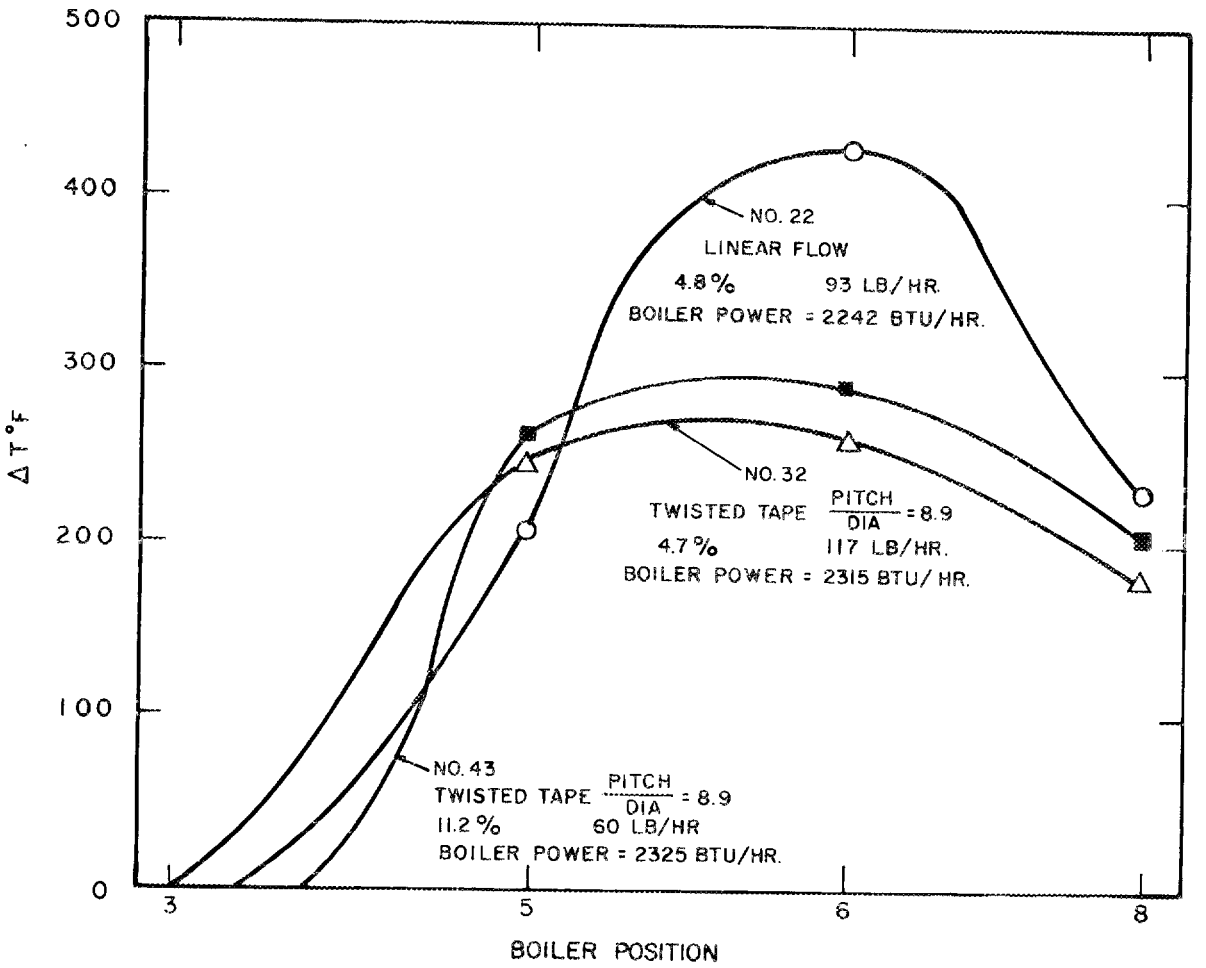

Figure 16. Linear and helical flow boiler wall temperature distributions.

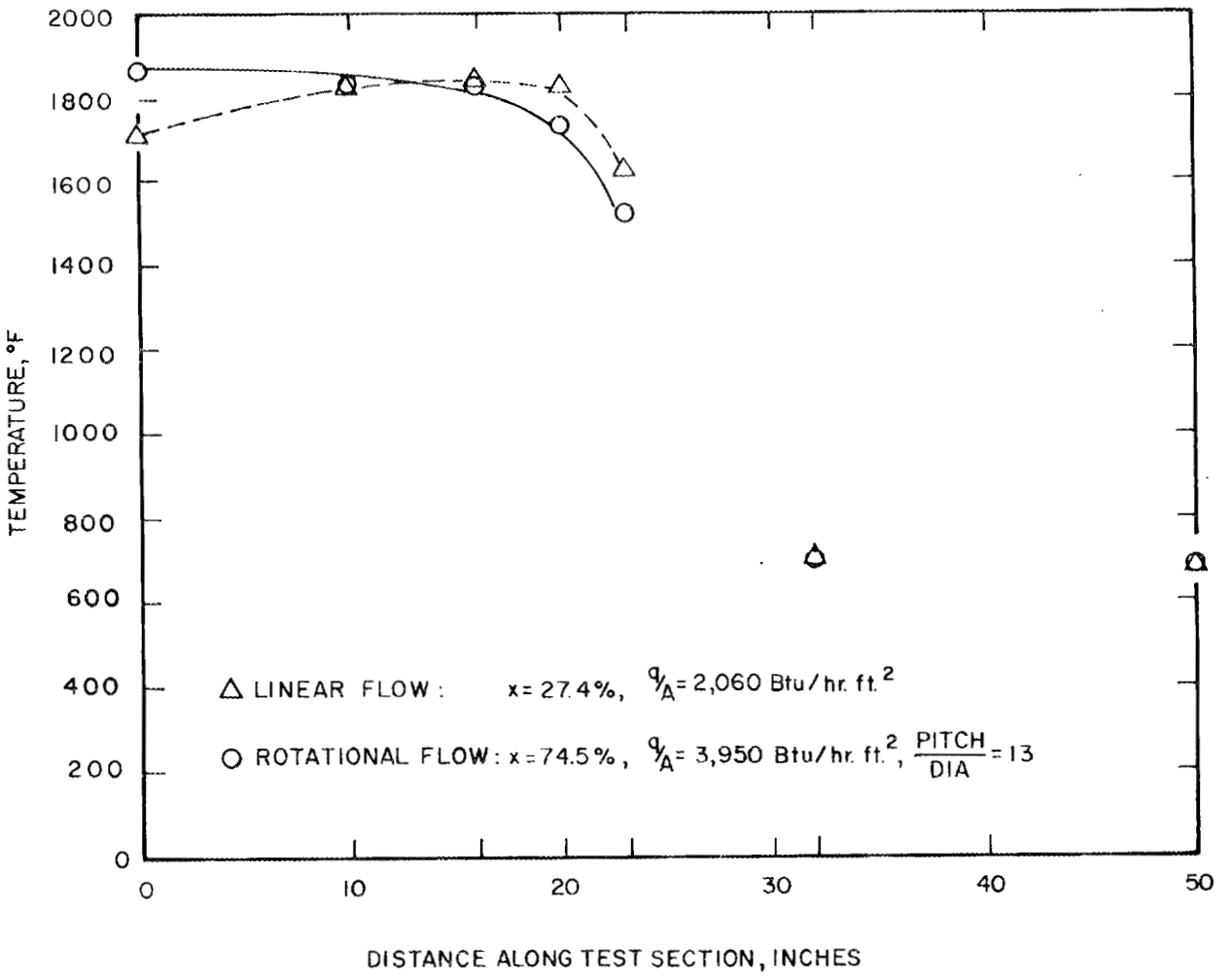

Figure 17. Wall temperature distributions for linear and helical flow boiling in auxiliary system.

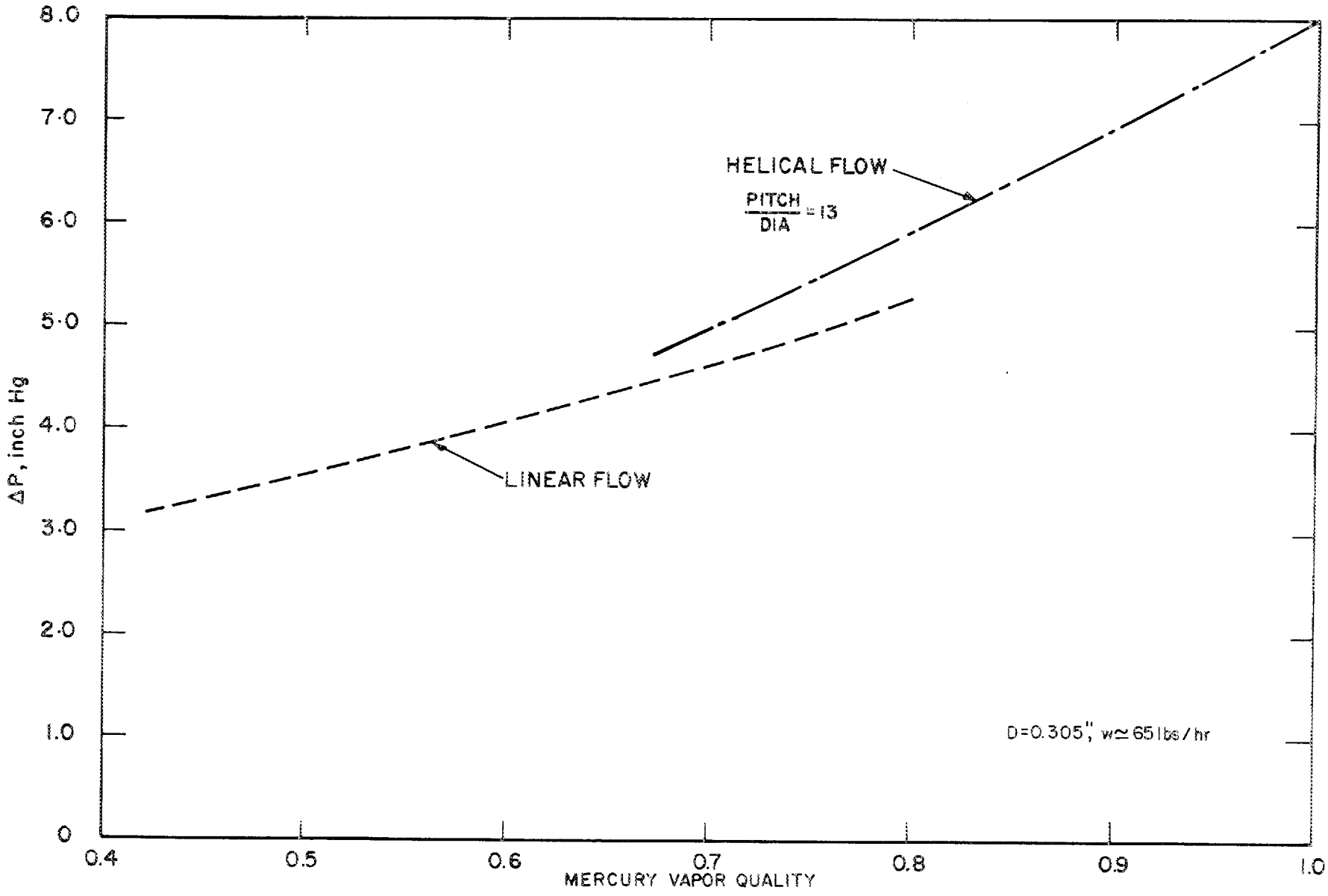

Figure 18. Boiling mercury pressure drop data for linear and helical flow.

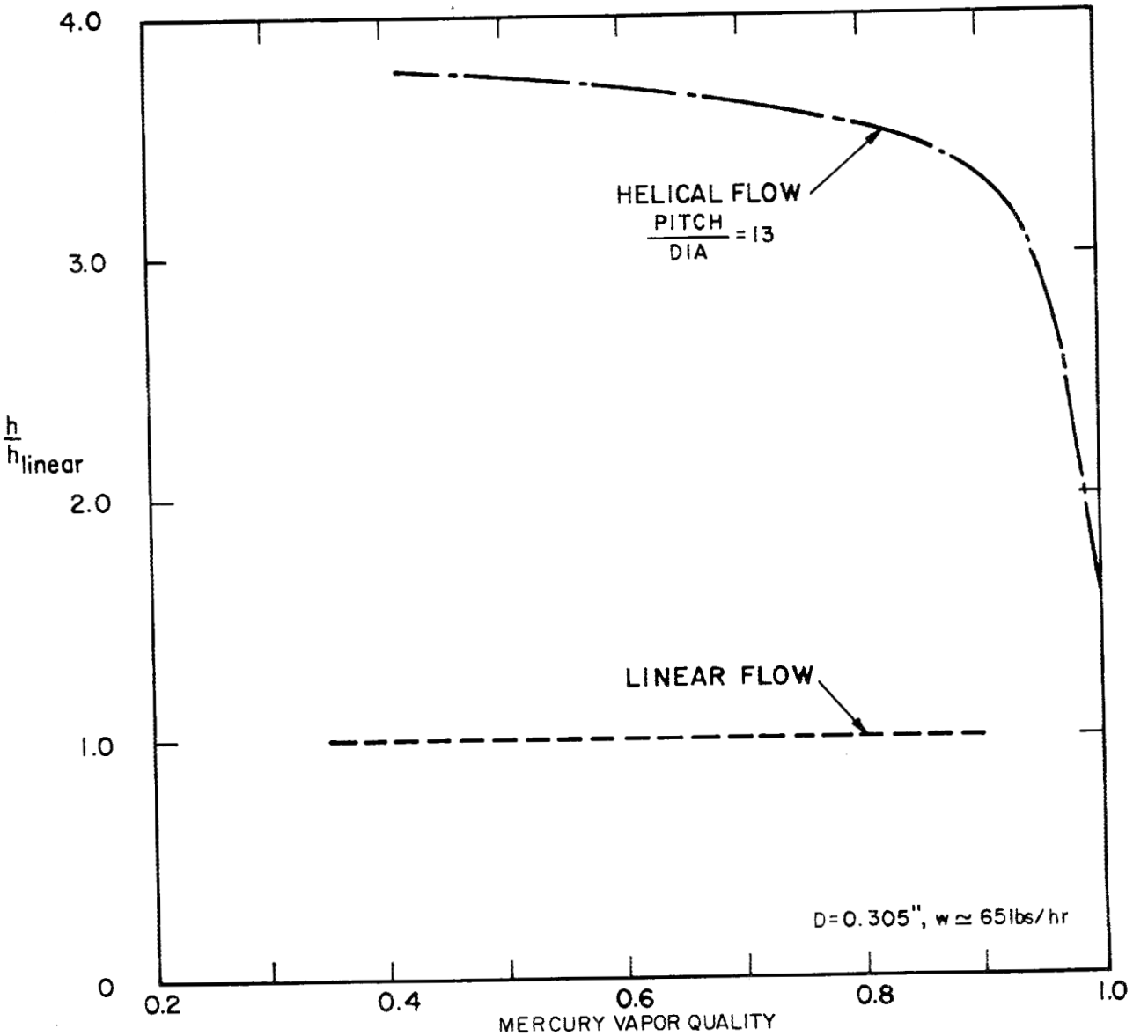

Figure 19. Boiling mercury heat transfer conductance ratios in linear and helical flow.

DISCUSSION

MR. HAYS: Do you have an explanation as to why the thermal power ranged as much as 15% greater than electrical, on the slide, and, secondly, what in general was the experimental scatter on the curves of h helical over h linear?

MR. GREENE: The data shown in the curve were based on the result of preliminary heat balances which were obtained with this system. We felt that from our measurements and observations a range of plus or minus 15% included all of the scatter.

What the accuracies of the experimental conductance data were at this time, I would not say definitely, but we feel that the data presented are correct within plus or minus 25%.

However, I would like to add that the comparison we made here between linear flow and helical flow was one for one. It was made with the same surface area in both cases, the same duct and the same tube. Secondly, this identical tube was used with the same pressure tap connections with the twisted tape inserted; thus, a total pressure drop was measured. While the magnitude is perhaps not precisely known, certainly the comparison between the two was.

MR. FISHER: The use of these models predicted drop diameter. Are you doing any work on this?

MR. POPPENDIEK: We are trying to calculate fog flow heat transfer using a number of possible cell-to-pipe radius ratios. We are going to make some more detailed examinations of what the possible practical ratios might be.

MR. GOLDMAN: I was also very interested in your droplet model. I think perhaps that the size of droplets is quite a bit smaller than the droplets we have been looking at. We have, some time ago, made estimates of what droplet size to expect in high-velocity steam-liquid systems, and it looked to us that the average droplet size might be around 40 microns, with a maximum size of about 200 microns.

Now the corresponding lifetime span for a droplet which moves into the boundary is also quite a bit shorter than that which you have indicated; and there is a considerable amount of data on spherical droplets, rather than cylindrical droplets. I believe much of this data can be used to develop droplet evaporation models.

MR. POPPENDIEK: The purpose of this model was just to show the relation between the various parameters. Certainly small-diameter droplets must be studied, as you indicate. It is not easy to watch little droplets while they are evaporating; we started with the larger ones. We have a microscope system, now, that is used in these studies. One can observe a number of interesting features while viewing the larger droplets. For example, when the ΔT is reduced sufficiently, then the lifetimes are drastically reduced because of nucleate boiling.

LITHIUM-BOILING POTASSIUM REFRACTORY METAL LOOP FACILITY

by Jerry P. Davis
Gerald M. Kikin
Wayne M. Phillips
Lawrence S. Wolfson

Jet Propulsion Laboratory
Pasadena, California
August 1, 1963

Abstract

A 30 kw lithium-boiling potassium two-loop facility is presently under construction at the Jet Propulsion Laboratory and is expected to be in operation during 1964.

The loop is totally constructed of columbium-1% zirconium alloy and will operate at temperatures up to 2100°F.

The primary purposes of this loop facility are as follows:

1. To investigate over-all transient and steady-state characteristics of a two-loop system which approximately simulates velocities, temperature, pressures, transit times, and heat fluxes in the range of actual system interest. The primary loop heat source is by direct-resistance heat generation in a section of tube wall and liquid metal, which lends itself to programming of reactor kinetic equations for simulation of power response to various system perturbations. A detailed study of regimes of boiling stability under various operating conditions, heat fluxes, exit vapor quality, inlet subcooling, etc. will be accomplished.

2. Steady-state local-boiling heat-transfer coefficients and two-phase pressure drop data will also be obtained for a variety of operating parameters.

3. Components such as throttling valves, centrifugal pumps, hot traps and experimental turbine-alternators, will be evaluated for potential application to actual systems.

I. Areas of Investigation.

The two loop lithium-boiling potassium facility under construction at JPL represents an attempt to simulate the major elements of a two-loop nuclear turboplant concept of potential interest for spacecraft propulsion application. The primary purpose of this facility is the investigation of overall transient and steady-state characteristics of a Rankine cycle alkali metal plant which approximately simulates operating conditions of actual system interest. Various programmed startups, power demand transients, control concepts for power range operation, etc. will be studied in parallel with an attempt to predict and/or formulate the necessary models to predict system behavior by analog representation.

In addition to the system dynamics program, a study will be attempted to define regimes of boiling stability as affected by various operating conditions, heat fluxes, exit vapor quality, inlet subcooling, liquid and two-phase pressure drop distribution, and their pertinent parameters. Various types of boilers are contemplated for investigation including tube side boilers and shell side cross-flow boilers. Steady state local and overall heat transfer coefficients and pressure drop data will also be obtained for a variety of boiler configurations and operating conditions.

Finally, a facility of this nature is, of necessity, engaged in component evaluation. Items such as throttling valves, centrifugal pumps, hot traps, liquid vapor separators, and experimental turbine-alternator components will be evaluated for potential application to space power systems.

II. Loop Design.

Fig. 1 represents a flow schematic of the system and loop operating conditions are shown in Table I. Briefly, the primary side lithium flow enters a direct current resistance heated helical coil to which reactor kinetic equations may be programmed for simulation of power response to various system perturbations. The lithium enters a centrifugal pump which employs a combination recirculation and liquid level indicator sump, through a bellows seal throttle valve, electromagnetic flowmeter, boiler, and return to the heater inlet. About 15% of the flow is bypassed to an yttrium hot trap located in the coolest part of the system for minimization of mass transfer effects.

The secondary side potassium enters a countercurrent annular flow boiler, exits through a flow orifice to the experimental turbine, or bypass bellows seal vapor throttling valve, to a radiating condenser. The condenser is surrounded by an array of rotating radiation shields to vary the effective condenser area. The potassium continues through a subcooler electromagnetic pump, electromagnetic flowmeter, preheater, zirconium gettered hot trap, liquid throttle valve, and returns to the boiler inlet.

The loop is contained in a 5 foot diameter by 7 foot long main enclosure with auxiliary enclosures for the condensing radiator and fill/dump system as shown in Fig. 2. The system will be run in a recirculating argon atmosphere slightly above atmospheric pressure. Make-up argon will have an oxygen content of about 1 ppm oxygen and 1/2 ppm water vapor. Equilibrium concentration in the enclosure is expected to be several orders of magnitude below these figures and unmeasurable by continuous stream analysis techniques.

The loop will be triple tantalum foil wrapped and insulated with about 3 inches of "Glass Rock" foamed high purity silica.

All materials in contact with fluids above 1500°F will be Cb-1Zr with the exception of higher alloy valve facings, hot trap getters, and turbine wheel. Fill and dump system is constructed of type 304 stainless steel.

III. Loop Components.

The design of loop and auxiliary components is essentially complete. All components and/or materials have been purchased for assembly of the loop. The development and fabrication of a test isolation diaphragm assembly for pressure measurements has been completed and a test program has been initiated. Compatibility experiments are in progress to evaluate various potential loop insulation materials. The inability to satisfactorily hydroform Cb-1Zr bellows has resulted in the investigation of alternate forming techniques, including a coreduction vapor deposition process.

Major loop components are shown in Figs. 3 through 10.

IV. Fabrication Status.

The loop design has been mocked up as a full-scale assembly, shown in Fig. 11. The purpose of this mockup is for locating components, associated piping and electrical wiring, heater power leads, piping supports, and the fitting up of insulation.

The loop is designed to permit the fabrication and assembly of the various loop components on the loop support frame outside the loop containment vessel. The containment vessel itself, shown in Fig. 12, is composed of two major sections, one of which can be traversed on tracks to permit the installation of the loop assembly and the associated power, instrumentation and dump system feedthroughs. The control shutter assembly shown on its preassembly stand, Figs. 13 and 14, will be installed in the vertical section of the movable portion of the containment vessel. The lithium circuit and potassium circuit hot traps and the lithium circuit liquid level indicator have been machined and are shown in Figs. 15, 16 and 17. The loop boiler assembly is in fabrication at JPL. The lithium and potassium electromagnetic flowmeters and the potassium electromagnetic pump

have been delivered and test preparations are in progress for calibration. All other components are in final fabrication.

The vacuum, argon cooling and dump systems are shown, Figs. 18, 19 and 20, in various stages of construction.

V. Materials Support Facilities.

The corrosion and compatibility test facility consists of three 3.2 kw Glowbar type furnaces, Fig. 21, containing two atmosphere test chambers, each (six independent experiments) manufactured by Hevi-Duty Electric Co. These furnaces are independently connected to a tilting mechanism capable of tilting 45° from the horizontal, from 1 to 4 cycles/min, as well as statically operated, for long time compatibility experiments at temperatures up to 2500°F. Associated equipment consists of a 16-point temperature recorder, alkali metal and radiological leak detectors, and an oxygen analyzer. The test chamber atmosphere is continuously monitored.

A TIG welding facility, including gas purification and moisture analysis equipment, is presently in operation, Fig. 22. Monitoring of the argon welding atmosphere, both before and after welding, indicates that moisture and oxygen impurity levels are readily maintained below 2 ppm.

The use of welding inserts, Fig. 23, for butt-welding tubing has proven satisfactory. Metallographic examination of these welds indicates melting and complete bonding of the tubing-insert interface has taken place. The insert, however, did not melt sufficiently to allow the metal to flow toward the inner surface of the tubing, as is commonly observed with stainless steel. As a result, the shape of the welding insert is retained on the inner surface of the tube. The welds produced with this technique were consistent, and the discontinuities produced on the inner

surface of the tube were approximately the same size as with standard butt-weld techniques.

Due to previously observed hardening of Cb-1Zr from contact with foamed silica, evaluation of other insulations was undertaken. Samples of insulation were outgassed at 2000°F for 24 hours under a cover of argon gas. Two tensile specimens of Cb-1Zr in contact with a sample of insulation were placed in direct contact with the insulation. In the others the tensile specimens and insulation were separated by tantalum foil, which allowed circulation of gas within the capsule.

These types of insulation have been tested: Cercor (a product of Corning Glass Works), Glassrock Foam #25, and Foamsil. These insulations as received, after outgassing and after testing, are shown in Figs. 24, 25 and 26. Results of tensile and microhardness measurements are shown in Table II. Metallographic examination showed no effect of contamination on microstructure. Microhardness measurements indicated that surface hardening had taken place, and tensile tests indicated that a slight amount of strengthening had also taken place.

The variations observed in microhardness with Foamsil were attributed to a variation in pore size in the material and, consequently, a variation in degree of outgassing obtained. Complete devitrification produced during testing released any remaining gas in the material.

Additional tests on foamed alumina and zirconia are being undertaken. To evaluate the effectiveness of foil wrapping in protecting Cb-1Zr from oxidation, a series of capsules were wrapped with molybdenum, tantalum, and zirconium foil. These were exposed at 2200°F for 100 hours to a stream of argon containing 2 ppm oxygen. The capsules after testing are shown in Fig. 27. The tantalum wrap was in the best condition, showing slight embrittlement. The molybdenum and zirconium foils were

completely embrittled. This is what would be predicted from the reaction rates of the three materials with oxygen.

To evaluate the stability of the oxide of each of the wraps, capsules of Cb-1Zr were filled with molybdenum oxide, tantalum oxide and zirconium oxide. The results of these tests shown in Figs. 28, 29 and 30 follow thermodynamic predictions. The molybdenum oxide reacted to completely embrittle the Cb-1Zr. No reaction was observed with tantalum oxide. The zirconium oxide produced a superficial reaction layer on the columbium. This was believed to be zirconium which resulted from a change in the stoichiometry of ZrO_2 at elevated temperatures.

Test capsules are presently being wrapped with a layer of zirconium foil covered with two layers of tantalum foil. This has been found to provide better protection than any of the foils separately and may ultimately be decided on as the technique for loop protection.

Table 1. 30 kw — 2100°F loop

Item	Operating conditions	Supplier and type
Lithium (liquid)		Foote Mineral Co.
Flow rate, Gpm	1 to 10	
Temperature, °F	2100	
Pressure, PSIG	Up to 20	
Potassium (liquid)		MSA Research Corp.
Flow rate, Gpm	0 to 1	
Temperature, °F	1500 to 2000	
Pressure, PSIG	Up to 200	
Centrifugal pump (lithium)	Up to 10 Gpm at 100 ft (TDH) 2100°F Service	Byron-Jackson
Swing gate valves (bellows seal)		Valcor Engineering Co.
Lithium	2100°F Li service	5/8 in. OD
Potassium	2000°F boiling K service	3/4 in. Sch. 80
EM flowmeters		
		MSA flowmeter FM-4
Lithium	2100°F service	5/8 in. OD 1/16 in. wall
Potassium	1500°F service	Cb — 1% Zr duct 3/8 in. OD Cb — 1% Zr duct
Diaphragm	Li and K pressure measurements	Cb — 1% Zr
K—boiler	Loop design conditions	JPL
K—vapor separator	Loop design conditions	———
Dump tanks and valves		
(Argon, vacuum and fill)	500°F service	Material S.S. 304

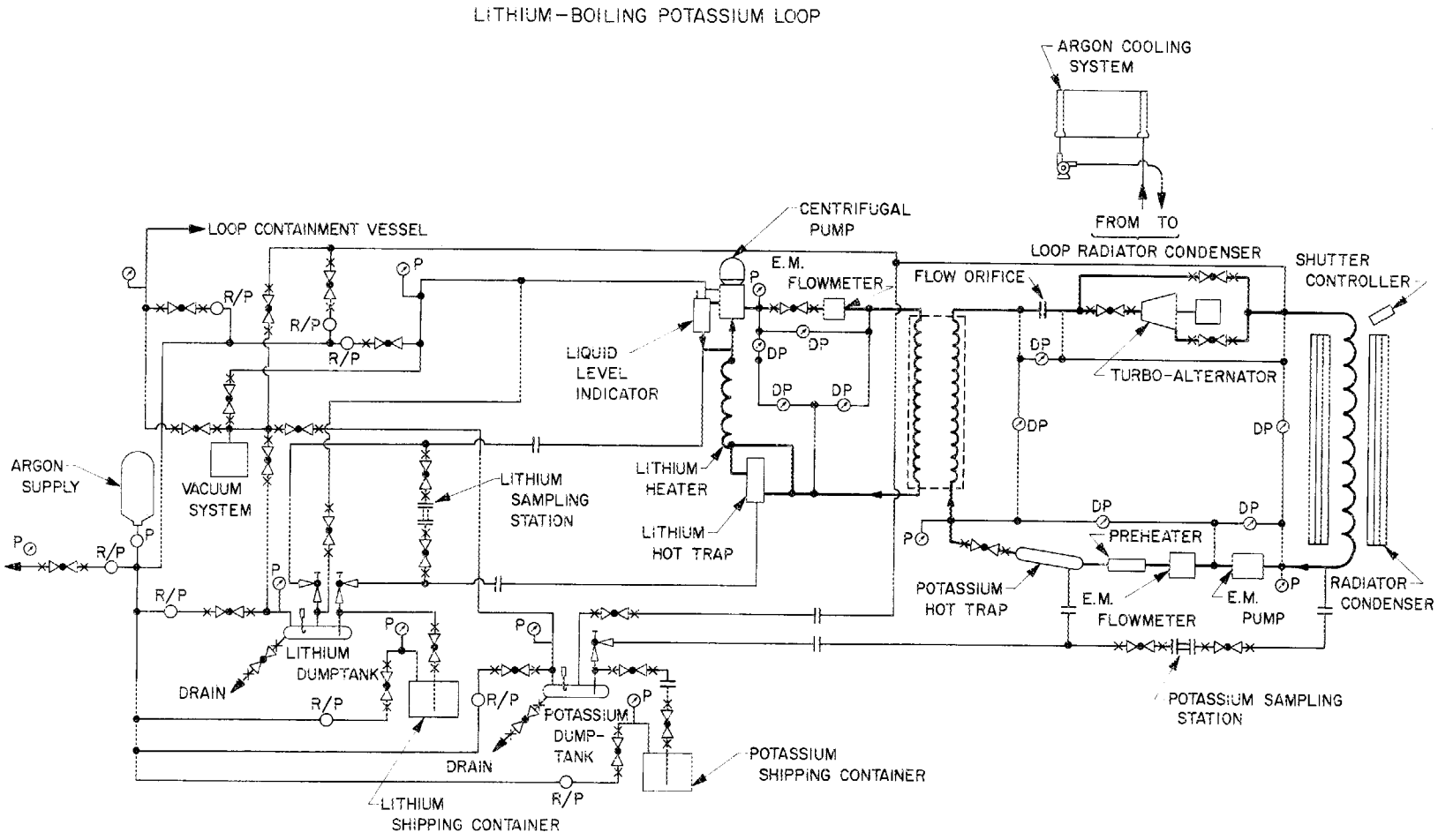
LITHIUM-BOILING POTASSIUM LOOP
ARGON COOLING SYSTEM
FROM TO
LOOP RADIATOR CONDENSER
SHUTTER CONTROLLER
CENTRIFUGAL PUMP
LOOP CONTAINMENT VESSEL
E.M. FLOWMETER
FLOW ORIFICE
LIQUID LEVEL INDICATOR
TURBO-ALTERNATOR
ARGON SUPPLY
VACUUM SYSTEM
LITHIUM SAMPLING STATION
LITHIUM HEATER
LITHIUM HOT TRAP
PREHEATER
POTASSIUM HOT TRAP
E.M. FLOWMETER
E.M. PUMP
RADIATOR CONDENSER
LITHIUM DUMPTANK
DRAIN
POTASSIUM DUMP-TANK
POTASSIUM SAMPLING STATION
POTASSIUM SHIPPING CONTAINER
LITHIUM SHIPPING CONTAINER
R/P
P
DP

Fig. 1.

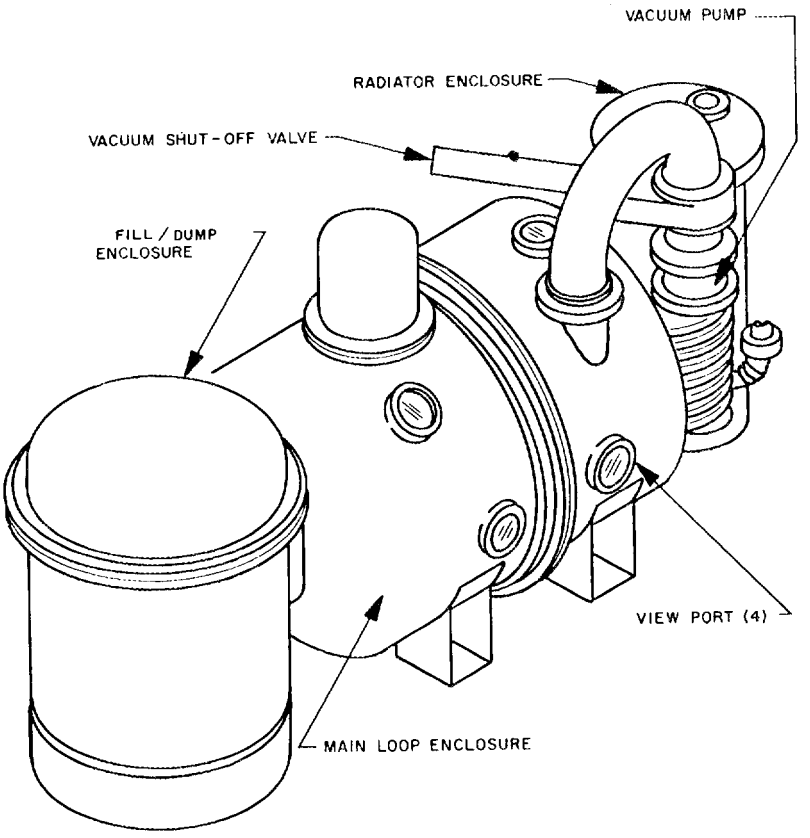

Fig. 2. Lithium—boiling potassium loop enclosure

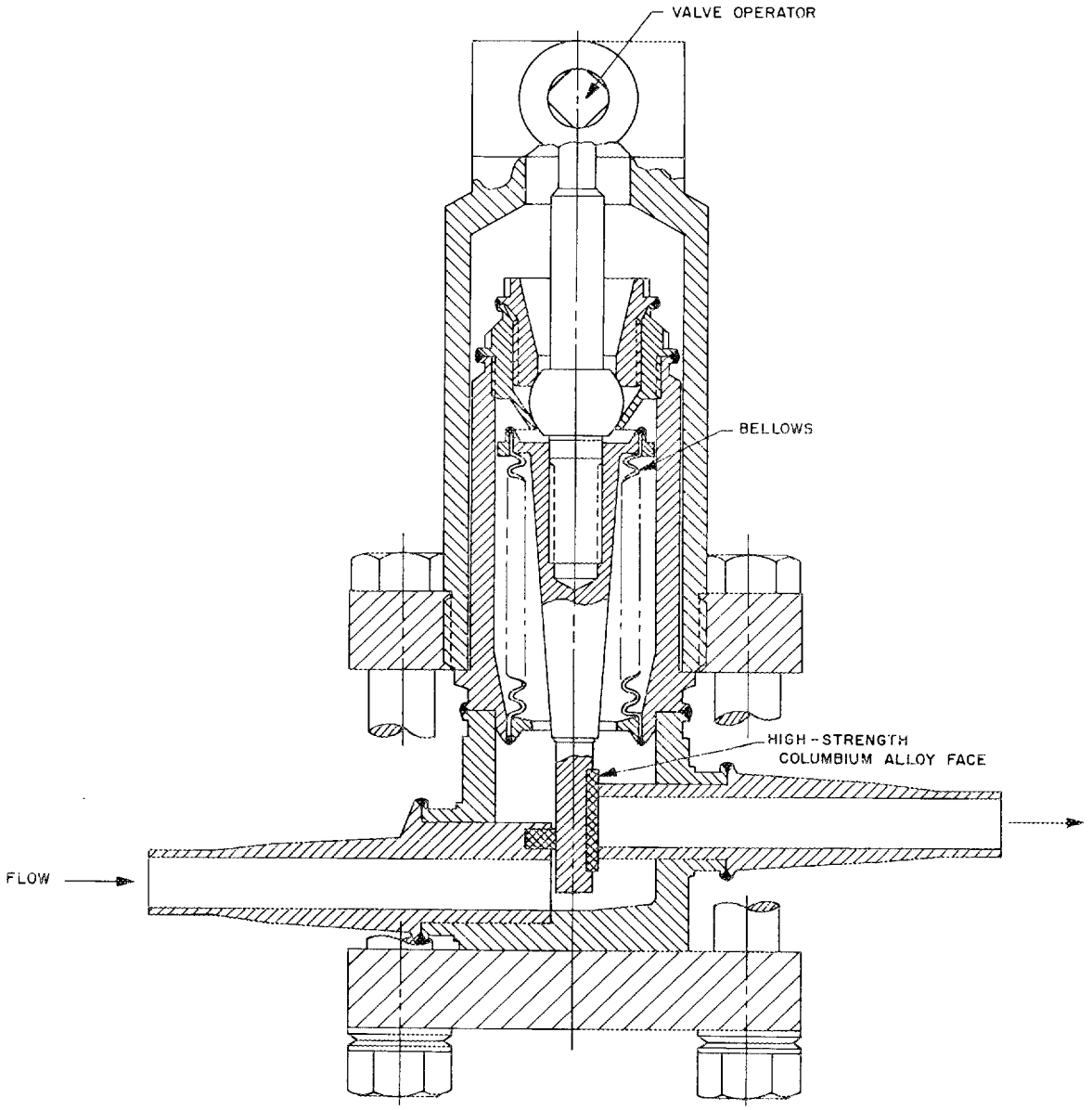

2100°F LIQUID METAL THROTTLE VALVE
(MATERIAL COLUMBIUM + 1% ZIRCONIUM)
MANUFACTURER: VALCOR ENGINEERING

Fig. 3. Lithium-boiling potassium loop valve design

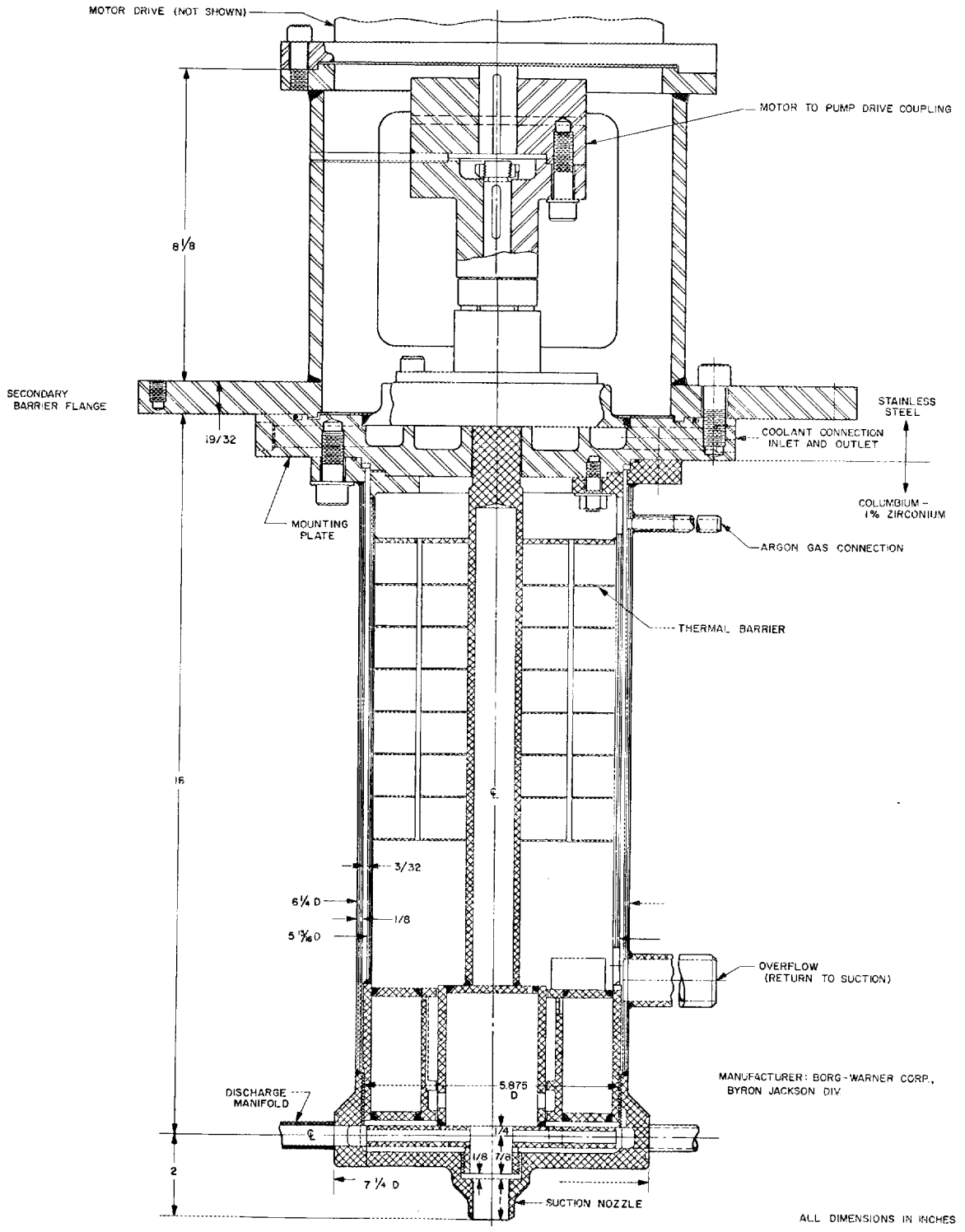

Fig. 4. 2100°F liquid metal centrifugal pump

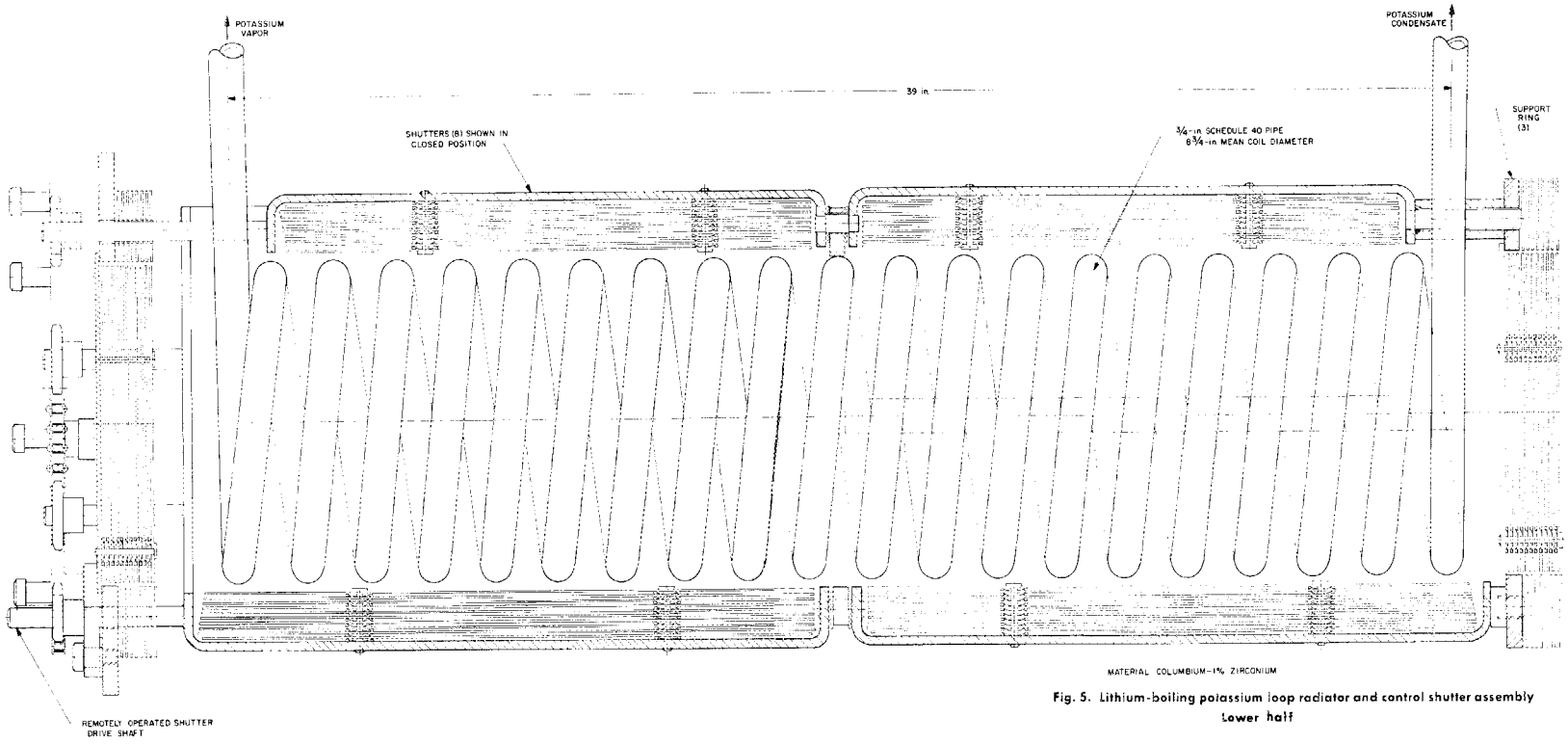

Fig. 5. Lithium-boiling potassium loop radiator and control shutter assembly Lower half

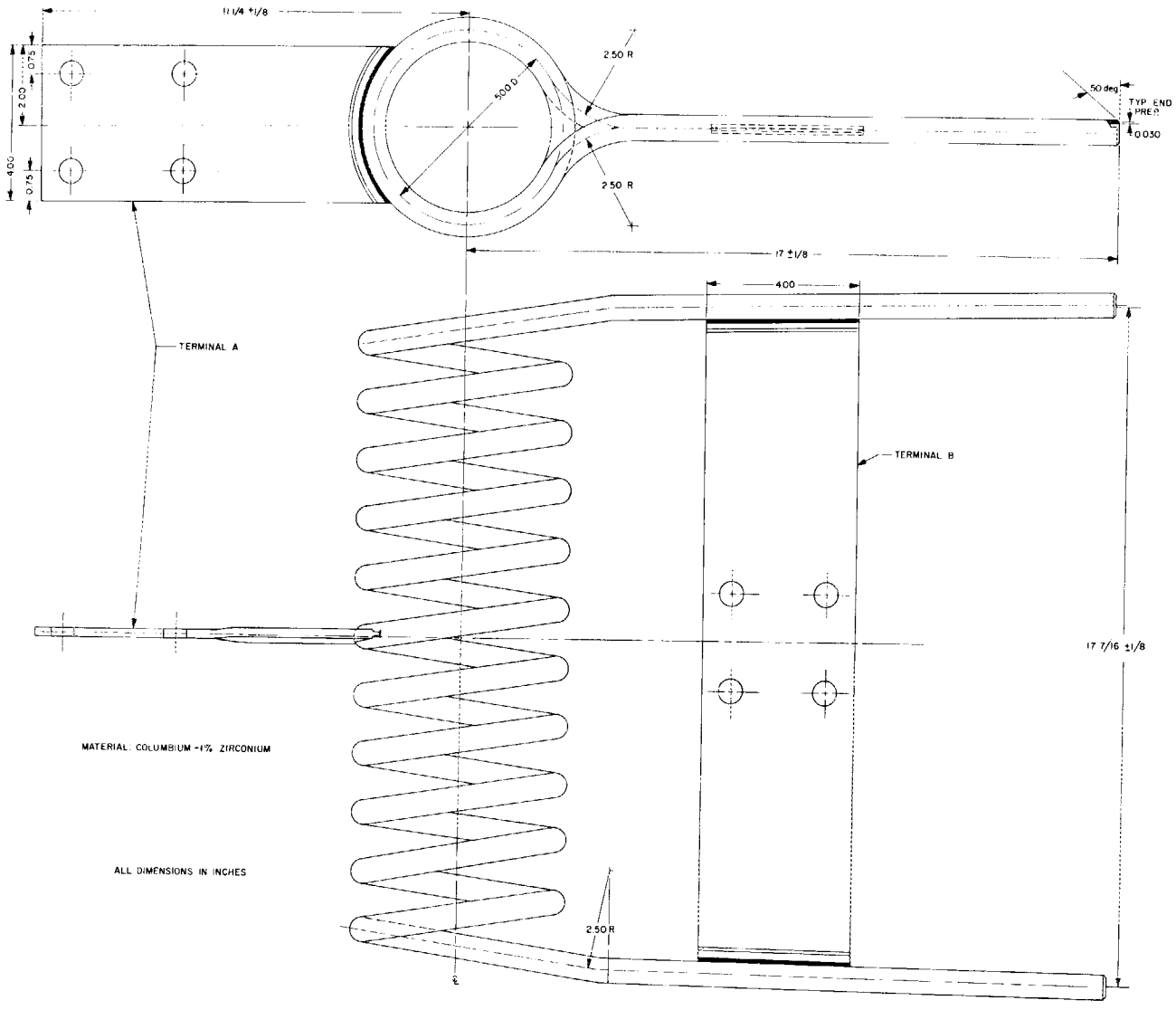

Fig. 6. Lithium circuit direct resistance heating coil

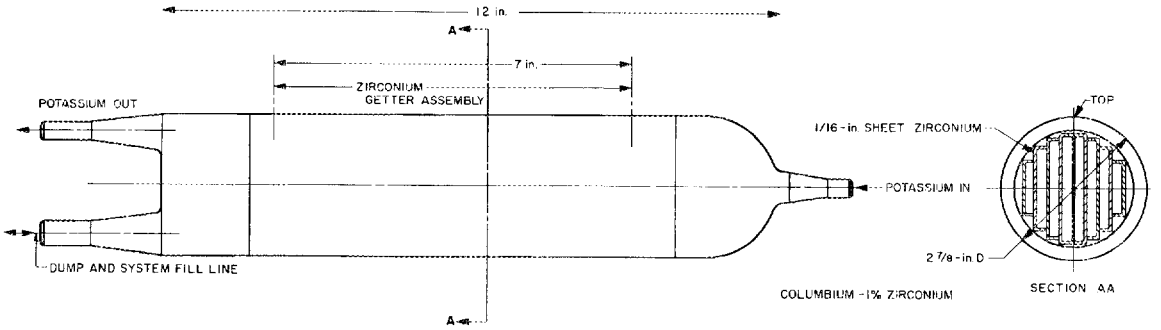

Fig. 7. Potassium circuit hold-up and hot trap assembly

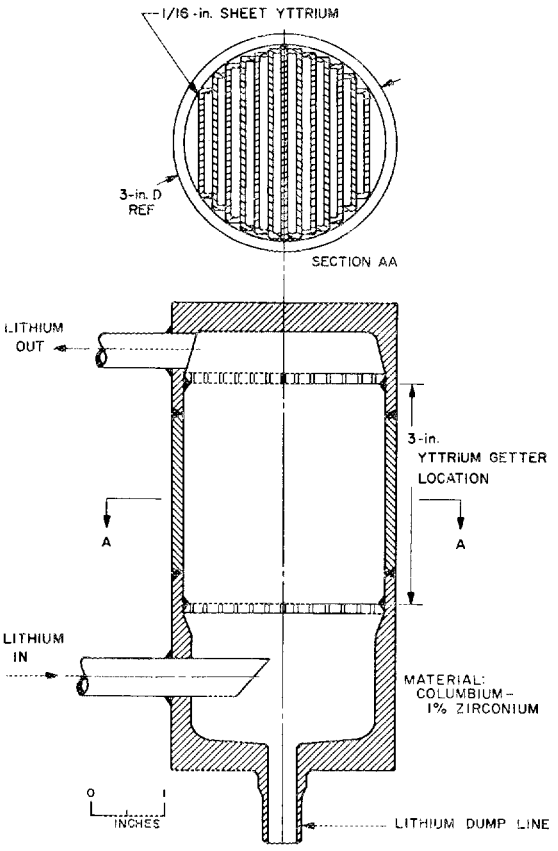

Fig. 8. Lithium circuit hot trap assembly

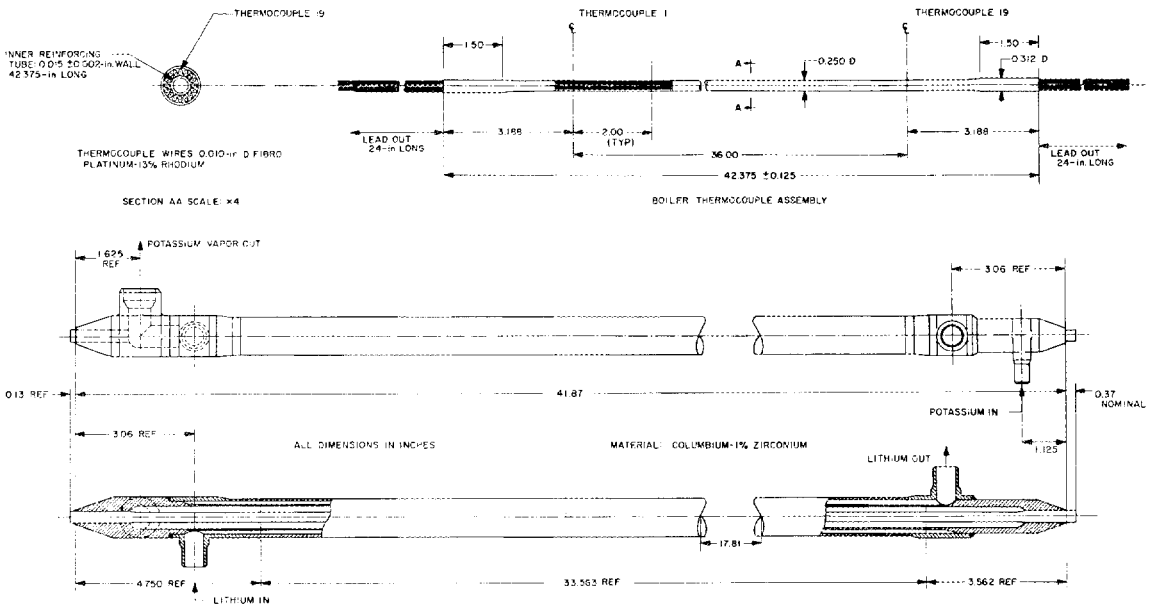

Fig. 9. Lithium-boiling potassium loop boiler assembly

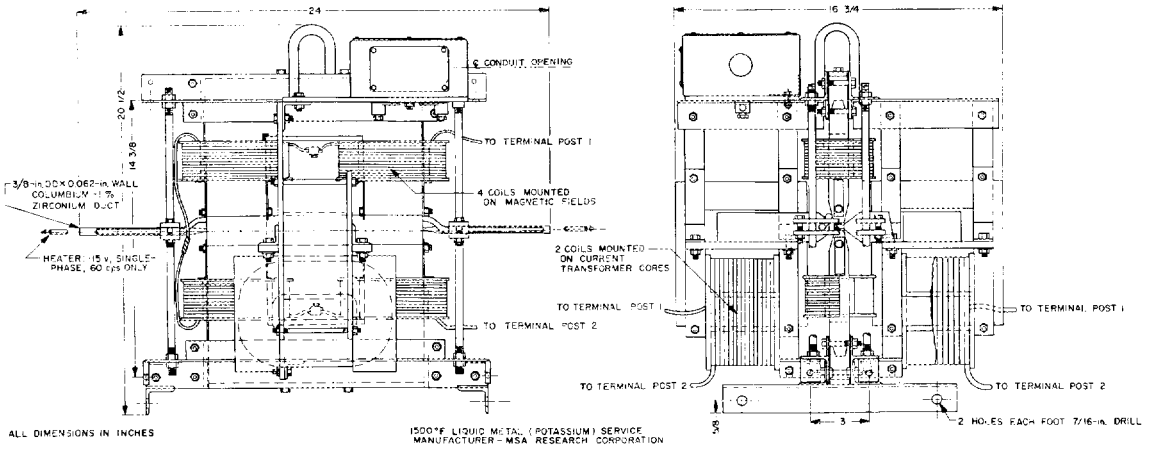

Fig. 10. Electromagnetic pump assembly

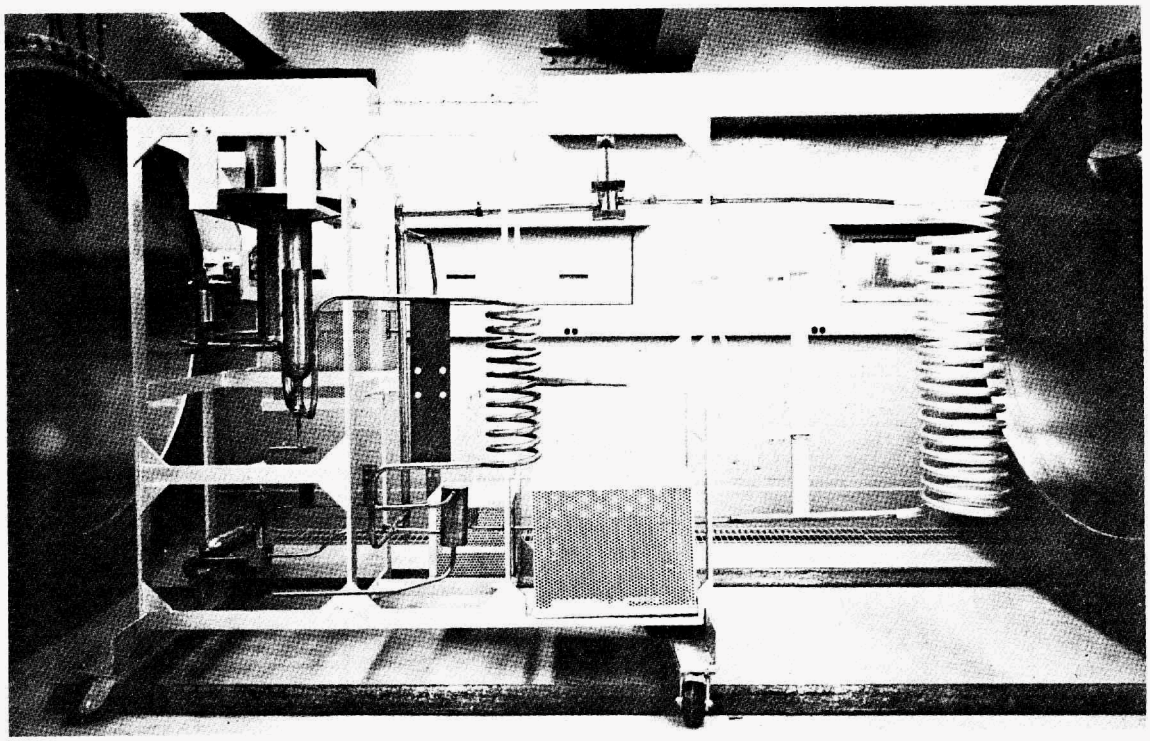

Fig. 11. Lithium-boiling potassium loop mock-up

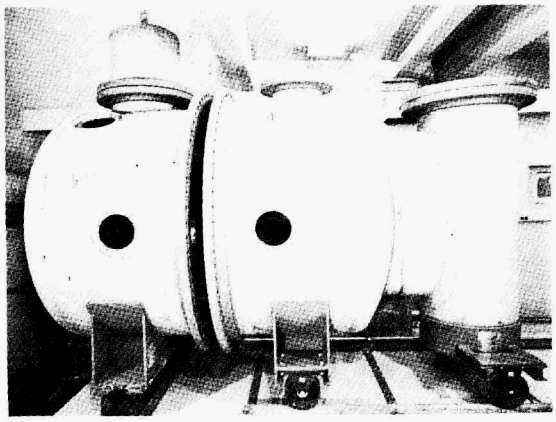

Fig. 12. Lithium-boiling potassium loop containment vessel

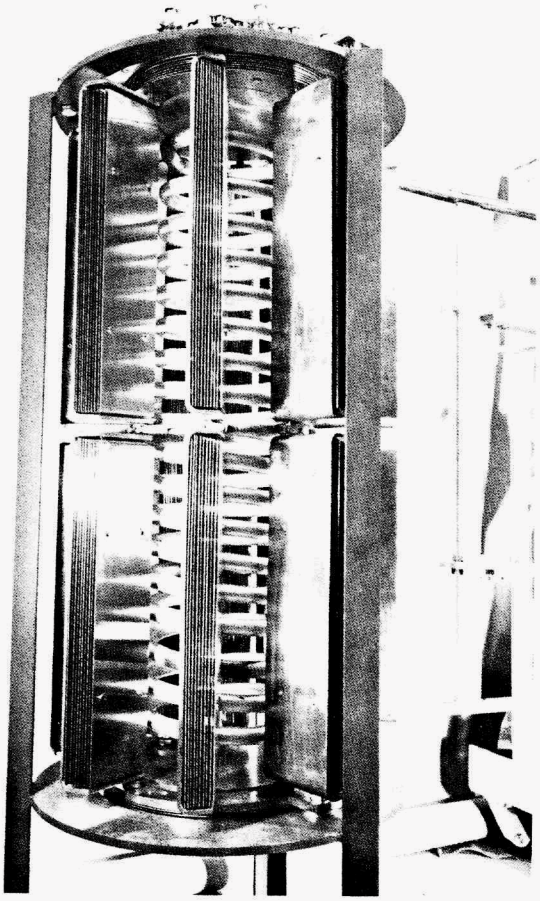

Fig. 13. Radiator shutter assembly—open position

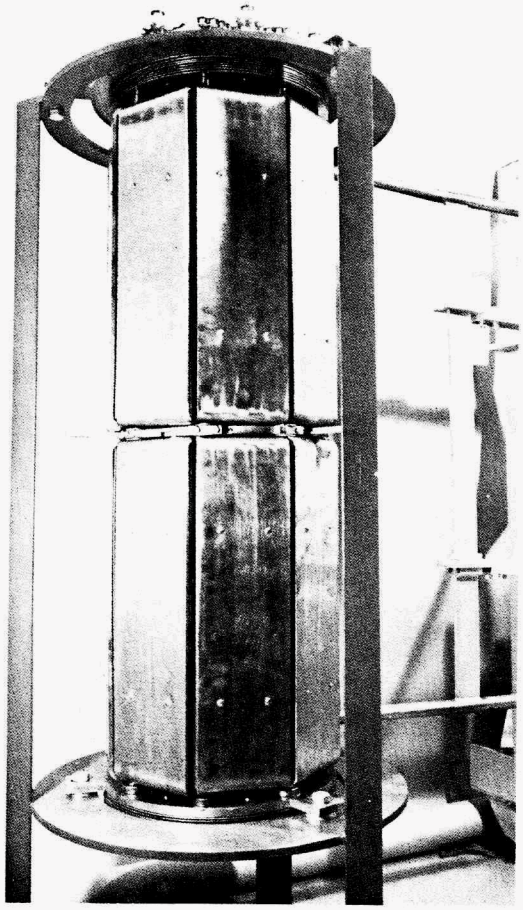

Fig. 14. Radiator shutter assembly—closed position

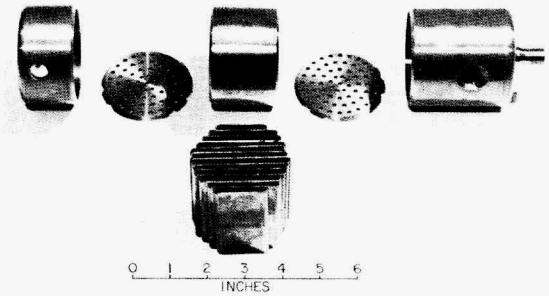

Fig. 15. Lithium circuit hot trap assembly

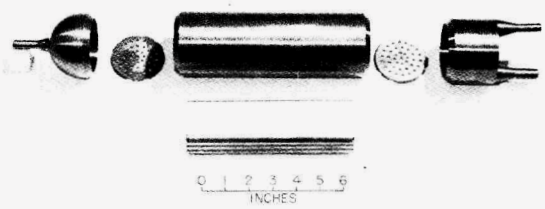

Fig. 16. Potassium circuit hot trap assembly

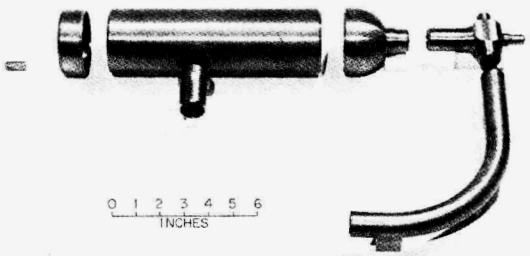

Fig. 17. Lithium circuit liquid level indicator assembly

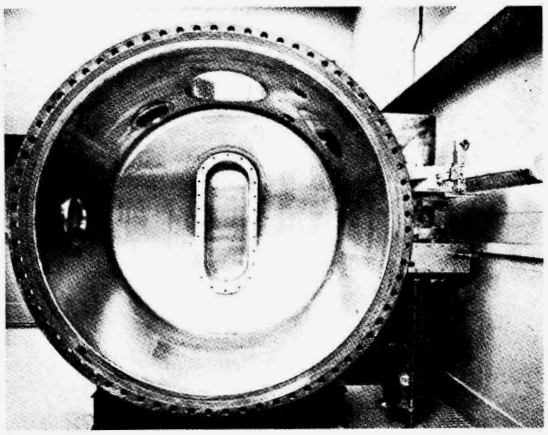

Fig. 18. 10-in. Vacuum system, attached to stationary section of containment vessel

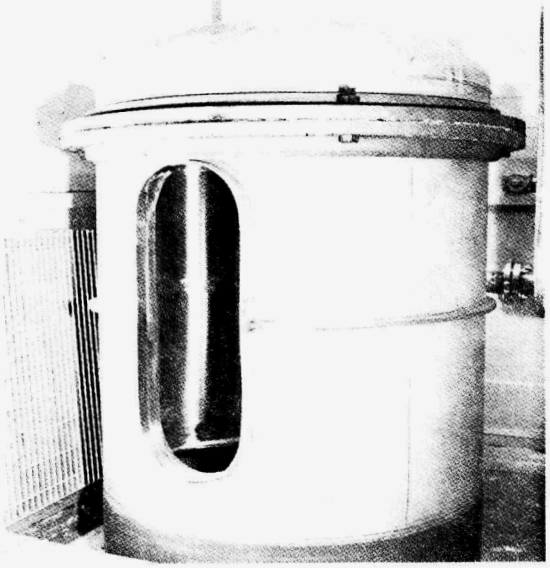

Fig. 19. Loop dump system containment vessel

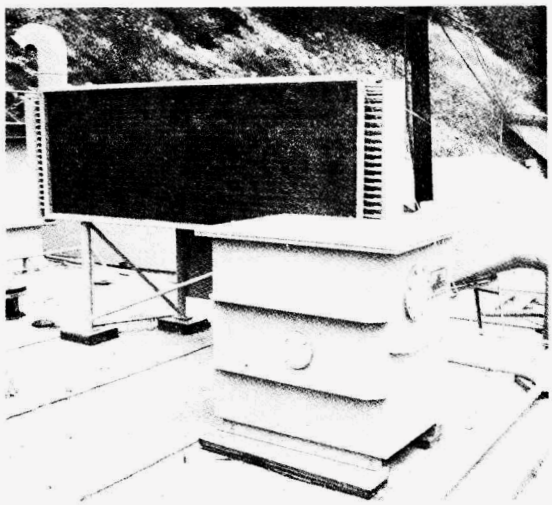

Fig. 20. Loop argon cooler and blower assembly

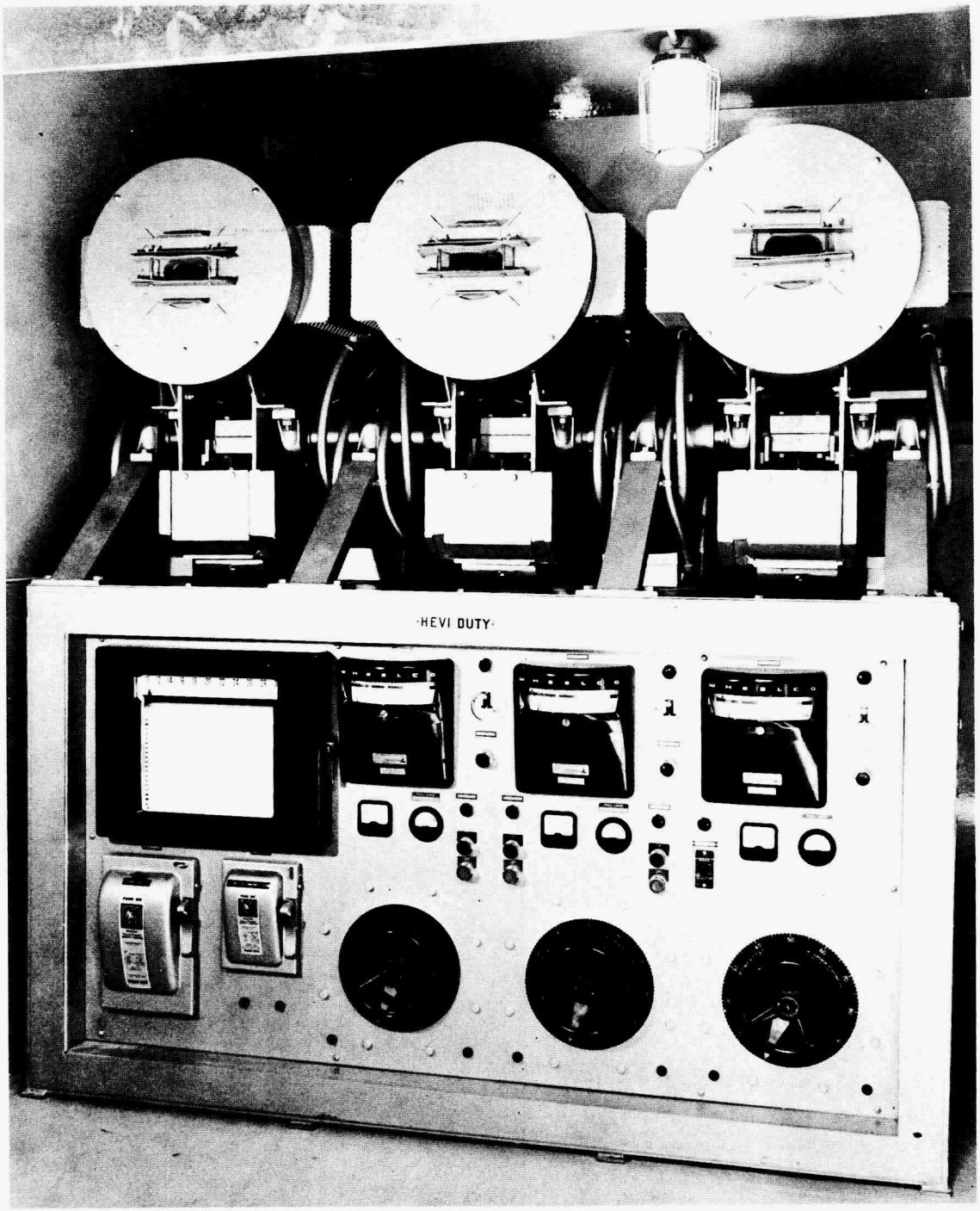

Fig. 21. Tilting furnace assembly

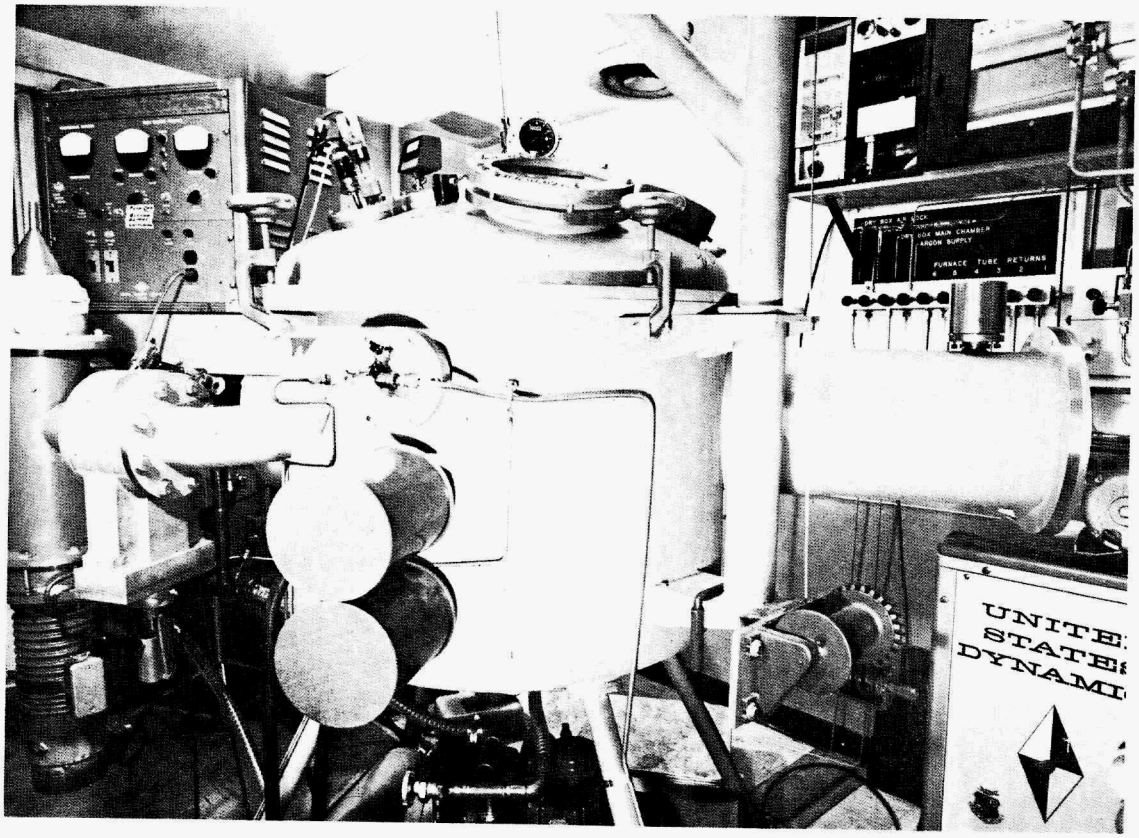

Fig. 22. TIG welding drybox with purification and analysis equipment

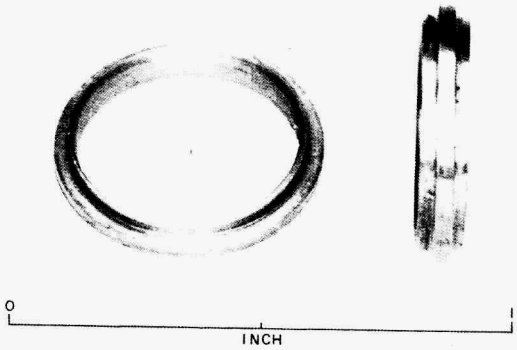

Fig. 23. Cb-1Zr welding inserts for 5/8-in. tubing

Table 2. Cb-1Zr compatibility tests for insulation

Insulation	Tantalum wrap	Tensile strength, psi	Elongation, %	Microhardness	
				Surface	Center
Cercor	No	35,300	54	118	112
Cercor	Yes	34,700	52	108	111
Glassrock #25	No	35,000	52	116	111
Glassrock #25	Yes	34,200	52	114	112
Foamsil	No	34,700	55	111	110
Foamsil	Yes	35,600	50	118	118
None	No	32,800	54	109	110
None	Yes	33,900	51	113	110

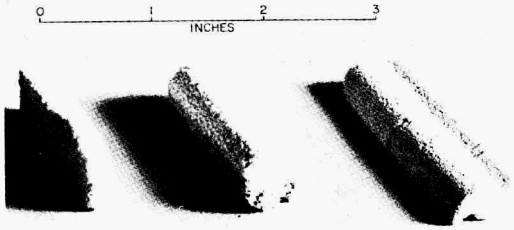

Fig. 24. Glassrock foam #25 as received after outgassing at 2000°F and after testing at 2200°F

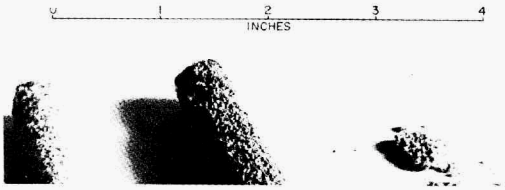

Fig. 25. Foamsil as received, after outgassing at 2000°F and after testing at 2200°F

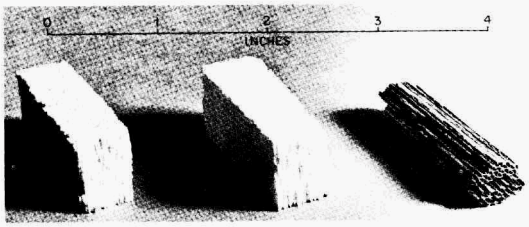

Fig. 26. Cercor as received, after outgassing at 2000°F and after testing at 2200°F

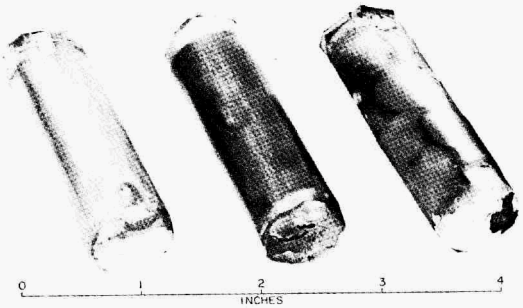

Fig. 27. Cb-1Zr capsules warpped with (from left to right) molybdenum, tantalum and zirconium foil after exposure to argon containing 2 ppm oxygen at 2200°F for 100 hr

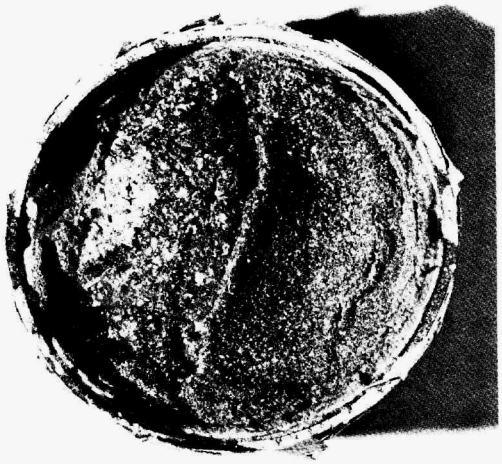

Fig. 28. Cb-1Zr capsule containing molybdenum oxide after 100 hr at 2200°F

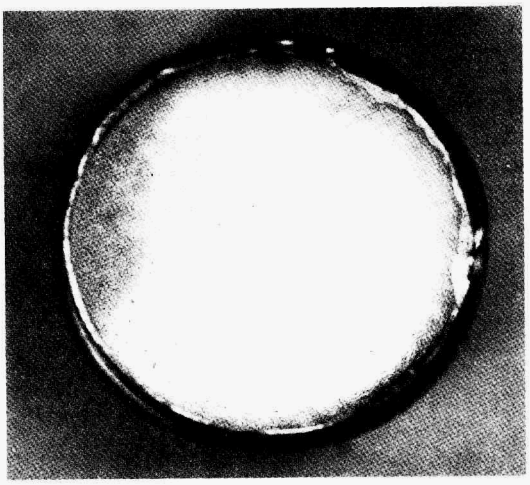

Fig. 29. Cb-1Zr capsule containing tantalum oxide after 100 hr at 2200°F

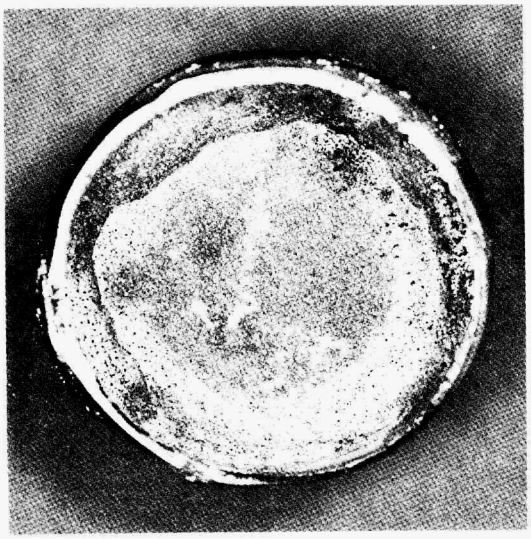

Fig. 30. Cb-1Zr capsule containing zirconium oxide after 100 hr at 2200°F

HEAT TRANSFER COEFFICIENTS IN LIQUID METAL CO-CURRENT FLOW DOUBLE PIPE HEAT EXCHANGERS

by

Ralph P. Stein

ABSTRACT

An analytical study of heat transfer in co-current flow double pipe heat exchangers is described. Although the analysis is based on plug flow models of the heat exchanging fluids, an approximation method is developed which allows application to the turbulent flow of liquid metals with good accuracy indicated up to Peclet numbers of 1000. The analysis is applied to the prediction of fully developed individual channel ("film") heat transfer coefficients. The following results are demonstrated.

(1) Values of fully developed heat transfer ("film") coefficients can be significantly less than those corresponding to the boundary condition of uniform wall temperature, but never larger than those corresponding to the boundary condition of uniform wall flux.

(2) The thermal resistance of the wall separating the two channels of the exchanger can have a significant effect on the heat transfer ("film") coefficient, with large wall resistance tending to result in larger values of the heat transfer coefficient.

(3) When operating with constant mass flow rate through one channel of the exchanger, while varying mass flow rate through the adjacent channel, the dependence of the fully developed heat transfer ("film") coefficient on Peclet number will be less than for the cases of uniform wall temperature or uniform flux. Under certain operating conditions, the heat transfer coefficient will decrease with increasing Peclet number.

These results suggest the possibility that the "inconsistent" values of heat transfer coefficients frequently obtained from experiments with double pipe heat exchangers, are actually a predictable effect of the exchanger operating conditions.

1. INTRODUCTION

The double pipe heat exchanger is one of the simplest of devices for transferring heat between two fluids. It is used not only as a practical heat exchange arrangement, but also as a laboratory tool for determining forced convection heat transfer coefficients by experiment. Design of such exchangers is also simple provided appropriate values of heat transfer coefficients can be obtained. Implicit in the customary use of heat transfer coefficients for this purpose are two essential assumptions. First, the

individual channel ("film") coefficients are assumed to be relatively insensitive to the longitudinal distribution of heat flux or surface temperature. Sometimes this assumption is implied by asserting that the actual heat exchanger operation will represent conditions intermediate to operation with uniform heat flux and uniform surface temperature, and that therefore actual heat transfer coefficients should have values somewhere between those appropriate to these two special boundary conditions. The second assumption is that the heat transfer coefficients are relatively independent of length or that the heat transfer is "fully developed" over most of the exchanger length. Customary analyses of laboratory data from double pipe heat exchangers for the purpose of determining heat transfer coefficients by experiment usually imply the validity of the first assumption, and sometimes the second also.

There appears to be substantial evidence that these assumptions lead to sufficiently accurate results in practical applications when the fluids are in turbulent flow and have moderate-to-high Prandtl numbers. These are conditions that favor the reasonableness of a stagnant film explanation of forced convection heat transfer. Under such conditions significant temperature gradients are localized near the heat transfer surface, and qualitatively at least, can be considered to occur over a small film or boundary layer thickness which is determined mainly by the state of flow.

For fluids in laminar flow or for the turbulent flow of liquid metals, which characteristically have very small Prandtl numbers, the stagnant film description is not always a very reasonable one. Significant temperature gradients can occur over the entire duct cross section, and can be strongly influenced not only by the state of flow but also by the heat transfer boundary conditions. As a result, for laminar flows and with liquid metals, the assumptions implicit in the customary methods of analysis of heat transfer in heat exchangers deserves to be questioned.

For this purpose, heat transfer in certain idealized co-current flow double pipe heat exchangers is analyzed in detail without use of these assumptions. Initially, the main idealization utilizes a plug flow model for the two heat exchanging fluids - i.e., velocity and effective conductivity distributions are taken as uniform. An approximation technique is then introduced which allows use of results from the plug flow idealization to approximate results for turbulent flows of liquid metals up to Peclet numbers of about 1000. In this introductory paper, application of the analysis is directed towards examination of the effects of heat exchanger operating conditions on fully developed individual channel ("film") heat transfer coefficients. Other applications, which will be described in a more complete report to be published in the near future, include thermal entrance region considerations, the behavior of over-all heat transfer coefficients, and comparisons of customary design calculations with more exact predictions of heat exchanger performance. A similar analysis with applications for the counter-current flow case presents certain mathematical difficulties which are being studied at present. To date, counter-current flow analyses based on the further simplification of a uniform heat transfer coefficient in one of the channels have been successful; and, although not completely studied as yet, indicate results similar to those for the co-current flow case.

Aside from adding to the basic understanding of convection heat transfer in general, the investigations relate to two areas of current practical interest: first, the proper design of liquid metal heat exchangers in general; second, the use of double pipe heat exchangers for the purpose of determining liquid metal heat transfer coefficients for general application by experiment. This paper relates more directly to the latter than the former.

Direct application of the quantitative results of the investigations reported here to these areas of current interest may be somewhat limited. Most technologically important liquid metal heat exchangers are not simple co-current flow double pipes. Most of the available liquid metal heat transfer coefficient data obtained from laboratory double pipe heat exchangers are based on counter current flow. But current design procedures and methods of interpreting laboratory data imply the same essential assumptions - that heat transfer coefficients are relatively insensitive to boundary conditions and/or are fully developed over most of the exchanger length. Thus, the analyses of the special simple cases treated here can serve to suggest possible qualitative effects to be expected with the more complicated cases. For example, as will be seen, the application presented here suggests the possibility that the "inconsistent" values of heat transfer coefficients frequently obtained from measurements made with double pipe heat exchangers, are actually a predictable effect of operating conditions, and may not require speculations concerning liquid metal "wetability" or inaccurate measurements to explain their occurrence.

2. FORMULATION OF GENERAL PROBLEM

The usual double pipe heat exchanger consists of two concentric circular pipes with fluids flowing through the annular space and the central tube. In a co-current flow exchanger, the fluids enter their respective flow channels at the exchanger inlet with different temperatures, transferring heat through the common wall as they flow in parallel along the length of the exchanger. In order to explore the effects of different duct shapes, a double pipe heat exchanger made up of adjacent infinitely wide parallel plane channels separated by a common wall, is considered also. These two "geometries" are illustrated in figure 1, which also identifies some of the nomenclature used.

In order to perform the desired analyses, the following problem must be solved first. Given the appropriate duct dimensions, physical properties, fluid mass flow rates and inlet conditions, the temperature distributions $t_i(x_i,\ell)$, $i = 1$ and 2, must be found. From the temperature distributions, the heat transfer coefficients and the rate of heat exchange between the two fluids can be computed. In order to be able to solve this problem in a relatively convenient manner, considerable simplification is necessary. Thus the following idealizations are made.

(1) At the inlet to the duct the temperature distributions within the fluids are uniform.

(2) Physical properties are temperature independent.

(3) Frictional heating is negligible.

(4) Longitudinal heat conduction in the heat exchanger walls is negligible.

(5) Longitudinal heat transport in the fluids other than by convection is negligible.

(6) The velocity distributions within the fluids are uniform.

(7) Heat transport within the fluids by turbulent diffusion (eddy conduction) is negligible compared to molecular heat conduction.

The first four idealizations are almost always reasonable. The fifth has been shown to be valid for a variety of special cases when Peclet numbers are larger than 50.[2][5] It seems reasonable to assume that this validity will carry over to the particular cases of interest here. The sixth and seventh idealizations are equivalent to the use of a "plug flow" model of the fluids. For the turbulent flow of liquid metals, a plug flow model is a fairly accurate representation for Peclet numbers less than 50,[2] which is not consistent with the fifth idealization which requires Peclet numbers to be larger than 50. Further, Peclet numbers in real double pipe heat exchangers are usually larger than 50. Nevertheless, the plug flow model is retained because of the resulting mathematical simplicity. In addition, it will be shown later that solutions to the general problem based on this simple model can be used to approximate the behavior of liquid metal flows for Peclet numbers up to 1000, which includes a region of practical interest.

The problem is simplified further by considering the annular space of the concentric tube geometry to be very narrow. This eliminates the need to include an annulus diameter ratio as an additional variable. Inclusion of this geometry variable at this time would not add greatly to the significance of the analysis, but would increase enormously the amount of computation required.

Mathematical Description of Problem

With the above simplifications, the principle of energy conservation, together with Fourier's heat conduction law, applied to each of the fluids flowing in its channel, results in the familiar simplified convection equation; viz.

$$\nabla^2 t_i = \frac{u_i}{\alpha_i} \frac{\partial t_i}{\partial \ell} \quad , \quad i = 1, 2 \tag{1}$$

where α_i represents the thermal diffusivity of the fluid in channel "i," and u_i represents its velocity. As associated with the coordinates x_i and ℓ identified in figure 1, the Laplacian, ∇^2, is given by

$$\nabla^2 t_i \equiv \frac{\partial^2 t_i}{\partial x_i^2} \quad , \quad i = 1, 2 \tag{2a}$$

for the narrow annular space and the parallel plane channels, and by

$$\nabla^2 t_i \equiv \frac{1}{x_i}\frac{\partial}{\partial x_i}\left(x_i \frac{\partial t_i}{\partial x_i}\right), \quad i = 1 \tag{2b}$$

for the circular tube. Also $0 \leq x_i \leq a_i$, and $x_i = a_i$ locates the heat transfer surface of channel "i," while $\ell = 0$ identifies the heat exchanger inlet.

Considering $t_i(x_i, \ell)$, the inlet conditions require

$$t_i(x_i, 0) = t_{io} \tag{3}$$

and at the insulated walls or at the circular tube center

$$\left.\frac{\partial t_i}{\partial x_i}\right|_{x_i = 0} = 0 \tag{4}$$

To assist in formulating the boundary conditions at the common wall, we arbitrarily consider $t_{20} > t_{10}$. Then the heat flux density at the wall, q_i in figure 1, is positive when flowing from channel "2" to "1," so that

$$q_1 = -\left(-k_1 \left.\frac{\partial t_1}{\partial x_1}\right|_{a_1}\right) \tag{5a}$$

and

$$q_2 = -k_2 \left.\frac{\partial t_2}{\partial x_2}\right|_{a_2} \tag{5b}$$

For the concentric tube exchanger

$$2\pi(a_1+b)\,q_2 = 2\pi a_1\, q_2$$

which results in

$$k_1 \left.\frac{\partial t_1}{\partial x_1}\right|_{a_1} = -\left(1+\frac{b}{a_1}\right) k_2 \left.\frac{\partial t_2}{\partial x_2}\right|_{a_2} \tag{6a}$$

while for the parallel plane geometry $q_1 = q_2$, and the relation

$$k_1 \left.\frac{\partial t_1}{\partial x_1}\right|_{a_1} = -k_2 \left.\frac{\partial t_2}{\partial x_2}\right|_{a_2} \tag{6b}$$

results. Equation (5a) and (5b) account for the equality of the heat flow on both sides of the common wall. We must now account for the temperature change resulting from heat conduction through the wall. For the circular tube wall the familiar log-mean area conduction equation can be expressed as

$$q_1 = \frac{k_w}{b'}\left[t_2(a_2,\ell) - t_1(a_1,\ell)\right] \tag{7}$$

with

$$b' = a_1 \ln\left(1+\frac{b}{a_1}\right) \tag{8a}$$

$$\approx b\left(1-\frac{1}{2}\frac{b}{a_1}+\cdots\right) \tag{8b}$$

Equation (7) also applies to the parallel plane geometry with b' = b.

Equations (1) through (8) are sufficient to describe the idealized double pipe heat exchangers mathematically. They constitute a two region linear boundary value problem, the solution of which will give the desired temperature distributions $t_i(x_i, \ell)$.

It is convenient at this point to introduce a dimensionless formulation, and then restate the problem in purely mathematical form. This will serve not only to simplify the nomenclature, but also, as the equivalent of a dimensional analysis, to assist in identifying the important parameters of the problem.

Dimensionless Formulation

First it is noted that as the heat exchanger length increases without limit, both fluid temperatures must approach an equal and uniform equilibrium value, t_∞, given by the simple heat balance

$$C_1 W_1 (t_\infty - t_{10}) = C_2 W_2 (t_{20} - t_\infty) \tag{9}$$

from which the relationship

$$t_\infty - t_{10} = \frac{H}{1+H} \Delta t_0 \tag{10}$$

is obtained with

$$H = \frac{C_2 W_2}{C_1 W_1} \tag{11}$$

and

$$\Delta t_0 = t_{20} - t_{10} \tag{12}$$

The heat capacity flow rate ratio, H, is a familiar one in heat exchanger analyses, and it will be advantageous to retain it as one of the dimensionless parameters in our analysis. Equation (10) also suggests the dimensionless temperature;

$$\xi_i = (t_i - t_{10})/\Delta t_0 \quad , \; i = 1, 2 \tag{13}$$

The following dimensionless space variables are now introduced: A dimensionless distance x, normal to the heat transfer surfaces defined by

$$x = \frac{x_i}{a_i} \quad , \quad i = 1, 2 \tag{14}$$

and a dimensionless length z, referenced arbitrarily to the properties of channel "1," defined by

$$z = \frac{\alpha_1 \ell}{u_1 a_1^2} \tag{15}$$

Note that $0 \leq x \leq 1$ with $x = 1$ identifying the heat transfer surface for all channels, and therefore subscripts are not required. Note also that $\xi_i(x,z)$ now replaces $t_i(x_i,\ell)$ and that $\xi_1(x,0) = 0$ while $\xi_2(x,0) = 1$. Further, from equation (10),

$$\lim_{z \to \infty} \xi_i(x,z) = \frac{H}{1+H}$$

The dimensionless length z can be expressed in more familiar terms by introducing the Peclet number defined by

$$Pe_i = \frac{D_i u_i}{\alpha_i}$$

with D_i, the hydraulic equivalent diameter, equal to $2a_i$ for all channels. Introduction of the Peclet number into equation (15) results in an alternate definition for z given by

$$z = \frac{4}{Pe_1}\left(\frac{\ell}{D_1}\right) \tag{15a}$$

Substitution of the dimensionless variables ξ_i, x, and z for their dimensional equivalents in the differential equations and boundary conditions given by equations (1) to (7) results in the following dimensionless mathematical statement of the general problem.

Differential Equations

For the concentric tube exchanger:

$$\frac{1}{x}\frac{\partial}{\partial x}\left(x\frac{\partial \xi_1}{\partial x}\right) = \frac{\partial \xi_1}{\partial z}$$
$$\frac{\partial^2 \xi_2}{\partial x^2} = \frac{1}{2} KH \frac{\partial \xi_2}{\partial z} \tag{16a}$$

For the parallel plane exchanger:

$$\frac{\partial^2 \xi_1}{\partial x^2} = \frac{\partial \xi_1}{\partial z}$$
$$\frac{\partial^2 \xi_2}{\partial x^2} = KH \frac{\partial \xi_2}{\partial z} \tag{16b}$$

Boundary Conditions (Both geometries)

$$\xi_1(x,0) = 0 \tag{17}$$

$$\xi_2(x,0) = 1 \tag{18}$$

$$\left.\frac{\partial \xi_i}{\partial x}\right|_0 = 0 \quad , \quad i = 1, 2 \tag{19}$$

$$K \left.\frac{\partial \xi_1}{\partial x}\right|_1 + \left.\frac{\partial \xi_2}{\partial x}\right|_1 = 0 \tag{20}$$

$$K_w \left.\frac{\partial \xi_1}{\partial x}\right|_1 + \xi_1(1,z) - \xi_2(1,z) = 0 \tag{21}$$

where

$$K = \left(\frac{k_1}{a_1}\right)\left(\frac{a_2}{k_2}\right) \qquad \text{(parallel planes)} \qquad (22a)$$

$$= \left(\frac{k_1}{a_1}\right)\left(\frac{a_2}{k_2}\right)\left(1 + \frac{b}{a_1}\right) \qquad \text{(concentric tubes)} \qquad (22b)$$

$$K_w = \left(\frac{k_1}{a_1}\right)\left(\frac{b}{k_w}\right) \qquad \text{(parallel planes)} \qquad (23a)$$

$$= \left(\frac{k_1}{a_1}\right)\left(\frac{b'}{k_w}\right) \qquad \text{(concentric tubes)} \qquad (23b)$$

The parameter H is a familiar one in heat exchanger analysis, as mentioned previously. The parameters K and K_w are not familiar ones but may be given simple physical significance when interpreted as relative thermal resistances. Thus, considering the ratio a_1/k_1 as a measure of the thermal resistance for heat flow to or from channel "1," K can be interpreted as the thermal resistance for heat flow to or from channel "2" relative to channel "1." Similarly K_w can be interpreted as the relative thermal resistance of the exchanger common wall.

Inspection of the above reveals that the dimensionless temperature distributions $\xi_i(x,z)$ depend exclusively on the three dimensionless groups H, K, and K_w in the sense that once these groups are assigned values, the mathematical solution is determined. Thus it is to be expected that quantities such as heat exchange rates and heat transfer coefficients, when expressed in appropriate dimensionless forms, will also depend on H, K, and K_w.

3. INDIVIDUAL CHANNEL NUSSELT NUMBERS

Clearly, the parameters H, K, and K_w characterize the operating conditions of the simple heat exchangers being considered. In this paper we are interested in the effect these operating conditions have on fully developed individual channel ("film") heat transfer coefficients, as compared, for example, to heat transfer coefficients appropriate to the channel boundary conditions of uniform heat flux or uniform surface temperature. In a sense, then, the parameters H, K, and K_w specify more exact channel boundary conditions for co-current flow double pipe heat exchangers.

The individual channel heat transfer coefficients, h_i, expressed as Nusselt numbers, Nu_i, are easily related to the dimensionless temperature distributions, $\xi_i(x,z)$. For example, by definition

$$h_1 = \frac{q_1}{t_1(a_1,\ell) - t_{B1}(\ell)} \tag{24}$$

where t_{B1} represents the heat content mean or "bulk" temperature of the fluid in channel "1." For the circular tube and uniform velocity distributions

$$t_{B1} = \frac{2}{a_1^2}\int_0^{a_1} t_1(x_1,\ell)\, x_1\, dx_1$$

while for the parallel plane channel

$$t_{B1} = \frac{1}{a_1}\int_0^{a_1} t_1(x_1,\ell)\, dx_1$$

Using equation (5a) for q_1 and introducing the dimensionless formulation described previously, equation (24) becomes

$$h_1 = \left(\frac{k_1}{a_1}\right) \frac{\left.\frac{\partial \xi_1}{\partial x}\right|_1}{\xi_1(1,z) - \xi_{B1}(z)}$$

with dimensionless bulk temperatures given by

$$\xi_{B1}(z) = 2\int_0^1 x\,\xi_1(x,z)\,dx \tag{25a}$$

for the circular tube, and

$$\xi_{B1}(z) = \int_0^1 \xi_1(x,z)\,dx \tag{25b}$$

for the parallel plane channel. Finally, by defining the Nusselt number in the usual way, i.e., by

$$\begin{aligned} Nu_1 &= \frac{D_1 h_1}{k_1} \\ &= \frac{2a_1 h_1}{k_1} \end{aligned} \tag{26}$$

the following is obtained

$$Nu_1(z) = \frac{2\left.\frac{\partial \xi_1}{\partial x}\right|_1}{\xi_1(1,z) - \xi_{B1}(z)} \tag{27}$$

The same expression is obtained for Nu_2 with subscripts changed.

In this paper we are interested in fully developed Nusselt numbers, which can be defined by

$$Nu_i(\infty) = \lim_{z \to \infty} Nu_i(z) \tag{28}$$

so that analytical solutions for $\xi_i(x,z)$ suitable for large values of z are needed. Before discussing such solutions and applying them to equation (28), let us consider first the approximation technique for turbulent liquid metal flows mentioned earlier.

4. AN APPROXIMATION FOR TURBULENT FLOWS

The mathematical formulation given thus far utilizes a plug flow model for the fluids, i.e., fluid velocities and conductivities are taken as uniform. As remarked previously, this kind of idealization will result in fairly accurate predictions for turbulent liquid metal flows when Peclet numbers are less than 50. But this limitation contradicts the requirement that Peclet numbers be larger than 50 in order to justify neglecting heat conduction in the longitudinal direction. Further, areas of practical interest usually correspond to Peclet numbers larger than 50. In order to alleviate this difficulty, an approximation technique is now presented which increases the Peclet number range over which use of a plug flow model can be expected to give fairly accurate results.

Basis for Approximation

The basis for the approximation is described for the case of turbulent convection heat transfer for flow through infinitely wide parallel plane channels. As will be seen, the same basic idea applies to the cylindrical geometry also.

The convection heat transfer equation analogous to equations (1) and (2a), but for turbulent flow, is

$$\frac{\partial}{\partial x}\left[(k + c\rho\epsilon)\frac{\partial t}{\partial x}\right] = c\rho a^2 u \frac{\partial t}{\partial \ell} \tag{29}$$

where the dimensionless distance variable x ($0 \leq x \leq 1$) has been used, and subscripts have been dropped for convenience. In this equation ϵ represents a turbulent diffusivity for heat transfer and, along with the fluid velocity u,

must now be considered a function of x. An implication is that the flow is fully developed in the sense that both ϵ and u are independent of the longitudinal position variable, ℓ.

The term $k + c\rho\epsilon$ can be interpreted as an effective total conductivity k_t. Thus,

$$k_t/k = 1 + \frac{\epsilon\rho}{\mu}\frac{c\mu}{k}$$

$$= 1 + \frac{\epsilon}{\nu} Pr \tag{30}$$

where ν is the kinematic viscosity and Pr the Prandtl number. Now we define an average effective conductivity k_m by

$$\frac{1}{k_m} = \int_0^1 \frac{dx}{k_t} \tag{31}$$

and a new distance variable $\eta(x)$ by

$$\eta(x) = k_m \int_0^x \frac{dx}{k_t} \tag{32}$$

so that $\eta(0) = 0$ and $\eta(1) = 1$.

By replacing x by η in equation (29) using

$$dx = \frac{k_t}{k_m} d\eta \tag{33}$$

and rearranging, the following is obtained:

$$\frac{\partial^2 t}{\partial \eta^2} = \frac{a^2 \bar{u}}{\alpha k^+} g(\eta) \frac{\partial t}{\partial l}$$

$$= g(\eta) \frac{\partial t}{\partial z} \tag{34}$$

where

$$\bar{u} = \int_0^1 u(x)\,dx$$

$$k^+ = k_m / k$$

$$g(\eta) = \frac{u(\eta)}{\bar{u}} \frac{k_x(\eta)}{k_m}$$

and

$$z = \frac{\alpha k^+}{a^2 \bar{u}} l$$

$$= \frac{4 k^+}{Pe} \left(\frac{l}{D}\right)$$

Current methods for computing values for ϵ have the ratio ϵ/ν as a function of dimensionless position x, the duct Reynolds number, and sometimes, especially with liquid metals, the Prandtl number. Thus η will be a function of these same quantities, while k^+ will be a function of Reynolds and Prandtl numbers.

As compared to the analogous plug flow expressions, e.g., equations (16b), solutions of equation (34) will give temperature distributions as $\xi(\eta,z)$ rather than $\xi(x,z)$ once the proper boundary conditions are specified, and equation (32) must be used to relate x to η. Since $\eta(0) = 0$ and $\eta(1) = 1$, this variable change influences only heat flux boundary conditions, for if q is the heat flux density at $x = \eta = 1$, then

$$q = -\frac{k}{a}\frac{\partial t}{\partial x}\Big|_1$$

$$= -\frac{k}{a}\left(\frac{d\eta}{dx}\right)\frac{\partial t}{\partial \eta}\Big|_1$$

$$= -\frac{k k^+}{a}\frac{\partial t}{\partial \eta}\Big|_1$$

since $k_t = k$ at $x = \eta = 1$. Obviously the same situation applies at $x = \eta = 0$. The change in variable introduces an effective fluid thermal conductivity equal to k_m or kk^+. As a result the parameters K and K_w in the dimensionless formulation of the parallel plane double pipe heat exchanger problem become

$$K = \left(\frac{k_1}{a_1}\right)\left(\frac{a_2}{k_2}\right)\left(\frac{k_1^+}{k_2^+}\right)$$

and

$$K_w = \left(\frac{k_1}{a_1}\right)\left(\frac{\delta}{k_w}\right)k_1^+$$

where the subscripts on k^+ indicate that appropriate values depend on the Reynolds and Prandtl numbers for channel "i."

So far no approximations have been introduced other than those implicit in the use of equation (29). But the form of $g(\eta)$ has been chosen intentionally so that for sufficiently small Peclet numbers, it is very close to unity over most of the duct cross section. In fact, the average value of $g(\eta)$ is exactly unity for all Peclet numbers, viz.

$$g_{av.} = \int_0^1 g(\eta)\,d\eta$$

$$= \int_0^1 \frac{u(\eta)}{\bar{u}}\frac{k_e(\eta)}{k_m}\,d\eta$$

$$= \int_0^1 \frac{u(x)}{\bar{u}}\, dx$$

$$= 1$$

If, as an approximation, $g(\eta)$ is set equal to its average value, i.e., unity, then equation (34) is equivalent to that obtained from the plug flow idealization based on a uniform effective thermal conductivity equal to kk^+ and with a change in variable from x to η. Clearly, in regions where this approximation results in sufficiently accurate temperature distributions, the extent of simplification it provides is considerable, since plug flow solutions are relatively easy to obtain compared to integrations of equation (29) or (34) with g a function of η.

Accuracy of the Approximation

A definitive analysis of the magnitude of errors introduced by taking $g(\eta) = 1$ in equation (34) has not been achieved as yet. Instead, turbulent flow Nusselt number predictions resulting from this approximation, which we shall now refer to as the "k^+ approximation," have been compared with several predictions obtained from detailed turbulent flow calculations reported in the literature. For this purpose, and for later application to the double pipe heat exchanger problem, it is noted that when the variable change and approximation are applied to the determination of Nusselt numbers for turbulent flow, for example, as applied to equation (27), the following simple relationship results,

$$Nu(z) \approx k^+ \left[Nu(z)\right]_p \tag{35}$$

where the subscript "p" denotes a plug flow value, and

$$z = \frac{4k^+}{Pe}\left(\frac{\ell}{D}\right) \tag{36}$$

Values of k^+ for the infinitely wide parallel plane channel were computed from its definition expressed as

$$\frac{1}{k^+} = \int_0^1 \frac{dx}{1 + \frac{\epsilon}{\nu} Pr} \tag{37}$$

using the von Karman universal velocity profile to determine $\epsilon(x)/\nu$, with ϵ/ν taken constant at its maximum value in the central regions of the duct. For comparison, k^+ was also determined from equation (35) using Seban's equation,[6]

$$Nu(\infty) = 5.8 + 0.02\, Pe^{0.8}$$

which is a close empirical fit of calculated results based on the same method for computing $\epsilon(x)/\nu$. Seban's equation is for fully developed heat transfer to turbulent flowing liquid metals in infinitely wide parallel plane channels with boundary conditions of uniform flux on one side, and the other side insulated. The corresponding plug flow Nusselt number for this case is 6.* Thus, according to equation (35)

$$k^+ \approx \frac{1}{6}\left(5.8 + 0.02\, Pe^{0.8}\right) \tag{38}$$

and k^+ should be mainly a function of the Peclet number and relatively insensitive to Prandtl number variations.

A further comparison was made based on equation (35) using fully developed liquid metal Nusselt numbers computed by Poppendiek.[5] These computations were for the boundary conditions of uniform surface temperature on both sides of a parallel plane channel, and were based on a simple linear representation for $\epsilon(x)/\nu$. Also u was taken as equal to $\bar{u}$. The corresponding fully developed plug flow Nusselt number for this case is π^2.**

The results of these comparisons are shown on figure 2. It is seen that the three procedures for computing k^+ agree quite well up to Peclet numbers of at least 1000. At a Peclet number of 1000, for example, the maximum disagreement over the Prandtl number range 0.001 - 0.01 is about 1% of the smallest value. The Prandtl number dependence of k^+, however, does not agree, except in the sense that the effect of Prandtl number is small, so that the disagreement is not too important.

A much more stringent test of the k^+ approximation is the prediction of Nusselt numbers in the thermal entrance region of a duct, for then k^+ is involved when computing appropriate values of both Nu and ℓ/D according to equations (35) and (36). For this purpose Nu as a function of ℓ/D for various Peclet numbers were predicted by the k^+ approximation for the case of turbulent liquid metal flow through a parallel plane channel with the boundary condition of uniform surface temperature at both walls. Poppendiek[5] presents results of detailed turbulent flow calculations for this case also. The corresponding plug flow solution, $[Nu(z)]_p$ was obtained from the analogous transient heat conduction problem given in

*Plug flow convection heat transfer equations are equivalent to the transient heat conduction equation. As a result, many plug flow Nusselt numbers are readily obtained from available solutions to various transient heat conduction problems. For example, the result cited is obtained easily from an example given on p. 112 of reference (1).

**See above footnote and pp. 100 and 308-310 of reference (1).

reference (1), pp. 100 and 308-310. Values of k^+ were obtained from equation (38) which, according to figure 2, represents a reasonable compromise relationship for Peclet numbers less than 1000.

Figure 3 shows this comparison for a Peclet number of 1000. Also shown are the predictions of the simple plug flow relation without the k^+ approximation. It is apparent from this graph that the k^+ approximation brings the plug flow solution into good agreement with Poppendiek's results in all but the very beginning of the thermal entrance region where it predicts Nusselt numbers that are larger. Disagreement in this region is to be expected since for very small ℓ/D temperature gradients will be localized within a thin temperature boundary layer near the wall where the total conductivity k_t is nearly equal to the fluid thermal conductivity. The k^+ approximation introduces an effective uniform conductivity which is always larger than the fluid thermal conductivity, and therefore Nusselt numbers will be larger also. For very small ℓ/D, Poppendiek uses an asymptotic approximation equivalent to the simple plug flow solution, and so the curves representing his computed values and the simple plug flow case should be equal at very small ℓ/D. Thus agreement is indicated on the figure as ℓ/D approaches zero. A more exact calculation which accounts for the velocity distribution close to the wall will result in somewhat lower values of the Nusselt number when ℓ/D is very small - e.g., less than unity. Thus, in the very beginning of the thermal entrance region, the k^+ approximation as a representation of this "more exact" case will not be as good as indicated on the figure. In this region, however, the developing of the velocity profile could be very important in real situations, and actual Nusselt numbers will depend on details of the duct inlet configuration.

Comparisons with Poppendiek's results at other Peclet numbers showed, as expected, that the accuracy of the k^+ approximation improves as the Peclet number decreases. For Peclet numbers significantly larger than 1000, the accuracy of the k^+ approximation becomes progressively poorer, although order-of-magnitude agreement is obtained for Peclet numbers as high as 10,000. At a Peclet number of 5000, the k^+ approximation predicts fully developed Nusselt numbers only 20% larger than Poppendiek's values, but become more inaccurate as ℓ/D decreases. For example, at an ℓ/D of unity, the approximation gives values about 60% larger.

For the circular tube the appropriate definition of k^+ equivalent to equation (37) is somewhat more cumbersome than for the parallel plane channel. For example, for cylindrical co-ordinates the equivalent of equation (33) is

$$\frac{dx}{x} = \frac{k_x}{k_m}\,\frac{dr}{\eta}$$

and integration to obtain the equivalent of equation (31) involves an indeterminancy at $x = 0$. But the same principles apply, and in particular, equations (35) and (36) summarize the Nusselt number approximation for the circular tube also.

The k^+ approximation for circular tubes was tested by comparing k^+ values computed from equation (35) using the fully developed turbulent liquid metal Nusselt number relations of Lyon[3] and Seban and Shimazaki.[7] The former, which correlates empirically Martinelli's[4] computed values, applies to the case of uniform heat flux; while the latter applies to uniform surface temperature. The corresponding plug flow values for these two cases are 8 and 5.8 respectively.[2]

Thus, the relations

$$k^+ \approx \frac{1}{8}(7 + 0.025\,Pe^{0.8}) \tag{39a}$$

results from Lyon's equation, and

$$k^+ \approx \frac{1}{5.8}(5.0 + 0.025\,Pe^{0.8}) \tag{39b}$$

results from the equation of Seban and Shimazaki. A comparison of these two equations is shown on figure 4. At a Peclet number of 1000 the equations disagree by about 15%.

The comparisons presented above indicate that for the purpose of computing Nusselt numbers for cases of uniform heat flux and uniform surface temperature, the k^+ approximation offers a reasonable compromise between accuracy and simplicity of computation when Peclet numbers are less than 1000, and perhaps somewhat larger. It seems reasonable to assume that the approximation will give equivalent accuracy with the double pipe heat exchanger problem, as well as a variety of others, but that this is a guess must be recognized.

Summary

In summary, the k^+ approximation converts plug flow solutions, $\xi_i(x,z)$, to approximate turbulent flow solutions, $\xi_i(\eta,z)$, by use of equation (32) or its equivalent for the circular tube, together with equation (36). There is evidence that the approximation will give satisfactory accuracy when Peclet numbers are less than 1000, and perhaps larger, especially when one considers the extent of computational simplicity it offers. In essense, the approximation introduces an effective uniform thermal conductivity equal to kk^+ which can be related to the Peclet number - for example by use of figures 2 and 4. Thus, when applied to the double pipe heat exchanger problem of this paper, plug flow results as obtained from solutions to the mathematical problem described by equations (16) to (21), can be converted to turbulent flow results by use of equations (35) and (36) with K and K_w now defined as follows:

For the concentric tube exchanger:

$$K = \left(\frac{k_1}{a_1}\right)\left(\frac{a_2}{k_2}\right)\left(1 + \frac{b}{a_1}\right)\left(\frac{k_1^+}{k_2^+}\right) \tag{40a}$$

$$K_w = \left(\frac{k_1}{a_1}\right)\left(\frac{b'}{k_w}\right) k_1^+ \tag{41a}$$

and for the parallel plane exchanger:

$$K = \left(\frac{k_1}{a_1}\right)\left(\frac{a_2}{k_2}\right)\left(\frac{k_1^+}{k_2^+}\right) \tag{40b}$$

$$K_w = \left(\frac{k_1}{a_1}\right)\left(\frac{b}{k_w}\right) k_1^+ \tag{41b}$$

With the above, the k_i^+ are taken as functions of Pe_i.

5. PLUG FLOW SOLUTIONS

Analytical solutions for the mathematical problem specified by equations (16) to (21) will now be discussed briefly. They can be obtained by Laplace transform techniques in a relatively straightforward manner following, for example, the procedures described in sections 12.8 and 13.8 of reference (1).

Details of the solutions will be described in the more complete report referred to in the introduction. In addition to Laplace transform techniques, the classical method of separation of variables was used also. The latter, although more cumbersome, is more interesting in two main respects. It involves the formulation of a Sturm-Liouville problem with boundary conditions not usually encountered with such problems. It then leads quite naturally to formal solutions for both laminar and turbulent flow cases to which various available approximation techniques for determining eigenvalues and eigenfunctions can be applied. Of special interest will be the use of these forms of solution as bases for specifying the size of errors introduced by the k^+ approximation.

Solutions for the dimensionless temperature distribution, convenient for moderate to large values of z, can be written as

$$\xi_i(x,z) = \frac{H}{1+H} + \sum_{m=1}^{\infty} A_m^{(i)}(\lambda_m, x)\, e^{-\lambda_m^2 z} \tag{42}$$

for both types of double pipe heat exchangers. In this equation, the $A_n^{(i)}$ are functions of an eigenvalue λ_n and the dimensionless distance variable x. The eigenvalues are the positive non-zero roots of an eigenvalue value equation

$$F(\lambda) = 0$$

and are infinite in number, depending on H, K, and K_w as well as the type of exchanger. For the concentric tube exchanger

$$F(\lambda) = \sqrt{\frac{2K}{H}}\, J_1(\lambda) \cos(\omega\lambda) + J_0(\lambda) \sin(\omega\lambda) - K_w \lambda J_1(\lambda) \sin(\omega\lambda) \tag{43a}$$

where $2\omega^2 = KH$. For the parallel plane exchanger

$$F(\lambda) = \sqrt{\frac{K}{H}} \sin\lambda \cos(\sigma\lambda) + \cos\lambda \sin(\sigma\lambda) - K_w \lambda \sin\lambda \sin(\sigma\lambda) \tag{43b}$$

where $\sigma^2 = KH$.

The eigenfunctions $A_n^{(i)}$ also depend on the type of exchanger. For the concentric tube exchanger, recalling from figure 1 that channel "1" identifies the circular tube and that channel "2" refers to the narrow annular space,

$$A_m^{(1)} = \frac{2 \sin(\omega\lambda_m) J_0(\lambda_m x)}{\lambda_m F'(\lambda_m)} \tag{44a}$$

and

$$A_m^{(2)} = -\frac{2K J_1(\lambda_m) \cos(\omega\lambda_m x)}{\omega \lambda_m F'(\lambda_m)} \tag{45}$$

where $F'(\lambda)$ represents the derivative of $F(\lambda)$ with respect to λ. Since the two channels of the parallel plane exchanger are geometrically similar, only one of the channels need be considered. For channel "1"

$$A_m^{(1)} = \frac{2 \sin(\sigma\lambda_m) \cos(\lambda_m x)}{\lambda_m F'(\lambda_m)} \tag{44b}$$

Note that the expressions for H, K, and K_w, and their physical interpretation given previously, consider them defined as properties relative to channel "1." As a result, when interest is directed towards the heat transfer performance of channel "2" as a function of H, K, and K_w and comparing with the performance of channel "1," consistency for the comparison requires interchanging subscripts in the expressions for H, K, and K_w (for example, in equations (11), (40), and (41)). If, for the moment, we denote values of these parameters as already defined with a subscript "1," and the interchange of subscripts in these definitions by subscript "2," then $H_2 = 1/H_1$ and $K_2 = 1/K_1$, but $K_{w2} = K_{w1}/K_1$. This will be important when we wish to compare the performance of the narrow annular space with the parallel plane channel, and the circular tube.

With the analytical solutions just summarized, and the k^+ approximation, we are now prepared to explore the behavior of fully developed individual channel heat transfer coefficients in co-current flow double pipe heat exchangers.

6. FULLY DEVELOPED HEAT TRANSFER COEFFICIENTS

Basic Relations

The definition of the local Nusselt number given by equation (27), together with the plug flow solution presented in the previous section, clearly show that as z increases without limit, an asymptotic value $Nu_i(\infty)$ is obtained. For the cylindrical tube application of the appropriate expressions results in

$$Nu_1(\infty) = \frac{2\lambda_1^2 J_1(\lambda_1)}{2 J_1(\lambda_1) - \lambda_1 J_0(\lambda_1)} \tag{46a}$$

while for the parallel plane channel the relation

$$Nu_1(\infty) = \frac{2\lambda_1^2 \sin\lambda_1}{\sin\lambda_1 - \lambda_1 \cos\lambda_1} \tag{46b}$$

results. The corresponding expression for the narrow annular space is found to be the same as that for the parallel plane channel with $\omega\lambda$, substituted for λ. In the above, λ_1 identifies the least eigenvalue as obtained from equation (43a) or (43b) and is, of course, a function of H, K, and K_w, so that $Nu_i(\infty)$ must also be a function of these parameters.

Magnitudes of the Parameters

Before examining the dependence of $Nu_i(\infty)$ on H, K, and K_w, let us determine the magnitudes of these parameters that are to be expected with actual double pipe heat exchangers. The heat capacity flow rate ratio, H, will be approximately proportional to the mass flow rate ratio, and in most practical cases can be expected to vary between 0.5 and 2. In special cases values from 0.1 to 10 are not too unlikely.

The fluid thermal resistance ratio, K, will be nearly proportional to the ratio of the duct equivalent diameters in most cases. For the parallel plane exchanger values in the range of 0.5 to 2 seem most likely, while for the concentric tube exchanger values near 0.1 are more reasonable - especially with the idealization of a narrow annular space. For applications to turbulent flow, K will also be proportional to the ratio of the channel k^+ values which, up to Peclet numbers of 1000, can introduce an additional variation by a factor of about 0.5 to 2.

With liquid metals, which have relatively large thermal conductivities, values of the relative thermal resistance, K_w, will be roughly proportional to the ratio of the wall thickness to the channel equivalent diameter and in most cases this ratio should be less than 0.1 and rarely larger than 0.5. But for turbulent flows, K_w is also proportional to k^+ which at Peclet numbers near 1000 can introduce a factor of nearly 2. Thus a range of values from near zero to unity is to be anticipated, with low values more likely.

General Trends

For the parallel plane channel, the special case of HK = 1 and $K_w = 0$ allows for a simple solution of the appropriate eigenvalue equation, and it is found that

$$\lambda_1 = \frac{\pi}{2}$$

When substituted into equation (46b), this gives

$$Nu_1(\infty) = \frac{\pi^2}{2}$$

which is simply the fully developed plug flow value for a parallel plane channel with one side kept at uniform temperature and the other side insulated.* In fact, a more detailed examination of the plug flow solution for the parallel plane exchanger for the special case of KH = 1 and $K_w = 0$, shows that the temperature of the common wall is truly uniform along the entire exchanger length.

For $K_w \neq 0$ and for the concentric tube exchanger in general, it is found that true operation with uniform surface temperature is not possible. This result is to be expected for $K_w \neq 0$ when one considers the effects of wall thermal resistance on surface temperature differences in the two channels. For the concentric tube exchanger, the differences in the shapes of the two channels apparently introduces an additional complicating effect. As will be seen later, however, there are special combinations of values of H, K, and K_w for which $Nu_1(\infty)$ is equal to the value corresponding to individual channel operation with uniform surface temperature even though actual operation is otherwise.

---

*See previous footnotes concerning available plug flow solutions.

Detailed examination* of the fully developed Nusselt number relations together with their appropriate eigenvalue equations, reveals that the maximum value of $Nu_1(\infty)$ corresponds to the individual channel boundary condition of uniform heat flux, while the minimum value is simply zero. For the concentric tube and parallel plane channel the maximum value is approached as H, K, or K_W increase. As H approaches zero, $Nu_1(\infty)$ does so also. Decreases in K or K_W cause decreases in $Nu_1(\infty)$, but for very small values of K or K_W $Nu_1(\infty)$ approaches non-zero limiting values. The same generalizations apply to the narrow annular space when H, K, and K_W are redefined relative to the properties of channel "2" as discussed at the end of the last section.

These generalizations, and their quantitative relationships to the magnitudes of H, K, and K_W, are illustrated in figure 5. In this figure the fully developed plug flow Nusselt number for the circular tube, normalized with respect to the appropriate uniform flux value, is graphed as a function of H with K and K_W as parameters. The normalized Nusselt number for this case is

$$N_1(\infty) = \frac{Nu_1(\infty)}{8}$$

where the number "8" is the circular tube uniform flux plug flow Nusselt number.

Normalization is this way is especially convenient for application to turbulent flows, for the k^+ approximation implies that $N_1(\infty)$, as defined above with plug flow Nusselt numbers, can be used with an appropriate uniform flux turbulent flow Nusselt number correlation to obtain corresponding double pipe heat exchanger turbulent flow Nusselt numbers. This also requires that K and K_W be defined by equations (40a) and (41a). Thus figure 5 applies to turbulent flows also, at least approximately.

Also shown on the graph is the value of the normalized Nusselt number corresponding to the boundary condition of uniform surface temperature. This is given by

$$\left[N_1(\infty)\right]_{\text{unif. temp}} \approx \frac{5.8}{8}$$

$$= 0.73$$

The graph shows that $K_W = 0.1$ is nearly equivalent to $K_W = 0$; and that $K = 10$ is nearly equivalent to $K = \infty$ except for very low values of H. Also, when K_W is small $K = 0.1$ is nearly equivalent to $K = 0$; and for $K > 2$, $H = 10$ is nearly equivalent to $H = \infty$.

---

*The mathematical details of this examination will be described in the more detailed report referred to previously.

For the parallel plane channel and the narrow annular space, the fully developed Nusselt number dependences on H, K, and K_w are qualitatively similar to those for the circular tube. There are quantitative differences, however, and these are illustrated in figure 6. In this figure, normalized Nusselt numbers for the three types of channels are plotted vs. H with K as a parameter for the case of $K_w = 0$. For the narrow annular space, K and H are redefined relative to channel "2" so that the three ducts can be compared on a consistent basis. Note that although the parallel plane channel and narrow annular space are equivalent geometrically, their respective adjacent channels with which they exchange heat are not the same. In a sense, they are equivalent channels with slightly different boundary conditions.

Figure 6 shows that Nusselt numbers for cylindrical tubes are significantly more sensitive to variations of H and K when compared with the other two types of channels, especially at low values of K. Nusselt numbers for the narrow annular space are slightly more sensitive than those for the parallel plane channel for moderately high values of K and values of H less than unity. At both very high and low values of K, however, the annular space Nusselt numbers are essentially equivalent to those for the parallel plane channel.

Also shown on figure 6 are the normalized Nusselt numbers for the boundary condition of uniform surface temperature. Values pertaining to the narrow annular space and to the parallel plane channel are the same and are equal to

$$\left[N_i(\infty)\right]_{\text{Unif temp.}} = \frac{\pi^2/2}{6}$$

$$\approx 0.82$$

where $\pi^2/2$ is the fully developed plug flow Nusselt number for uniform surface temperature, and 6 is the value for uniform heat flux.

A detailed tabulation of normalized Nusselt numbers as a function of H, K, and K_w is given in table 1.

Double Pipe Heat Exchanger Experiments

Occasionally the assertion is made that heat transfer in double pipe heat exchangers corresponds to operation somewhere between uniform heat flux and uniform surface temperature, and that therefore Nusselt numbers should fall between values corresponding to these simple boundary conditions. For the special cases treated here, which should be applicable to liquid metal heat transfer with Peclet numbers less than 1000, figures 5 and 6 indicate that this assertion is reasonable when H is larger than unity. But the figures also show that for values of H less than unity, fully developed heat transfer coefficients can be significantly less than those corresponding to a uniform surface temperature boundary condition unless K and K_w are unusually large.

It is possible that this result can explain the "low" values of liquid metal heat transfer coefficients frequently obtained with double pipe heat exchanger experiments, for these values are always judged to be too low when compared with values corresponding to uniform heat flux or uniform surface temperature boundary conditions. Also, the complicated dependence of the Nusselt number on three different parameters H, K, and K_w, together with an implicit Peclet number dependence involving both channels, could explain the large scatter of experimental data usually observed.

As an illustration of the kind of results possible when using double pipe heat exchangers for the determination of liquid metal Nusselt numbers by experiment, the plug flow solutions and the k^+ approximation were used to predict the Nusselt number vs. Peclet number relations that would be obtained with the concentric tube exchanger illustrated in figure 7. The fluids flowing through both sides of the exchanger were imagined to be liquid sodium. Two different types of operation were considered. In the first, the mass flow rates were taken as equal in both channels, i.e., H = 1; in the second, the Peclet number of the fluid flowing in the narrow annular space was kept fixed at a value of 100. For both types of operation, tube side Nusselt numbers were predicted for both copper and stainless steel tubes. The different thermal conductivities of the two tube materials results in about a factor of 20 difference between corresponding K_w values, so that the results for the copper tube can also be interpreted as a stainless steel tube with a 5 mil wall.

The results are shown on figure 8 where tube side Nusselt numbers are plotted vs tube side Peclet number for the various cases. Also shown are the corresponding curves for uniform heat flux and uniform surface temperature boundary conditions. Most striking of these results are those for operation with constant Peclet number in the annular space. For this case, tube side Nusselt numbers decrease with increasing tube side Peclet number, a result which if obtained by experiment might tempt the experimenter to consider his apparatus at fault, or perhaps to speculate about the possibility of non-wetting or corrosion problems. His speculations might receive further encouragement after observing the differences between results obtained with copper and stainless steel tubes, especially since copper does not behave too well with liquid sodium.

Even with the perhaps more usual method of operation of nearly equal mass flow rates in both channels, the differences between results obtained with copper and stainless steel tubes and the generally lower Nusselt number values obtained with copper, might lead to erroneous speculation about corrosion or non-wetting problems.

These conclusions can be given as possibilities only, since nearly all of the double pipe heat exchanger liquid metal data available were obtained with counter-current flow, and the analysis given here pertains to co-current flow. But it is clear that the parameters H, K, and K_w will also appear in a counter-current flow analysis, and therefore similar effects are at least possible.

7. SUMMARY

The material presented in this paper represents an introductory analytical investigation of liquid metal heat transfer in co-current flow double pipe heat exchangers without use of the usual heat transfer coefficient assumptions implicit in the more customary methods of analysis.

In order to provide mathematical simplicity, plug flow models of the heat exchanging fluids were utilized for analysis, and an approximation method developed for application of plug flow results in general to the turbulent flow of liquid metals. Evidence was presented which indicates that the approximation will give satisfactory accuracy up to Peclet numbers of 1000 and perhaps larger.

The plug flow analysis and approximation method were applied to the prediction of the dependence of fully developed individual channel ("film") heat transfer coefficients on the operating conditions of two types of liquid metal co-current flow double pipe heat exchangers. It was found that operating conditions and exchanger type can be important in this regard, and that fully developed heat transfer coefficients can be significantly lower than normally expected.

ACKNOWLEDGEMENT

Solutions of the eigenvalue equations, as well as a variety of other computations, were performed on an IBM 704 under the direction of Miss Irene Baksys of Argonne National Laboratory. Many exploratory calculations were performed by Mr. Thomas W. Petrie, a mechanical engineering student at Marquette University and summer employee at Argonne. The author wishes to thank both of these people for their assistance.

(1) Carslaw, H. S. and J. C. Jaeger, Conduction of Heat in Solids, 2nd Ed., Oxford, London (1959).

(2) Eckert, E.R.G. and R. M. Drake, Jr., Heat and Mass Transfer, McGraw-Hill, New York (1959), pp. 298-301.

(3) Lyon, R. N., "Liquid Metal Heat Transfer Coefficients," Chem. Eng. Prog. 47, 75 (1951).

(4) Martinelli, R. C., "Heat Transfer to Molten Metals," Trans. ASME 69, 947 (1947).

(5) Poppendiek, H. F., "Turbulent Liquid-Metal Heat Transfer in Channels," Nuc. Sci. Eng. 5, 390 (1959).

(6) Seban, R. A., "Heat Transfer to a Fluid Flowing Turbulently Between Parallel Walls with Asymmetric Wall Temperatures," Trans. ASME 72, 789 (1950).

(7) Seban, R. A. and T. T. Shimazaki, "Heat Transfer to a Fluid Flowing Turbulently in a Smooth Pipe with Walls at Constant Temperature," Trans. ASME 73, 803 (1951).

NOMENCLATURE

Dimensional Quantities

a_i	Width or radius of channel "i," ft.
b	Wall thickness, ft
b'	Effective wall thickness of circular tube, ft, equation (8a).
c_i	Heat capacity of fluid in channel "i," Btu/(lbm)($^{\circ}$F).
k_i	Thermal conductivity of fluid in channel "i," Btu/(hr)(ft)($^{\circ}$F).
k_w	Thermal conductivity of wall, Btu/(hr)(ft)($^{\circ}$F).
ℓ	Heat exchange length measured from inlet, ft.
q_i	Heat flux density at wall in channel "i," Btu/(hr)(ft^2).
t_i	Temperature of fluid "i," $^{\circ}$F
t_{io}	Inlet temperature of fluid "i," $^{\circ}$F.
u_i	Velocity of fluid in channel "i," ft/hr.
W_i	Mass rate of flow of fluid in channel "i," lbm/hr.
x_i	Distance variable, ft.
α_i	Thermal diffusivity of fluid in channel "i," ft^2/hr.
ϵ	Turbulent diffusivity, ft^2/hr.
ν	Kinematic viscosity, ft^2/hr.
μ	Viscosity, (lb$_f$)(hr)/ft^2
ρ	Density, lbm/ft^3.

Dimensionless Quantities

H	Heat capacity flow rate ratio, equation (11).
K	Fluid thermal resistance ratio, equations (40a) and (40b).
K_w	Wall thermal resistance ratio, equations (41a) and (41b).
k_i^+	Thermal conductivity multiplier for turbulent flow in channel "i."
N_i	Normalized Nusselt number for channel "i."

NOMENCLATURE (cont.)

Dimensionless Quantities

Nu_i Nusselt number for channel "i," equation (26).

Pe_i Peclet number for channnel "i."

z Dimensionless heat exchanger length, equation (36).

ξ_i Dimensionless temperature of fluid in channel "i," equation (13).

TABLE 1

NORMALIZED* FULLY DEVELOPED NUSSELT NUMBERS

K	H	CONCENTRIC TUBE EXCHANGER: TUBE SIDE, $N_1(\infty)$	CONCENTRIC TUBE EXCHANGER: ANNULUS, $N_2(\infty)$**	PARALLEL PLANE EXCHANGER: $N_1(\infty)$
		$K_w = 0$		
0.1	0.1	0.155	0.996	0.253
	0.5	0.445	0.983	0.598
	1.0	0.565	0.972	0.702
	2.0	0.646	0.952	0.765
	10	0.727	0.792	0.822
0.5	0.1	0.167	0.978	0.276
	0.5	0.519	0.922	0.662
	1.0	0.653	0.877	0.764
	2.0	0.739	0.801	0.822
	10	0.870	0.359	0.903
1.0	0.1	0.187	0.956	0.310
	0.5	0.616	0.866	0.732
	1.0	0.747	0.806	0.822
	2.0	0.824	0.707	0.874
	10	0.932	0.294	0.947
2.0	0.1	0.242	0.914	0.398
	0.5	0.755	0.812	0.822
	1.0	0.848	0.749	0.888
	2.0	0.900	0.645	0.924
	10	0.966	0.269	0.973
5.0	0.1	0.527	0.840	0.658
	0.5	0.892	0.774	0.917
	1.0	0.934	0.711	0.949
	2.0	0.958	0.607	0.967
	10	0.986	0.256	0.989

* Normalized with respect to uniform heat flux value.

** In this table K and K_w are defined relative to Channel "1" for the narrow annular space as well as for the other channels. See text at the end of Section 5.

TABLE 1 , CON'T.

K	H	CONCENTRIC TUBES $N_1(\infty)$	CONCENTRIC TUBES $N_2(\infty)$	PARALLEL PLANES $N_1(\infty)$
		$K_w = 0$		
10	0.1	0.765	0.820	0.822
	0.5	0.945	0.761	0.957
	1.0	0.966	0.698	0.974
	2.0	0.978	0.594	0.983
	10	0.993	0.252	0.995
		$K_w = 0.1$		
0.1	0.1	0.164	0.996	0.270
	0.5	0.495	0.984	0.643
	1.0	0.623	0.975	0.744
	2.0	0.704	0.958	0.802
	10	0.778	0.829	0.853
0.5	0.1	0.178	0.978	0.294
	0.5	0.568	0.928	0.699
	1.0	0.699	0.892	0.793
	2.0	0.776	0.827	0.845
	10	0.877	0.406	0.909
1.0	0.1	0.199	0.956	0.331
	0.5	0.655	0.878	0.758
	1.0	0.774	0.826	0.840
	2.0	0.841	0.736	0.885
	10	0.934	0.314	0.949
2.0	0.1	0.260	0.915	0.422
	0.5	0.772	0.825	0.835
	1.0	0.858	0.766	0.895
	2.0	0.905	0.665	0.928
	10	0.966	0.278	0.973

TABLE 1 , CON'T.

K	H	CONCENTRIC TUBES $N_1(\infty)$	CONCENTRIC TUBES $N_2(\infty)$	PARALLEL PLANES $N_1(\infty)$
		$K_w = 0.1$		
5.0	0.1	0.544	0.845	0.671
	0.5	0.895	0.781	0.920
	1.0	0.936	0.720	0.950
	2.0	0.958	0.616	0.967
	10	0.986	0.259	0.989
10	0.1	0.770	0.823	0.826
	0.5	0.946	0.766	0.957
	1.0	0.967	0.703	0.974
	2.0	0.979	0.599	0.983
	10	0.993	0.254	0.995
		$K_w = 0.5$		
0.1	0.1	0.211	0.996	0.349
	0.5	0.674	0.989	0.772
	1.0	0.782	0.984	0.846
	2.0	0.837	0.976	0.885
	10	0.881	0.907	0.916
0.5	0.1	0.232	0.979	0.382
	0.5	0.718	0.950	0.800
	1.0	0.814	0.930	0.867
	2.0	0.863	0.893	0.901
	10	0.909	0.587	0.933
1.0	0.1	0.263	0.958	0.426
	0.5	0.764	0.913	0.830
	1.0	0.847	0.880	0.888
	2.0	0.889	0.818	0.918
	10	0.941	0.405	0.954

TABLE 1 , CON'T.

K	H	CONCENTRIC TUBES $N_1(\infty)$	CONCENTRIC TUBES $N_2(\infty)$	PARALLEL PLANES $N_1(\infty)$
		$K_w = 0.5$		
2.0	0.1	0.346	0.922	0.518
	0.5	0.827	0.865	0.872
	1.0	0.890	0.819	0.917
	2.0	0.923	0.733	0.941
	10	0.968	0.316	0.974
5.0	0.1	0.607	0.863	0.713
	0.5	0.908	0.809	0.929
	1.0	0.943	0.751	0.955
	2.0	0.962	0.650	0.970
	10	0.987	0.273	0.989
10	0.1	0.788	0.836	0.839
	0.5	0.949	0.782	0.960
	1.0	0.969	0.721	0.975
	2.0	0.979	0.617	0.984
	10	0.993	0.260	0.995
		$K_w = 1.0$		
0.1	0.1	0.302	0.996	0.472
	0.5	0.794	0.993	0.850
	1.0	0.865	0.990	0.901
	2.0	0.900	0.985	0.926
	10	0.927	0.942	0.946
0.5	0.1	0.333	0.981	0.505
	0.5	0.814	0.966	0.864
	1.0	0.879	0.953	0.910
	2.0	0.910	0.929	0.933
	10	0.937	0.724	0.952

TABLE 1 , CON'T.

K	H	CONCENTRIC TUBES $N_1(\infty)$	CONCENTRIC TUBES $N_2(\infty)$	PARALLEL PLANES $N_1(\infty)$
		$K_w = 1.0$		
1.0	0.1	0.376	0.963	0.549
	0.5	0.836	0.938	0.878
	1.0	0.893	0.916	0.920
	2.0	0.921	0.872	0.941
	10	0.950	0.526	0.962
2.0	0.1	0.467	0.933	0.617
	0.5	0.868	0.897	0.901
	1.0	0.915	0.862	0.935
	2.0	0.939	0.793	0.953
	10	0.970	0.372	0.976
5.0	0.1	0.668	0.882	0.755
	0.5	0.920	0.836	0.939
	1.0	0.950	0.784	0.961
	2.0	0.965	0.689	0.973
	10	0.987	0.291	0.989
10	0.1	0.807	0.850	0.853
	0.5	0.953	0.799	0.963
	1.0	0.971	0.741	0.977
	2.0	0.980	0.639	0.985
	10	0.993	0.268	0.995

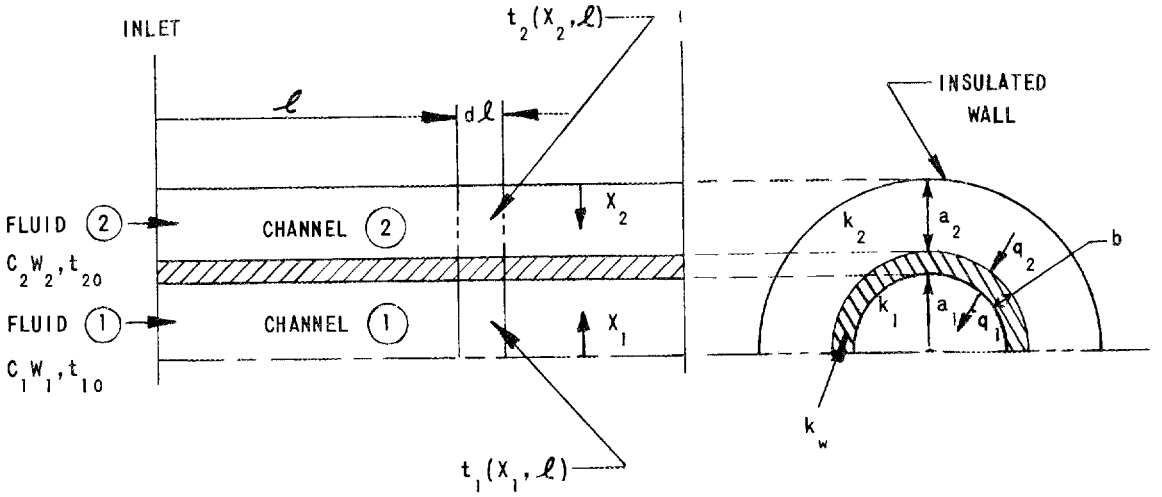

(a) CONCENTRIC TUBES

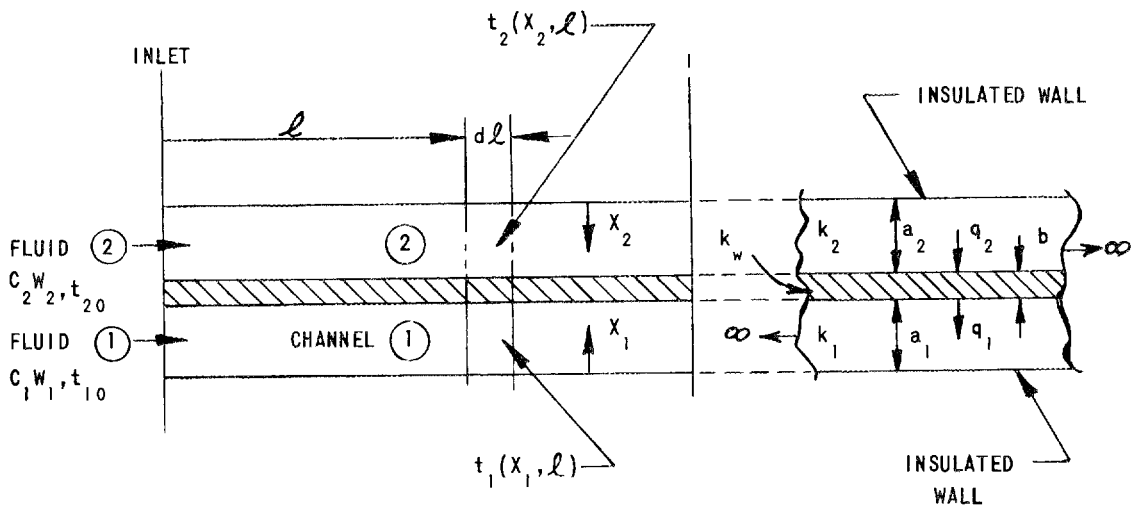

(b) ADJACENT PARALLEL PLANES

FIG. 1

DOUBLE PIPE HEAT EXCHANGER GEOMETRIES

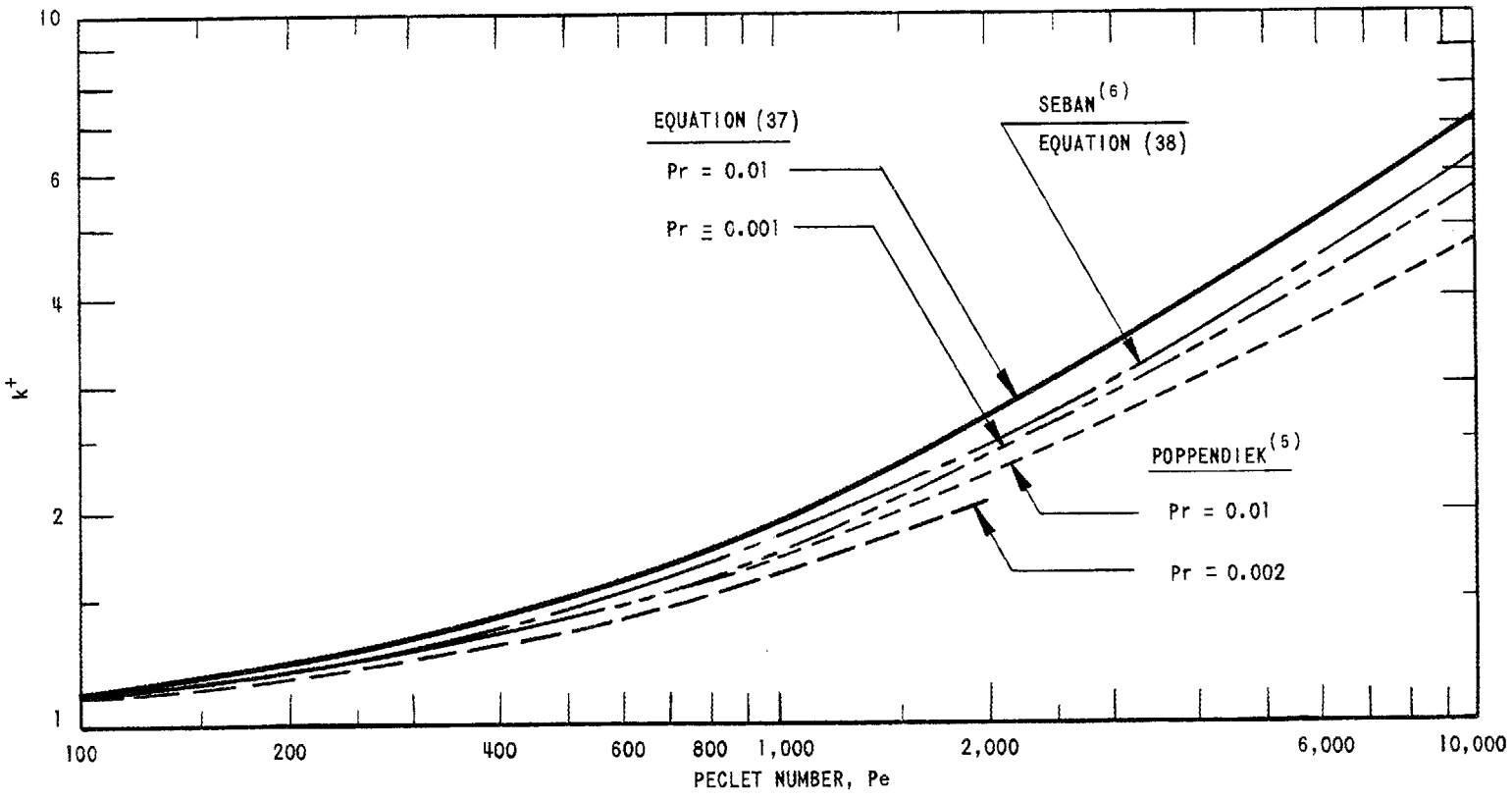

FIG. 2

COMPARISON OF k^+ COMPUTED BY VARIOUS METHODS, PARALLEL PLANE CHANNELS

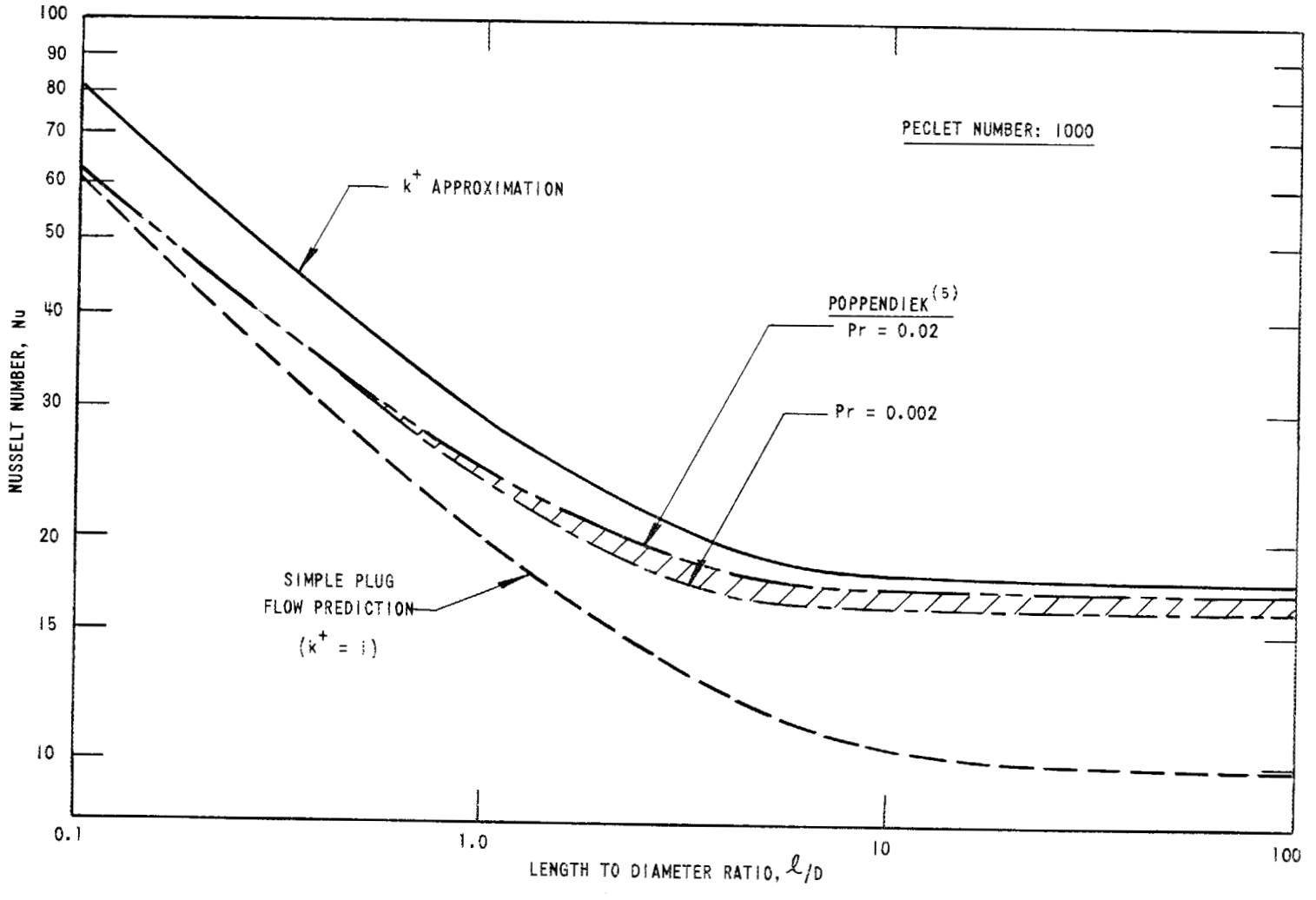

FIG. 3

NUSSELT NUMBER VS LENGTH PREDICTIONS,
UNIFORM SURFACE TEMPERATURE IN PARALLEL PLANE CHANNEL

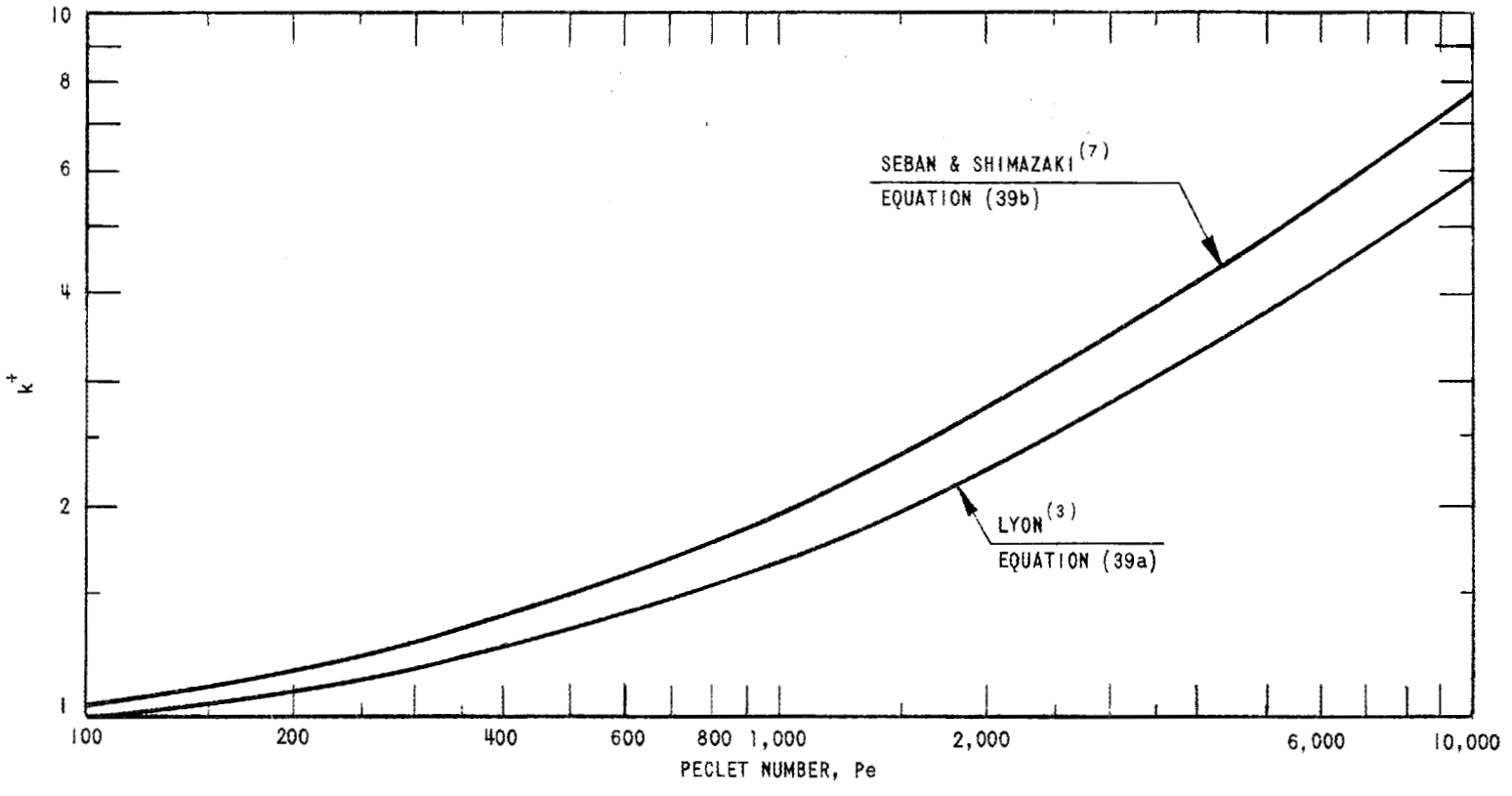

FIG. 4

COMPARISON OF k^+ COMPUTED BY VARIOUS METHODS, CIRCULAR TUBES

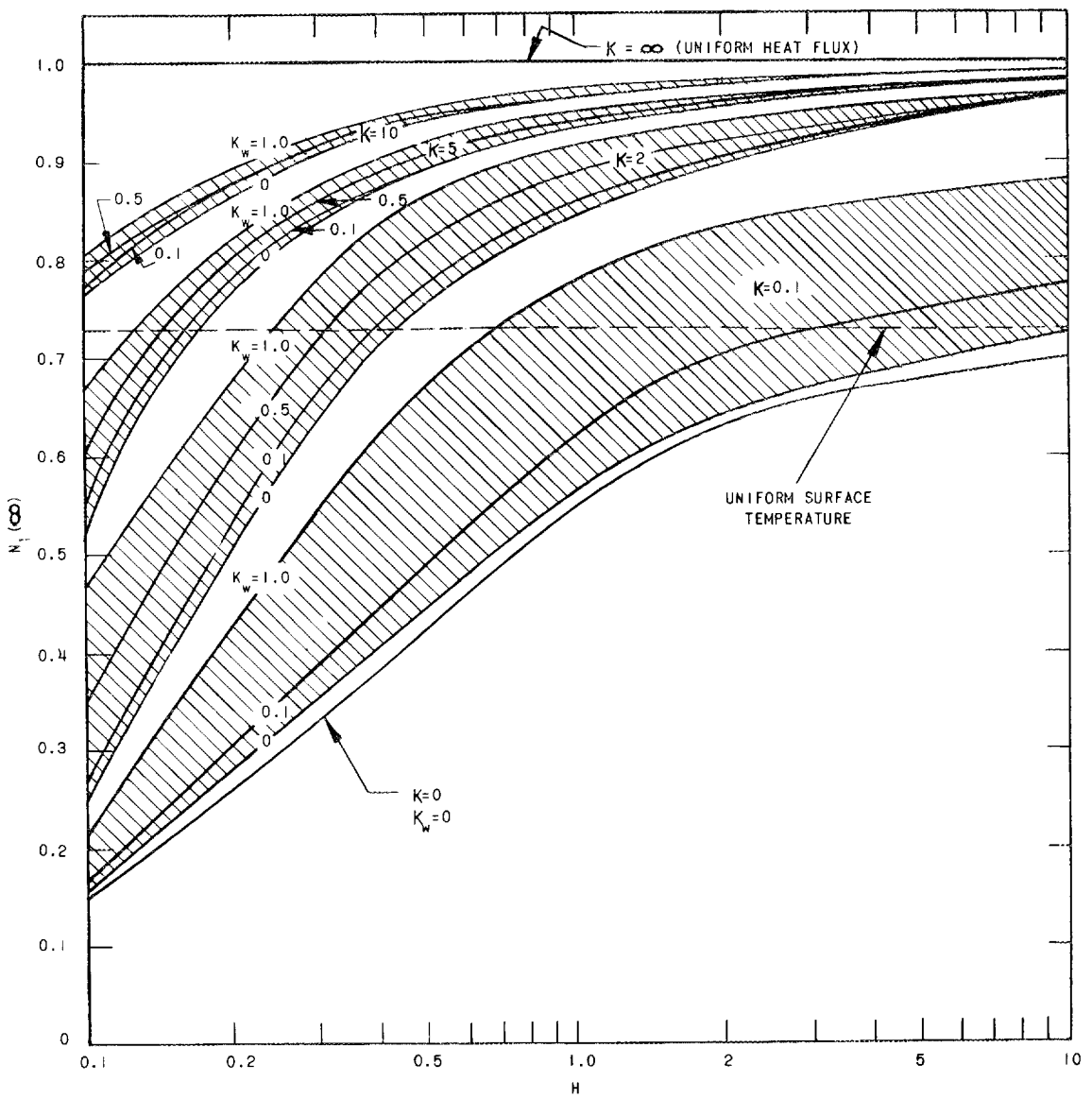

FIG. 5
NORMALIZED FULLY DEVELOPED TUBE SIDE
NUSSELT NUMBERS

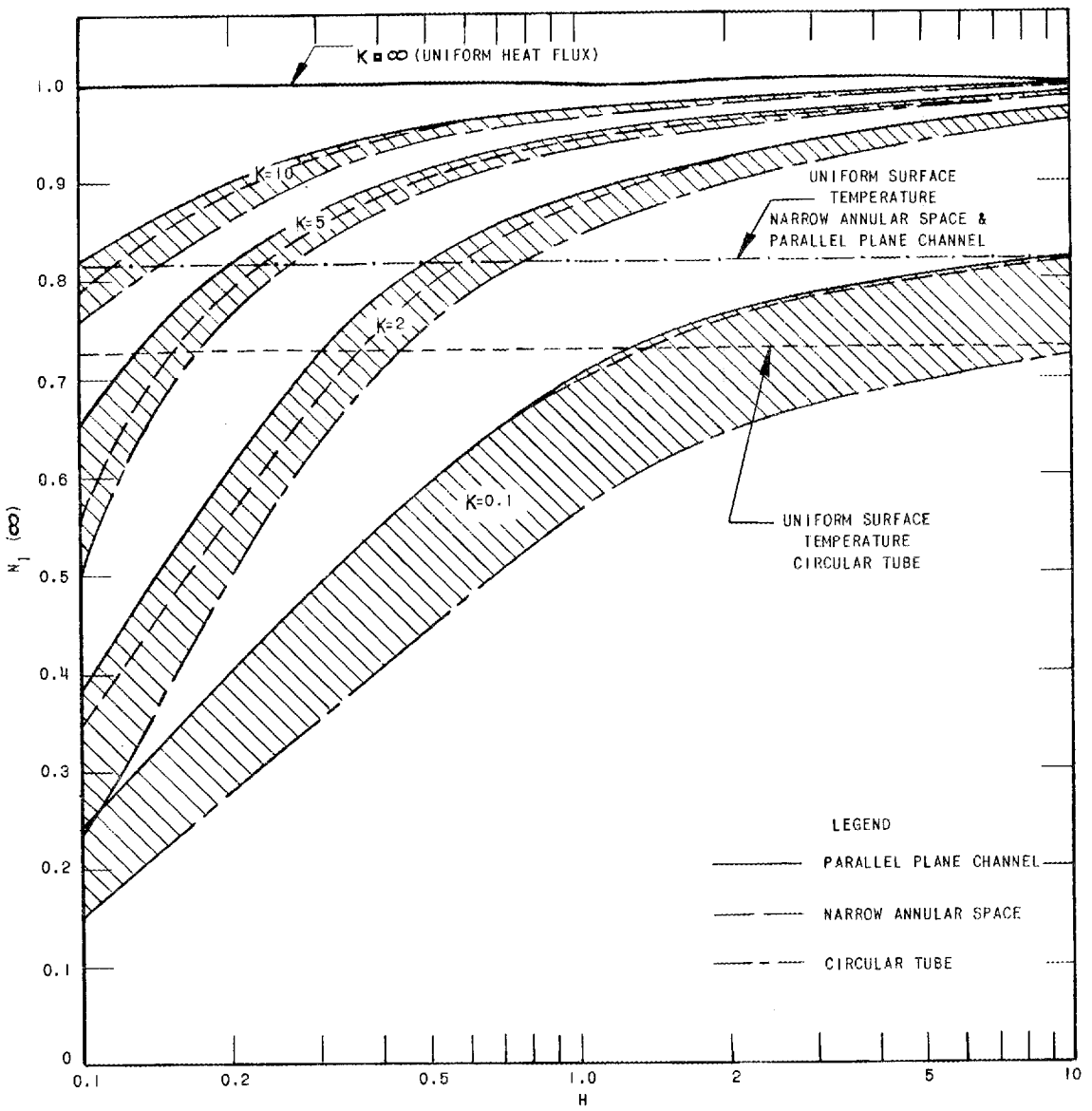

FIG. 6
NORMALIZED FULLY DEVELOPED NUSSELT NUMBERS FOR VARIOUS DUCT SHAPES

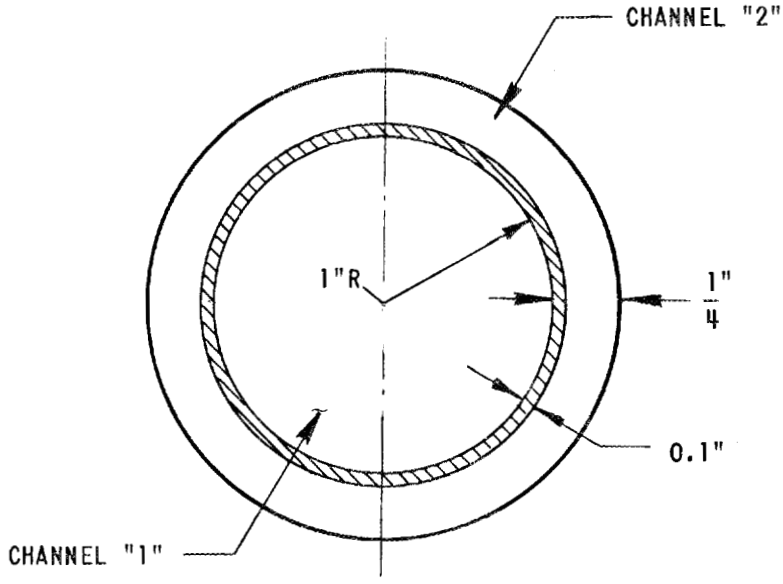

FIG. 7
CROSS-SECTION OF DOUBLE PIPE
HEAT EXCHANGER FOR
TURBULENT FLOW CALCULATIONS

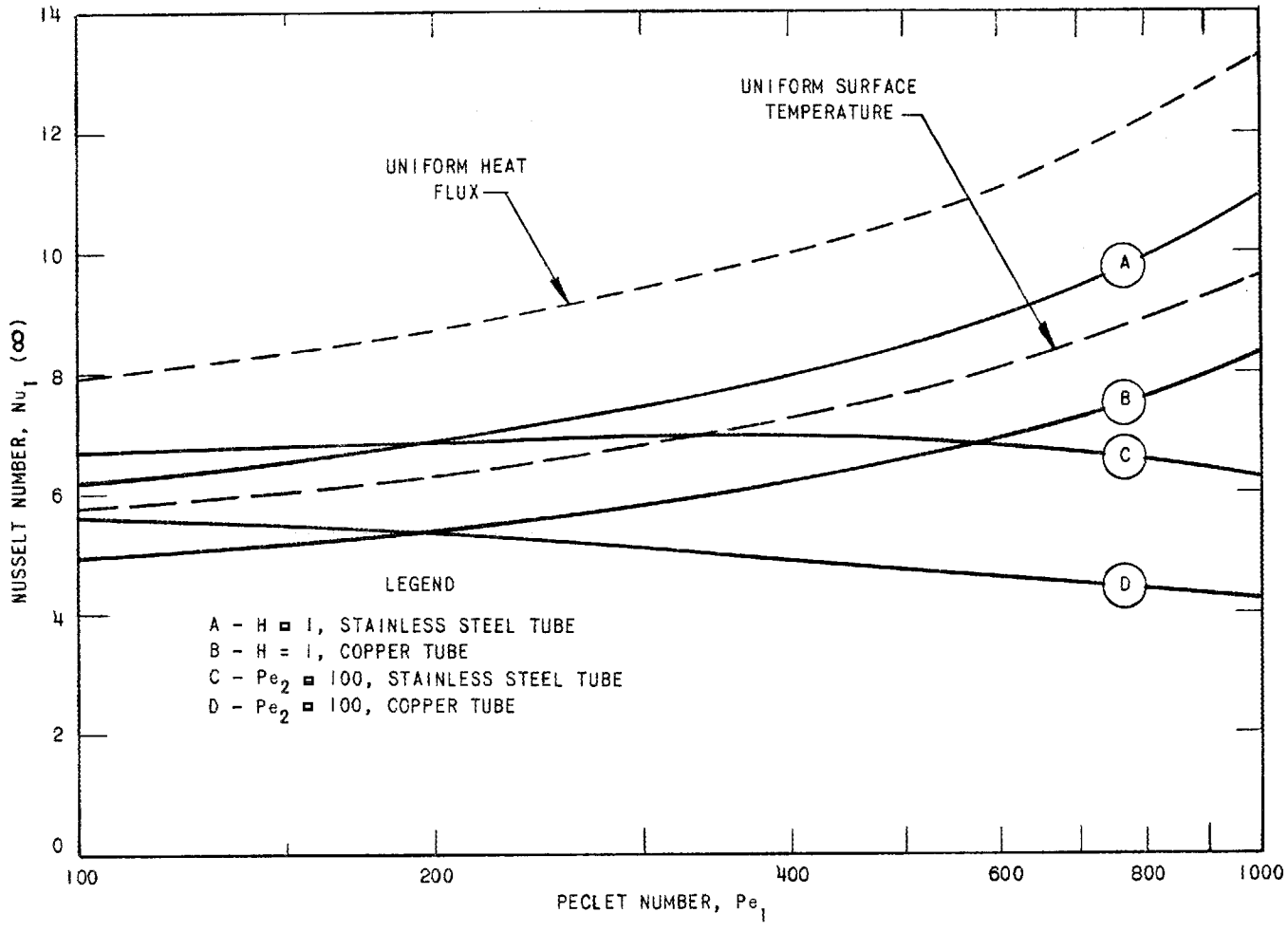

FIG. 8

TUBE SIDE FULLY DEVELOPED
NUSSELT NUMBERS VS PECLET NUMBER
DOUBLE PIPE HEAT EXCHANGER OF FIGURE 7

DISCUSSION

Mr. Stein mentioned other aspects not covered in the prepared paper. Of special interest was the finding that although actual fully developed heat transfer coefficients in co-current flow liquid metal heat exchangers can be significantly smaller than normally expected, customary design procedures, which use larger values, still seem to give sufficiently accurate results in most cases of practical interest. The reason appears to be a result of the assumption that heat transfer coefficients are independent of length. This assumption decreases the overall heat transfer rate as calculated, and tends to correct the results of using larger than actual fully developed heat transfer coefficients.

Dr. Dwyer asked what relationship between thermal and momentum eddy diffusivities was used for the turbulent flow calculations, and whether the trends shown in Fig. 8 would be influenced by the relationship chosen. Mr. Stein replied that for k^+ values computed from Eq. (37), the thermal and momentum eddy diffusivities were assumed to be equal. The results shown in Fig. 8 were based on k^+ values computed from Eq. (38) for the annular space, and Eq. (39a) for the tube, and both of these equations imply the assumption of equal thermal and momentum eddy diffusivities. Mr. Stein stated that he did not believe that reasonable alternate assumptions, such as the diffusivity relationship recently proposed by Dr. Dwyer, would influence the illustrative trends shown in Fig. 8.

Dr. Dwyer then asked whether results for various annular space diameter ratios had been obtained.

MR. STEIN: Yes, but only for the simplified model I mentioned in which I was able to get co-current and counter-current solutions.

MR. POPPENDIEK: I think your solution would be very valuable for the next person who goes over a critical analysis of all the liquid-metal data; I think your solution would be very valuable to help sort it out.

MR. STEIN: I haven't had enough time to do this myself to any great extent. Also, solutions for the counter-current flow case would be needed. But there are some interesting possibilities - especially with respect to the data of Doody and Younger who used both counter-current and co-current flow. There is the equivalent of a parallel plate exchanger at the International School at Argonne, and maybe we can get data from that to verify the effects predicted by the analysis.

NATURAL CONVECTION HEAT TRANSFER COEFFICIENTS FOR LIQUID TIN AT HIGH HEAT FLUXES

ABL/Z

By

Akbar F. Brinsmade and Leland G. Desmon

HERCULES POWDER COMPANY
ALLEGANY BALLISTICS LABORATORY

Cumberland, Maryland

ABSTRACT

Natural convection liquid metal heat transfer measurements were made in a rocket nozzle containing refractory metal calorimetric devices utilizing tin as a heat transfer agent. Test variables included propellant gas throat stagnation temperatures in excess of 5000°F, acceleration to 1.18 g and heat fluxes to 1.72×10^6 Btu/hr x ft^2. Test data, a natural convection correlation for tin, and a comparison with sodium and lithium are presented.

I. INTRODUCTION

"Research" reported in this publication was supported by the Advanced Research Projects Agency and the Bureau of Naval Weapons over a period of five years. One of the techniques in solid propellant rocket nozzle heat transfer that was developed involves measurements with liquid metals, for which little if any heat transfer data have been available in the associated high heat flux range. Therefore, part of the work involved a program of fundamental research on liquid-metal heat transfer in experimental rocket nozzles. The United Nuclear Corporation, Development Division, NDA, collaborated with ABL in this effort.

Some of the possible advantages of using tin as a heat transfer medium (when compared to sodium and lithium) are:

1. No safety hazard exists and no special atmosphere is necessary to store or handle it at ordinary temperatures to retain purity.
2. It has the highest boiling point (with a melting point only slightly above that of lithium), and a boiling point liquid heat content of only about 315 Btu/pound compared to about 2500 for lithium, thereby permitting a low heat drain application at a relatively high container wall temperature.
3. On the other hand, for a volume limited system, the boiling point enthalpy per unit liquid volume of tin is about 1.6 times that of lithium, thereby permitting a high heat absorption.
4. It is readily available in high purity at low cost.

II. TEST PROGRAM

A solid propellant rocket motor was used as the heat source and a large centrifuge on which the rocket was mounted was used in some of the tests to provide high gravitational forces. This equipment was supplied by ABL and ABL personnel operated the centrifuge, fired the rocket, and collected the data. United Nuclear handled the mechanical aspects of design, fabricated the test sections, and participated in the assembly of test pieces on the centrifuge.

The variables that were studied in the overall heat transfer program were heat flux, magnitude and direction of acceleration forces, type of liquid metal, and type of liquid metal container material.

Although the overall investigation included sodium and lithium, the data for liquid tin only are reported here.

III. DESCRIPTION OF APPARATUS

Nozzle, Rocket, and Centrifuge

The nozzles were machined at ABL from solid molybdenum and were designed to have one-inch long by one-inch diameter cylindrical throats and to accept two test sections in the throat. The nozzles with test inserts installed were assembled on a solid propellant rocket and mounted either on the centrifuge or in a static firing bay.

The centrifuge used is located in a concrete shielded bay and can rotate at speeds up to 66 rpm. The arm on the centrifuge is 28 feet long. The rocket was mounted radially on the centrifuge arm and the exhaust was directed outward (see Figure 1). This equipment was instrumented to provide centrifuge rpm, rocket chamber pressure, motion pictures of the nozzle area, and closed circuit television of the centrifuge bay. Temperatures were recorded on instruments mounted on the centrifuge at its center.

The letters CNDA and UNCS represent the name of the fabricator and serve only to help identify the test series.

Test Section

The general arrangement of the CNDA test section in the nozzle is shown in Figures 1 and 2. The test section consisted of the following components:

1. Test section cup--to contain the liquid metal and to be inserted and sealed in the nozzle so that the truncated portion of the cup formed part of the nozzle throat through which the heat from the propellant gases was transferred to the liquid metal;
2. Separator tube--to separate entrained liquid from the vapor, if any, and to direct the vapor to the trap;
3. Trap--in which the vapor is condensed and the condensate prevented from returning to the cup;
4. Exhaust tube--to provide additional surface for condensation.

Test Section Cup (Insert)

The test section cup (see Figure 2) was an open inverted cone. The truncated portion was bounded by a surface whose geometry is that of a cone intersecting a cylinder. This surface formed part of the nozzle throat.

This design was pretested using a transparent plastic model with compressed air to simulate metal vapor and water or mercury to simulate the liquid metal under large accelerations. The tests indicated that, with high vapor generation rates at the heat transfer surface, the surface would remain covered with liquid.

All portions of the test section cups were fabricated of pure tantalum, except for the heat transfer surface window which was made of tantalum-10% tungsten. These were welded to the tantalum conic sections. The tests reported used a 0.150-inch thick curved wall heat window to obtain instantaneous heat flux readings using two thermocouples in the wall.

Each cup was instrumented with the thermocouples located at the following points:*

1. heat transfer wall, 0.05 inch from the gas side,
2. heat transfer wall, 0.05 inch from the liquid side,
3. liquid, 0.080 inch from the wall,
4. liquid, bulk temperature, one inch from wall,
5. insulation.

Each cup was insulated with silica cast in place. The heat transfer surface was machined and hand-fitted to the opening in the nozzle throat. The top flange was sealed by a rubber O-ring.

In addition to tin, sodium and lithium have also been used as heat transfer agents in the overall program.

---

* These values vary slightly from cup-to-cup.

Separator Tube

The one-inch diameter separator tube was inclined 30° from the vertical in the direction of lower acceleration so that any liquid carried into the separator tube would tend to be pulled back to the cup while the vapor was free to travel up the tube and enter the trap. The angle of inclination was the maximum permitted to clear the nozzle housing.

The tubes were wrapped with mineral-type blanket insulation and instrumented with chromel/alumel thermocouples to provide a temperature - time history for heat balance data.

Other Components

The stainless steel trap was baffled to prevent any liquid carried into the trap from entering the condensing regions. The trap was instrumented with thermocouples and connected by a flexible stainless steel joint to the 10-foot long, one-inch diameter exhaust tube. The exit of the exhaust tube was filled with stainless steel mesh to provide additional surface for condensation in the event that vapor reached that point. No vapors were detected during any of the tests reported here.

All thermocouple signals from the test section were recorded throughout the firing on Minneapolis Honeywell Visicorders.

Figure 3 is a photograph of a nozzle with test inserts assembled on motor and mounted in static firing bay. This set-up is typical for the firings not made on the centrifuge. The design operating pressure for the UNCS test section is considerably above that for the CNDA test section, but the design differences are not sufficient to warrant detailed description here.

IV. CALCULATION METHODS

The test calorimetric system is defined as consisting of all of the liquid metal, all the metal parts, and one-half of the cast silica insulation surrounding the calorimeter cup (the other half of the silica insulation is assumed to absorb heat only from the molybdenum block surrounding it). Given the temperatures at any instant and the weights of the various materials and their specific heats, (Ref. 1 through 4), the total quantity of heat absorbed by the system up to the given instant may be readily calculated. Dividing the total quantity of heat by the time interval and the heat window area on the propellant gas side yields the average gas side heat flux over the time interval considered. Theoretically, this time interval could be any part or all of the test firing interval. Given the gas side heat flux, translation to a liquid metal side heat flux has involved deducting from the former only the heat absorbed by the heat window during the time interval considered and multiplying by the ratio of heat window liquid metal side to gas side heat transfer areas. The assumption was also made that none of the heat passed from the heat window directly to the walls of the cup.

The liquid metal film heat transfer coefficient, averaged over a given time interval, was calculated by dividing the liquid metal side average heat flux over the interval by the average temperature difference between the heat window surface on the liquid metal side and the measured liquid metal temperature 0".092 to 0".106 away from the heat window surface (depending on the "film" thermocouple location for the particular test firing involved). The heat window surface temperature was not measured directly; it was calculated by extrapolation from the measured temperature or temperatures within the heat window metal, using the distance between thermocouple and heat window surface, the thermal conductivity of the heat window[1], and the corresponding heat flux (corrected for the heat absorbed by the portion of heat window involved).

The above method of calculation based on the calorimetric system provides average values of heat flux and heat transfer coefficient within selected time intervals.

V. TEST RESULTS

A series of firings has been made with the test apparatus and the data for calorimetric inserts charged with tin are reported.

Operating conditions and test results are shown in Table I. Typical temperature records are given in Figure 4.

TABLE I

Heat Transfer Results with Tin

Test	CNDA-9		UNCS-1
Duration of Firing, Seconds	104		16.9
Gravity Force			
Magnitude, g	1.18		1.0
Angle with Heat Window	-23.9°		30°
Test Section No.	1	2	1
Tin Charged, Grams	193	193	175
Seconds of Data	Total	Total	9*
Heat Transfer			
Heat Window, Diameter. Ft.	0.0743		0.0766
Area, Ft.^{2}	0.00528		.00363
T_s, Calc. Throat Stagnation, °C	2730		2778
Flux x 10^{-6}, Btu/Hr x Ft^2	0.780	0.780	1.72
T_{wc}, Wall Tin Side, °C	1039	1011	1065
T_c, Tin Nearest Wall Temperature, °C	843	762	686
Distance from Wall, Inch.	0.106	0.099	0.092
ΔT, $= T_{wc} - T_c$, °C	196	249	379
h_c, Tin Film Coefficient, Btu/Hr x Ft^2 x °F	2210	1740	2520

*The data are given for the last 9 seconds of the run during essentially "steady-state" conditions.

3918

VI. CORRELATIONS

In addition to the heat transfer measurements set forth above, all of the data obtained in this program have been analyzed and correlated as detailed in Table II and Figures 5 and 6. In these correlations, the properties for tin were evaluated at the film temperature and are as given in Figure 7 and Reference 2 through 4.

a. Natural Convection Coefficient for Tin

The film heat transfer coefficient data of Table I are plotted on Figure 5 along with the line representing Eckert's general equation (Reference 5) for natural convection in vertical planes at low Prandtl Numbers.

$$Nnu^* = 0.68 \left[Npr/(0.952 + Npr)\right]^{.25} (Ngr \times Npr)^{.25} \qquad (1)$$

The maximum deviation of Prandtl Number from the average of all test values (with any given liquid metal) when raised to the 0.25 power amounted to about 2 percent and hence the substitution was made in the first term of equation (1) so that the lines could be included in the correlation figures. For tin, with an average Npr of 0.00563 for these tests, equation (1) reduces to:

$$Nnu = 0.188 \, (Ngr \times Npr)^{.25} \qquad (1a)$$

The data are well represented by this line. The variation of gravity, although not significant in the tests with tin, is accounted for by the term ($g^{0.25}$) in the Grashof Number (data as yet unpublished).

---

* Eckert's equation for the general case (1) was used here instead of $Nnu = 0.508 \left[Npr/(0.952 + Npr)\right]^{.25} (Ngr \times Npr \cos \alpha)^{.25}$, a form of which is seen in Reference 6, because this latter equation was derived specifically for the case of laminar free-convection heat transfer from a moderately inclined surface.

b. Comparison with Sodium and Lithium

In Table II, the film heat transfer coefficients of lithium, sodium, and tin are compared under what appears to be reasonably similar conditions. The lithium coefficient is about 25% higher than the tin coefficient and about 46% higher than the sodium coefficient. Note, however, that although the heat flux values were about equal, the film temperature for sodium was much lower than that for the other two metals.

For sodium, with an average Npr of 0.00482 for the tests, in this overall program equation (1) reduces to:

$$Nnu = 0.179\ (Ngr \times Npr)^{.25} \qquad (1b)$$

and for lithium, with an average Npr of 0.0199 for these tests, equation (1) reduces to:

$$Nnu = 0.257\ (Ngr \times Npr)^{.25} \qquad (1c)$$

Equations (1a), (1b), and (1c), which represent equally well the experimental data for tin, sodium and lithium respectively, are plotted in Figure 6. At constant values of heat flux and film temperature of 0.712×10^6 Btu/hr x ft^2 and 782°C respectively (Table II for lithium), calculations based on these curves result in a lithium coefficient about 35% higher than the tin coefficient and about 12% higher than the sodium coefficient. It is obvious that film temperature significantly affects the coefficient.

TABLE II

Comparison of Lithium, Tin and Sodium Heat Transfer Coefficients

Heat Transfer Metal	Li	Sn	Na
Test and Insert No.	CNDA-8, #1	CNDA-9, #1	CNDA-8, #2
Seconds of Data	135.2	104	135.2
Flux x 10^{-6}, Btu/Hr x Ft^2	0.712	0.780	0.752
Tc, Liquid Metal Film Temperature, °C	782	843	439
h_c, Btu/Hr x Ft^2 x °F	2770	2210	1900

3919

VII. SUMMARY AND CONCLUSIONS

As part of a program of research on solid propellant rocket nozzle heat transfer at Allegany Ballistics Laboratory, fundamental research on liquid-metal heat transfer in experimental rocket nozzles has been pursued. In the latter, ABL worked with United Nuclear Corporation, Development Division, NDA.

A series of tests has been made with a nozzle designed with two calorimeter test inserts for determining film heat transfer coefficients at the nozzle throat. The variables that were studied in the overall program included heat flux, magnitude and direction of acceleration forces, type of liquid metal, and type of liquid metal container material. The data for liquid tin are reported here. Wall surface temperature to 1065°C, liquid metal heat flux to 1.72×10^6 Btu/hr x ft^2, film temperature to 843°C, propellant gas throat stagnation temperatures in excess of 2760°C (5000°F) and accelerations to 1.18 g were experienced.

The liquid metal natural convection heat transfer results obtained thus far suggest the following conclusions:

1. The highest tin film heat transfer coefficient measured was 2520 Btu/hr x ft^2 x °F.
2. The dimensionless heat transfer coefficients are well represented by Eckert's equation (Reference 5):

$$Nnu = 0.68 \left[Npr/(0.952 + Npr)\right]^{.25} (Ngr \times Npr)^{.25}$$

3. The final equation for tin, with an average experimental Prandtl Number of 0.00563, takes the form

$$Nnu = 0.188 (Ngr \times Npr)^{.25}$$

4. At constant values of heat flux and film temperature of 0.712×10^6 Btu/hr x ft^2 and 782°C respectively, calculations based on Eckert's equation result in a lithium coefficient about 35% higher than the tin coefficient and about 12% higher than the sodium coefficient.

VIII. SYMBOLS AND NOMENCLATURE

C_p	Specific heat, Btu/lb x °F
D	Diameter
Ngr	Grashof Number = $D^3\rho^2 g\ \beta\Delta T/\mu^2$, dimensionless
g	Acceleration of gravity
h_c	Liquid metal film heat coefficient, Btu/hr x ft^2 x °F
k	Thermal conductivity, Btu/hr x ft^2 x °F/ft
Nnu	Nusselt Number = hD/k, dimensionless
Npr	Prandtl Number = $C_p\ \mu/k$, dimensionless
T_s	Gas stagnation temperature at nozzle throat
T_{wc}	Wall surface temperature on the liquid metal side
ΔT	Temperature difference

Greek Letters

α	Angle between gravity force and heat window
β	Volumetric coefficient of expansion, 1/°F
μ	Coefficient of viscosity, lb/ft x hr
ρ	Density, lbm/ft^3

IX. REFERENCES

1. A. Goldsmith, T. E. Waterman, H. J. Hirschhorn, "Thermophysical Properties of Solid Materials", WADC Technical Report 58-476, Revised Edition, Volumes I-IV, Wright Air Development Division, Wright-Patterson Air Force Base, Ohio, August, 1960.
2. "Liquid Metals Handbook", Second Edition, AEC and Department of the Navy, Washington, D. C. , June, 1952.
3. S. S. Kutateladze, V. M. Borishanskii, I. I. Novikov and O. S. Fedynskii, "Liquid-Metal Heat Transfer Media", Supplement No. 2, Atomnaia Enegiia, Atomic Press, Moscow, 1958. Translated from Russian by Consultants Bureau, Inc., New York. Chapman and Hall, Ltd., London.
4. A. D. Kirshenbaum and J. A. Cahill, "The Density of Liquid Tin from its Melting Point to its Normal Boiling Point and an Estimate of its Critical Constants", Transactions of the ASM, Volume 55, 1962, p. 845.
5. McAdams, Heat Transmission, Third Edition, McGraw Hill (1954), p. 171, Eq. 7-3a.
6. Kreith, Principles of Heat Transfer, International Textbook Company (1958), p. 309, Eq. (7-21).

GENERAL VIEW OF
INSTALLATION ON CENTRIFUGE

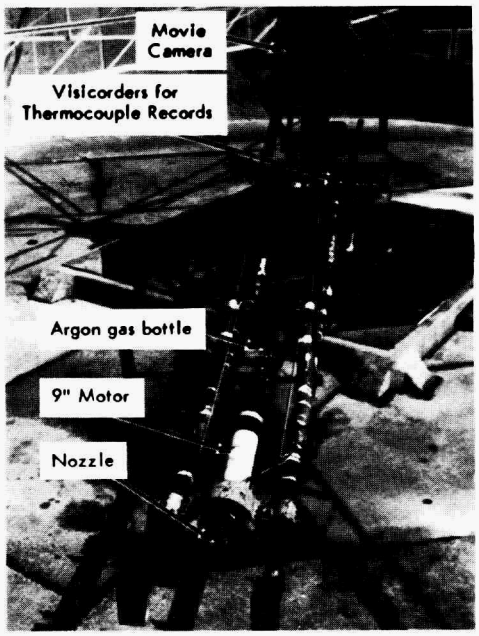

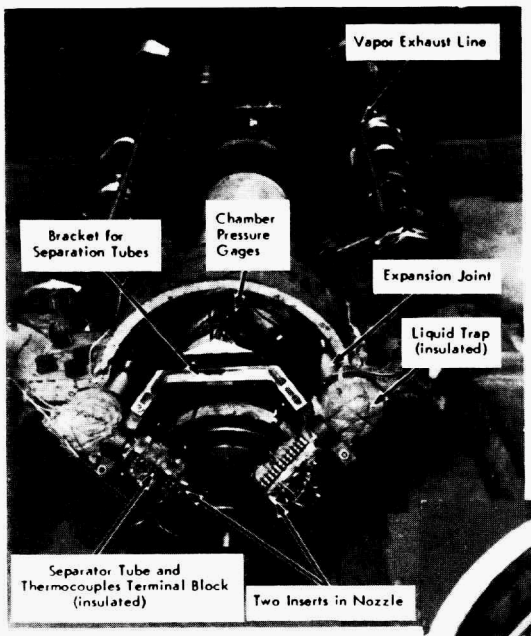

CLOSEUP OF MOTOR AND
NOZZLE WITH TEST INSERTS

CLOSEUP OF NOZZLE EXIT CONE
AFTER TEST FIRING CNDA-1

PHOTOGRAPH OF NOZZLE WITH TEST INSERTS ASSEMBLED
ON MOTOR AND MOUNTED ON CENTRIFUGE

Fig. 1.

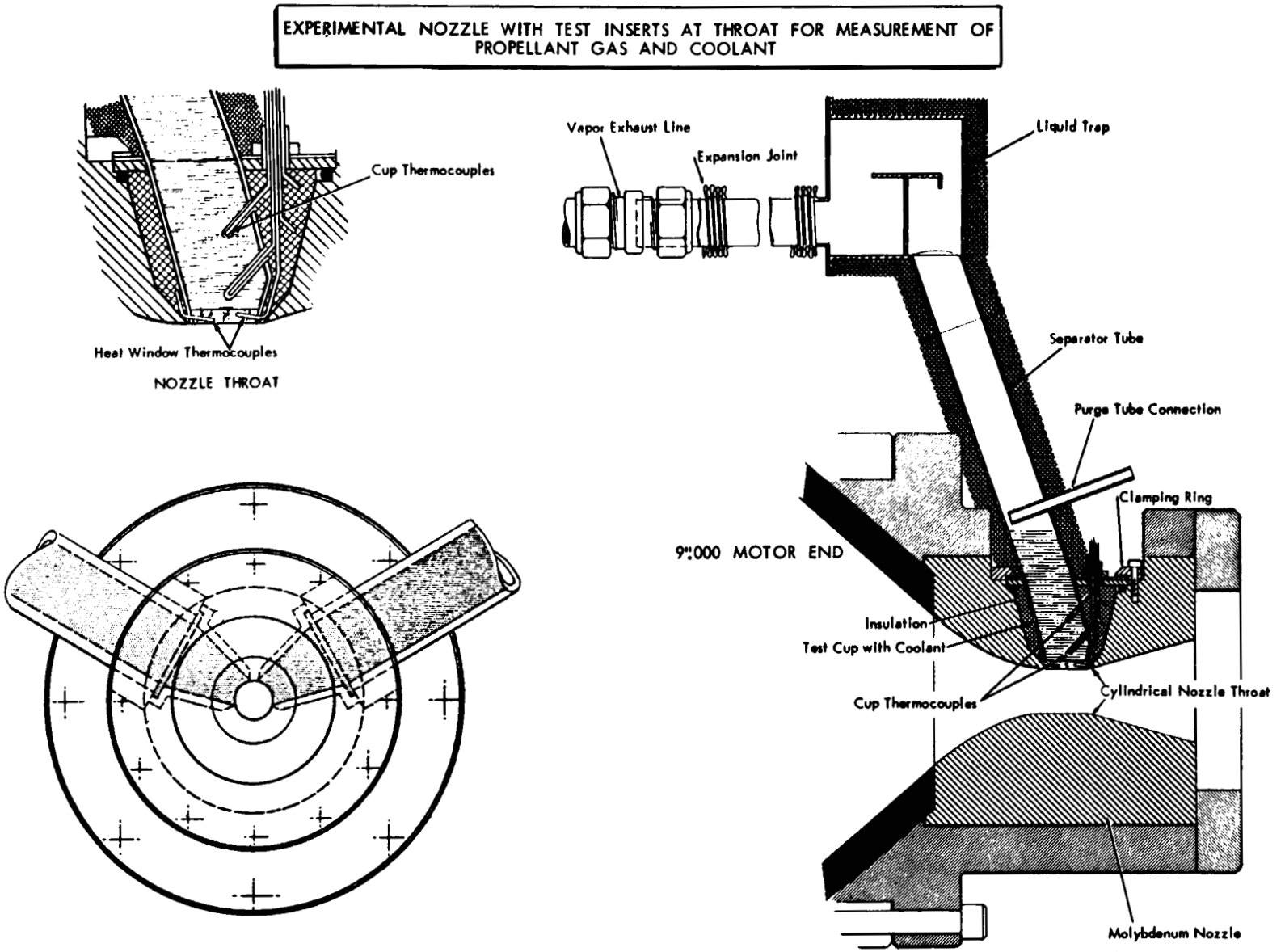
EXPERIMENTAL NOZZLE WITH TEST INSERTS AT THROAT FOR MEASUREMENT OF PROPELLANT GAS AND COOLANT
Cup Thermocouples
Heat Window Thermocouples
NOZZLE THROAT
Vapor Exhaust Line
Expansion Joint
Liquid Trap
Separator Tube
Purge Tube Connection
Clamping Ring
9".000 MOTOR END
Insulation
Test Cup with Coolant
Cup Thermocouples
Cylindrical Nozzle Throat
Molybdenum Nozzle

Fig. 2.

PHOTOGRAPH of NOZZLE with TEST INSERTS ASSEMBLED ON MOTOR and MOUNTED in STATIC FIRING BAY

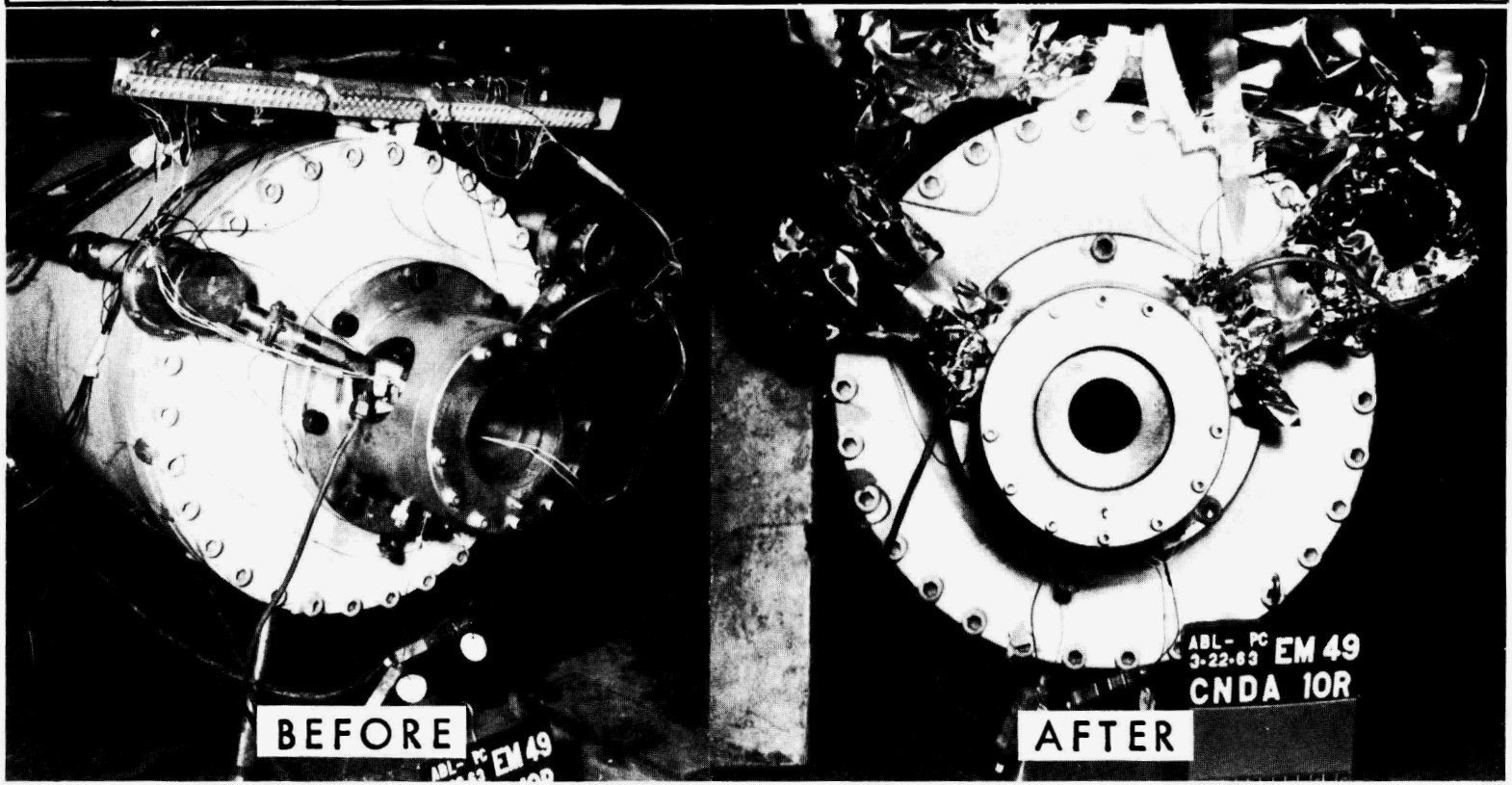

Fig. 3.

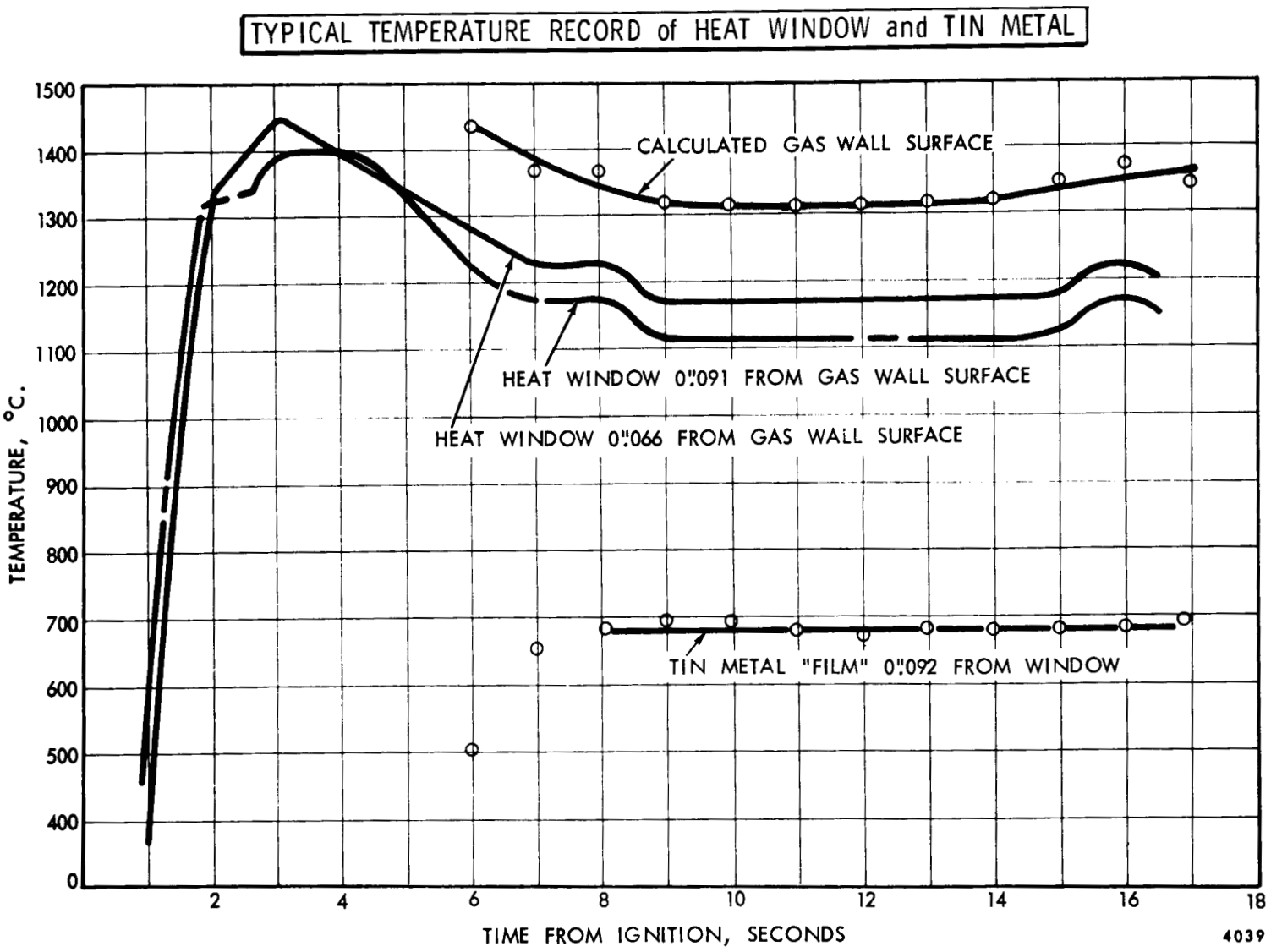
TYPICAL TEMPERATURE RECORD of HEAT WINDOW and TIN METAL
CALCULATED GAS WALL SURFACE
HEAT WINDOW 0".091 FROM GAS WALL SURFACE
HEAT WINDOW 0".066 FROM GAS WALL SURFACE
TIN METAL "FILM" 0".092 FROM WINDOW
TEMPERATURE, °C.
1500
1400
1300
1200
1100
1000
900
800
700
600
500
400
0
2
4
6
8
10
12
14
16
18
TIME FROM IGNITION, SECONDS
4039

Fig. 4.

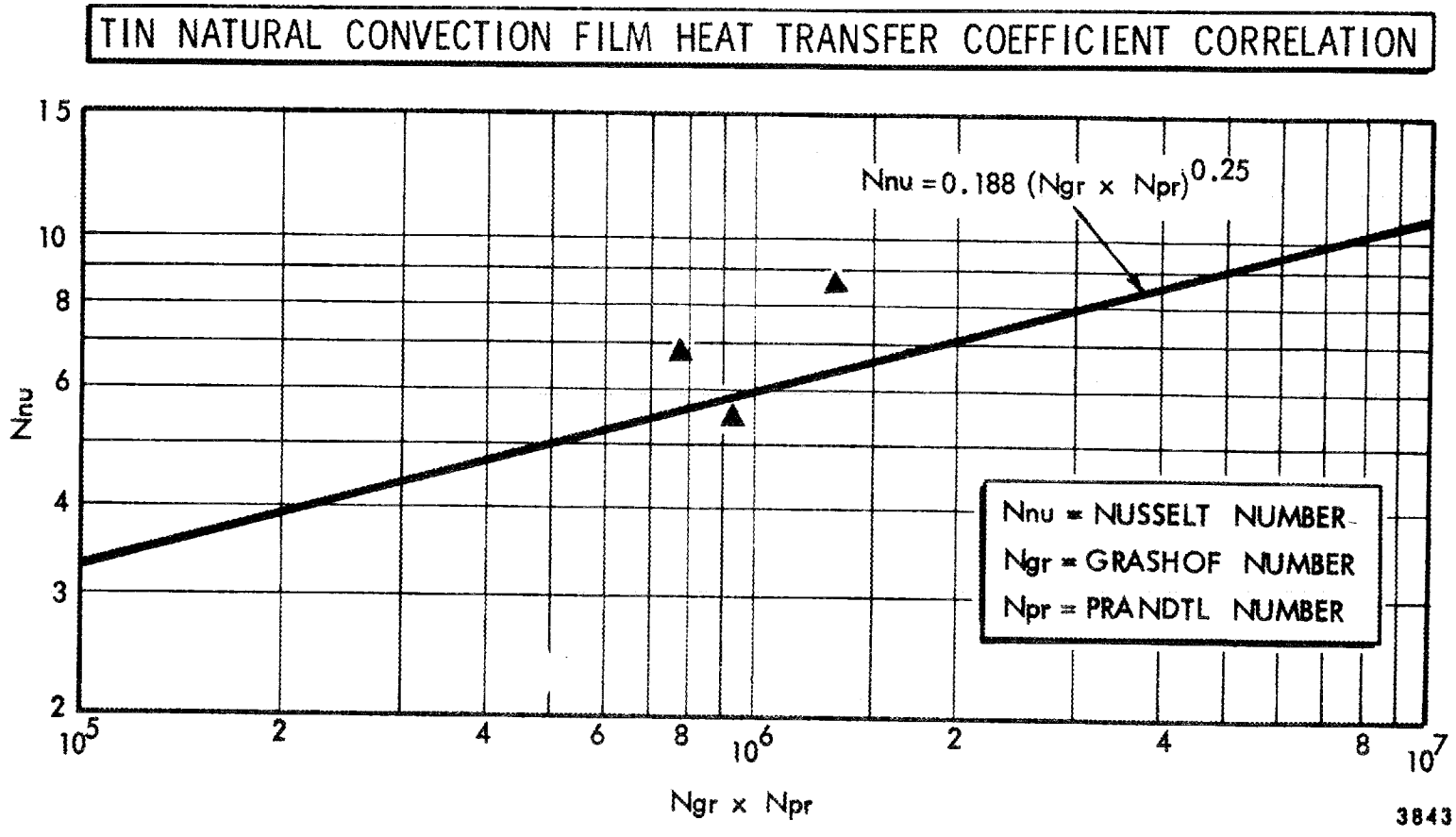
TIN NATURAL CONVECTION FILM HEAT TRANSFER COEFFICIENT CORRELATION
Nnu = 0.188 (Ngr x Npr)^0.25
Nnu = NUSSELT NUMBER
Ngr = GRASHOF NUMBER
Npr = PRANDTL NUMBER
Nnu
15
10
8
6
4
3
2
10^5
2
4
6
8
10^6
2
4
8
10^7
Ngr x Npr
3843

Fig. 5.

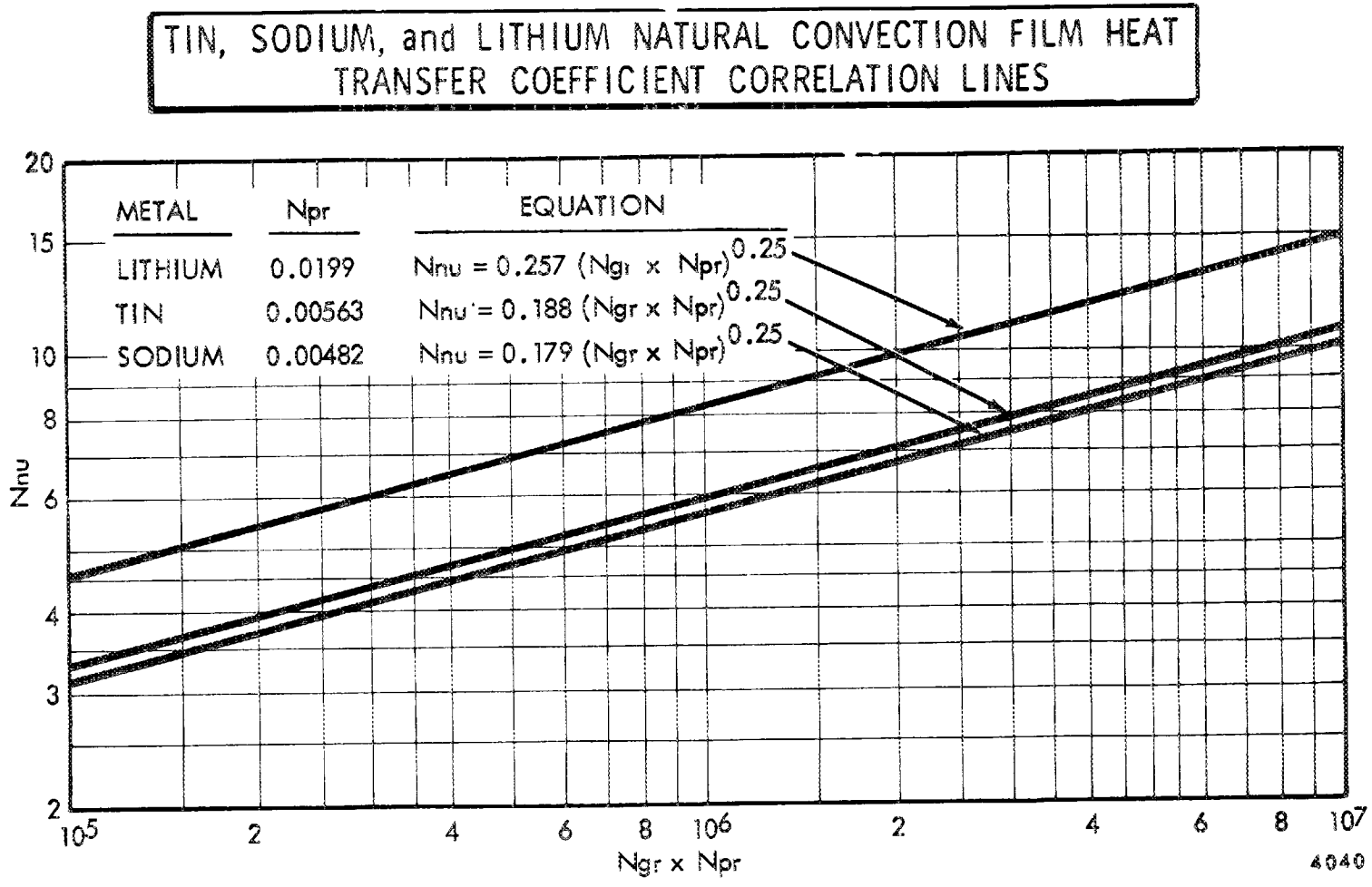
TIN, SODIUM, and LITHIUM NATURAL CONVECTION FILM HEAT TRANSFER COEFFICIENT CORRELATION LINES
METAL
Npr
EQUATION
LITHIUM 0.0199 Nnu = 0.257 (Ngr x Npr)^0.25
TIN 0.00563 Nnu = 0.188 (Ngr x Npr)^0.25
SODIUM 0.00482 Nnu = 0.179 (Ngr x Npr)^0.25
Nnu
20
15
10
8
6
4
3
2
10^5
2
4
6
8
10^6
2
4
6
8
10^7
Ngr x Npr
4040

Fig. 6.

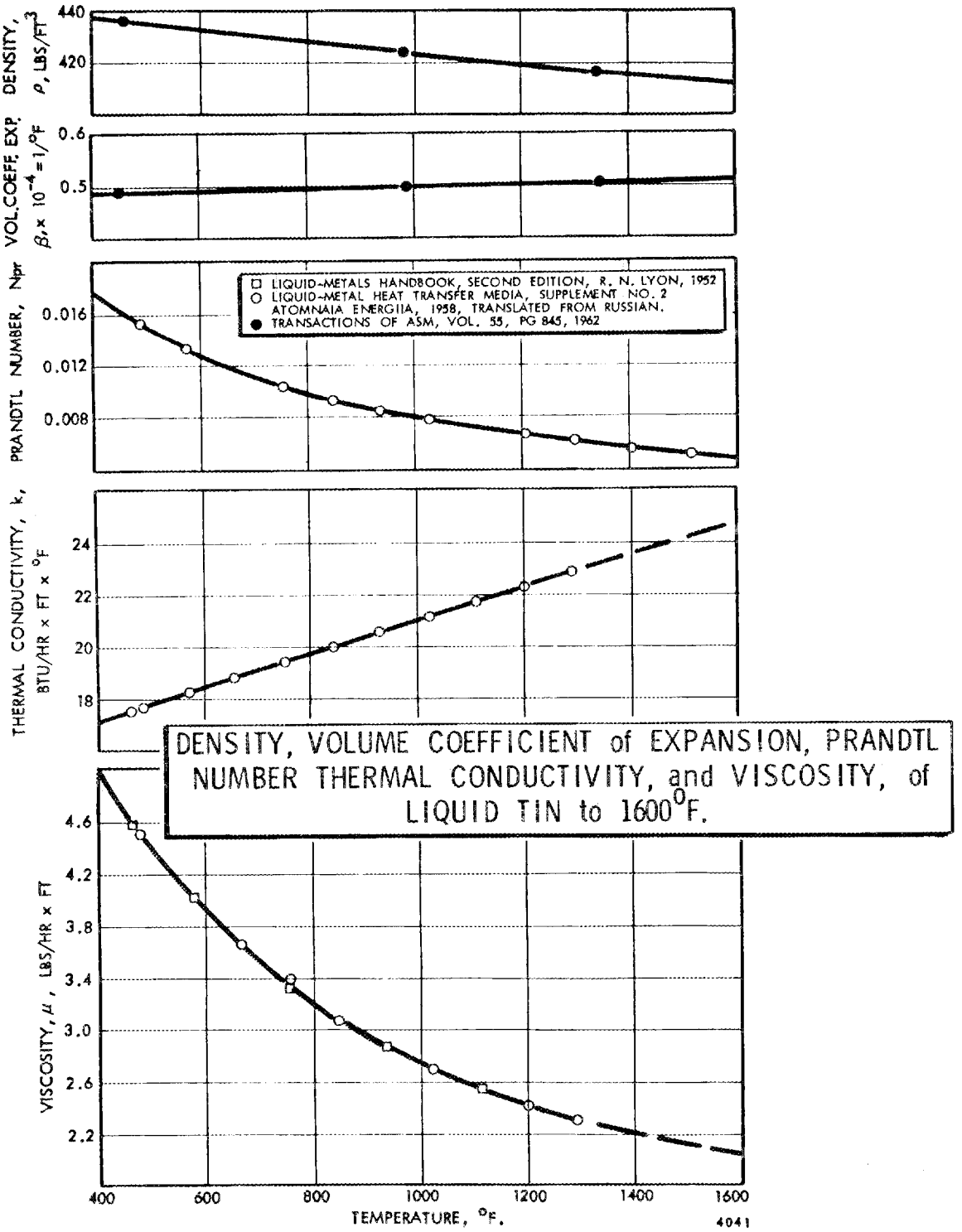

DENSITY, VOLUME COEFFICIENT of EXPANSION, PRANDTL NUMBER THERMAL CONDUCTIVITY, and VISCOSITY, of LIQUID TIN to 1600°F.

Fig. 7.

DISCUSSION

MR. STEIN: Just one remark of amazement: that Eckert's relationship derived for a certain specific situation, could represent the results obtained from transients and confined space, with gravity oriented in a peculiar way.

MR. DESMON: In a rocket-nozzle firing, the transients don't last too long. The total firing times were of the order of one hundred to two hundred seconds; and the transients are pretty well over with by six to ten seconds. They just contribute to the scatter in the data; that's all.

We have a lot more data which doesn't appear in this paper, which, in its final form, will be given at the AICHE meeting in December at Houston.

MR. CHEN: I thought that I noticed g-values of 1.18 and 1.0. I wondered why you went to all the trouble of a centrifuge device, if that's all you are getting.

MR. DESMON: This overall program had three liquid-metal investigations; tin, sodium and lithium. This is one-third of the data, the data of liquid tin. With liquid lithium we had accelerations up to 14.25 g, and found in that investigation that g to the .25 in the Grashof number did an adequate job of incorporating acceleration into the dimensionless correlation.

THE EFFECT OF SURFACE CONDITIONS ON POOL BOILING HEAT TRANSFER OF SODIUM

P. J. Marto

W. M. Rohsenow

Massachusetts Institute of Technology
Cambridge 39, Massachusetts

Presented at the Third Annual Liquid Metal Heat Transfer Meeting
Oak Ridge National Laboratory
Oak Ridge, Tennessee

September 4-6, 1963

Work performed under NSF Contract GP-14421

I. INTRODUCTION

Recent advances in the technology of nuclear power reactors such as FERMI, and of experimental breeder reactors such as SRE and HNPF, and also of rocket auxiliary power systems such as SNAP (where liquid metal vaporization will occur in an advanced Rankine cycle) have created a great demand for investigating and understanding the process of boiling liquid metals.

Liquid alkali metal pool boiling data is quite sparse, and the small amount of available data scatters considerably[1,2,3,4] (as shown in Fig. 1 and Fig. 2) so that good engineering designs of the above-mentioned systems are very difficult.

It is felt that the primary cause of a lack of reproducibility in boiling liquid metal data is due to poor control of surface conditions (i.e., poor control of surface physical roughness and surface contamination, and also the wide use of many different surface materials).

II. OBJECTIVE

The main purpose of this research program is to establish an experimental procedure for cleaning, evacuating and filling a piece of equipment which will yield reproducible pool boiling sodium data for a given set of boiling surface conditions, and to investigate the effect of various surface finishes and additives on the nucleate pool boiling sodium curve.

III. BACKGROUND

Theoretical Results

It is now generally agreed that in nucleate pool boiling, the heat transfer coefficient can be written as

$$h \sim (n/A)^a \, (T_w - T_{sat})^b \qquad \ldots (1)$$

where (n/A) is the number of active cavity sites per unit area of the boiler surface. Several investigators[5,6] have shown that the critical wall superheat necessary to initiate the growth of a bubble from a cavity also depends on the surface geometry

$$(T_w - T_{sat})_{crit} \sim \frac{1}{r_c} \qquad \ldots (2)$$

where r_c is the cavity mouth radius of a nucleating site.

Thus, it is evident from the form of equations (1) and (2) that the condition of the boiler surface plays a twofold role in nucleate boiling heat transfer; first, surface conditions can alter the cavity size distribution of a boiler surface and second, surface conditions can alter the stability of a nucleating site and thereby control the degree of superheat necessary to initiate nucleate boiling.

Experimental Results

Corty and Foust[5] were among the first to extensively study the effect of surface roughness on nucleate boiling heat transfer coefficients. They boiled Freon 113, diethyl ether and n-pentane off copper and nickel plates for different surface polishes, and found that notonly the position of the boiling curve, but also the slope depends on the degree of surface polish. Later, Berenson[7] showed that for boiling of n-pentane off copper, nickel and inconel flat plates, the surface roughness can increase the heat transfer coefficient by as much as 500%, as shown in Fig. 3. More recently, Bonilla, Grady and Avery[8] found that by applying sharp parallel scratches onto the boiling surface, heat transfer coefficients for water increased by as much as 88% and for mercury with 0.1% sodium by as much as 116%.

Since different solid metals have different grain structures which can alter the size and shape of microscopic cavities on the boiling surface, we would expect that surface material would also affect the nucleate pool boiling curve. Both Stock[9] and Berenson[7] show similar results for the effect of surface material. Fig. 4 shows that the heat transfer coefficients increase by as much as 200% depending on the material used.

Other variables which affect the surface energy of a given metal (chemical contamination in the form of oxides, chemical contamination due to additives, the state of stress, etc.) can alter the wetting characteristics of a boiling fluid and also cause changes in the nucleate boiling curve[10,11,12].

Since none of the above effects have been systematically investigated for alkali metal boiling systems, the importance of this research work is quite evident.

IV. EXPERIMENTAL DESIGN

Since this research program is the first of its type at M.I.T., in order to begin the design of the equipment, the following conditions were established:

1. The working fluid should be sodium because it is inexpensive, its properties are well tabulated, and because its corrosive capabilities are rather well known.
2. The boiling system should be a static, closed capsulewith no loop operation.
3. The boiler surface should be a horizontal flat plate because this is a simple geometry, a large amount of horizontal flat plate boiling data is available for comparison, and because it is the simplest geometry on which to regulate surface finishes.
4. The boiler surface must be easily removable to allow for different surface polishes, surface materials, etc.
5. The system must be designed as simply, as safely, and as flexibly as possible.

With these "parameters" in mind, the final design resulted in a system where sodium would boil off a flat plate, rise up a vertical pipe, and condense due to forced convection of air. The boiling system is shown schematically in Fig. 5.

The major components are the main heater, boiler-condenser, high vacuum system, helium cover gas line, sodium fill and drain system, and instrumentation. These main components are now described more fully.

Main Heater

In order to interchange boiler surfaces quickly and with relative ease, it is necessary that the main heater should not be an integral part of the boiling test plate; therefore, radiant type heating was decided upon. The heater consists of three tantalum-10% tungsten filaments clamped in series between two molybdenum bus bars. The filaments are .010" thick, 1" wide and 4" long. They are corrugated with an internal angle of 30° for two reasons: first, to give added strength at high temperatures and second, according to Sparrow and Lin[13], the effective emissivity increases by roughly 200%. A large DC power supply, rated at 1200 amps, 20 volts, will pass up through internally water cooled copper electrodes to the molybdenum bus bars and across the electrical filaments. High temperature electrical insulators made of high purity aluminum oxide are used to channel the current so that the three filaments are connected in series. Fig. 6 shows the heater assembled, with six concentric radiation shields (the two inner made of .010" thick molybdenum, the four outer of .019" thick stainless steel 304) and nine horizontal .019" thick stainless steel 304 radiation shields to reflect as much heat as possible toward the boiler plate. These shields have been polished on the inner face to a mirror finish. The electrical filaments will operate up to a maximum temperature near 4500 ^{o}F (the melting point of tantalum-10% tungsten is approximately 5300 ^{o}F), and it is expected that heat fluxes as high as 500,000 Btu/hr ft^2 will be reached. To prevent complete oxidation and burnout of the filaments, a vacuum between 10^{-4} mm Hg and 10^{-5} mm Hg must be maintained.

Boiler-Condenser

The boiler is a 2-1/2" schedule 40 stainless steel 316 pipe, 1 ft. long. Fig. 7 shows an exploded view of this piece of equipment. Boiling will take place from a horizontal, flat, nickel disc 2-7/8" in diameter and 3/4" thick, electron beam welded by means of a .030" thick collar onto the stainless steel 316 pipe wall. This method of attachment was decided upon because the electron beam weld can be ground off the collar, leaving the boiler plate ready for refinishing and for re-welding to the pipe wall. It is expected that each collar can be re-welded about four times. Also, electron beam welding is the purest weld possible and eliminates any oxide formation. The bottom of the boiler test plate is flame sprayed with a thin coating of "Rokide A" aluminum oxide to increase its emissivity. Thermocouple wells, 1/16" in diameter, have been drilled at a number of axial and radial positions in the test plate to insure an accurate recording of the temperature distribution. The boiler pipe is flanged 9" above the boiler surface to allow for easy dismantling. This flange is grooved to accommodate a thin nickel gasket. Stainless steel knife edges, machined in the groove, provide a tight seal. The condenser section is a 2 ft. length of stainless steel 316 pipe with 18 copper fins, 18" long, 1-1/4" wide and 1/16" thick, hydrogen brazed on the outside.

High Vacuum System

The boiler and heater are contained within a 14" OD, 18" long, stainless steel 316 vacuum chamber, flanged at the top and bottom for easy access. Aluminum "O" rings are used in these flanges for a high temperature vacuum seal. The high vacuum line is a 4" schedule 40 pipe line connected to a flexible steel connector, a 90° elbow and a 4" vacuum diffusion pump.

Helium Cover Gas Line

In order to maintain the sodium as free of oxides as possible, helium will be used as a cover gas. Pressures will range from 10 mm Hg to 760 mm Hg. The helium will be dried and filtered by flowing through a molecular sieve bed (1/16" diameter pellets of an alkali metal alumino silicate) at liquid nitrogen temperatures. The entire helium gas line is 1/4" stainless steel 316 tubing and all valves are Hoke type TY440.

Sodium Fill and Drain System

Sodium will be stored in two tanks (one for filling, one for draining), 4-1/2" OD, 6" high with Viton "O" ring seals. The fill and drain lines are 3/8" stainless steel 316 tubing. Both the tanks and lines are electrically heated to keep the sodium molten. Sodium will be filtered before entering the boiler by passing through packed, fine grade, stainless steel wool. All valves are Hoke type TY445.

Instrumentation

Six platinum-platinum 10% rhodium "Ceramo" type thermocouples will be used at different axial and radial positions in the test plate. These thermocouples are 1/16" OD, inconel sheathed, magnesium oxide insulated, and are specially calibrated at 1400, 1600, 1800 and 2000 ^{o}F by the Thermoelectric Company to within an accuracy of less than 0.25%. Four chromel-alumel "Ceramo" type thermocouples, 1/8" OD will be contained inside 1/4" OD horizontal stainless steel 316 wells to measure the sodium pool temperature distribution. These thermocouple wells are located 1/2", 1", 1-1/2" and 2" above the boiler surface. Another chromel-alumel "Ceramo" type thermocouple 1/16" OD will be contained within a 1/8" OD stainless steel 316 tube and will dip down vertically into the sodium pool. Pressure in the helium line is measured by a Marsh compound pressure gage, and an open end manometer.

The heat flux can be calculated directly, knowing the thermal conductivity and thermocouple locations accurately, by measuring the temperature differentials between paired thermocouples in the boiler plate. The wall

temperature can be determined by extrapolating the plate thermocouple readings to the boiler surface. The saturation temperature of the sodium can be determined either by measuring the temperature distribution in the sodium pool, or by using the temperature corresponding to the measured saturation pressure in the vapor space.

V. TIME SCHEDULE

The boiling apparatus is about 80% complete. Fig. 8 shows the partial assembly of the system including the air blower, condenser cover, vacuum chamber, vacuum pumps, cooling water connections, steel enclosure, etc.

The vacuum system has been tested and a vacuum as low as 2.5×10^{-5} mm Hg has been reached. The electrical heaters will be tested next, and the system will be "debugged" throughout September.

Experimental runs should begin sometime in October.

VI. REFERENCES

1. Lyon, R. E., A. S. Foust, Katz, D. L., "Boiling Heat Transfer with Liquid Metals", Chem. Engr. Progr. Symposium Series No. 17, 51, (1955).
2. Madsen, N. and C. F. Bonilla, "Heat Transfer to Boiling Sodium-Potassium Alloy", Third National Heat Transfer Conference, Storrs, Conn., (1959).
3. Noyes, R. C., "An Experimental Study of Sodium Pool Boiling Heat Transfer," NAA-SR-6769, (1962).
4. Brooks, R. D., "Alkali Metals Boiling and Condensing Investigations", Quarterly Report No. 1, NAS 3-2528, (1962).
5. Corty, C. and A. S. Foust, "Surface Variables in Nucleate Boiling," AIChE Heat Transfer Conference, St. Louis, Mo., (1953).
6. Griffith, P. and J. D. Wallis, "The Role of Surface Conditions in Nucleate Boiling," Third National Heat Transfer Conference, Storrs, Conn., (1959).
7. Berenson, P. J., "Experiments on Pool Boiling Heat Transfer," Int. Jour. of Heat and Mass Transfer, 5, October (1962).
8. Bonilla, C. F., J. J. Grady and G. W. Avery, "Pool Boiling Heat Transfer from Scored Surfaces," Sixth National Heat Transfer Conference, Boston, Mass., (1963).
9. Stock, B. J., "Observations on Transition Boiling Heat Transfer Phenomena," ANL-6175, (1960).
10. Harrison, W. B. and Z. Levine, "Wetting Effects on Boiling Heat Transfer," ASME-AIChE Heat Transfer Conference, State College, Penna., (1957).
11. Dunskus, T. and J. W. Westwater, "The Effect of Trace Additives on the Heat Transfer to Boiling Isopropanol," ASME-AIChE Heat Transfer Conference, Buffalo, N.Y., (1960).
12. Denny, V. E., "Some Effects of Surface Micro-Geometry on Natural Convection and Pool Boiling Heat Transfer to Saturated Carbon Tetrachloride," Ph.D. Thesis, Univ. of Minnesota, (1961).
13. Sparrow, E. M. and S. H. Lin, "Absorption of Thermal Radiation in a V-groove Cavity," International Jour. of Heat and Mass Transfer, 5, November, (1962).

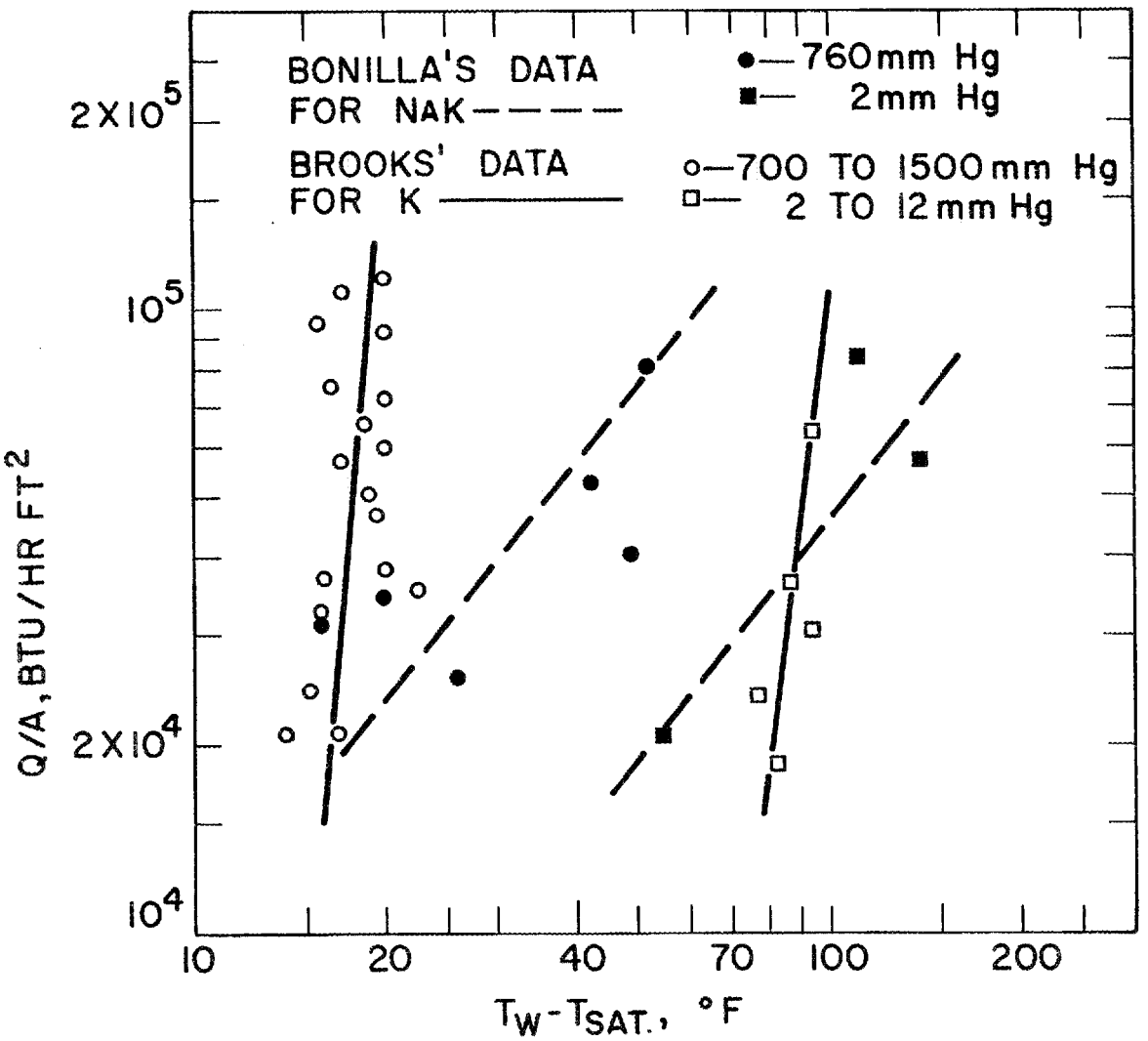

FIG.1 COMPARISON OF POOL BOILING NaK AND POTASSIUM DATA FOR HORIZONTAL FLAT PLATE

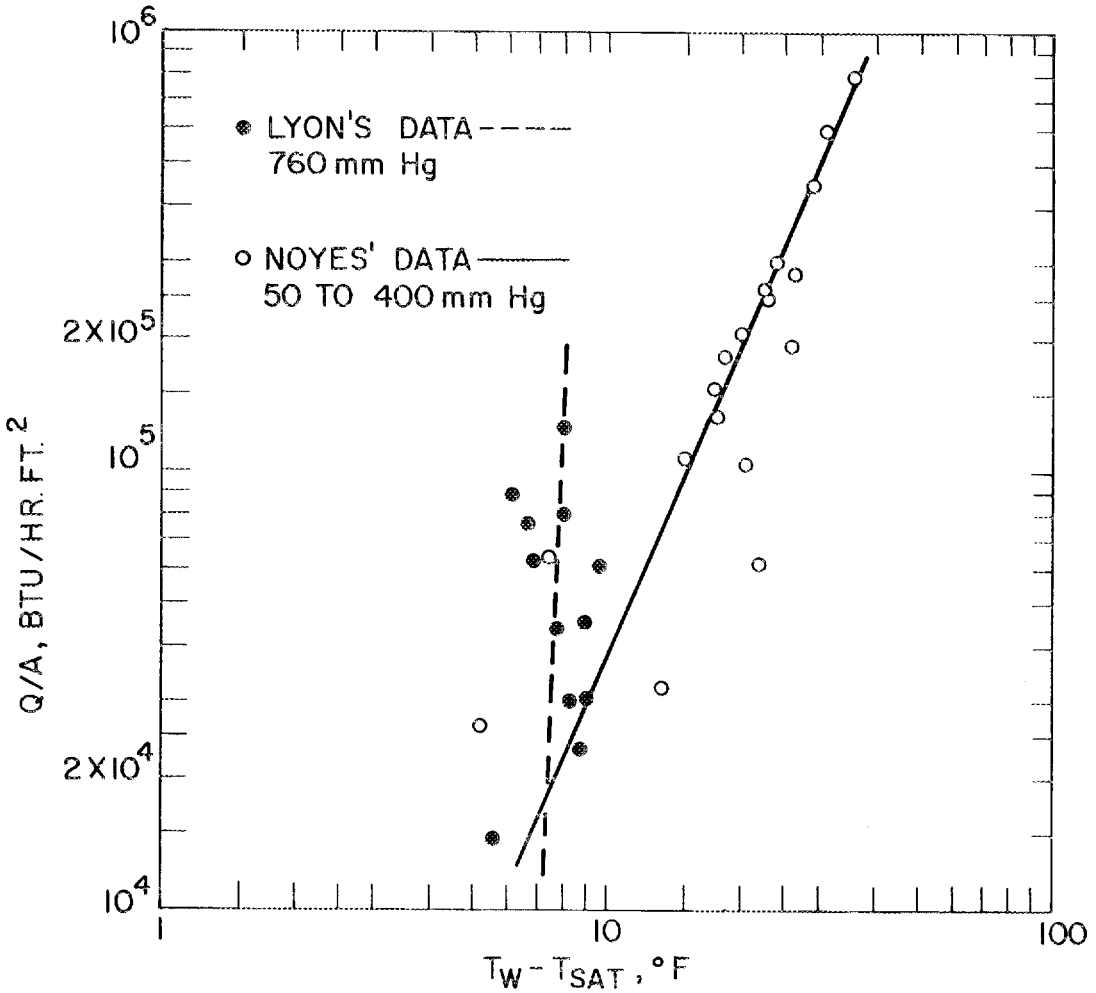

FIG. 2 COMPARISON OF SODIUM POOL BOILING DATA FROM HORIZONTAL TUBE

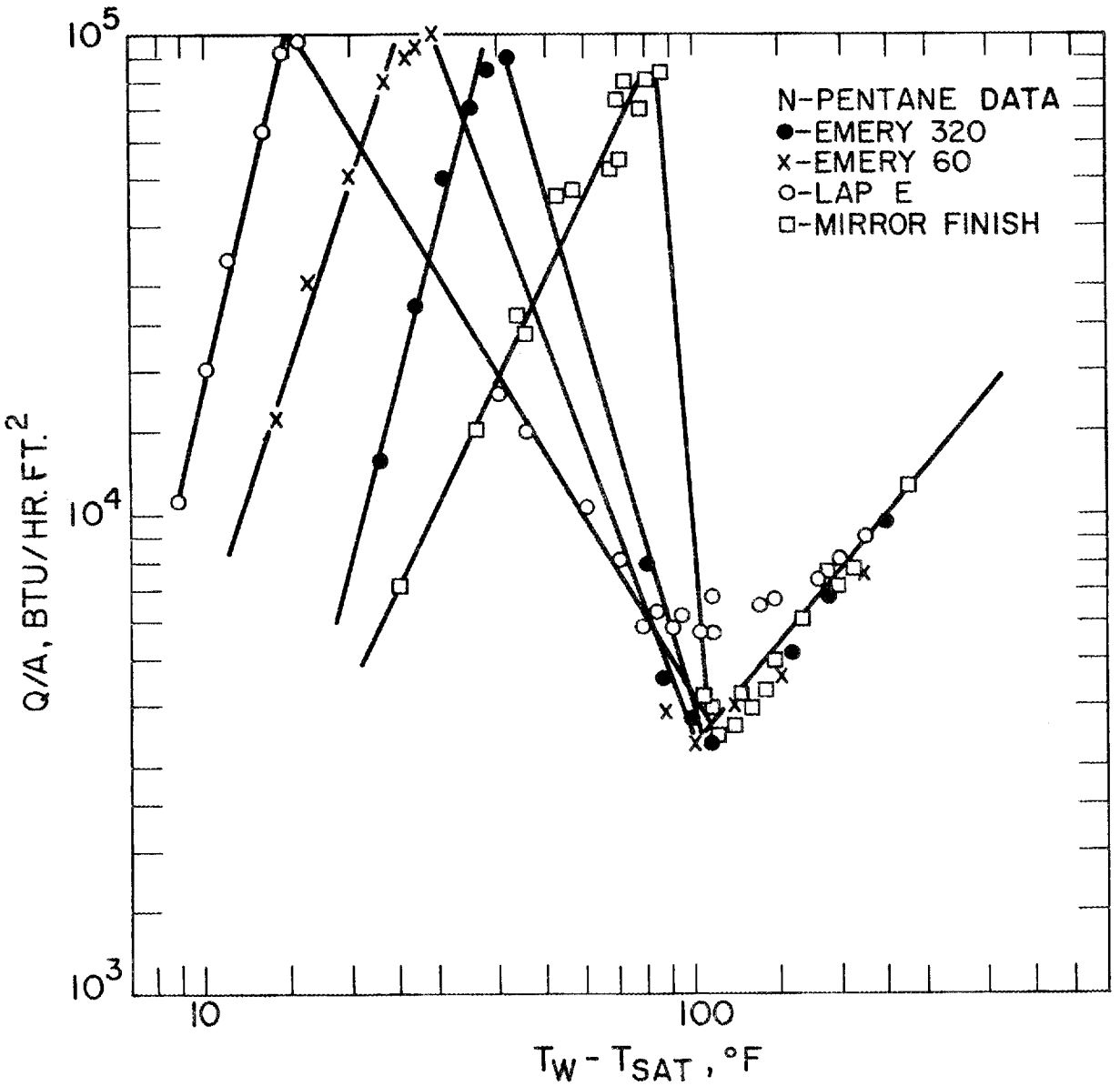

FIG. 3 EFFECT OF SURFACE ROUGHNESS ON POOL BOILING FROM A HORIZONTAL FLAT PLATE

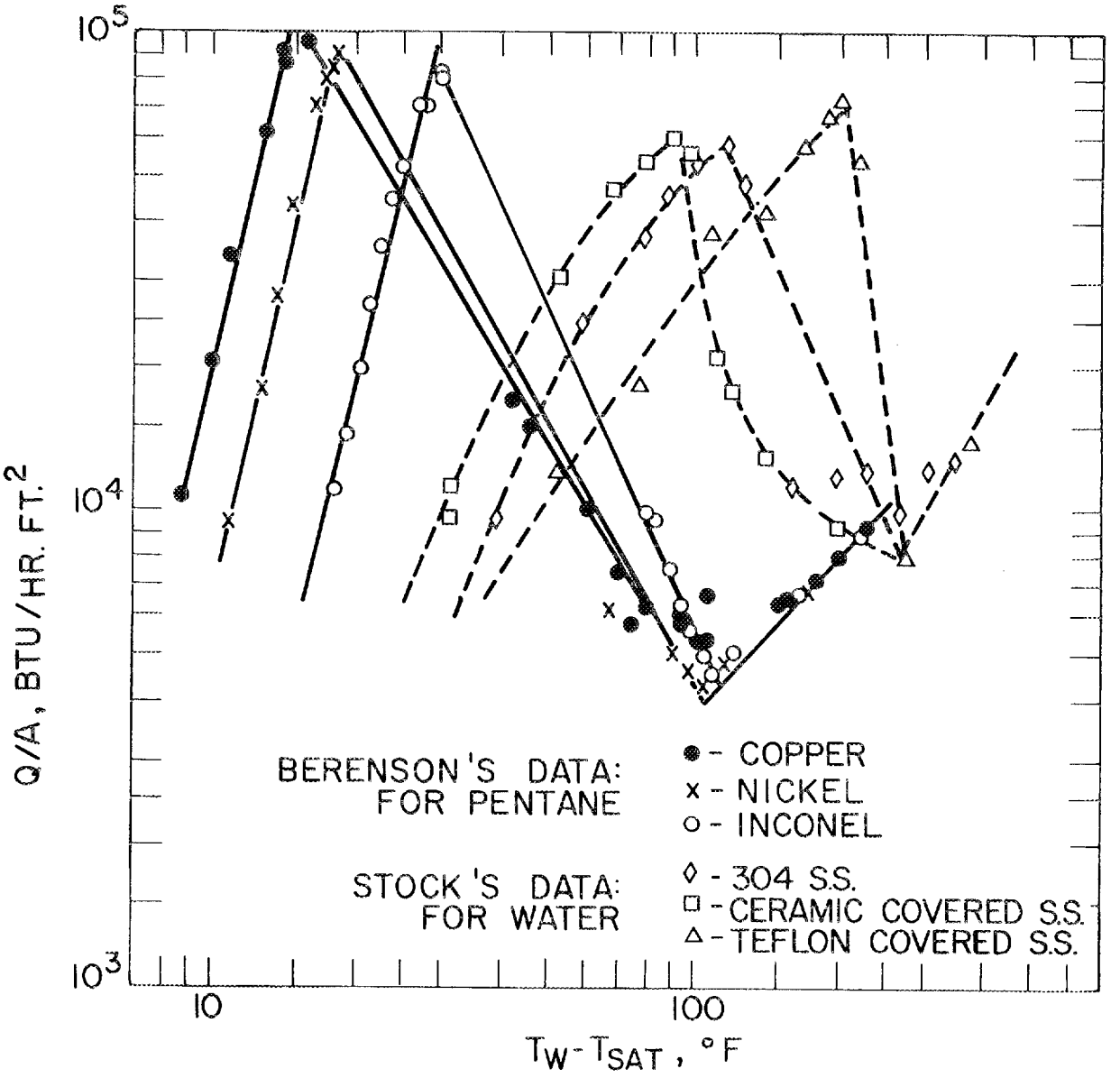

FIG. 4 EFFECT OF SURFACE MATERIAL ON POOL BOILING FROM A HORIZONTAL FLAT PLATE

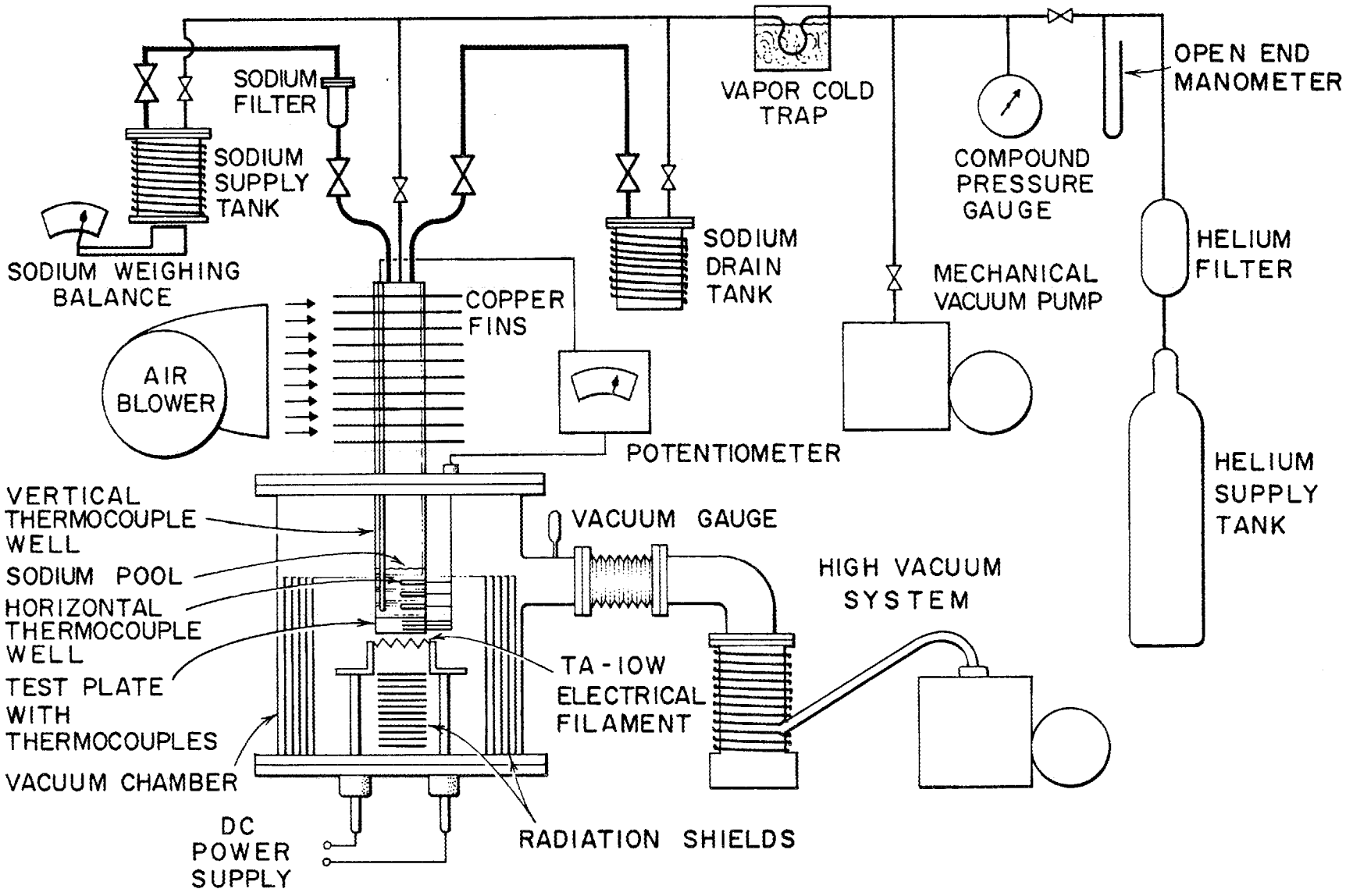

FIG. 5 SCHEMATIC DIAGRAM OF APPARATUS

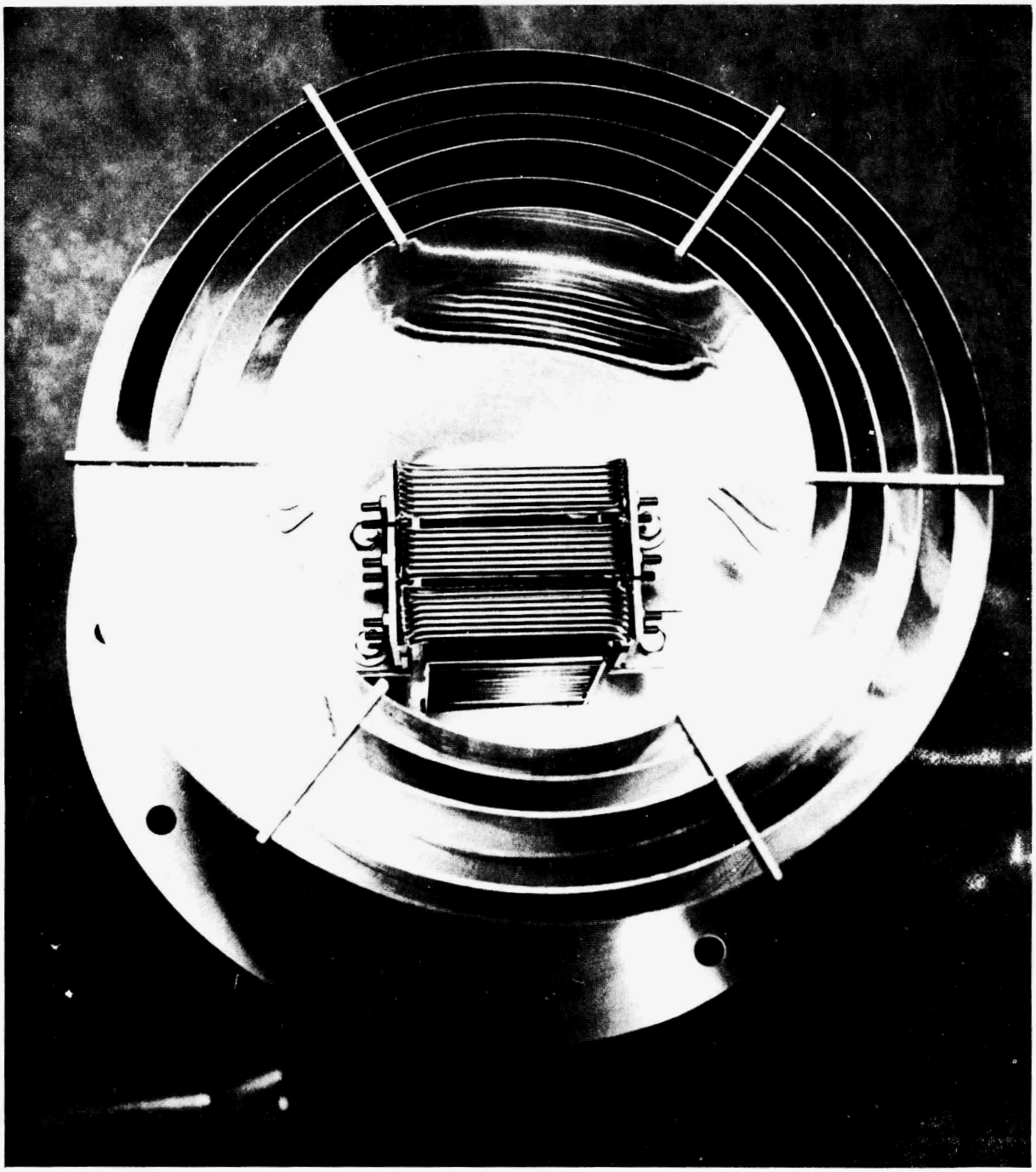

Fig. 6 ASSEMBLY OF MAIN HEATER WITH RADIATION SHIELDS

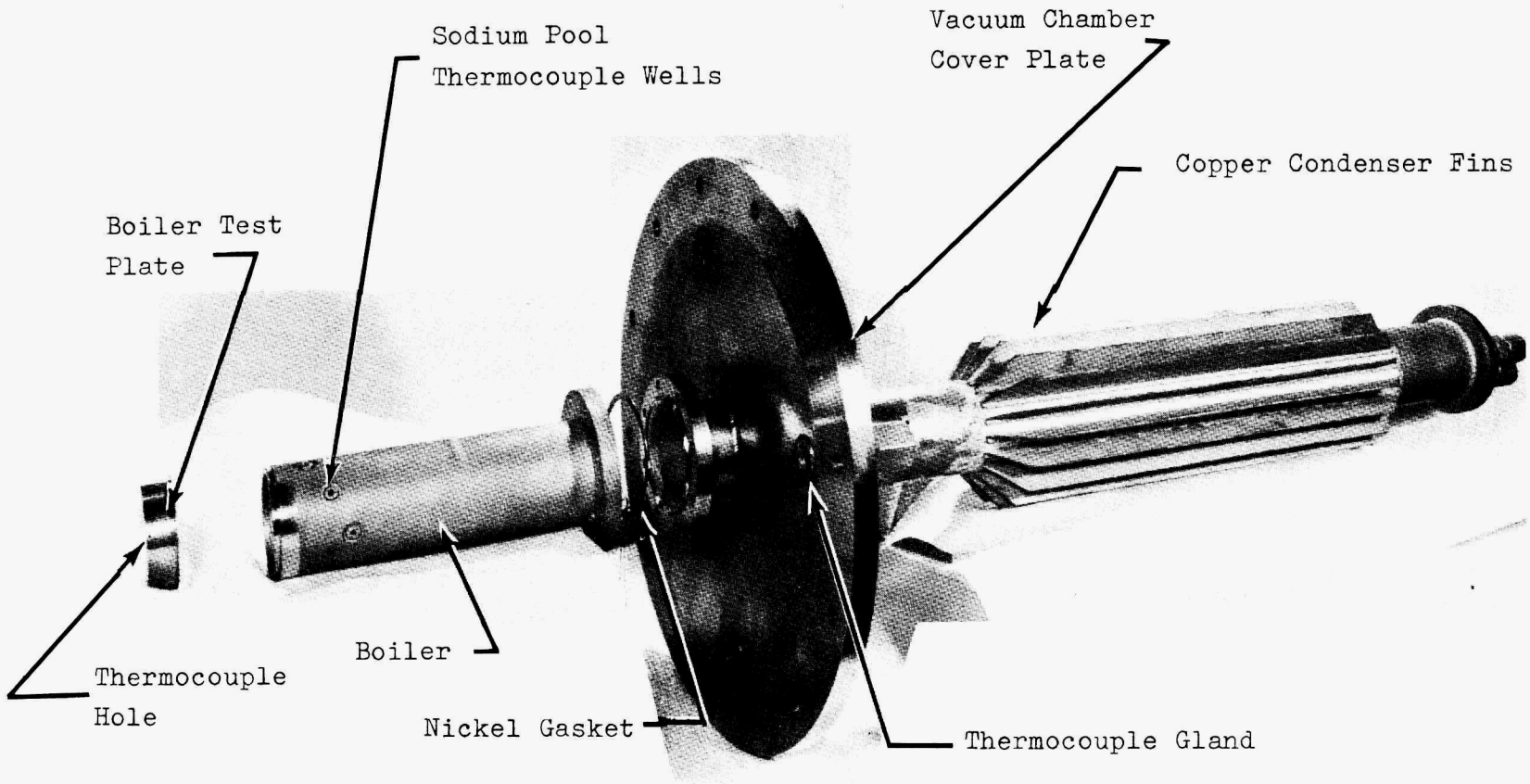

Fig. 7 EXPLODED VIEW OF BOILER-CONDENSER SECTION

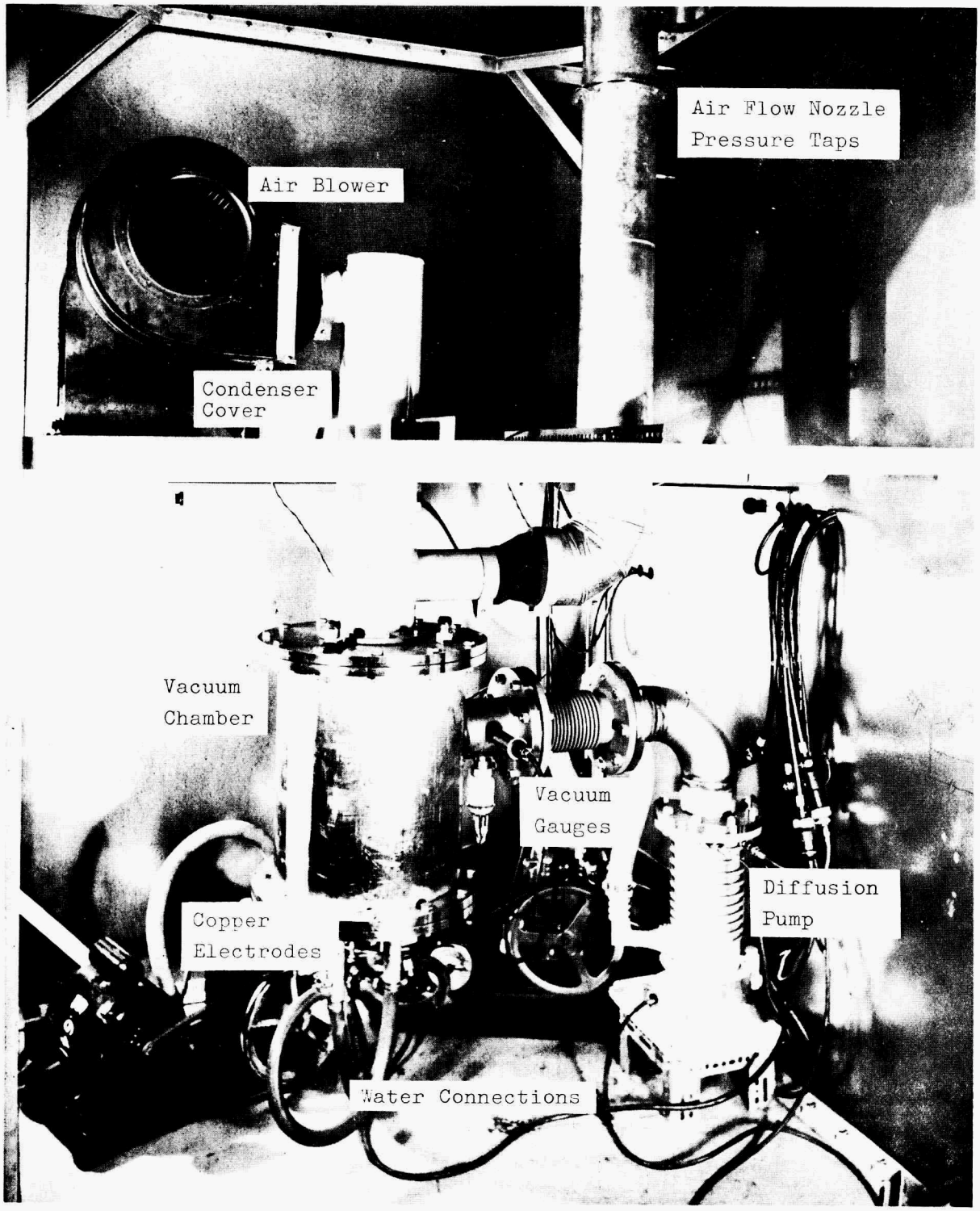

Fig. 8 PARTIAL ASSEMBLY OF POOL BOILING SODIUM SYSTEM

DISCUSSION

MR. BALZHISER: First, you made a statement which intrigued me. The fact you wouldn't expect the type material used in the surface to affect the results, and second, I wonder--our experience with nucleate boiling, I assume by the way you are going to extrapolate and use the thermocouple readings in the plate and get the flux--our experience with nucleate boiling is that the fluctuations are extreme, and might cause a bit of trouble in trying to extract flux from this sort of reading.

MR. ROHSENOW: This is in liquid metal? You have more fluctuations?

MR. BALZHISER: Substantially more.

MR. ROHSENOW: We hadn't been aware of that, with liquid metals.

MR. BALZHISER: We plan to do this same thing with a film-boiling regime. It appears, there, there is greater stability. But when we are inclined to go up and get down in the nucleate regime, we observe rather sizable fluctuations, which poses a problem.

MR. ROHSENOW: You have two questions, there. The one, so far as whether the material surface itself, the kind of material of the heated surface, has any influence. Peter Griffith and John Wallis investigated this kind of a thing with a boiling apparatus very much like the kind we have here; the kind Paul Berenson used. They counted a number of points where boiling took place on the surface. Plotting n/A against the wall temperature, minus saturation, he got three curves, one each for water, methanol and ethanol.

Then they went through $\Delta P = \frac{2\sigma}{r}$ and with this ΔT took every point on the curves for the different fluids each with different properties, and computed r. When they plotted n/A against the computed r, all of these curves fell on a single line. This suggests, then, that this is the minimum cavity size active for a given boiling condition, or a given ΔT; actually this is the integral of a kind of a distribution function which is n/A between D and D plus ΔD, say, plotted against diameter, or cavity radius.

There is a hint, here, pretty strong hint, that cavity size distribution is important.

As to surface temperature fluctuation, this technique of measuring with the thermocouple in the surface is used with non-liquid metals, and if we have trouble with liquid metals, I guess--we will find that out in October, and do something about it.

MR. BERENSON: If I may, I would like to expand on your answer to Dick's question. I think the effect that was shown in the slide, where we tested copper, inconel and nickel, part of it is probably due to a difference in hardness-yielding, different cavity distributions on the surface, even with the same surface-finishing technique; but I suspect--I don't have any proof of this--that part of it is also due to the thermal properties of the surface material, and I think this is--the property that I think of is the thermal diffusivity. Right above the surface you get temperature fluctuations as the bubbles grow in the pores, and these have been measured with surface thermocouples that were developed measuring the temperature fluctuations right at the point where a bubble breaks off. As this surface temperature fluctuates, this must have associated with it a certain heat-transfer resistance as the temperature recovers under the bubble after the bubble leaves; and I would think that this thermal diffusivity for the surface very low diffusivities, for instance with inconel, could begin to contribute to the overall boiling resistance. When I plotted the data as the temperature difference versus thermal diffusivity, the temperature required at a given thermal heat flux increased drastically as you got to inconel, which has a very low thermal diffusivity.

This is just a conjecture. I think there might be a material effect.

MR. ROHSENOW: We have always wondered about this influence. On the other hand, the material effect seems not to be present when we are getting our burnout points except for very thin material. With a thin ribbon, of .001 of an inch, as opposed to 1/16 of an inch, the measured $(q/A)_{crit}$ is lower. But that evidence would say that the properties of the surface itself ought not to play a role, perhaps only the lateral conduction resistance. We don't know the answer to that.

MR. GROSSMAN: Just to be sure the paper is technically accurate, in your introduction you made a couple of errors I think you want corrected. You refer to the STR and HNPF reactors as "breeder reactors". They are not. They are thermal reactors.

MR. ROHSENOW: Experimental thermal reactors.

MR. GROSSMAN: Experimental sodium reactors.

The other one is on SNAP--I hope I don't hurt any feelings here--but the SNAP cycles have not been settled, as such. So if you want to specifically refer to it as SNAP mercury cycles--but there may be Brayton cycles or other cycles in SNAP. This is not heresy, here, but I just wanted to say that.

MR. ROHSENOW: Thank you for those refinements.

MR. CHEN: We have been thinking along the same line and have reached the same general conclusions that you have indicated for the study. We ran into some difficulty that perhaps would give us an insight on it at this time. First, when you mentioned the distribution of cavities, the thought is that with a change in cavity size, you get a different free energy required for nucleation of a bubble, corresponding to that dimension. For this reason I believe we and you are looking into cavity distribution on the surface, and the trouble is we find that most cavities on surfaces are not pits or cones, so much--unless you go to the trouble of putting them in that way. Most of them are grooves and scratches. We have some difficulty in visualizing why in, say, a unit area, with all scratches running pretty much in one direction, how many pits would you have; or how many cavities would you count along the length of a groove. We have difficulty in characterizing the so-called surface cavity distribution.

MR. ROHSENOW: We agree--by the way! That's difficult!

MR. CHEN: Experimentally we also have a 2-inch disk--yours is 2 1/8-inch. When we find that conditions for which we have been working with a very smooth, polished surface, so that there are very few nucleation sites, it is extremely difficult to iliminate the condition where the edge of the test section joins into either your test vessel or skirt, to eliminate

cavities there, which are much larger and more likely to nucleate than the test surface of the mass which you measure.

MR. ROHSENOW: We are expecting some trouble there. We may have to move the joint up higher, away from the heated surface. We may have to put in a little cooling, there, to prevent cavity nucleation at those points. We have this in mind, but we thought we would try it first.

The other question on nucleation: Peter Griffith has made up, some while ago, a boiling slide that we have exhibited around the country in various places. We put it in a lantern and have an electric wire with water right before your eyes, boiling, and put the experiment on the slide.

If you go up to the extreme and have nucleate boiling coming off of a point on the wire, and you put your finger there, pull the electric plug stopping all boiling, then replace the plug, boiling comes back right at that same point.

So as far as whether grooves are really important here, or not, I just don't know. But it is possible that the cavities that we are talking about are in the grooves, within the groove itself. And in that case you wouldn't have much difficulty.

This kind of a study, suggested here, seems to be valid only at low heat fluxes, that is, under conditions of pool boiling. Whether this kind of an analysis is true with liquid metals, is another question, where perhaps the heat fluxes would be a little higher, with a lower ΔT.

This simple analysis doesn't work in forced convection. There is a dynamic effect that Hsu and Graham are espousing. We modified their suggestion in a paper that we presented last month at the National Heat Transfer Conference [Bergles and Rohsenow, ASME Paper No. 63-HT-22].

MR. TEPPER: This might not be germane to the talk, but I was wondering what would your feelings be with regard to the effect of the application of an ultrasonic beam to the wall on the number of nucleation sites, on formation of a large number of smaller bubbles, and on rate of departure of the bubbles from the wall?

MR. ROHSENOW: I guess you would have a more rapid departure by the jiggling. But what seems to happen is that more rapid departure is associated with smaller bubbles. The net effect of ultrasonics is that the frequency increases, but the diameter goes down. The net effect of this seems not to influence the heat transfer very greatly, except at the burn-out condition, the maximum flux. With the smaller bubbles, you would be able to go to higher burn-out heat fluxes, but it doesn't seem to influence the position of the boiling curve very greatly. That hasn't been investigated as thoroughly as it should be.

MR. BALZHISER: The way you have that last picture on the board, I would like to make one comment. It might be interesting to contrast that sort of behavior, which you might expect with water, with what we would expect for liquid metals, where we have extremely high thermal diffusivity. You may actually experience lines on that scale which are essentially horizontal; and when we are well out away from the wall, we have actually measured this.

MR. ROHSENOW: Yes. This is what happens at low heat fluxes with water at very low forced convection, or natural convection pool boiling. The slopes of actual temperature curves are very shallow, being tangent to the $2\sigma/r$ curve at larger cavity sizes which do not exist in the surface. Therefore higher superheats are required to nucleate the smaller available cavities. At the lower heat fluxes (natural convection, or very low forced convection) this theory doesn't hold very well. It simply means that the ΔT's predicted are very much lower than those actually measured. This is probably what happens with liquid metals.

POOL BOILING OF POTASSIUM

BY

Charles F. Bonilla
Mark M. Wiener *
Hans Bilfinger **

Liquid Metals Research Laboratory
Department of Chemical Eng.
Columbia University
New York, N.Y., 10027

Present Addresses:

* Pratt and Whitney Aircraft, East Hartford, Conn.

* * Fa. Lurgi, 6 Frankfurt/M, Germany

This work was sponsored by the Space Electric Power Office of the National Aeronautics and Space Administration through contracts NAS 5-681 and 3-2528 with the Space Power and Propulsion Section, Missile and Space Division, General Electric Co., Cincinnati 15, Ohio.

POOL BOILING OF POTASSIUM

Introduction

The use of liquid metals in space-oriented Rankine cycles necessitates a thorough understanding of flow, quality and gravity effects, as well as the effects of temperature, pressure and heat flux on boiling phenomena. The sparcity of such information makes it difficult to engineer these systems. The urgency in obtaining boiling heat transfer data for liquid metals flowing in tubes and other channels is great, and such experimental investigations have now become an integral part of the overall space program.

Information on pool boiling can be of considerable value in the interpretation and correlation of forced convection boiling. For instance, low vapor quality forced convection boiling heat transfer coefficients would not be expected, normally, to fall below pool boiling coefficients. Thus pool boiling data can serve as a guide as to whether proper boiling is being obtained in a loop, e.g., whether good wetting occurs, whether some unexpected resistance in the heating path or error in the temperature-measuring instrumentation is present, etc. Furthermore, the effect of additives and other changes of operation in loops can be readily obtained, at least qualitatively. In addition, it may well be found feasible and desirable to express forced convection liquid metal boiling by means of pool boiling correlations or results with an additional forced convection term or multiplying factor, similar to the correlation of Clark and Rohsenow[1] for water. This might be particularly true for burn-out heat flux.

Previous Liquid-Metal Pool-Boiling Experimental Work

The first broad boiling study of several metals was published by R.E. Lyon, et al[2] [3] in 1953. The metals studied were mercury, mercury plus 0.10% sodium, mercury plus 0.02% magnesium and a trace of titanium, sodium, sodium-potassium alloy and cadmium. These metals were boiled on a single horizontal type 316 stainless steel tube five inches long. All data were obtained at atmospheric pressure with nitrogen cover gas. Heat fluxes up to 130,000 BTU/hr ft^2 were obtained. Nucleate boiling heat transfer coefficients of nearly 15,000 BTU/hr ft^2 ^{o}F were reported for sodium boiling at 1620°F and sodium-potassium alloy boiling at 1500°F with a temperature difference of less than 10°F. Lyon reported, however, that temperature difference in this region was independent of heat flux. Cadmium and pure mercury experienced only film boiling upon reaching the saturation temperature. This phenomenon was attributed to non-wetting, since when wetting agents were added to mercury, nucleate boiling and high heat transfer coefficients were observed.

Starting in 1952 more extensive data on heat transfer to pool-boiling mercury and mercury with wetting agents were obtained by Bonilla, et al[4]. Mercury was boiled on an electrically-heated horizontal low-carbon steel plate at pressures from 4 mm. of mercury to 45 psia, depths of 2 to 10 centimeters and heat fluxes from 4000 to 200,000 BTU/hr ft^2. These data agreed well with those of Lyon[3] on mercury. Some of the conclusions drawn from this investigation were: (a) Nucleate boiling at a given heat flux requires decreasing temperature differences with increasing pressure for all pool depths, (b) for pure mercury both the addition of wetting agents and a long boiling period tend to increase the heat transfer coefficient, the former having a greater effect than the latter, (c) higher noise levels are generally observed at higher heat fluxes in nucleate boiling, (d) pool boiling mercury - a dense metal, of low kinematic viscosity - mixes well, showing little or no superheat in the liquid.

Lin[5] boiled mercury at lower heat fluxes at pressures from one to eleven atmospheres. Contrary to the results of other investigations, he indicated that as pressure increases the heat transfer coefficient to boiling mercury decreases.

In 1960 Avery and Bonilla[6,7] boiled mercury and mercury with 0.1% sodium near atmospheric pressure and studied the effect of surface roughness. Boiling was accomplished on the same smooth horizontal low-carbon steel plate apparatus previously used[4], and on another similar one. Despite efforts to reproduce surface conditions, the two smooth plates gave considerably different heat transfer coefficients. The authors concluded that boiling coefficients can be improved by deeply scratching the surface, the (fairly critical) optimum spacing of parallel scratches being approximately twice the bubble release diameter given by Jakob & Linke's formula. The use of cover gas does not appreciably affect the heat transfer characteristics of the boiling pool and the effect of surface grooves increases percentage-wise with increasing heat flux over the range covered of up to 100,000 BTU/hr x sq.ft.

Madsen and Bonilla[8,9] boiled sodium-potassium alloy on a horizontal low-carbon nickel plate. Pressures ranged from 2 mm. of mercury to one atmosphere and heat fluxes from 20,000 to 135,000 BTU/hr ft^2. Using a statistical analysis of the data, which exhibited considerable scatter, the authors showed that boiling heat flux was proportional to the 1.24 power of the temperature difference between the boiling surface and the vapor space. For a given heat flux Madsen and Bonilla's data showed a temperature difference roughly five times that determined by Lyon[9]. Unlike Lyon, Madsen and Bonilla found a considerable temperature gradient within the boiling pool, with much superheat at the bottom. This might be explained by the difference in pool geometry, Lyon's larger pool and smaller horizontal tubular element promoting a stronger convection current, which tended to eliminate temperature gradients. Evidently the higher thermal conductivity of alkali metals does not cause greater temperature uniformity in the pool than with mercury, as might have been expected. Instead, the larger Rayleigh number of mercury yields stronger natural circulation, and transport is the dominant process of sensible heat transfer from the heated surface to the liquid-vapor interface, rather than conduction.

Another recent investigation is that of Noyes[10] on pool boiling sodium. The liquid metal was boiled from the surface of a 3/8 inch O.D. horizontal test section. Measurements of surface temperature and heat flux during nucleate boiling were made at pool temperatures from 1200 to 1500°F and at heat fluxes up to 800,000 BTU/hr ft^2. Correlation of nucleate boiling data showed heat transfer coefficients somewhat higher than previous predictions. Heat flux was found to be proportional to the 2.35 power of the temperature difference. Burn-out heat fluxes were determined at low pressures, and correlated and extrapolated to higher pressures, yielding 1.9 x 10^6 BTU/hr sq ft at atmospheric pressure.

Englebrecht and Bonilla[11] have pool-boiled potassium and rubidium in conjunction with a study of condensation of these vapors. Heat fluxes were low, ranging up to 5,000 BTU/hr ft^2, and pressures were in the range of 0.1 to 1 psia. Boiling was at the cylindrical inside walls of large vertical 304 stainless steel tubes, the boiling temperature difference being measured by differential solid-liquid metal thermocouples. Heat transfer coefficients were, surprisingly, found to agree closely with Madsen and Bonilla's empirical lines of q/A vs Δt for NaK, extended downwards.

At present, results are becoming available from Balzhiser et al[12] on their program on the pool boiling of potassium. As they are preliminary, and generally circulated to this group, they will not be discussed at present.

Present Pool-Boiling Program with Potassium

The current General Electric program for NASA under contracts NAS 5-681 and 3-2528 has as its principal objective the evaluation of potassium for Rankine cycles. It has been seen that when this program started there was no information on the boiling of potassium at substantial heat fluxes. Accordingly, for rapid early orientation in the overall program it was decided to carry out any feasible preliminary pool-boiling potassium experiments on equipment already in existence, and to simultaneously undertake the design and construction of a more adequate apparatus for a later extensive study. This paper describes the results of the first study, and the equipment that has been completed for the second one.

Equipment

The equipment available for the first study was basically that employed by Madsen and Bonilla [8,9] with NaK. Figure 1 shows the general arrangement. Boiling was accomplished on a submerged horizontal nickel plate. The boiling chamber, consisting of a 3 in. Sch. 40 type 316 stainless steel pipe, was welded to the heater plate at one end and to a stainless steel block serving as a reflux condenser at the other end. The heat was supplied electrically by means of a molybdenum resistor wire wound around and electrically insulated from molybdenum fins which were brazed into slots milled on the underside of the nickel plate. The heat was removed from the condensing surface by cooling water passing through channels drilled transversely through the condenser block.

The bottom of the pool for this study was made from a high purity-low carbon nickel plate provided by the International Nickel Company. The plate was turned in a lathe to the desired dimensions (Figure 2) and then vacuum-brazed onto the bottom half of the A-nickel heater plate and its attached heater and housing that had been constructed by Madsen and Bonilla[8,9]. The A-nickel was topped with low-carbon nickel because it had been found in the previous study that graphite separation in the A-nickel at some 800°C soon rendered it porous.

Three holes 0.041 inch in diameter were drilled into the low-carbon nickel plate parallel to the heat transfer surface. The holes varied in length, and in depth or distance from the heating surface. The length differences were intentional, for the purpose of observing any variation over the boiling area. The depth variation resulted from the difficulty of controlling the path of the very small drill through the nickel plate, but was not a significant disadvantage.

In order to minimize conduction from the heater plate to the chamber wall, it was decided to make the bottom of the wall relatively thin over a reasonable length, as in the previous pool-boiler[9]. Also, it was desired to avoid a weld or undue thermal stress directly at the outer edge of the boiling surface. Accordingly, the boiling plate was made by turning down a 3/4 inch thick plate, leaving a thin rim at its outer edge, as shown in Figure 2. Unfortunately, a short thickened shoulder remained above the plane of the boiling surface due to an oversight. In addition, a fall-through in the weld of the plate rim to the pipe wall could only be repaired by building up the thin wall thicker at that point. For symmetry the welder then built up the rest of the thin wall. Fortunately the added metal was stainless steel weld rod, of low thermal conductivity. Neither defect was corrected because of the impossibility of turning the whole apparatus in available lathes and fear of damaging the boiler if done otherwise.

Stainless steel sheathed, chromel-alumel Ceramo type thermocouples were used to measure the temperature in the heater plate and in the boiling pool. Three 40 mil thermocouples were placed in the 42 mil holes in the heater plate. The close clearance supported the assumption that the effective positions of the hot junctions could be taken as at the axis of the thermocouple holes. After many hours of operation it was found that the thermocouples could not be removed from the holes. The oxide formation between the sheaths and the holes had obviously cemented the two, further strengthening the assumption as to location of the thermocouples in the holes. The thermocouple used to measure the vapor space temperature was a 1/16 inch stainless steel clad chromel-alumel couple. This thermocouple could be raised or lowered in the well and could thus be used to determine the temperature profile in the pool. All thermocouples, with the exception of two only used in the heat loss runs were calibrated against a standard Pt-Pt 10% Rh thermocouple. The 40 mil heater plate thermocouples were found to agree very well among themselves and with the standard. A correction of only 1°F at 1500°F was found, and since this error is within the accuracy of the standard no correction was applied to these thermocouples.

The Ni-K-Ni differential thermocouple consisted of a nickel wire dipping into the boiling metal and another nickel wire connected to the nickel heater plate. The nickel wires were made of high-purity low-carbon nickel as was the heater plate. However, a slight difference in composition between the wires and the plate resulted in a small emf being generated at their junction. This emf was measured vs. temperature and taken into account when considering the actual emf of the differential thermocouple. The Ni-K-Ni differential thermocouple emf was converted to boiling Δt by available calibration data[13].

For the lead into the boiling metal a ball was made on the end of a nickel wire by striking an electric arc between the end of the wire and a graphite slab under a pool of glycerine. The wire was then threaded through a 1/8 inch I.D. stainless steel tube and pulled tight until the ball was firmly seated, then welded to the end of the tube. It was electrically insulated from the tube by ceramic beads. This tip was placed 3/8 inch above the boiling surface. The other wire was welded to the bottom of a thermocouple well in the heater plate by condenser discharge.

Experimental Procedure

Before assembling the apparatus, the boiling chamber was filled with concentrated hydrochloric acid and allowed to stand for one hour in order to dissolve oxide and welding flux. After the acid was drained the chamber was flushed several times with distilled water and helium leak-tested. The apparatus was not considered ready for charging until a vacuum of less than 1 mm Hg. abs. could be maintained overnight at 1000°F with the vacuum pump turned off.

The heat loss from the heater housing was determined in order to calculate the net flux to the boiling plate by subtraction from the total electrical energy input. This was accomplished by heating the empty apparatus under a high vacuum before charging. At several power inputs the plate temperatures, condenser block temperature, heater resistance, temperature profile along the chamber wall from heater plate to condenser block, and temperature profile along the inside wall of the stovepipe were recorded. Subtracting the loss through the insulation along the chamber wall plus the loss from the condenser block to the atmosphere from the power input gave the net loss from the heater to the room through its thermal insulation. This loss is plotted in Figure 3 against heater resistance, the resistance being a good measure of the average temperature of the winding, and thus of its housing. This figure has been published previously[14]. At the highest temperatures the heat loss amounted to some 25% of the heat input at high heat fluxes. However, it was believed to be known to some 5%, thus was not a substantial source of error.

The first group of data (see later) was taken without argon cover gas. The valve to the manometer system was closed to prevent potassium vapor from entering the system tubing from the boiling chamber. The boiling pressure during these runs was taken as the saturation pressure corresponding to the observed vapor space temperature[15].

After one day of operation without cover gas, it was decided to switch to operation with argon at pressures above atmospheric. In this manner pressure control was much more accurate and rapid. Also, operation might be continued in the event of a slight leak, since the leak would be outward from the chamber or tubing and could possible be sustained or even repaired without contamination of the liquid potassium. Pressure was controlled by setting the argon to the desired boiling pressure. It was noticed that when sizable rates of cooling water were passed through the condenser, the pressure fluctuations normally observed with pool boiling ceased. This was attributed to plugging of the line to the manometers by solidifying potassium in the hole in the block. The plug could be removed by applying a Bunsen flame to the condenser block.

When steady state operation was reached, as evidenced by the lack of drift of the heater plate thermocouples, the following measurements were recorded; plate, differential and vapor space thermocouple emfs, manometer readings and ammeter, voltmeter and wattmeter readings. The raw data are tabulated elsewhere[16,17,18].

Data Reduction

The rate of heat transfer through the horizontal surface was determined by subtracting the heater loss and the conduction loss up the chamber wall from the total power input, which was the wattmeter reading less the I^2R drop in the leads from the wattmeter to the heater. Dividing the results by the horizontal heat transfer area gave the heat flux q/A.

As a first rough method of analysis[17], the heat escaping up the walls of the boiling chamber was taken at 15% of the total, based on an estimated average effectiveness of the walls as uniform infinitely long fins. Recognizing that the walls are not uniform in thickness or material, a second process employed was the construction of a large scale model of the cross section of the wall in Teledeltos paper, simulating the poorer thermal conductivity of the stainless steel weld metal overlay by perforations[19]. The analog was run with a number of different values of constant heat transfer coefficient at its inner surface and the results correlated graphically. Trial and error was of course required in finding the resultant boiling heat flux in order to compute the boiling heat transfer coefficient to be used also on the wall.

Although the results obtained using these two methods of correcting for wall heat loss did not differ widely, it was decided to use yet a third procedure for the final results[18]. This method employed a formula derived for heat lost up the walls which assumes the walls uniform in structure but allows for the variation of h (or q/A) to the boiling potassium with change in Δt along the wall. This method can only be applied to individual points of a succession of the data points at varying heat flux, so that the correction effect of Δt on h or on q/A is available. It also requires trial and error, but only 1 or 2 approximations are required, and it is convenient in application. The derivation follows:

Let $T = t_{wall} - t_{potassium}$, where t_{wall} is assumed uniform in each horizontal plane through the wall and $t_{potassium}$ is assumed uniform throughout the boiling liquid.

Let x = distance up the wall from its base, the wall being assumed, for convenience, infinite in height with the same structure as over its bottom portion (thin nickel and stainless steel). This assumption is permissible because the values of h are high. The heat transfer equation can be presented as follows:

$$q/A = aT^c \qquad (1)$$

where a and c are obtained from a plot on log-log paper of all of the points of the runs. These points were heat loss corrected q/A plotted vs. the net boiling Δt, which was corrected for the Δt lost between the thermocouples and the boiling surface. The chromel-alumel thermocouples were employed to measure temperature, since the Ni/K/Ni differential thermocouples read too high, as if a nickel wire were shorted to stainless steel.

The heat conduction equation for the wall, in terms of the internal diameter D, and kS, the sum of the products of the thermal conductivity k and the cross section S of each material is:

$$\frac{d^2T}{dx^2} = \frac{\pi D h}{kS} T \qquad (2)$$

Replacing h by $q/(AT) = aT^{c-1}$ from equation 1:

$$\frac{d^2T}{dx^2} = \frac{\pi Da}{kS} T^c \qquad (3)$$

The first integration of equation 3, which is all that is needed here,

$$\frac{dT}{dx} = N - \sqrt{\frac{2\pi D a}{k S (c+1)}} \; T^{(c+1)/2} \qquad (4)$$

From the condition that at $x = \infty$, $T = 0$ and $dT/dx = 0$, N must = 0. Equation 4 with N = 0 can readily be verified to give equation 3 by differentiation. Finally:

$$q_o = \left| kS \left(\frac{dT}{dx}\right)_o \right| = \sqrt{\frac{2\pi Da \; k \; S}{c+1}} \; T_o^{(c+1)/2} \qquad (5)$$

FINAL RESULTS

Applying the above method of data reduction, the preliminary and final values shown in Table I result[18]. To calculate these data the thermal conductivity of the high purity nickel was estimated[20,21]. To obtain at an early time the maximum amount of information on the effect of pressure, the initial runs were made either at low pressures or in the 1 to 2 atmospheres range. Additional runs were carried out later, but had to be discarded as less accurate when it was determined that after run D-11 the potassium had penetrated through the nickel plate at a peripheral spot near the welding fall-through and had attacked the braze metal beneath the plate. This was discovered by comparing the run numbers with the thermal resistance from the molybdenum wire to the boiling plate, employing the electrical resistance of the Mo wire to obtain its temperature.

TABLE I

POOL BOILING OF POTASSIUM (ref. 18)

Run No.	Pressure mm Hg.	Saturation Temp. (°F)	Preliminary Values (1st Approximation) q/A BTU/hr ft^2	Preliminary Values (1st Approximation) $t_w - t_{sat}$ (°F)	Final Values (2 Re-iterations) q/A BTU/hr ft^2	Final Values (2 Re-iterations) $t_w - t_{sat}$ (°F)
A-1	2.25	682.6	16,530	31.8	15,500	33.9
A-2	2.67	696.1	38,300	73.6	24,100	77.4
A-3	11.60	821.7	37,100	77.4	18,700	81.3
A-4	2.66	693.1	56,200	81.7	35,500	82.0
A-5	5.40	752.9	55,400	87.4	29,900	94.4
A-6	2.67	697.9	82,300	83.1	63,200	92.9
A-7	993	1452.0	67,700	15.9	78,100	18.9
B-1	771	1391.5	12,930	11.2	12,100	12.0
B-2	772	1391.5	23,200	13.6	21,000	16.3
B-3	771	1391.5	32,850	14.5	32,400	16.0
B-4	775	1392.4	47,200	16.5	46,400	19.0
B-5	768	1390.7	69,700	17.8	71,300	20.0
C-1	1198	1482.5	24,870	13.8	24,100	15.0
C-2	1189	1480.9	35,850	14.9	35,700	16.3
C-3	1198	1492.5	41,100	19.2	34,900	22.4
C-4	1186	1480.2	59,700	17.5	59,800	19.9
C-5	1198	1482.5	71,200	14.9	75,800	17.3
C-6	1198	1482.5	85,500	14.5	95,400	15.8
D-1	1501	1532.6	21,400	12.8	20,900	13.8
D-3	1500	1532.5	39,400	17.7	35,700	20.2
D-4	1503	1532.7	50,500	15.7	50,400	18.7
D-5	1500	1532.5	54,100	16.0	55,900	17.5
D-6	1498	1532.1	71,500	17.0	65,400	18.9
D-7	1498	--	--	--	76,700	17.5
D-8	1498	1532.1	78,900	16.6	83,700	18.1
D-9	1498	1532.1	86,600	18.4	91,500	20.0
D-10	1498	1532.1	98,000	16.4	107,300	17.3
D-11	1498	1532.1	106,800	18.5	115,500	19.7

These points have been plotted in Figure 4.

The first series of runs, series A, was taken without argon cover gas. Most of them were at low pressures, but run A-7 was in the higher pressure range, as well as at a representative heat flux. A-7 is seen in Figure 4 to agree well with the other higher pressure runs, all of which employed argon to control the pressure. Therefore it is concluded that the boiling potassium heat transfer coefficients provided by this apparatus are not affected by the presence or absence of cover gas, and thus would apply in either type of operation on a larger scale, provided that any cover gas is kept sufficiently away from the liquid surface. It is evident that a clear-cut separation of the experimental data into low pressure and high pressure values is obtained, the latter having approximately 5 times as high a heat transfer coefficient at the same heat flux. This is evidently the effect of gross pressure difference, the (much smaller) relative variation among pressures in each group of the data points not showing any substantial trend. h is seen to be approximately proportional to the (log 5/log (1200/5)) = 0.293 power of pressure. This is in excellent agreement with 0.30 found for pure mercury (4), and close to 0.20 found (9) for the binary mixture NaK.

Film boiling is not involved in any of these runs, as bubbling was heard during all of them. In addition, the slopes (8.7 as drawn for the low pressure points) of the lines are typical of nucleate boiling, not film boiling. The high value of the slopes agress with Lyon[2], and is presumably due to the highly uniform roughness of the (polished) nickel plate.

An empirical equation approximately fitting the data, and thus presumably other comparable and intermediate pressures is:

$$\Delta t = 41.5\ (q/A)^{0.115}\ P^{-0.293} \qquad (6)$$

where Δt is in ^{o}F, q/A in BTU/hr x sq.ft. and P in mm. of mercury absolute.

Comparison with Available Correlations

Available theoretical and empirical correlations[22,23,24,25] proposed for liquid metals, or possibly applicable, have been calculated for the representative condition of 1400°F and plotted on Figure 4. It is seen that moderate agreement is reached, but that the correlations spread over the full range of the experimental points, are yet less self-consistent than the experimental points, and have less steep a slope. Evidently further improvement in correlations, including the effect of roughness and metal, is necessary before pool boiling predictions for liquid metals can be made with confidence.

Advanced Apparatus

The advanced type of potassium pool boiler for work at higher pressures, heat fluxes and roughness has been completed and installed, and operation on it is commencing. It is illustrated in Figures 5,6,7 and 8[20].

The bottom assembly of the pool boiling apparatus is illustrated in Figure 5. Power is supplied through tantalum leads held in pressure contact against the molybdenum heater element. A Cb-1Zr alloy cylinder, which is brazed to the molybdenum disc, provides the transition between the molybdenum boiler and the L-605 alloy condenser section. The L-605 alloy bottom shell,

not shown in Figure 5, contains thermal shielding and provides the vacuum or inert environment necessary to protect critical molybdenum and Cb-1Zr alloy components. Instrumentation consists of ten thermocouples, positioned as shown in Figure 7, within the Mo-0.5 Ti alloy boiler plate. The plate thermocouple wells shown as meeting are pairs located at different depths. The other two wells are for Mo-0.5 Ti wires, to use in differential connection with similar wires into the potassium pool. Two L-605 alloy thermocouple wells provide temperature measurement within the potassium pool, including the separate Mo wires.

Using standard metallographic procedures, the Mo-0.5 Ti alloy boiling plate (3-inch diameter x 0.382-inch thick) was polished on one side. The final polishing operation employed 0.25-micron alumina powder abrasive. From interferometer photographs as shown in Figure 9 the initial roughness can be determined.

The heating element was produced in the following sequence. Initially, 99.5% purity alumina was flame sprayed to a 0.045-inch thickness. Slots, 0.120-inch wide, were then ground in the alumina so the remaining alumina was 0.020-inch thick. A 0.030-inch wide alumina spacing was maintained between slots. Near the circumference, these spacings were removed to produce the continuous configuration shown in Figure 5. At this point, the heater was exposed to 2700°F for 1 hour in a vacuum to convert the alumina from metastable gamma phase to the stable alpha phase. Unalloyed molybdenum was then flame sprayed over the entire surface and ground to expose the alumina separators at a molybdenum thickness of 0.020-inch. Visual inspections were made after each processing step to verify the integrity of the sprayed deposits. To determine the uniformity of the molybdenum heating element, resistance measurements were made on each segment. A constant current was introduced at the terminal points and millivolt readings were taken across each straight segment of the element. A high degree of uniformity was obtained, with a total hot resistance of roughly 1 ohm.

Two brazed joints were used to attach the Mo-0.5 Ti alloy boiling plate to the L-605 alloy containment vessel. The initial joint between the Cb-1Zr alloy transition cylinder and the Mo-0.5 Ti plate used AS-514 (V-35 Cb) brazing alloy. Brazing was conducted at 3400°F for 5 minutes. This alloy possesses excellent metallurgical compatibility with both Mo-0.5 Ti and Cb-1Zr alloys. Liquid metal capsule tests had also shown no attack at 1850°F after a 1,000-hour exposure. The second braze employed H-33 alloy (21 Cr - 8 Si - 21 Ni - 3.5 W - 0.4 C - 0.8 B Bal. Co)to form the bimetallic joint between the Cb-1Zr alloy cylinder and the L-605 alloy containment vessel. Brazing was accomplished at 2150°F in two 5-minute cycles. The tongue-in-groove joint configuration is illustrated in Figure 6. Radiographic inspection of both joints revealed no significant defects. Ultrasonic inspection of the AS-514 braze indicated a minor defect in the outside braze fillet. The joint cross section, however, was not affected.

Final assembly of the pool boiler consisted of routine fusion welding of the L-605 alloy and stainless steel components. Radiographic inspection of each liquid metal containment weld revealed no defects. The final configuration is shown in Figure 8. Both the bottom (left) vacuum jacket and the liquid metal containment tube, independently helium leak-tested, were free of defects.

BIBLIOGRAPHY

(1) Clark, J.A. and Rohsenow, W.M., (Trans. ASME 76, 553 (1954)

(2) Lyon, R.E., Ph.D. Thesis, University of Michigan, Ann Arbor (1953)

(3) Lyon, R.E., et al, Chem. Eng. Prog. Symp., 51, 41 (1955)

(4) Bonilla, C.F., et al, Chem. Eng. Prog. Symp., 53, 21 (1957); Report NYO-3148 (April 24, 1952) et seq. under AEC Contract AT(30-1)-1048

(5) Lin, C., et al, JPRS - 3512, JPRS-3531

(6) Avery, G., M.S. Thesis in Chemical Engineering, Columbia University (1960)

(7) Bonilla, C.F., Grady, J.J. and Avery, G, AIChE Paper No. 32, Sixth National Heat Transfer Conference (Boston, 1963)

(8) Madsen, N., Ph.D. Thesis, Columbia University, New York (1960)

(9) Madsen, N., and Bonilla, C.F., Chem. Eng. Prog. Symp., 56, No. 30 (1960) Report NYO-3156 (Nov. 15, 1955)

(10) Noyes, R.C., ASME Journal of Heat Transfer, 85, 125 (1963)

(11) Englebrecht, J.C., M.S. Thesis in Chemical Engineering, Columbia University, New York (1961)

(12) Balzhiser, R.E., Reports to Flight Accessories Laboratory, Wright-Patterson Air Force Base, USAF, under Contract AF 30(616)-8277 (July 1963) et seq.

(13) Kyi, R., M.S. Thesis in Chemical Engineering, Columbia University (1961)

(14) "Alkali Metal Boiling and Condensing Investigations", Qtr. Rept. 4, Ctr. 5-681, SPPS, MSD, General Electric Co., Jan. 20, 1962, Page 67

(15) Bonilla, C.F., Sawhney, D.L. and Makansi, M.M., Trans. Amer. Soc. Metals, 55, No. 3, 877 (1962)

(16) Wiener, M.M., M.S. Thesis in Chemical Engineering, Columbia University (1961)

(17) "Alkali Metal Boiling and Condensing Investigations", Qtr. Rept. 5, Ctr. NAS 5-681, SPPS, MSD, General Electric Co., March 1962

(18) "Alkali Metal Boiling and Condensing Investigations", Qtr. Rept. 1, Ctr. NAS 3-2528, SPPS, MSD, General Electric Co., Sept. 1962

(19) Bonilla, C.F., Ed. "Nuclear Engineering", p. 488, McGraw-Hill Book Co. (1957)

(20) "Alkali Metal Boiling and Condensing Investigations", Qtr. Repts. 2 and 3, Ctr. NAS 3-2528, SPPS, MSD, General Electric Co., April 1963, Page 344

(21) Goldsmith, A. and Waterman, T.E., "Thermo-Physical Properties of Solid Materials", Rept. TR 58-476, Vol. IV, WADC, Jan. 1959, pp 1-4.

(22) Chang, Y.P. and Snyder, N.W., Chem. Eng. Prog. Symp. 30, 56 (1960)

(23) Forster, H.K. and Zuber, N., AIChE Journal, 1, 531 (1955)

(24) Forster, H.K. and Greif, R., ASME Journal of Heat Transfer, 81, 43 (1959)

(25) Levy, S., ASME Journal of Heat Transfer, 81, 37 (1959)

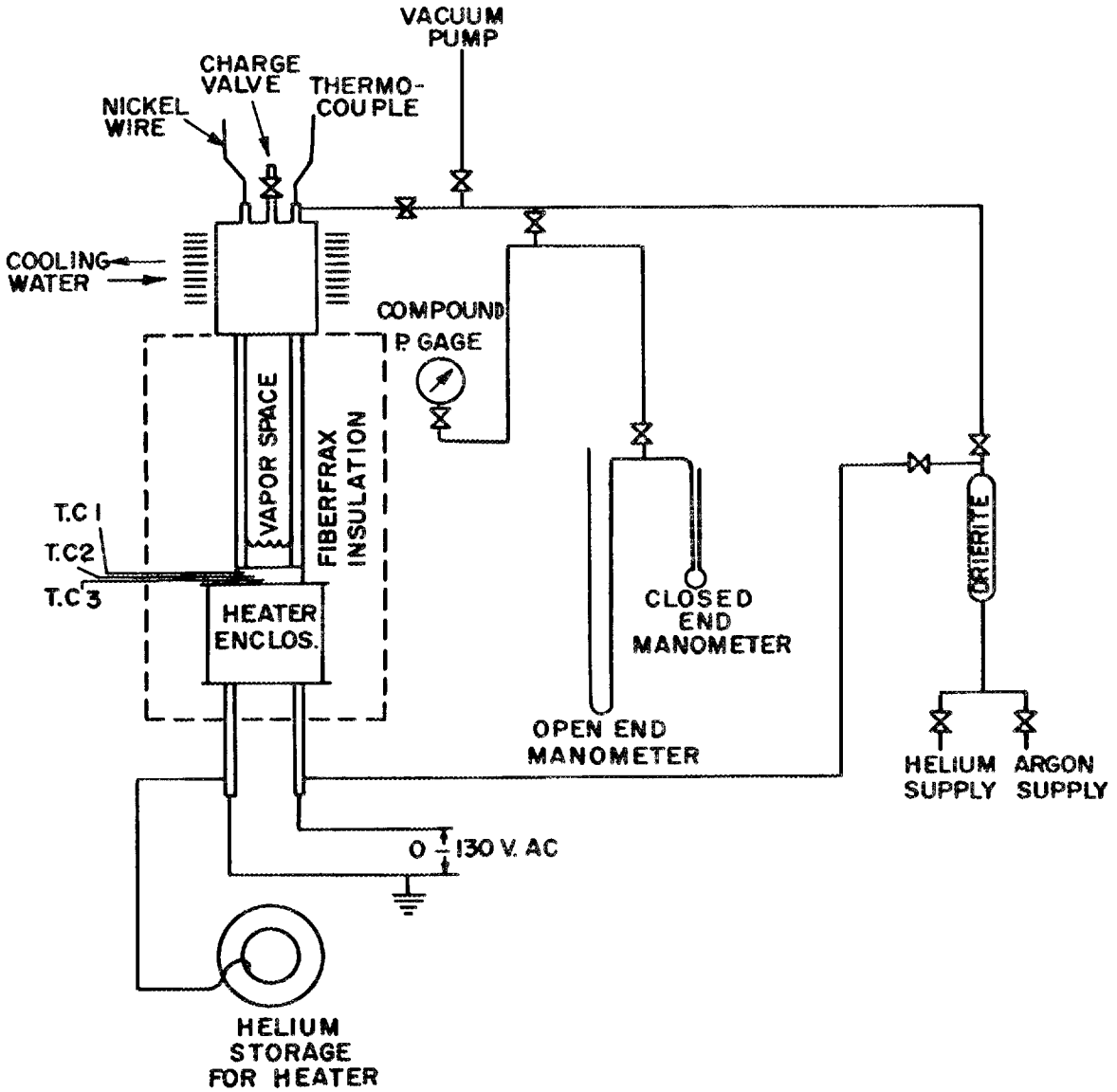

FIGURE I. POOL BOILING APPARATUS

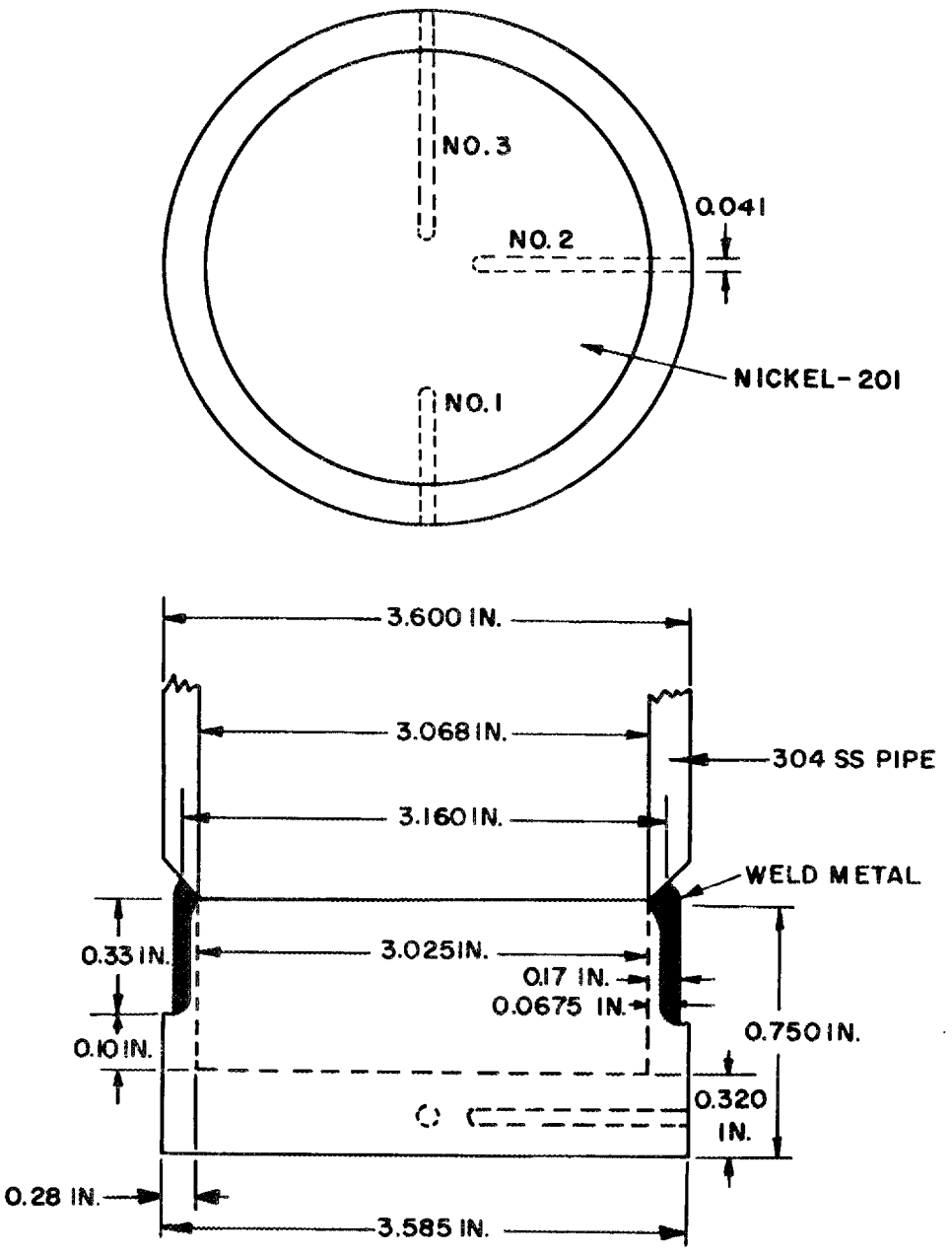

T.C. NO.	TOTAL LENGTH	HOLE CENTER TO SURFACE
1	.850 IN.	0.1715
2	1.215 IN.	0.1500
3	1.745 IN.	0.1655

FIGURE 2. HEATER PLATE

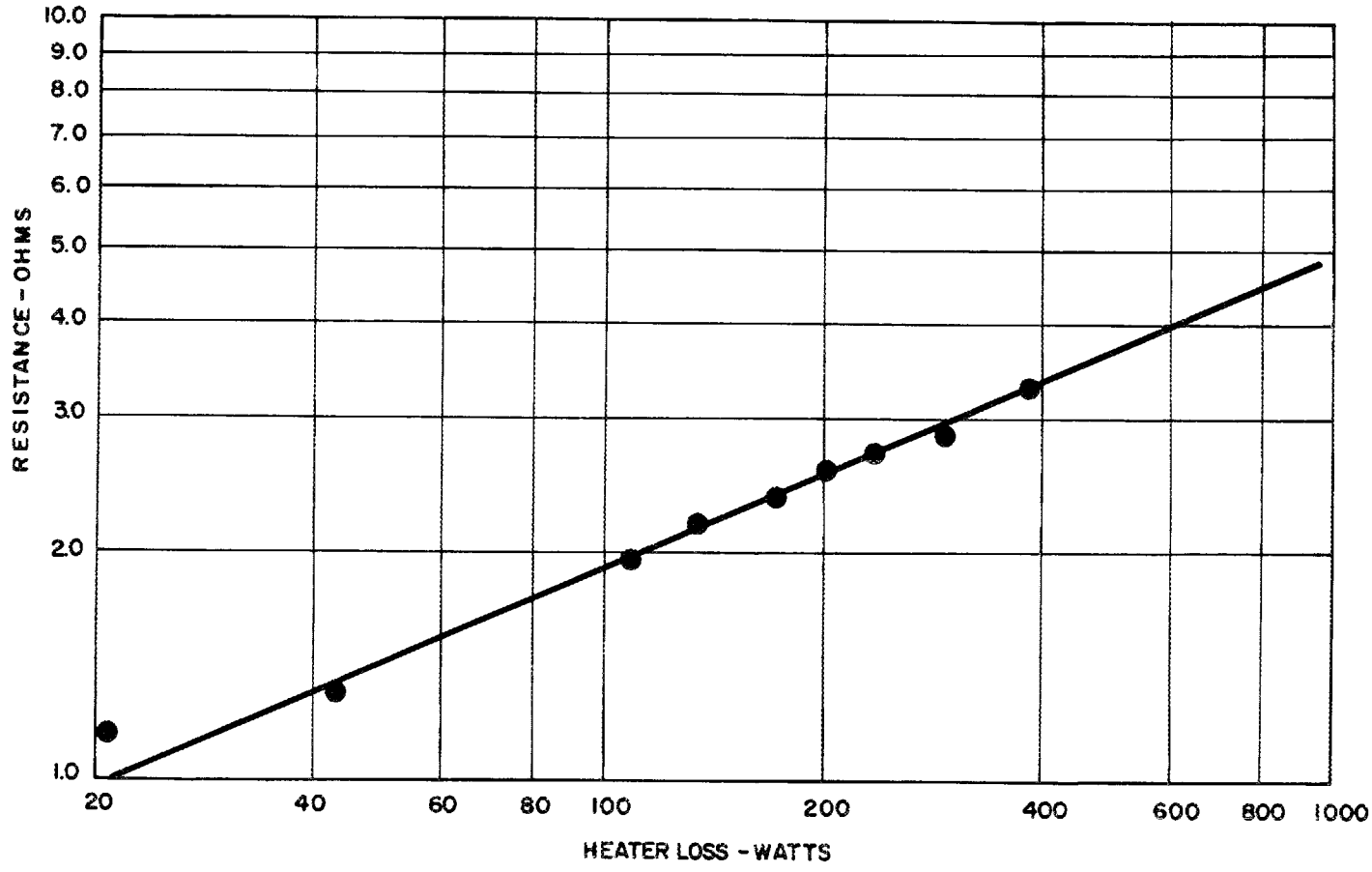

FIGURE 3. HEATER LOSS CALIBRATION

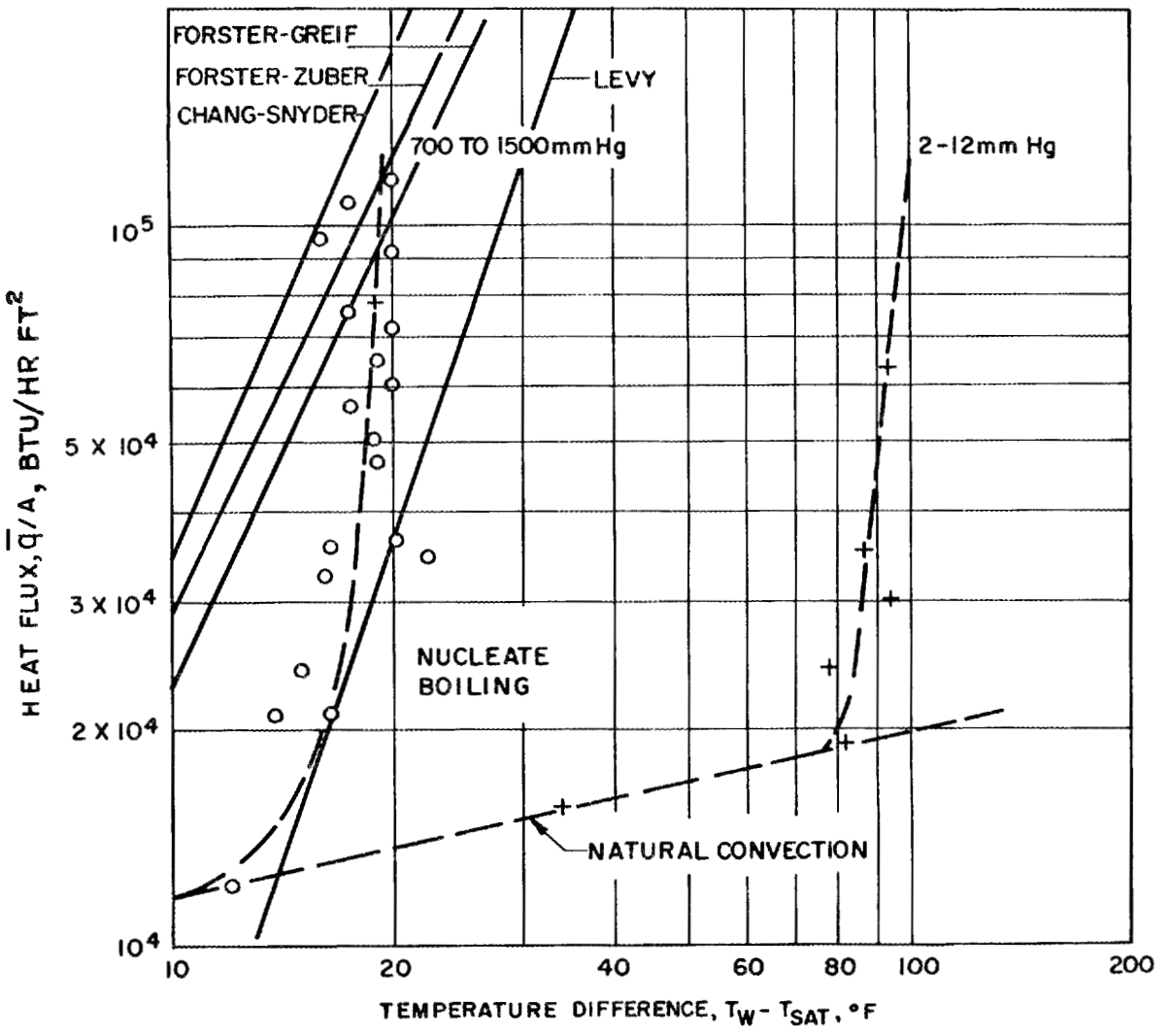

FIGURE 4. POTASSIUM POOL BOILING

L-605 Alloy Containment Vessel

Cb-1Zr Alloy Cylinder Thermocouple Holes

Molybdenum plate

Molybdenum heater

Figure 5. The Pool Boiler Bottom Sub-Assembly.

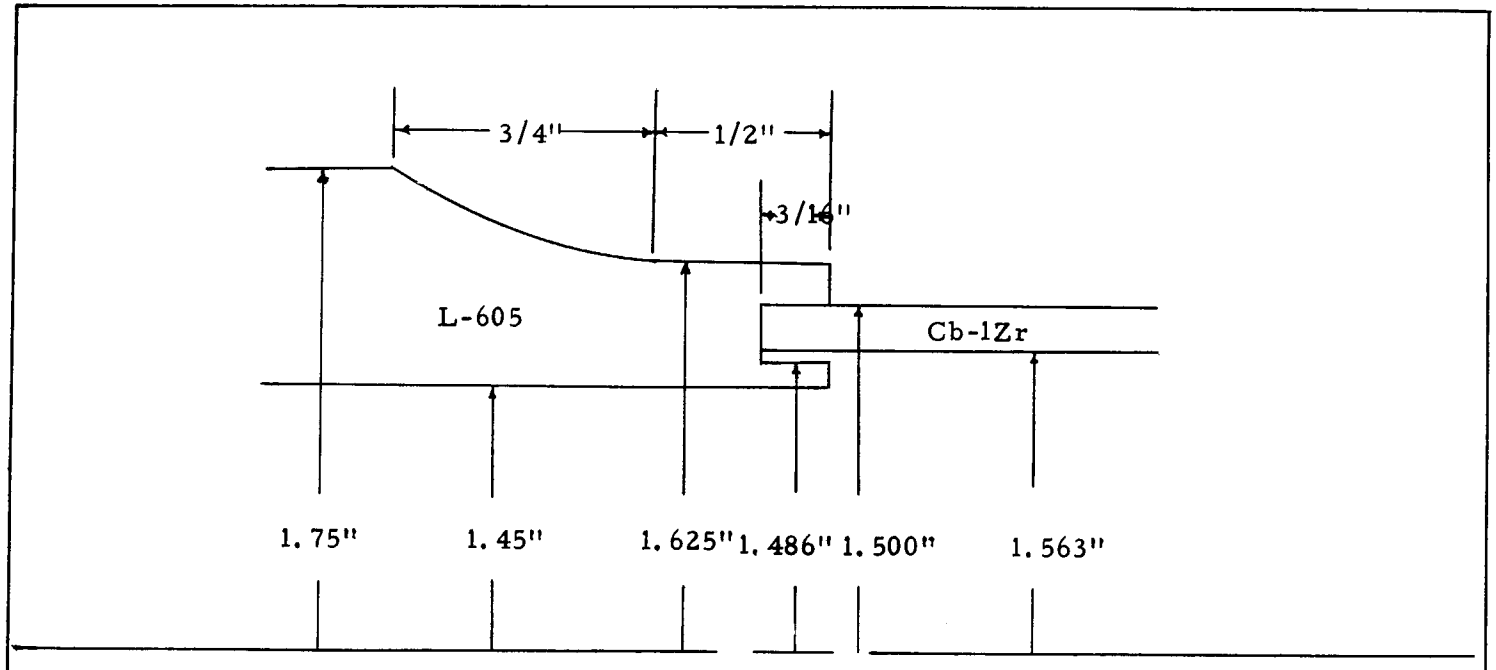

Figure 6. Cb-1Zr to L-605 Alloy Bimetallic Joint Used in Pool Boiler Fabrication.

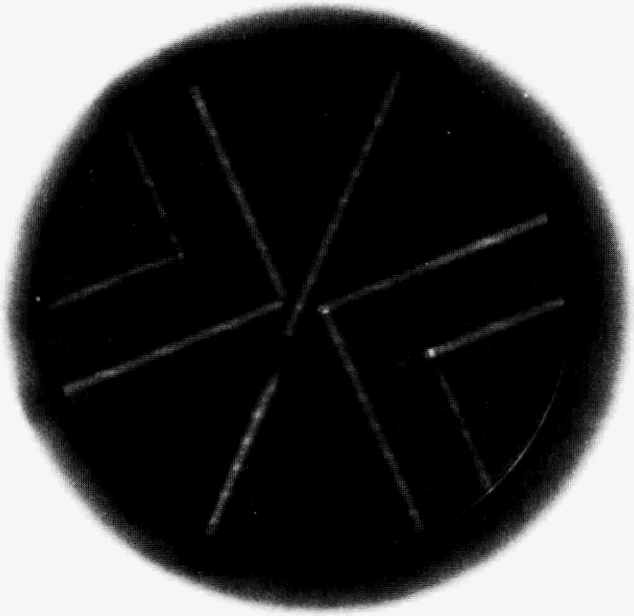

Figure 7. Radiograph of Thermocouple Holes in the Mo-0.5Ti Alloy Pool Boiler Plate. Viewed from the Polished Surface.

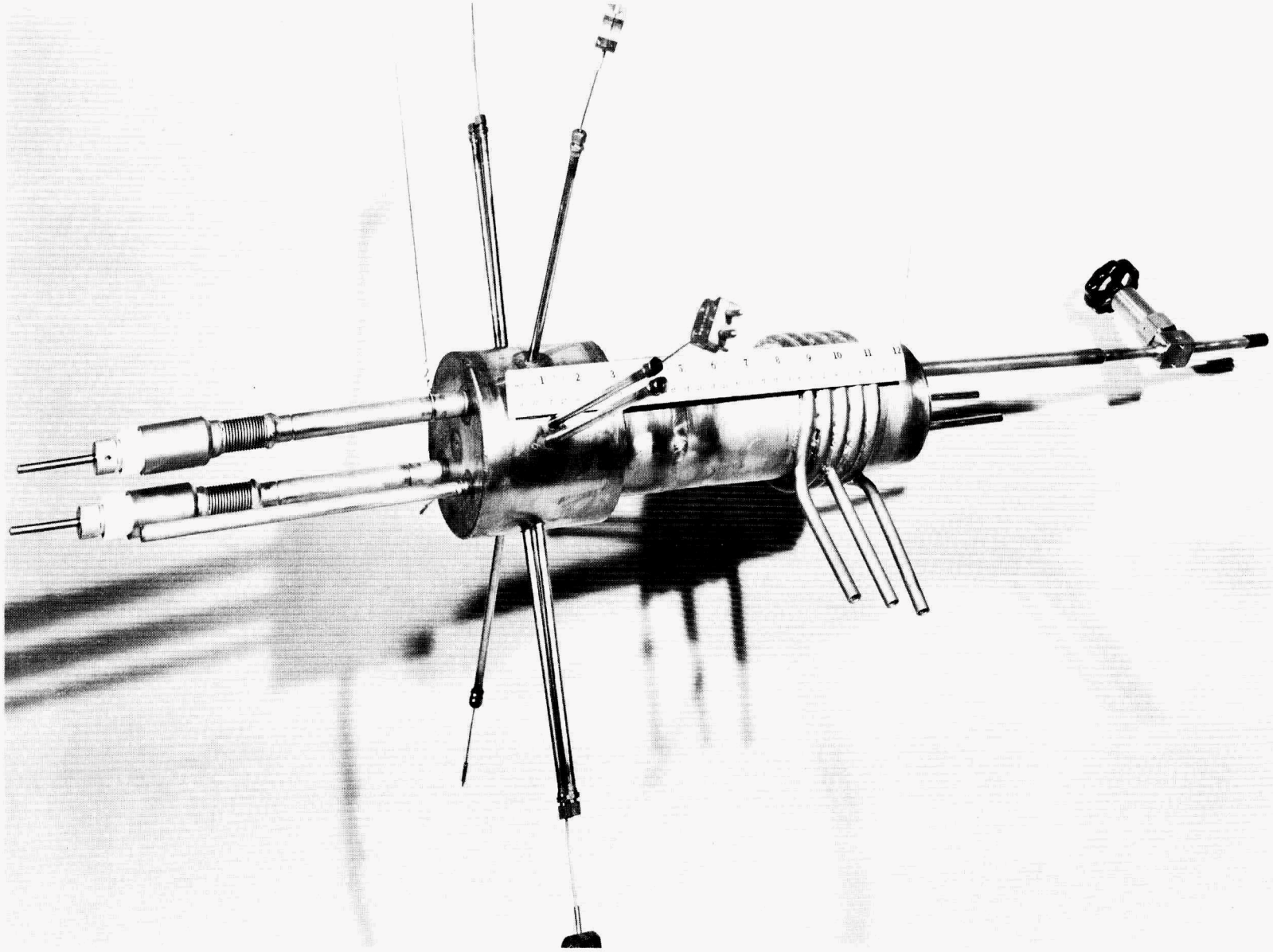

Figure 8. The Pool Boiling Apparatus After Final Assembly.

FIGURE 9. Interferometer Photograph of Mo-0.5 Ti Alloy Boiling Plate 180X Magnification Using 4500 Angstrom Oblique Light Source.

DISCUSSION

MR. HAYS: I was wondering, yesterday and today, about using the liquid metal as one leg of the thermocouple. I notice the traces were about 200 microvolts, full scale. Is there any possibility of some kind of electromagnetic currents occurring when you have the resulting liquid metal here, and the electric heater, and resulting magnetic field that could produce the fluctuation.

MR. BONILLA: I don't believe so. The heater employed 60-cycle AC.

The measurements are fluctuating DC, showing only much lower frequencies. It is possible with a potentiometer and an uninsulated thermocouple even to measure the temperature of the central electrode of a spark plug during firing. So I don't think there will be any interference on the reading itself. Another question would be whether the AC heating affects circulation of the metal, altering the heat transfer. We could do comparative tests with DC heating as a check, but I don't anticipate that there would be any effect.

There is quite a thickness of good electrical conductor, nickel and/or molybdenum, around or between the heater and the pool. But it is one of the things that certainly could readily and will be investigated if it cannot be ruled out by analysis.

MR. GOLDMAN: Perhaps of some concern too, when you have liquid metal flow, is that you could get voltages due to the zeta potential between the liquid metal and the wall; just a flowing fluid will cause the voltage to occur.

MR. BONILLA: The Z-potential? That requires a nonconducting liquid, doesn't it?

MR. GOLDMAN: No. Any liquid in contact with the wall has a Z-Potential; and if you have a flow of the potential along the wall, you create voltages which are measureable.

MR. BONILLA: There is, of course, a Peltier potential between any liquid and solid metal, as well as Thomsen potentials along each if there is a temperature gradient. Their effects could be investigated by putting in baffles of some type to change the current flow, and see if there is any change in the heat transfer performance. I doubt that one would be able to demonstrate anything like that; but of course we will operate with different depths, and with a very shallow pool there might be quite a difference compared to a deep pool. Previous work with NaK and mercury have shown no effect, over a sizable depth range; but that is another good point to investigate.

SUPERHEAT REQUIREMENTS WITH BOILING LIQUID METALS

A. I. Krakoviak
Oak Ridge National Laboratory
Oak Ridge, Tennessee

ABSTRACT

A brief review of boiling for ordinary fluids with emphasis on the wall superheat required for bubble initiation from a heated surface is presented. Calculations based on an equation valid for normal fluids indicate that superheats from two to eight times that for water are required to initiate a vapor bubble in some of the alkali metals. This high superheat and the high thermal conductivity peculiar to liquid metals are combined to explain the unstable liquid-metal boiling phenomenon in natural- and forced-circulation loops.

INTRODUCTION

A brief review of the boiling phenomenon in ordinary fluids (water, alcohol, etc.) with emphasis on the superheat required to initiate a bubble from a surface may be useful in explaining the erratic behavior observed in the natural- and forced-circulation boiling-potassium loops at the Oak Ridge National Laboratory.

The condition for dynamic equilibrium of a spherical vapor bubble in a liquid pool is given by:

$$P_v - P_\ell = \frac{2\sigma}{r} , \qquad (1)$$

which relates the pressure, P_v, of a vapor within a bubble and the pressure in the liquid external to the bubble, P_ℓ, to the surface tension, σ, of the liquid at the liquid-vapor interface and the bubble radius, r. Then for bubble formation, P_v must be greater than P_ℓ; for boiling, the temperature of the liquid must be greater than that corresponding to the saturation temperature of the liquid at pressure, P_v. This excess temperature over the saturation value at P_ℓ is termed the liquid superheat.

If Eq. (1) is combined with the Clausis-Clapyron relation, as was done by Ellion,[1] there results the expression:

$$T_v - T_{sat} \cong \frac{2 R T_{sat}^2 \sigma}{h_{fg} P_\ell r} , \qquad (2)$$

wherein it has been assumed that the specific volume of the liquid can be neglected in comparison with that of the vapor and that the gas law relation, PV = RT, describes the specific volume of the vapor. In Eq. (2), T_v is the absolute temperature of the vapor within the bubble; T_{sat}, the

absolute temperature of the saturated liquid at P_ℓ; R, the gas constant; h_{fg}, the latent heat of vaporization of the liquid. This equation then predicts the approximate liquid superheat required for equilibrium for a bubble of radius, r.

Equation (2) has been tested and found adequate by a number of experimenters. Griffith and Wallis[2] studied nucleation of water, ethanol, and methanol from a copper surface containing conical cavities of 0.0018-in. diameter at the base. With this value for r, the calculated liquid superheat agreed well with the experimental results for the superheat required to maintain ebullition. Berenson[3] obtained similar results in his investigation of the effects of surface roughness on the superheat involved in the boiling of liquid pentane. Farber and Scorah[4] found an additional effect of pressure on the superheat with boiling water.

SUPERHEAT AS APPLIED TO LIQUID METALS[5]

Since Eq. (2) appears to represent the results for water and several organic fluids, it is presumed that the equation may also be applicable with liquid metals. For ease of calculation, the evaluation of the liquid superheats required for boiling with the several liquid metals is made in comparison with water by use of

$$\frac{(T_v - T_{sat})_w}{(T_v - T_{sat})_x} = \frac{(\sigma\, T_v\, V_{fg})_w}{(\sigma\, T_v\, V_{fg})_x} \times \frac{(h_{fg}\, r)_x}{(h_{fg}\, r)_w} , \qquad (3)$$

where the subscripts, w and x, denote water and liquid metal, respectively, and V_{fg} is the specific volume change between liquid and vapor ($\cong V_v$, the vapor volume). Using the physical property values listed in Table 1 and taking 30°F as the superheat required to sustain bubble formation from a

Table 1. Physical Properties of Water and Several Alkali Liquid Metals Evaluated at their Respective Normal Boiling Points

Liquid	Normal Boiling Point, °F	Spec. Vol. Vapor ft^3/lb	Density of Liquid, lb/ft^3	Latent Heat of Vaporization, Btu/lb	Thermal Conductivity, Btu/hr·ft·°F	Surface Tension,[a] lb/ft	Heat Capacity, Btu/lb·°F
Water	212	26.82	59.83	970	0.393	0.00403	1.0
Potassium	1400	32.47	41.58	851	18.1	0.0043	0.187
Sodium	1618	60.6	46.4	1609	30.1	0.0077	0.307
Rubidium	1270	16.67	82.15	347.5	11.8	0.003	0.088
Cesium	1260	10.42	104.7	213.8	10.6	0.002	0.057

[a]Surface tensions at the normal boiling temperature were estimated from data given in the following sources:

H_2O – T. F Young and W D Harkins, p. 1721 in Handbook of Chemistry and Physics, edited by C. D Hodgman, Chemical Rubber Publishing Co., Cleveland, Ohio, 13th ed., 1947.

K – J. W. Cooke, Thermophysical Properties of Liquid Metals, "Space Power Program Semiann. Prog. Rep. June 30, 1963, USAEC Report ORNL-3489, Oak Ridge National Laboratory, to be published.

Na – J. W. Taylor, "Solid Metal-Liquid Metal Interaction Studies, Part 1: The Surface Tension of Sodium," British Atomic Energy Authority Report AERE M/R 1247, September 1953.

Rb, Cs – R. N. Lyon (ed.), Liquid-Metals Handbook, 2nd ed., pp. 40-43, Atomic Energy Commission and Department of the Navy, Washington, D. C., 1952.

particular surface with cavities of radius, r, immersed in water at atmospheric pressure, the superheats required to form vapor bubbles from the same surface immersed in several liquid metals at their normal boiling points are shown in Table 2. Data obtained at ORNL with potassium boiling in natural-[6-7] and forced-circulation loops[6-9] and in reflux capsules[8,10,11] indicate liquid superheats in the range of 70 to 340°F.

Table 2. Estimated Liquid Superheats Required to Sustain Boiling with the Alkali Liquid Metals at 1 Atm Pressure

Fluid	Calculated Superheat Based on 30°F for Water, °F	Measured Superheat, °F	Calculated Superheat Based on 90°F for Water, °F
Na	258	–	774
K	125	342*	375
Rb	101	135*	303
Cs	67	–	201

*E. E. Hoffman, "Metals and Ceramics Division Annual Prog. Rep. 1963," USAEC Report ORNL-3470, Oak Ridge National Laboratory, to be published.

One further factor may be determined in relation to the superheat problem. The boiling sites (cavities) available on a natural surface (such as a pipe wall) will show a normal distribution of sizes. From Eq. (2), it is seen that as the temperature of the surface rises, bubble formation will begin in the cavities of largest radius first. As these sites are used up, the wall temperature will continue to rise and smaller and smaller cavities will be brought into action. Presumably these cavities are not wet by the fluid; i.e., the fluid does not displace trapped or adsorbed gases. On the other hand, liquid metals wet most metals easily. It is to be expected then that the boiling site distribution will be drastically skewed, predominating in very small cavities.

The superheats required to initiate bubble formation with the liquid-metal will thus significantly exceed that required with water. In addition, since the liquid metals used are generally of very high purity and are in contact with clean surfaces in the absence of inert gases, the comparison of Eq. (3) should be made with water under similar conditions. It has been observed that for distilled, deaerated water in contact with a very clean surface the liquid superheat is of the order of 90°F. For the liquid metals, then, the values in the second column of Table 2 should be increased by a factor of 3 as shown in the column on the right.

UNSTABLE BOILING[12]

From the data of Table 1, it can be determined that the thermal diffusivities of the liquid metals grossly exceed that for water; e.g., the diffusivity ratio, K to H_2O, is calculated to be 355. To illustrate the widely different temperature profiles and thus the different boiling behavior between water and liquid metals, imagine an infinitely long 1-in.-OD solid rod surrounded by an infinitely long radiant heater (as shown in Fig. 1). After a sufficient length of time with energy radiating to the rod at a constant rate of, say, 30,000 Btu/hr·ft^2 (maximum heat flux of all but one boiling-potassium loop at ORNL), the temperature profile within the rod will assume the paraboloids of revolution shown in Fig. 1a. Paths a and b represent the temperature gradients in a rod of thermal conductivities equivalent to potassium (18.1 Btu/hr·ft·°F) and water (0.393), respectively. Now if this rod is replaced with a 1-in.-ID tube filled with water under 1 atm of pressure, then when the wall temperature rises to 30°F above saturation temperature (depending on the cavity size of heated surface), tiny "explosions" of liquid into vapor take place at the

wall and grow rapidly in the 0.005-in. superheated annulus depicted in Fig. 1b and either collapse after leaving the wall if the bulk liquid is subcooled or remain stable if the bulk fluid is saturated. In contrast, if the water in this tube were replaced with potassium under 1 atm of pressure, then the wall temperature would rise 375°F above saturation temperature before bubble nucleation at the wall. However, because of the conductivity of potassium, the entire volume of potassium in the tube would be at a superheat of not less than 340°F (Fig. 1c). Now when a bubble nucleats, the energy of superheat from the entire volume is released in a matter of microseconds in a sudden "explosion" of liquid into vapor. The energy of superheat in a unit volume of potassium when released under these conditions produces a vapor quality in excess of 7 wt %, resulting in a momentary high-pressure surge and supplies a large amount of vapor to the condenser, thus increasing the condenser temperatures. This cycle repeats itself at a frequency depending on the heat flux and thermal gradient in the bubble-producing cavity. If the heated surface contains a re-entrant-type cavity with a sufficiently high thermal gradient to maintain a liquid-vapor interface at the cavity mouth, then stable boiling without excessive liquid superheat can be expected. The mechanism pictured is consistent with the pattern of temperature oscillations observed in the low-flux boiler[8,9] during the condition described as "unstable boiling" and in natural-circulation loops.[6,7] A cyclic variation in boiler wall temperature was found in which the temperature first increased slowly (over ~20 sec) to a level of 150 to 250°F above the saturation temperature and then decreased extremely rapidly (~0.1 sec) to the saturation value (in association with equally rapid increases in boiler pressure and condenser temperature). This type of unstable boiling existed only when

liquid entered the boiler subcooled (that is, single-phase flow existed).

STABLE BOILING

In contrast, stable performance (i.e., no oscillations in temperature, pressure, or flow) has been observed in forced-convection boiling-potassium loops when some finite inlet quality condition existed (i.e., two-phase flow was present at boiler entrance). This was generally accomplished by allowing flashing across the flow restriction at the boiler inlet. It is possible that this stability resulted from the presence of the bubbles in the liquid so that the high superheat required for bubble initiation was circumvented. Alternatively, a different mechanism may be operative.

From a map of the forms of flow for air-water mixtures in a vertical tube by Radovcich and Moissis,[13] a graph was constructed for potassium showing the minimum quality requirements for the existence of annular flow as a function of tube diameter and mass flow rate. It is thus estimated from Fig. 2 that annular flow will exist in a 1-in.-ID tube at a quality $\geq 0.4\%$ and a mass flux of 10^5 lb/hr·ft^2. The thickness of the liquid film on the wall of a 1-in. tube under these conditions (assuming zero slip) is calculated to be ~0.040 in. If, as indicated by Eq. (2), 375°F of superheat is necessary for bubble initiation, then by conduction alone a film of this thickness will sustain a thermal flux of the order of 2×10^6 Btu/hr·ft^2 without nucleation. There would also exist a convective contribution,[14] however, this was not considered in this analysis. Thus nucleate boiling is "supressed" in "forced-convection boiling" because the high thermal conductivity of the liquid film and subsequent vaporization at the gas-liquid interface preclude the development of sufficient wall superheat to intitiate bubble formation at the heated surface. Hence, the total heat

transferred in the tests to date can be amply accounted for by this conduction-evaporation mechanism.

Pool boiling tests with potassium at ORNL[6,11] have shown that the wall superheat required for bubble nucleation can be reduced appreciably by the addition of appropriate nucleation sites on the heated surface. Experiments to determine the wall superheat required to activate a pore of a controlled size have been initiated; the capsule designed for this work is shown in Fig. 3. The inside surface of the capsule has been polished to a mirror finish with diamond dust. Thermocouples are located at the bottom of the capsule to meter the axial heat flow from a 1/16-in.-OD calrod heater brazed in the form of a spiral to the bottom of the capsule. Extrapolation of the temperature gradient through the capsule to the liquid-solid interface will provide a measurement of the liquid temperature at the wall and the pressure gage and thermocouples in the vapor space will provide a check on the saturation temperature.

The assumptions and correlations presented here are admittedly oversimplified. It is hoped that the difference between liquid metals and ordinary fluids presented in this paper will elicit more quantitative study of boiling-liquid-metal heat transfer.

REFERENCES

1. M. Ellion, "Study of Mechanism of Boiling Heat Transfer," Jet Propulsion Laboratory Memorandum 20-88, March 1954.

2. P. Griffith and J. D. Wallis, "The Role of Surface Conditions in Nucleate Boiling," Chemical Engineering Symposium Series, Vol. 56, pp. 49–63 (1960).

3. P. Berenson, "Transition Boiling Heat Transfer from a Horizontal Surface," MIT Technical Report No. 17, Heat Transfer Laboratory, Massachusetts Institute of Technology, March 1960.

4. E. A. Farber and R. L. Scorah, "Heat Transfer to Water Boiling under Pressure," Trans. Am. Soc. Mech. Engrs., 70: 369–384 (May 1948).

5. A. I. Krakoviak, "Notes on the Liquid Metal Boiling Phenomenon," USAEC Report ORNL TM-618, Oak Ridge National Laboratory, July 10, 1963 (to be published).

6. E. E. Hoffman, "Metals and Ceramics Division Annual Prog. Rep. 1963," USAEC Report ORNL-3470, Oak Ridge National Laboratory (to be published).

7. E. E. Hoffman and D. H. Jansen, "Space Power Program Semiann. Prog. Rep. June 30, 1962," USAEC Report ORNL-3337, pp. 113–123, Oak Ridge National Laboratory (Classified).

8. A. I. Krakoviak and H. W. Hoffman, "Space Power Program Semiann. Prog. Rept. Dec. 31, 1961," USAEC Report ORNL-3270, pp. 73–79, Oak Ridge National Laboratory (Classified).

9. H. W. Hoffman and A. I. Krakoviak, Forced-Convection Saturation Boiling of Potassium at Near-Atmospheric Pressure, pp. 182–203, "Proceedings of 1962 High-Temperature Liquid-Metal Heat Transfer Technology Meeting," USAEC Report BNL-756, Brookhaven National Laboratory.

10. J. C. Amos and C. H. Gabbard, "Space Power Program Semiann. Prog. Rep. June 30, 1962," USAEC Report ORNL-3337, pp. 60–61, Oak Ridge National Laboratory (Classified).

11. L. W. Evers and A. G. Grindell, "Space Power Program Semiann. Prog. Rep. June 30, 1963," USAEC Report ORNL-3489 (to be published) [Classified].

12. M. E. LaVerne, "Space Power Program Semiann. Prog. Rep. Dec. 31, 1962," USAEC Report ORNL-3420, pp. 113–122 (Classified).

13. N. A. Radovcich and R. Moissis, "The Transition from Two-Phase Bubble Flow to Slug Flow," MIT Report No. 7-7673-22, Department of Mechanical Engineering, Massachusetts Institute of Technology, June 1962.

14. P. A. Nelson, "Heat Transfer to Boiling Metal by Convection," USAEC Report ANL-6507, Argonne National Laboratory, June 1961 (Classified).

UNCLASSIFIED
ORNL-DWG 63-802

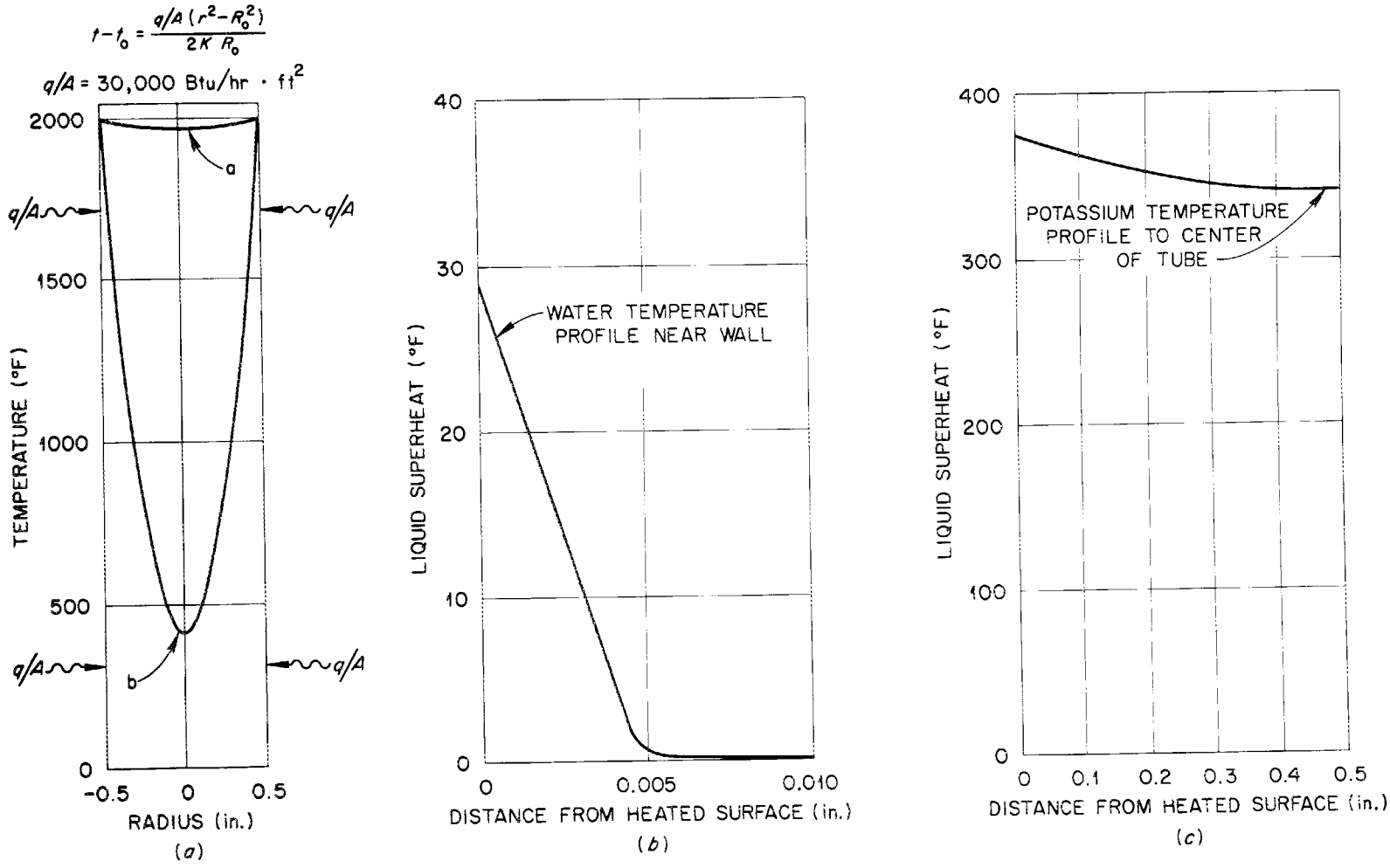

Fig. 1. Comparison of Temperature Profiles Within a Rod.

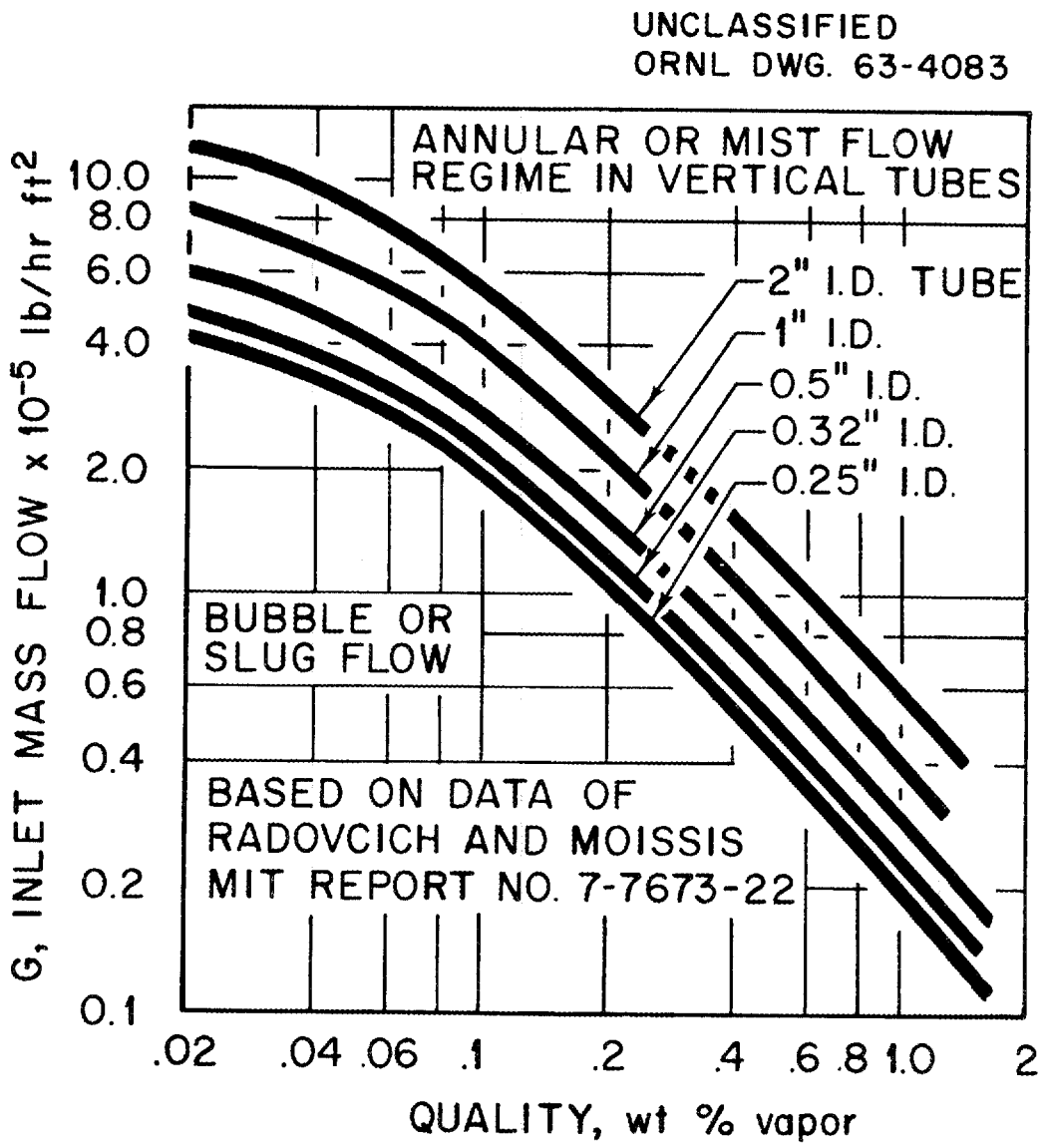

Fig. 2. Calculated Minimum Mass Flows Required for Annular Flow as a Function of Quality and Tube Diameter.

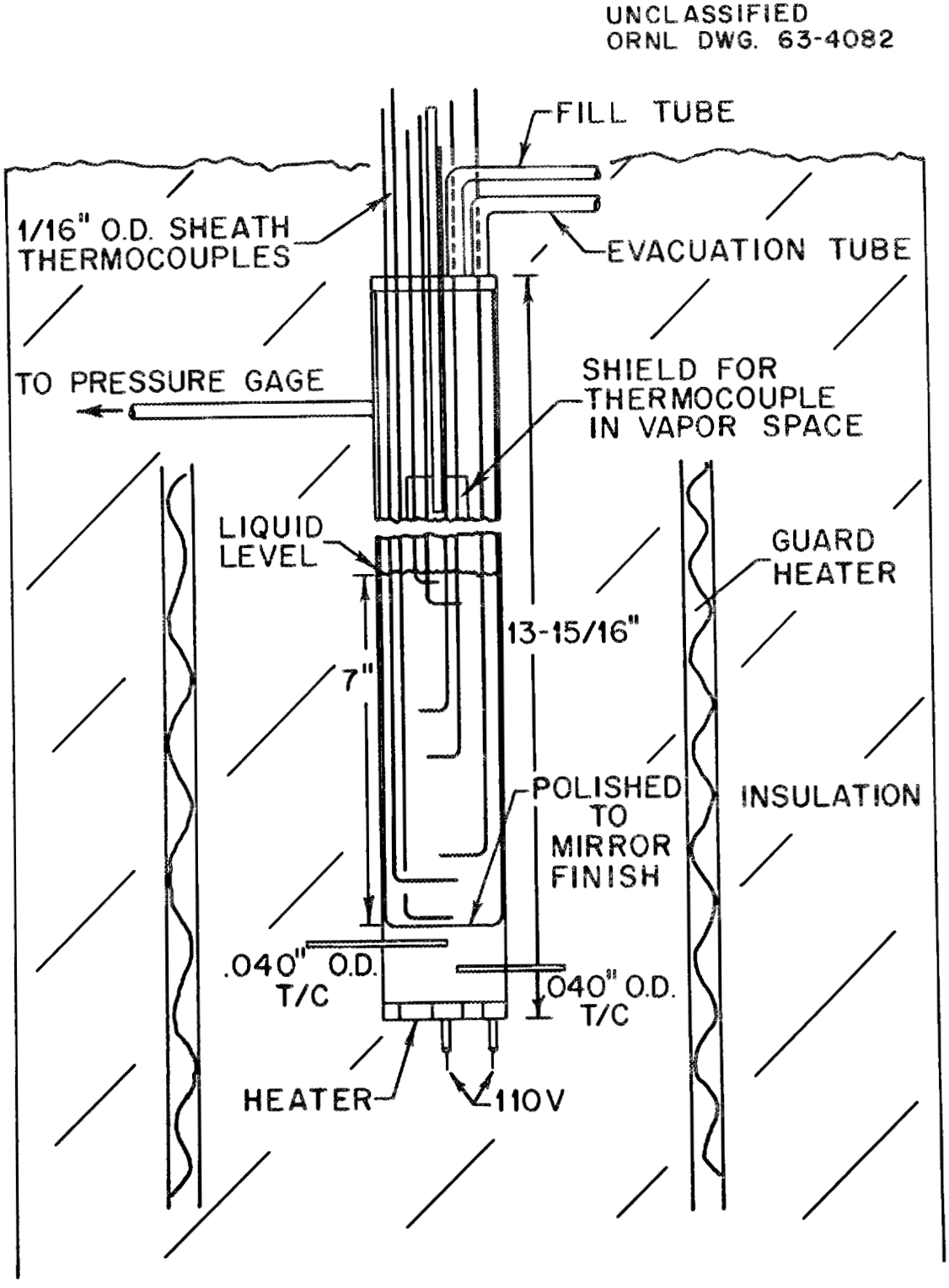

Fig. 3. Superheat Capsule.

DISCUSSION

MR. GOLDMAN: I think you are very much on the right track. I have only one question, relating to your statement that you believe that the surface of the film is sufficient to evaporate all the liquid which is evaporating. I was wondering whether you have any data which shows that such evaporation rates from free surface are possible.

MR. KRAKOVIAK: I wondered about that; however, I don't have any data on this.

MR. GOLDMAN: Let me suggest that until you have found such data, that we don't accept the model.

MR. ROHSENOW: This kind of scares us a little bit. Would you say that with low heat flux boiling, pool boiling, that we ought to have some wide swings? And yet Bonilla had some data, there, at low heat flux. I wonder what he has got to say about the operation of that apparatus? Do you get these wide swings?

MR. BONILLA: We have some pool-boiling data at still lower heat fluxes that I don't recall--I know they never have been published. They were submitted to Thompson-Ramo-Wooldridge, because they were obtained as a part of a condensation sub-contract from the Air Force, in which we condensed potassium and rubidium vapor. Of course we had to produce that vapor; and since we were studying condensation, we did not want to run into any problems on producing the vapor. So we used very low fluxes of about 2,000 to about 5,000. We saw no instabilities; it always boiled beautifully.

It seems to me there are so many possible parameters in pool boiling. For instance, at low fluxes I think you undoubtedly get vaporization from the top, more than any other way. And of course it also depends on the pressure at which it is boiling, since boiling at a low pressure with even a relatively small hydrostatic head, will increase the boiling point greatly.

So unless you have very shallow depth, it would be impossible to boil down from the bottom.

There are an awful lot of angles. It seems to me, though, that my own approach is let's make the boiling better instead of worrying about how bad it can be.

MR. LYON: I would just like to make a qualitative comment on Dr. Goldman's question. I think if one were to look at the evaporation rate, when bumping is occurring, super-evaporation rates, or flux, at the surface, would be quite demonstrable.

MR. GOLDMAN: I agree with you that if the evaporation is a bumping kind of phenomenon, you get tremendous releases of vapor from a surface but this, then, would no longer imply that you have this nice, annular flow. The model you have described here is that you have an annular flow; you have a thin liquid film. I believe that once such a bump occurs, the liquid film gets completely blown off the wall.

MR. LYON: My comment was directed at the idea that the mechanism of evaporation would be the same, whether it is steady-state, as in the case of annular flow, or unsteady-state, in the case of bumping. As long as the heat is being supplied to the surface. Or maybe I misunderstand your point.

MR. GOLDMAN: No. My point is that when you try to evaporate from the free surface at very high heating rates, the free surface doesn't remain a smooth, free surface. As you increase fluxes from a free surface you find that the surface starts wobbling, and some people actually have described them as "schizophrenic" surfaces. But the schizophrenic surfaces occurred at vapor-release rates which are very much lower than the kind of vapor-release rates which you are talking about here.

So I believe you must have a lot of surface available, to evaporate liquid; and in the annular flow (heat flux of 2,000,000, for instance) gives you such a high vaporization rate that you just don't have enough surface there.

MR. KRAKOVIAK: Of course in annular flow, you have quite a few ripples on the surface, resulting from the shear forces of liquid.

MR. LYON: Let me propose a compromise. Suppose what is suggested is only that if there is an interface of some undefined shape, which is close enough to the wall so that the heat can be supplied with the small ΔT available, then the evaporation can occur; the temperature of the wall will not rise out of bounds. This may be a somewhat fluctuating situation, as you suggest. I misunderstood your comment. I thought originally your question was whether you could actually get molecules leaving the surface at this rate, and the answer is, you can. But if your question is whether you have a nice, smooth, annular layer of liquid, I am inclined to agree with you. It is probably quite random in shape, with lumps jumping off; and of course if it is evaporating rapidly, you also have a force against the annulus because of the reaction from the acceleration there.

MR. GOLDMAN: My proposition, of course, is that after the initial bump, all you have left is a whole bunch of droplets, and you have an evaporation of droplets.

MR. LYON: You are proposing an additional mechanism. The droplets come off and continue to evaporate after they get into the stream.

MR. GOLDMAN: Then you have droplets, instead of liquid film at the wall. Maybe you have a few rivulets, but when you really look at the wall, you have droplets rather than a continuous liquid film, at these high heat fluxes.

MR. H. W. HOFFMAN: I only wish to comment, in regard to your mentioning a 2,000,000 Btu/hr·ft^2 heat flux, that this really is not the level of heat flux we have in our systems. The capability of most apparatus we have been working with is in the range 30,000 to maybe 300,000 Btu/hr·ft^2.

MR. ROHSENOW: Lacey and the fellows at Harwell have got a pretty convincing argument that you can have a film along the wall and not have nucleate boiling, if the film is thin enough to have plain conduction in the water and evaporation at the interface (and they have interpreted it this way, certainly) one can conceive some vapor models of this which are pretty convincing. With liquid metals--

MR. DWYER: At what fluxes?

MR. ROHSENOW: I don't have the numbers here, but they are in the higher quality ranges. You have this annular flow model. Some of Silvestri's data can be interpreted in the same way. The same model holds.

If this is possible with water, it is even more possible with liquid metals. Particularly in light of this retarded nucleation, of getting the high super-heats. If the wall can go up with modest super-heats, then with the high conductivity of the liquid alkali metals, a liquid layer could exist right along the wall, and you don't have the fog flow with liquid metals.

MR. E. HOFFMAN: I would like to make a few remarks regarding boiling instabilities which we at ORNL have encountered in the course of conducting potassium corrosion experiments. The instabilities have led to liquid carryover which complicated the determination of corrosion in condenser regions and in some cases to actual container system failure due to thermal fatigue induced by the boiling instabilities. Recently we have conducted a series of capsule experiments to determine means of stabilizing boiling to eliminate the problems cited above.

First I will show two slides which illustrate the problem which we have encountered in our natural-circulation boiling potassium loop experiments. Slide 1 is a top view of 0.8-inch O.D. x 0.1-inch wall x 1.5-inch long insert specimen which was located at the approximate liquid level in the condenser region of a Type 316 stainless steel--potassium loop test. The specimen shown is one of approximately 40 that lined the condenser and subcooled liquid regions of the loop which operated for 3,000 hours at an approximate boiler temperature of 1600°F (871°C). Pressure and temperature fluctuations occurred every one to three minutes during the experiment due to boiling instabilities and the resulting thermal fluctuations led to fatigue of the insert specimen illustrated in the first slide. Two adjacent specimens had similar thermal fatigue cracks.

Slide 2 illustrates the boiling instabilities which have been observed in several natural-circulation boiling potassium loops during startup. The temperature plotted is that measured by a two-color pyrometer sighting on

the loop wall above the condenser. The severity of the thermal shock and the frequency of the unstable boiling is illustrated. As the heat to the boiler was increased, this system very abruptly began to boil stably and continued to boil stably for the remainder of the 2,800 hr experiment.

As a result of the difficulties cited above, a series of capsule experiments were conducted in an attempt to discover a practical method of achieving stable boiling. Analysis of the oscillations in the temperature of the liquid potassium in the boiler in the various experiments suggested that liquid superheat and periodic flashing due to lack of continuous vapor bubble nucleation might be the problem.

For this reason, a test program was initiated to evaluate the effectiveness of various devices in promoting nucleation of vapor bubbles in alkali metals.

The most successful solution to this problem found during these experiments, which included a total of nine tests with both potassium and rubidium, is illustrated in the third slide. The vapor bubble nucleation site or "hot-finger" was located at the bottom of the capsule. The bulk of the heat to the capsule was supplied by the resistance heater which surrounded the entire liquid length of the capsule. A very localized hot region of liquid was obtained in the 0.50-in. diameter x 0.25-in. long potassium well in bottom of the capsule by heating the 0.25-in. diameter rod with a gas flame. The liquid and vapor temperatures were measured by thermocouples located in wells in the condenser and liquid regions. A typical experimental run which illustrates the effectiveness of the "hot finger" as a vapor bubble nucleation site and boiling stabilizer is given in slide 4. The boiling activity inside the capsule during these tests was determined by a contact microphone mechanically linked directly with the capsule. The cyclic behavior of the boiling in the capsule is apparent. When the temperature of the hot-finger reached a value approximately 100°C in excess of the liquid temperature, the potassium began to boiling continuously and the cyclic thermal behavior ceased. On lowering the hot-finger temperature gradually, it was observed that when the ΔT between hot-finger and liquid reached a value of approximately 60°C the potassium

again started to boil in the unstable manner. This pattern could be reproduced over a wide range of liquid temperatures in both the potassium and the rubidium experiments. A final experiment in which more precise temperature measurements were obtained indicated that a temperature differential of approximately 70°C between the hot-finger and the bulk liquid was sufficient to achieve stable boiling initially and that reducing the temperature differential to approximately 55°C caused the onset of unstable boiling.

Following these results, the loop referred to in slide 2 above was re-examined more closely and a favorable vapor bubble nucleation site was found in the boiler where a thermocouple well penetrated the boiler wall. It is postulated that the activation of this site was responsible for the sudden transition from unstable to stable boiling observed while the loop temperature was being increased.

In closing, I would like to suggest that special attention be given to the possibility of accelerated corrosion at favorable nucleation sites in boiling alkali metal systems. It seems quite possible that the violent liquid agitation at these sites might cause preferential dissolution in these regions, even with materials having relatively good corrosion resistance.

Thank you.

MR. DWYER: We will take a few more questions on this other controversial issue.

MR. BALZHISER: I would like to support what Krakoviak has presented here, and also some of the work that Gene Hoffman put forth. We have observed exactly the same thing, particularly at low fluxes - very pronounced temperature rises. We will discuss this work later, but I think it appropriate to mention it at this time. We have three thermocouples located 12:00 o'clock, 3:00 o'clock, and 6:00 o'clock, in the boiling tube. We observe the low fluxes rise just as Gene Hoffman's slides indicate, with the sudden drops. In our apparatus these fluctuations may be overall as much as 150°; these thermocouples are located about 20 mils below the surface. All three respond exactly in phase. It appears as though there

is something triggering this response. When it goes, the entire system is nucleated and all the thermocouples are simultaneously depressed; a bump occurs at the same time.

I might also add--and I am not sure of the flux levels--but as we go up in flux (somewhere above 150,000 Btu/hr·ft^2), the period of the fluctuations has decreased substantially and the amplitude (at least as indicated by our detectors and recorders) appears to have decreased significantly. Incidentally at the lower fluxes, the period appears to be of the order of 15 sec; very distinguishible.

MR. KRAKOVIAK: I would like to add that any liquid-metal system that does not show these temperature fluctuations during nucleate boiling probably has somewhere in that system an appropriately-sized nucleation site resulting from either a faulty weld, a flaw in the material, or some other discontinuity.

I would also question any nucleate boiling data that does not have a contact microphone to detect nucleation and boiling in a capsule.

MR. E. HOFFMAN: I didn't mention this, but when we put the swage thermocouple in the bottom of this hot finger, we got about 70° temperature differential between the end of the finger and the liquid temperature, both on heating and cooling. It appeared very reproducible. It was quite different when we had the thermocouple located below, as you might expect.

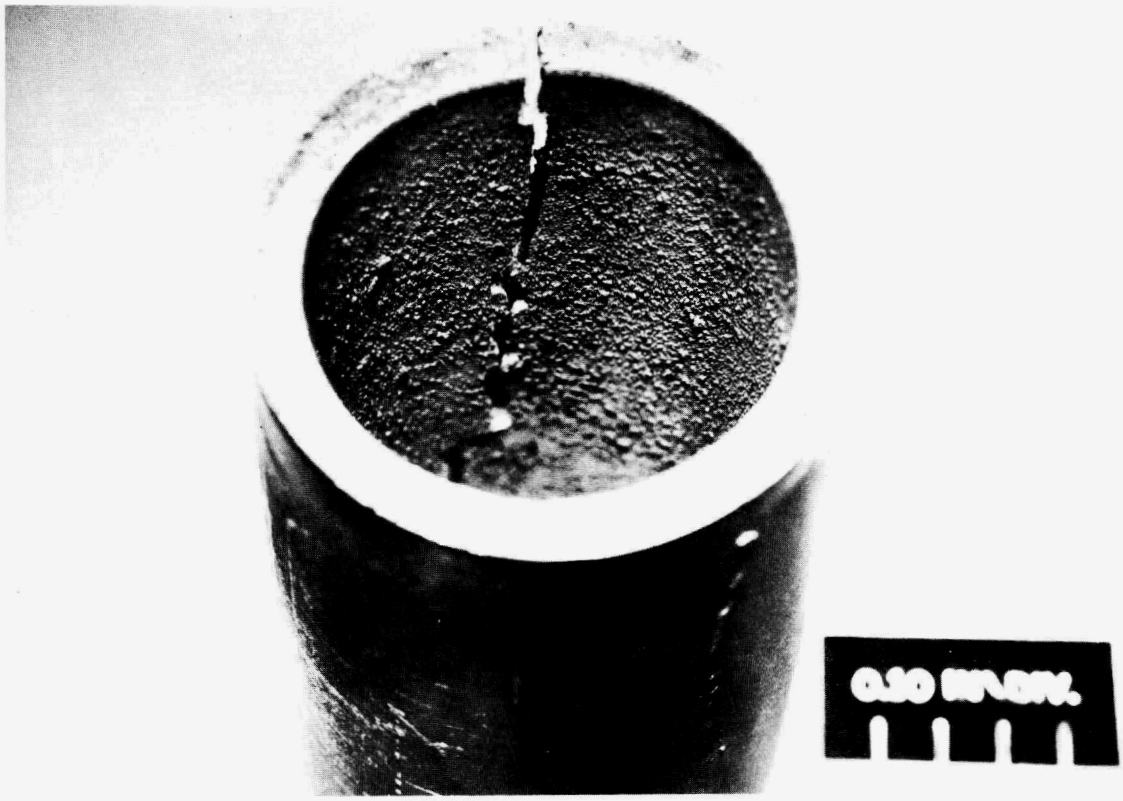

Slide 1 Type 316 stainless steel insert which was located at the approximate liquid level in the condenser. Note the thermal fatigue crack and mass transfer deposition which occurred during the 3,000 hour test.

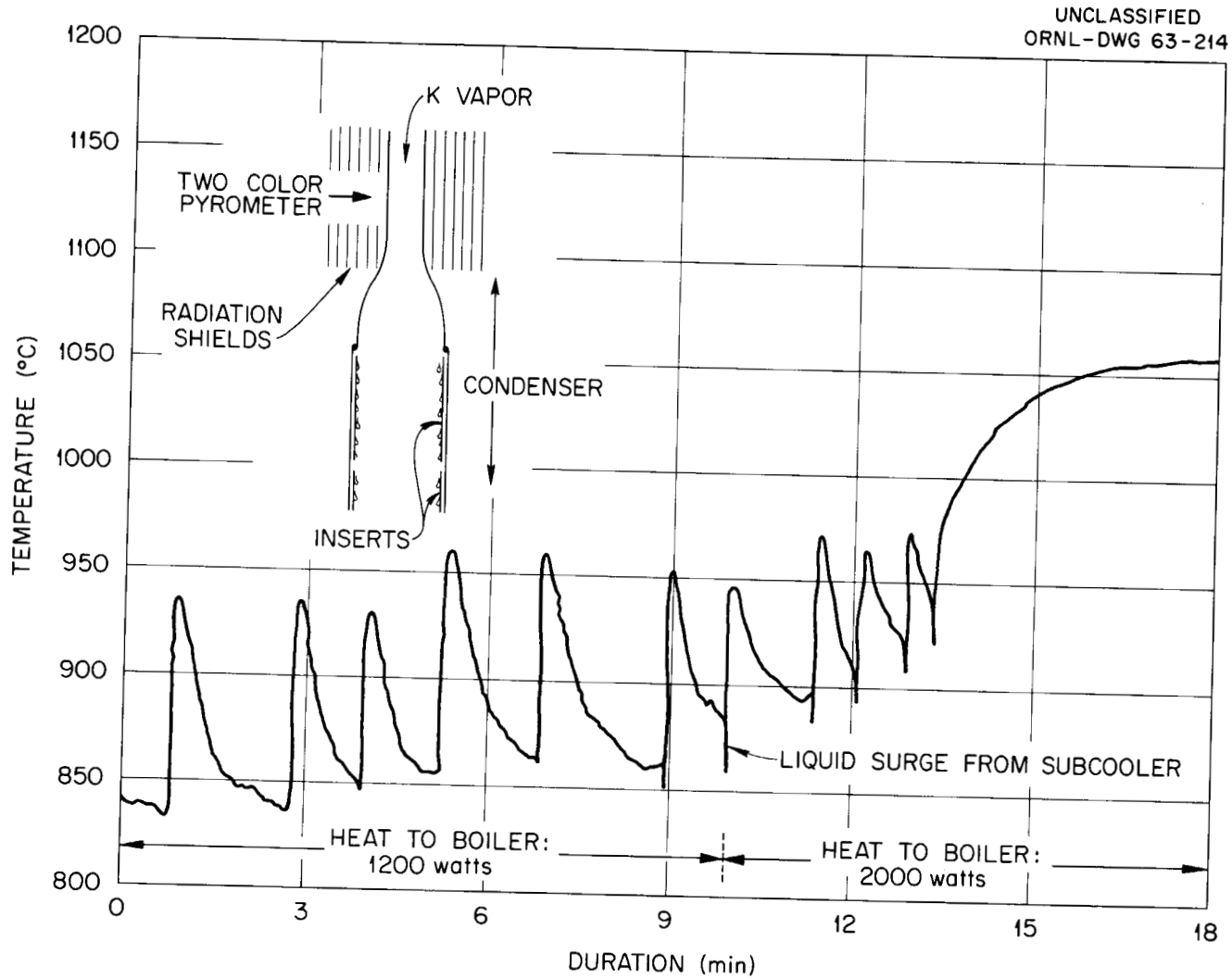

Slide 2 Temperature Profile of Condenser of Natural-Circulation Boiling-Potassium Loop During Start-up.

UNCLASSIFIED
ORNL-LR-DWG 77560

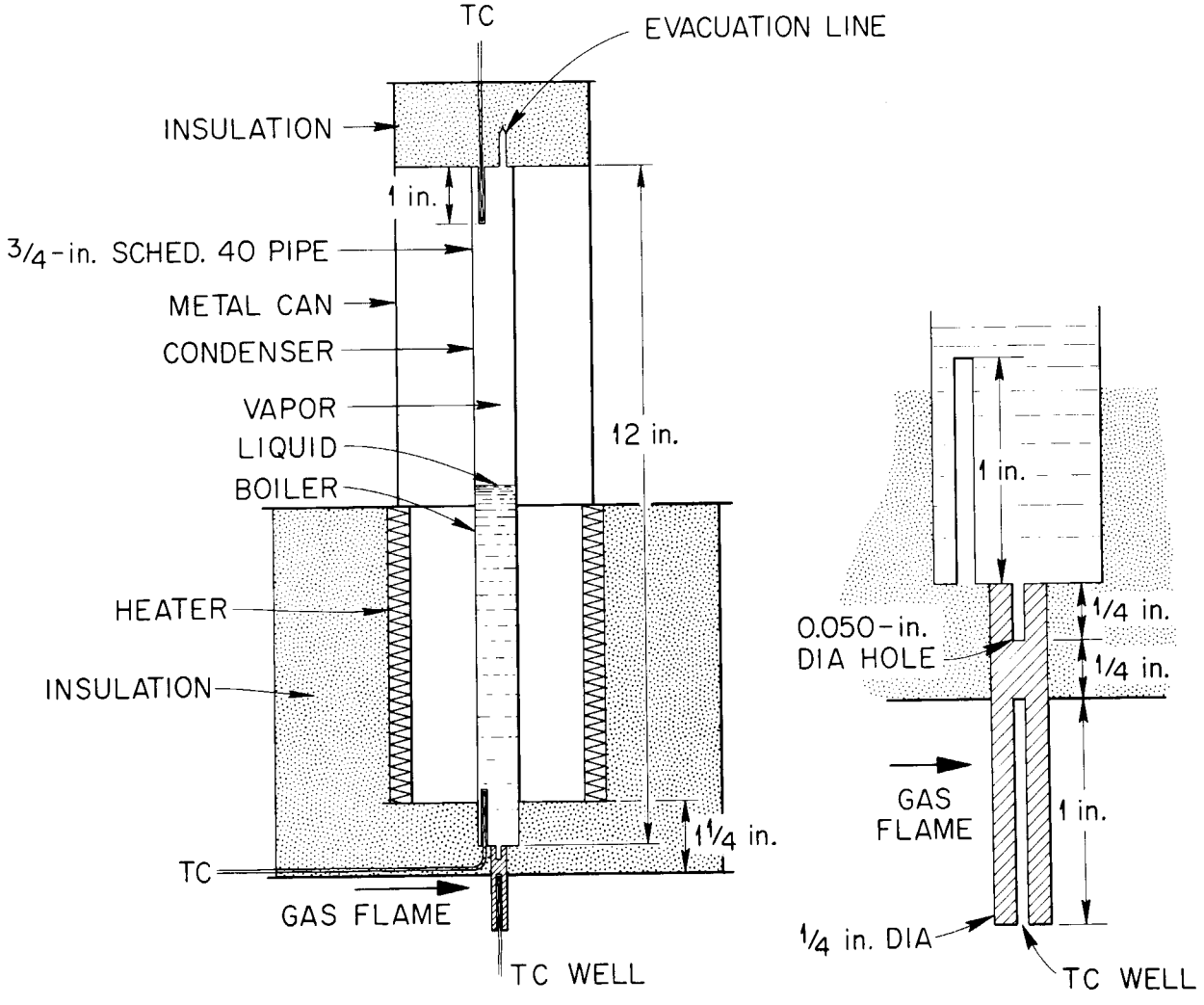

Slide 3 Refluxing Test Capsule.

UNCLASSIFIED
ORNL-DWG 63-408

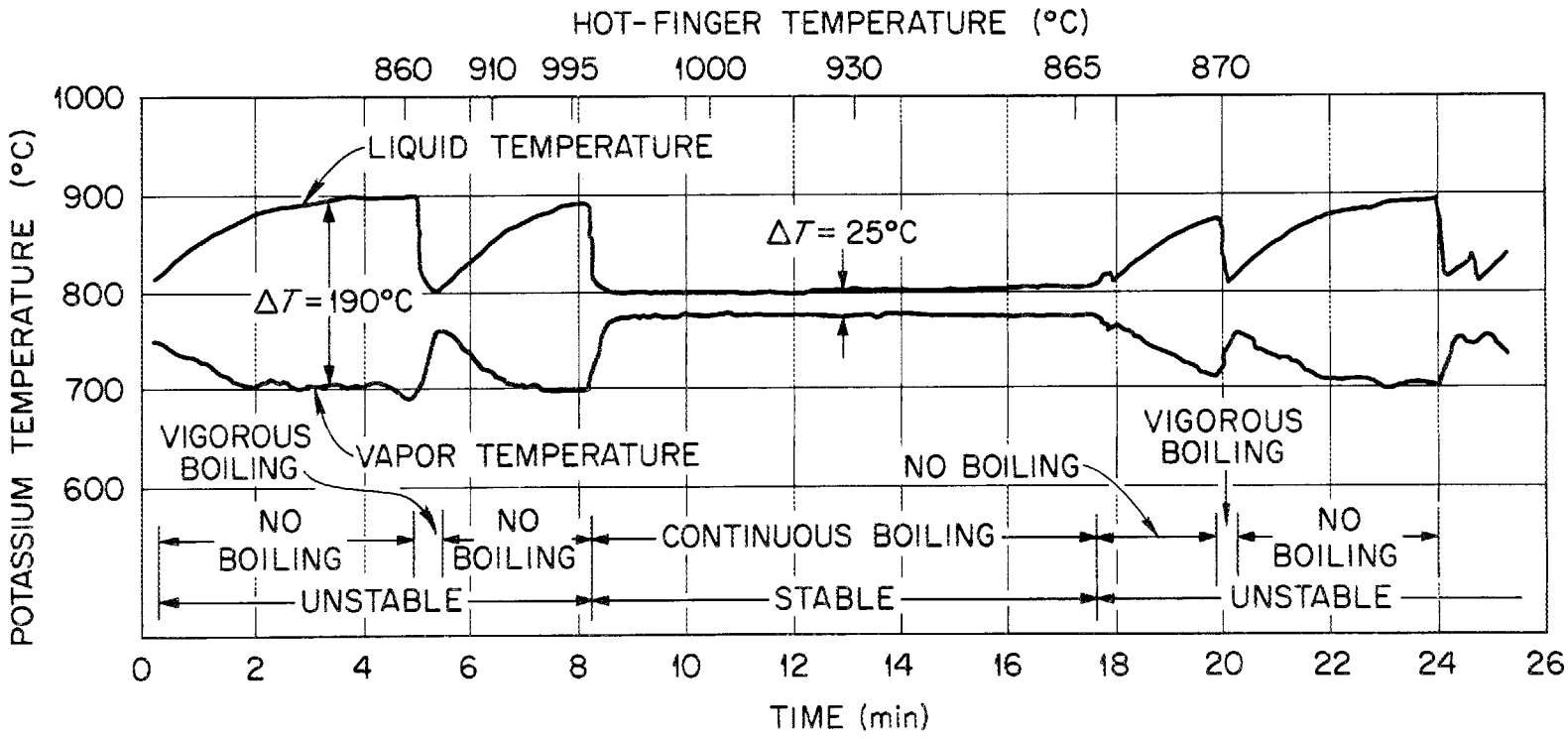

Slide 4 The Effect of Hot-Finger Temperature on the Boiling of Potassium in a Refluxing Capsule.

RECENT EXPERIMENTAL RESULTS IN ORNL STUDIES WITH BOILING POTASSIUM

H. W. Hoffman
Oak Ridge National Laboratory
Oak Ridge, Tennessee

ABSTRACT

Recent results of continued studies into the forced-convection saturation boiling of potassium in a vertical, circular tube are reported. Heat-transfer data, for conditions below the critical heat flux, were explained in terms of an annular flow with surface evaporation. Critical heat flux values continued to agree with a correlation developed for water by Lowdermilk, Lanzo, and Siegel. A consistent pattern was observed for the pressure drop across the boiler; the data, however, include indeterminate losses at the boiler entrance and exit. New boiler sections, designed to provide data on the fluid-temperature distribution, are described. A program to obtain data on the critical heat flux in a multirod geometry as a function of rod spacing is discussed.

INTRODUCTION

The Oak Ridge National Laboratory has continued a significant effort into the study of the heat transfer and flow aspects of boiling potassium. As indicated at the 1962 meeting[1] of this group, our over-all program remains broad in scope. However, our principal studies thus far continue to be restricted to the determination of heat transfer (including the critical heat flux) with potassium at saturated conditions in vertical upward flow through a circular tube and of selected thermophysical properties of the alkali metals. These latter measurements are discussed by Cooke[2] in a separate paper. The next phase of our studies with boiling potassium (hopefully beginning within the next year) will be concerned with either a swirl-flow situation or with flow parallel to the longitudinal axis of a rod bundle (or a simulated unit channel from such a geometry). A decision has not yet been reached as to which of these alternatives will be elected. However, we have initiated a study with water boiling in a multi-rod geometry to study the effect of rod spacing on the magnitude of the critical heat flux and the location of the region of "burnout"; this is discussed in more detail later in this paper.

BOILING-POTASSIUM STUDIES

Experimental studies into the forced-convection saturation boiling of potassium have continued with the accummulation of some additional data on the critical heat flux and on the pressure drop for flow vertically upward within a circular tube. The experimental apparatus used in this investigation is adequately described in the previous proceedings;[1] for reference, a cut-away sketch of the 0.325-in.-ID boiler is shown in Fig. 1.

The results of the most recent experiments are summarized in Table 1. As noted, the data were extended to heat-flux levels of the order of 350,000 Btu/hr·ft^2 with exit qualities in excess of 50%. Attempts at achieving higher heat fluxes and at resolving some uncertainties in the data were hampered by a deterioration of the bond between the stainless steel boiler tube and the surrounding copper blocks and by the failure of a significant number of thermocouples.

Data obtained for conditions below the critical heat flux are given in Fig. 2. It should be noted again that the superheat temperature difference shown is a mean across the boiler assuming a linear variation in the fluid temperature. The trend exhibited by the data remains consistent with that reported previously. However, the dispersion in ΔT at any flux level, which previously seemed to relate systematically to the exit quality, now appears more random; this may result from errors introduced by the breakdown of the thermal bond in the boiler as mentioned above. It has been indicated in the paper by Krakoviak[3] that an annular-flow condition can occur with potassium at very low qualities. Such a situation almost certainly existed in these experiments in that stable loop operation was achieved only when vapor existed at the boiler inlet as the result of flashing across the inlet restriction; it has been estimated that the inlet quality was of the order of 0.5%. This mode of obtaining stability relates, of course, to the question of the superheat required for bubble nucleation in liquid-metal systems as also discussed by Krakoviak. It is to be expected then that the slope of the q/A versus ΔT curve will deviate from that which obtains under strictly nucleate boiling conditions and that the data will show a velocity dependence. As indicated later in this paper, it is planned to continue studies toward a better definition of this effect.

Table 1. Summary of Results on Potassium Boiling in a 0.325-in. ID Vertical Tube

Series A Run No.	$10^{-5} \times$ Inlet Mass Flow ($lb/hr \cdot ft^2$)	Inlet Fluid Temp. (°F)	Exit Fluid Temp. (°F)	Exit Quality (wt % Vapor)	Boiler ΔP (psi)	Heat Flux Q/A (fluid) ($Btu/hr \cdot ft^2$)	Heat Balance $Q_{electric}/Q_{fluid}$	Heat Balance $Q_{thru\ copper}/Q_{fluid}$	ΔT ($T_{w,i} - T_{sat}$)
23	1.42	1424.4	1394.5	19.4	3.9	106,900	1.12	0.86	14.3
24	1.13	1418.9	1392.8	24.3	3.6	107,700	1.03	0.79	12.5
25	1.44	1448.6	1403.0	31.7	5.4	145,700	1.08	0.98	19.6
26	1.23	1442.6	1401.6	37.2	4.8	146,200	1.09	1.07	16.4
27	1.78	1461.1	1382.3	35.4	8.6	197,200	1.12	1.06	39.7
28	1.58	1460.7	1386.5	40.5	7.8	201,600	1.09	1.08	35.8
29	1.84	1466.4	1386.7	36.8	8.9	292,600	1.09	0.98	40.7
30	2.12	1479.0	1397.3	32.2	9.6	290,000	1.10	1.00	41.1
31	1.47	1472.1	1402.0	46.5	7.7	297,400	1.10	1.02	36.4
32	1.15	1465.9	1402.6	58.6	6.7	296,400	1.10	1.02	34.8
33	0.94	1460*	1402*	73.4	6.5	305,000	1.07	–	–
34	–	–	–	–	–	–	–	–	–
35	2.06	1447.4	1415.7	17.1	3.7	174,000	1.00	0.92	–
36	2.06	1481.9	1401.9	34.2	8.3	343,200	1.07	0.98	45.2
37	1.54	1463.7	1393.5	45.5	6.9	349,500	1.04	0.98	39.8
38	1.27	1450.6	1388.0	53.8	6.1	345,100	1.05	0.99	42.2
39	1.20	1462.4	1395.8	57.5	5.0	347,100	1.05	0.98	55.5
40	2.08	1434.1	1405.3	34.2	8.7	346,900	1.07	0.99	43.4
41	1.81	1472.8	1394.4	39.9	7.8	357,000	1.03	0.95	41.1

*Estimated.

Under these circumstances, the critical heat flux values reported relate to a "dry-wall" condition. In the data of Table 1, runs 30 through 33 again constitute a critical heat flux determination following the procedure of decreasing the flow while maintaining a constant heat input. From this latest measurement, "burnout" occurred at $G = 9.37 \times 10^4$ $lb/hr \cdot ft^2$ for a heat flux of 305,000 $Btu/hr \cdot ft^2$ and an exit quality of 73.4%. This result is compared in Fig. 3 with the previously reported values. Again, agreement with predictions based on the Lowdermilk, Lanzo, and Siegel[4] correlation for the forced-convection saturation boiling of water in a vertical tube is good; note that this correlation is dimensional and that the curves shown in Fig. 3 pertain to the specific geometries of this investigation. It was found, however, that for equivalent values of heat flux and mass flow the critical heat flux condition with potassium occurred at somewhat higher exit qualities (~15% increase at atmospheric pressure). In these experiments, "burnout" was evidenced by a sharp rise in wall temperature with an equally sudden reduction in the over-all pressure drop; a wall-temperature increase of 50°F was taken as the power cut-off criterion. With this annular-flow situation, oscillations in wall temperature prior to achieving the critical flux were not observed.

Results obtained for the pressure drop across the boiler are shown in Fig. 4 as the variation of the pressure-loss ratio (total two phase to equivalent liquid-only at the same inlet mass flow) with the Lockhart-Martinelli[5] parameter; a consistent pattern, with the total two-phase pressure drop increasing as the exit quality increased, was observed. In view of this result, it should be kept in mind that the pressure taps were located approximately 2 ft upstream of the boiler entrance and about 1 ft beyond the exit. Thus, the data include undetermined losses associated

with flow through an inlet mixing chamber, around exit-end thermowells, and through an exit expansion. Corresponding data for water, similarly presented but with the exclusion of losses incurred outside the confines of the boiler, fall about a factor of three higher. A better comparison between potassium and water would be in terms of the frictional portion only of the pressure drop; however, information on the slip ratio in a potassium liquid-vapor flow needed to account for the acceleration contribution to the total momentum change is not readily available.

APPARATUS MODIFICATIONS

Interpretation of the results of this study and the development of local heat-transfer information has not been possible due to the lack, primarily, of data on the fluid-temperature distribution. To correct this situation, a new boiler has been fabricated. In most details, this test unit is similar to that used thus far in these experiments. However, the design has been modified to include the direct measurement of tube-surface temperatures at three equally spaced locations along the tube and of the pressure at the midpoint and ends of the boiler section. The Chromel-Alumel thermocouples previously used were replaced with Pt vs Pt-10% Rh couples in the hope of increasing thermocouple life and of providing for in-place annealing and calibration subsequent to boiler fabrication. Unfortunately, this study has been temporarily delayed as the result of extensive damage to the new boiler prior to installation. Salvage and rebuilding of the unit is proceeding, and it is anticipated that experiments will be resumed within six months.

In the interim, the design and construction of an alternate boiler (capable of fluxes of the order of 100,000 Btu/hr·ft^2 at the boiling

surface) has been initiated; operation with this boiler should begin by the first of November. The test section will be constructed from a 0.84-in.-OD, 0.29-in.-ID, type 347 stainless steel tube. Thermocouples (Pt vs Pt–10% Rh) will be inserted radially into shallow wells in the tube wall. In addition, gunbarrel-type thermocouples[9] will be located in the wall at two levels near the boiler exit. With several such couples positioned at various depths within the wall at each measuring station, it is hoped to gain better data on wall-temperature fluctuations near the critical heat-flux condition as well as information on the heat flux and the inside tube surface temperarature. Pressure taps will be located at five positions along the tube. Heat will be supplied radiantly to the boiler from a set of surrounding clamshell heaters. The power input to these heaters will provide an additional measure of the heat flux; losses from these primary heaters will be minimized by a second jacketing set of clamshell heaters.

BOILING IN A MULTIROD GEOMETRY

In a related phase of the ORNL program, a study of the magnitude of the critical heat flux in a multirod geometry has been started. Although considerable attention has been given to this problem in recent years (in particular, reference can be made to the work of Levy et al.[7] and of Becker[8]), there still remain significant areas of uncertainty. It is generally agreed that the burnout heat flux is lower for rod-cluster geometries (with an unheated channel wall) than for single round ducts at the same conditions of quality, mass velocity, and pressure; however, questions still exist as to the location of the "burnout" region on the rods and the influence of rod spacing. It is with this latter question

that this investigation will be initially concerned. In addition to rod spacing, the effects of inlet subcooling and outlet quality on the critical heat flux will be considered at near-atmospheric pressures using deareated, demineralized water as the test fluid. In a later aspect of this study, an apparatus will be constructed to examine boiling with potassium in a seven-rod geometry.

A photograph of the experimental system being assembled is shown in Fig. 5. The outer shells of all major loop components have been fabricated from flanged sections of glass piping to allow visual observation of phenomena occurring during boiling runs; at the same time, easy removal and exchange of individual units will be possible. The boiler will contain a cluster of seven $\frac{1}{2}$-in.-diam Firerods of 10-in. heated length arranged in a triangular pattern with six rods surrounding the central seventh rod. Surface heat fluxes to 160,000 Btu/hr·ft^2 will be possible. Thermocouples embedded in the rods near the surface will provide both information on the surface temperatures and the input signal to a device for protection against actual physical burnout. Boiler clusters with rods at spacings of 1/16, 1/8, and 3/16 in. in channels of 1 3/4-, 2-, and 2 1/4-in. diameter, respectively, are being constructed for the first studies; the corresponding ratios of heated-to-total perimeter are 0.67, 0.64, and 0.61. Dummy-rod sections may be inserted in the channel to simulate the hydrodynamic conditions of an infinite array of rods. The effects of roughness elements attached to the channel wall will also be considered. Operation under both natural- and forced-circulation conditions will be possible.

FUTURE STUDIES

A program has been initiated to examine methods for circumventing the problems created by the high superheat requirement with boiling potassium . Since these studies have just barely started, and at the moment are still restricted to the development of techniques of surface preparation, further discussion will be postponed to a later meeting. When available, a short section of a treated tube will be located in the inlet region of the boiler.

As indicated earlier in this paper, it is planned to extend the boiling potassium studies to other geometries during the coming year. Two possible situations, both of much interest, are being considered: (1) boiling with the fluid in swirl flow through a circular tube or (2) boiling within a simulated unit channel of a multirod arrangement. Both geometries present some problems in construction and instrumentation, and it has not yet been decided as to which course will be pursued.

Finally, manpower permitting, it is hoped to initiate experimental studies into regime transitions for a flow in a rod bundle geometry. Water-air in transparent channels will be used in early phases of these experiments; the use of a capacitance-type probe, previously tested with some success, will be essayed.[9] It is hoped to modify this probe eventually to be of use in similar experiments in a potassium liquid-vapor system.

REFERENCES

1. H. W Hoffman and A. I. Krakoviak, "Forced-Convection Saturation Boiling of Potassium at Near-Atomospheric Pressure," pp. 182–203, Proceedings of 1962 High-Temperature Liquid-Metal Heat Transfer Technology Conference, USAEC Report BNL-756, Brookhaven National Laboratory.

2. J. W. Cooke, "Thermophysical Property Measurements of Alkali Liquid Metals," paper to be presented at the Third Annual Conference on High-Temperature Liquid-Metal Heat-Transfer Technology to be held at Oak Ridge National Laboratory on Sept. 4-6, 1963.

3. A. I. Krakoviak, "Superheat Requirements with Boiling Liquid Metals," paper to be presented at the Third Annual Conference on High-Temperature Liquid-Metal Heat-Transfer Technology to be held at Oak Ridge National Laboratory on Sept. 4-6, 1963.

4. W. H. Lowdermilk, C. D. Lanzo, and B. L. Siegel, "Investigation of Boiling Burnout and Flow Stability for Water Flowing in Tubes," Nat. Adv. Comm. Aero. Technical Note 4382, September 1958.

5. R. W. Lockhart and R. C. Martinelli, "Proposed Correlation of Data for Isothermal Two-Phase, Two-Component Flow in Pipes," Chem. Eng. Prog., 45: 39–48 (1949).

6. J. J. Keyes, Jr., and J. E. Mott, "An Investigation of Thermal Transient Decay at a Fluid-Solid Interface and in Turbulent Flow Through Circular Ducts," USAEC Report ORNL-2603, Oak Ridge National Laboratory, Dec. 2, 1958.

7. S. Levy, E. E. Polomik, C. L. Swan, and A. W. McKinney, "Eccentric Rod Burnout at 1000 $lb_f/in.^2$ with net steam generation," Int. J. Heat-Mass Transfer, 5: 595–614 (July 1962).

8. K. M. Becker, "Burnout Conditions for Flow of Boiling Water in Vertical Rod Clusters," A.I.Ch.E. Journal, 9: 216–222 (March 1963).

9. J. J. Keyes, Jr., "Two-Phase Hydrodynamic Studies," pp. 168–170, Space Power Program Semiann. Prog. Rep. Dec. 31, 1962, USAEC Report ORNL-3420, Oak Ridge National Laboratory.

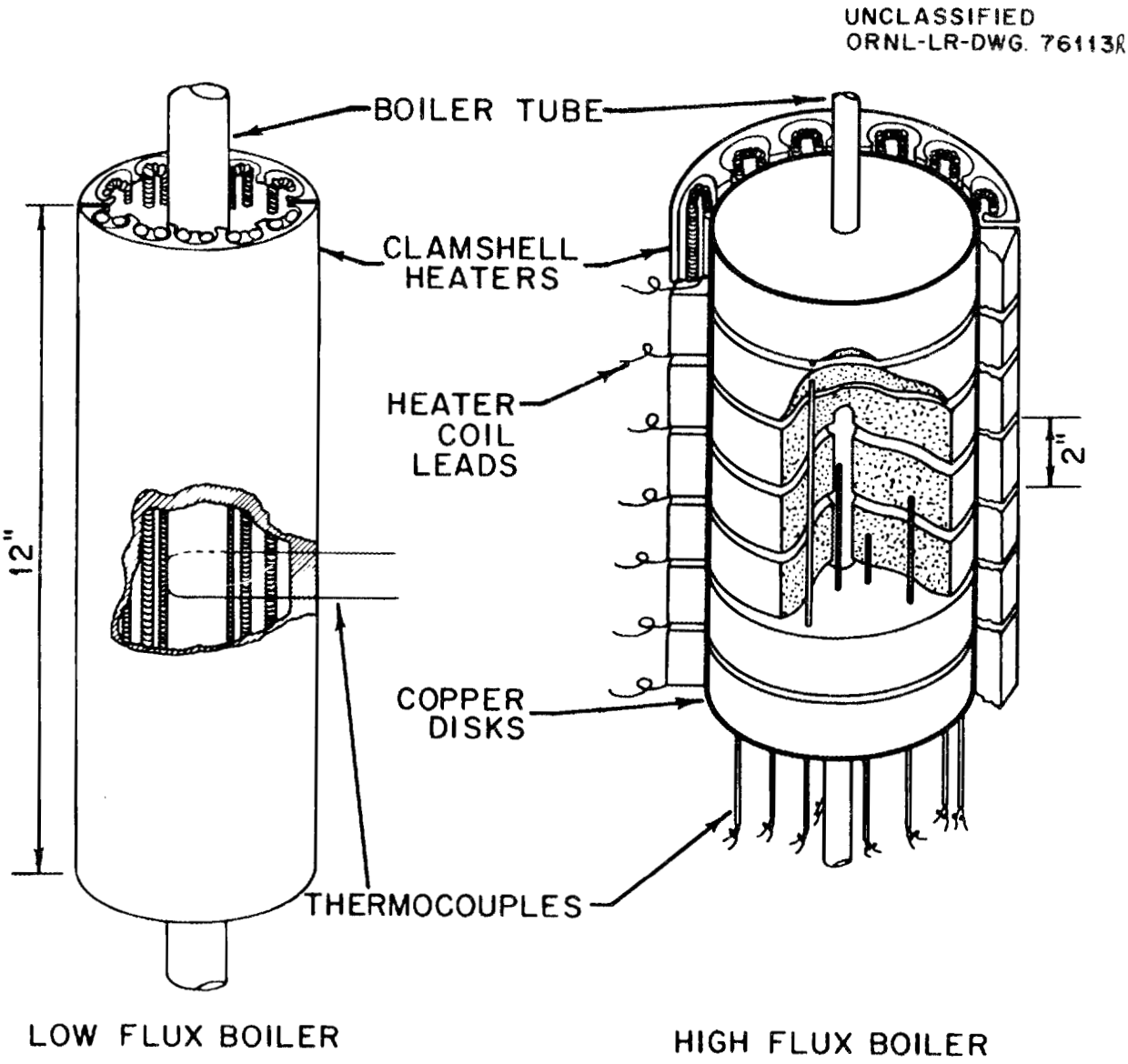

Fig. 1. Cutaway View of Test Section for Boiling Potassium Experiment.

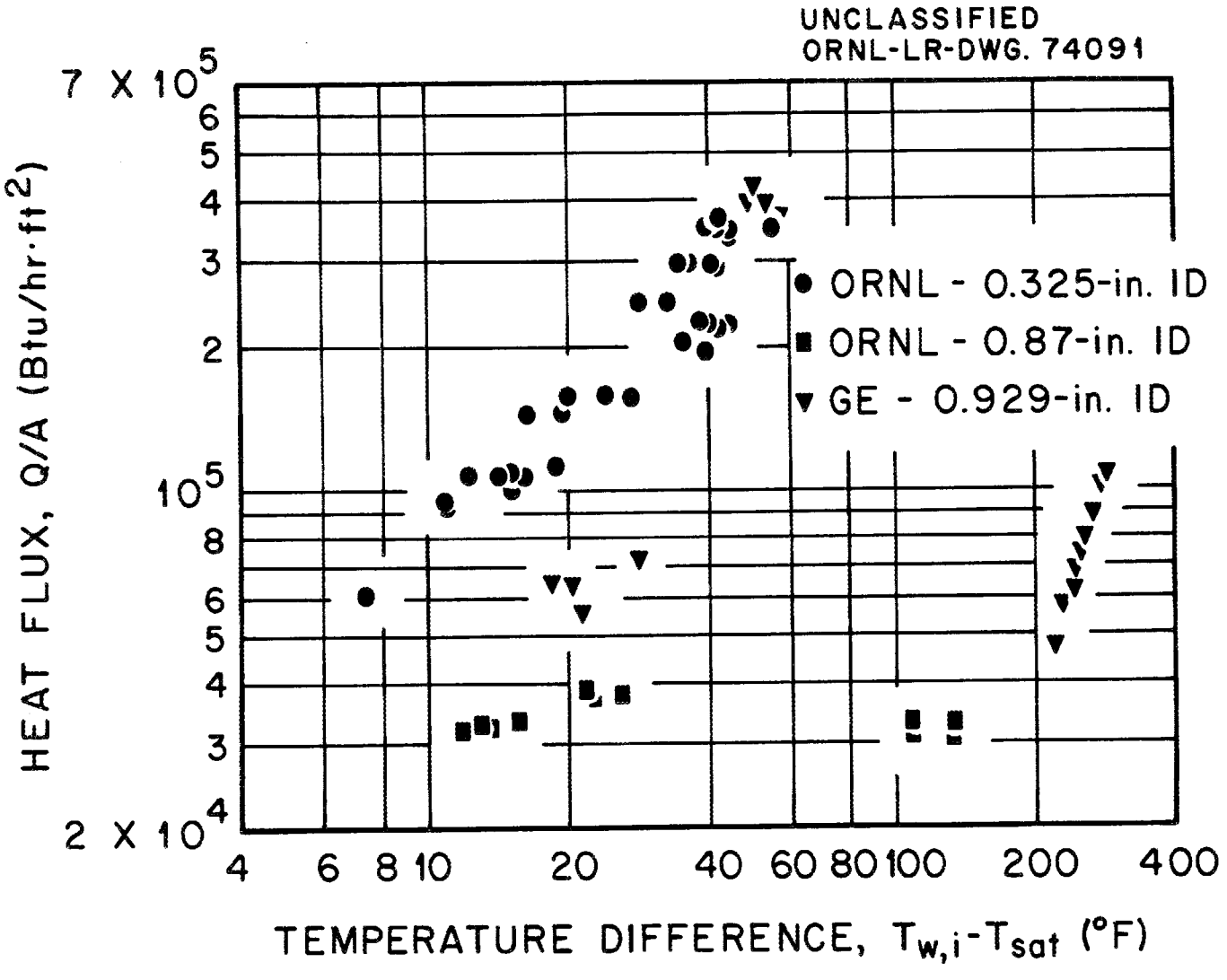

Fig. 2. Boiling Potassium Heat Transfer.

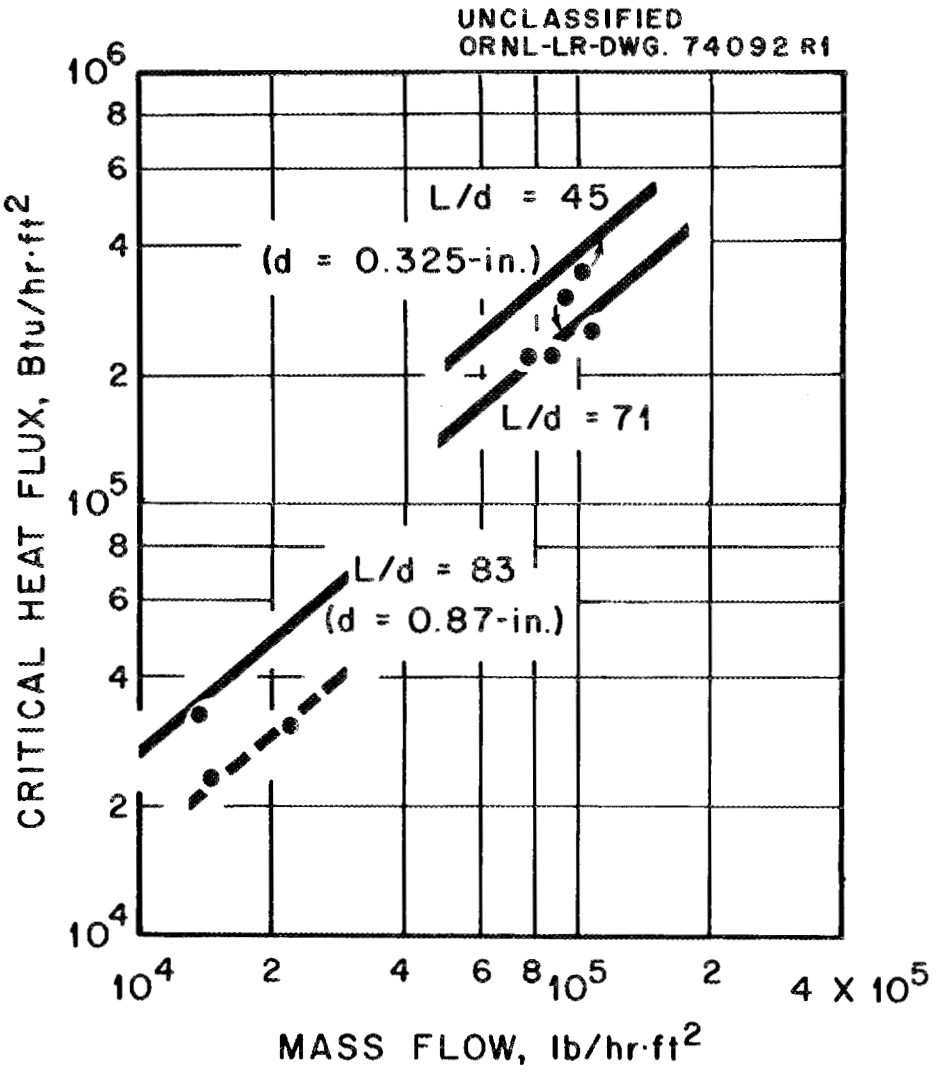

Fig. 3. Critical Heat Flux with Boiling Potassium.

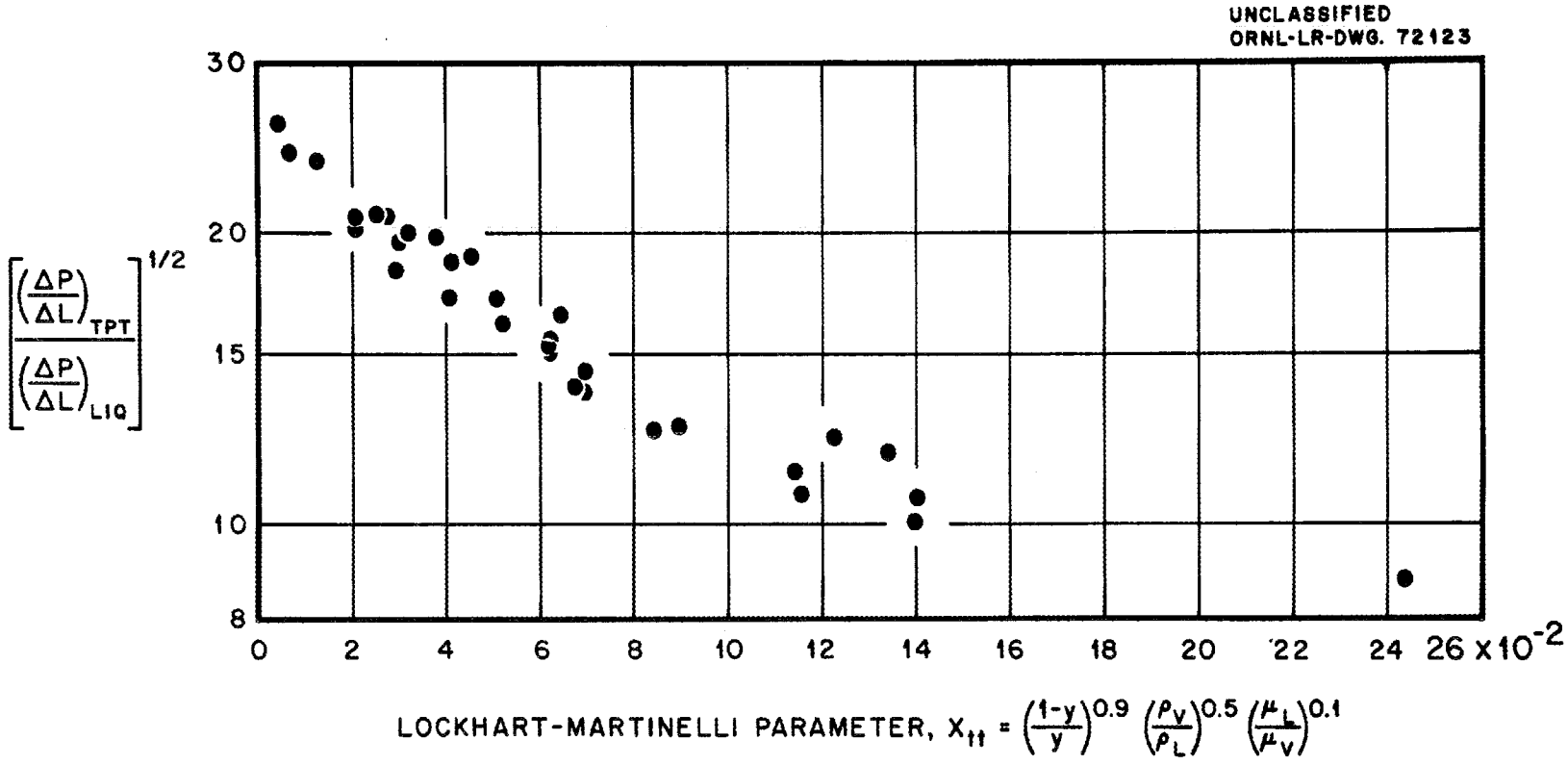

Fig. 4. Pressure Drop with Flow of Boiling Potassium Through a 0.325-in.-diam Tube.

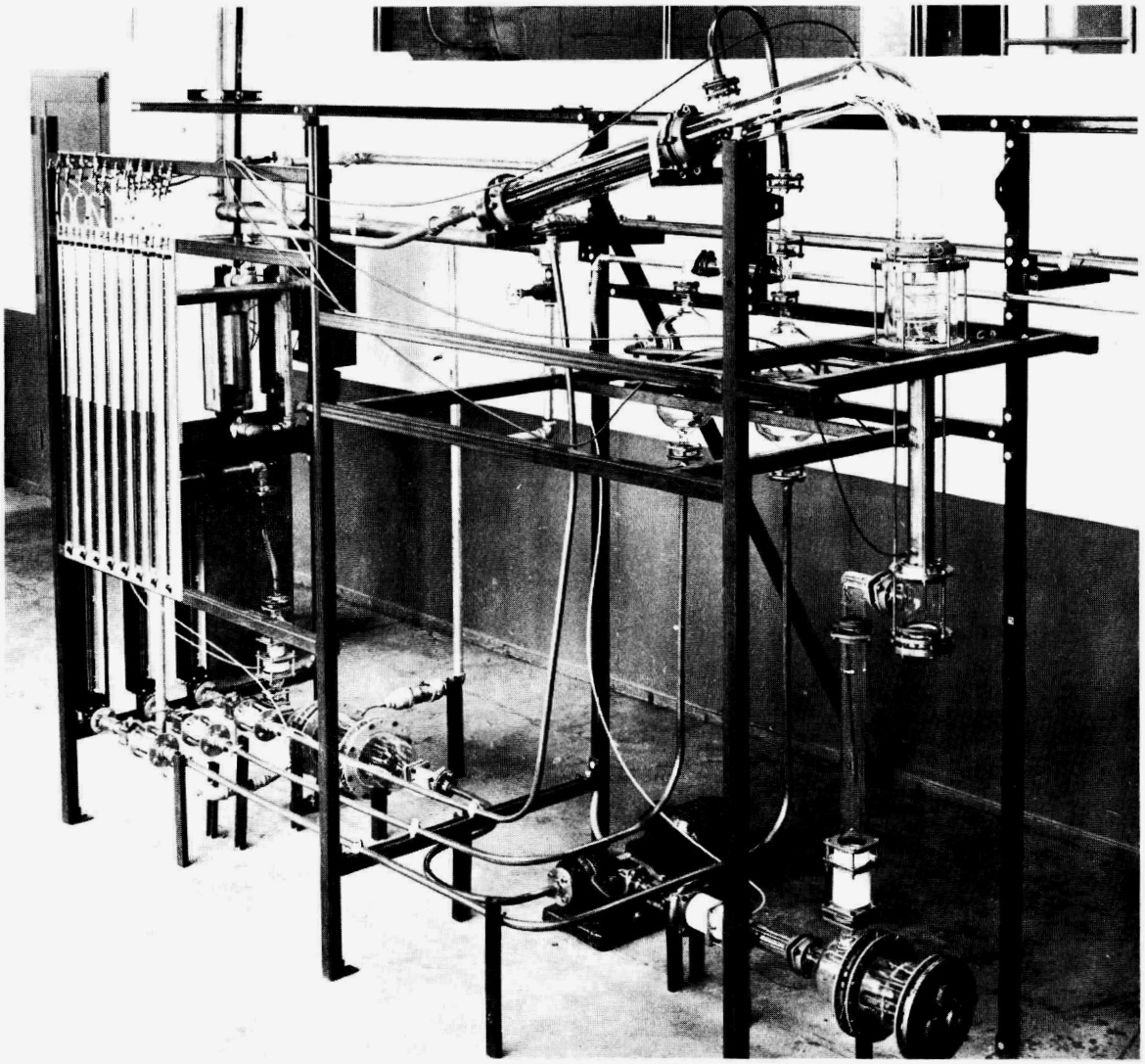

Fig. 5. View of Apparatus for Study of Critical Heat Flux with Water Boiling in a Multirod Channel.

DISCUSSION

MR. ROHSENOW: What is the quality in Fig. 3 that causes burnout flux? Is this in the quality region?

MR. H. W. HOFFMAN: The last burnout point I indicated was 73%.

MR. ROHSENOW: Fig. 3 shows the critical heat flux increasing with mass flow rate. With water there is a reverse effect at high quality. What is the explanation of that?

MR. H. W. HOFFMAN: I have none at the moment. The critical flux values given are not at constant quality. The qualities for the data shown vary from about 60% to about 92%.

MR. BERENSON: In regard to your plot of your Martinelli parameter (Fig. 4) in which you mentioned that the water data (and by this I assume you mean the data that Martinelli and Nelson originally used to plot their parameter), we have observed that the predicted pressure drop, using the Martinelli water data, was approximately a factor of 2 higher. In our paper we offered an explanation of this. Maybe an explanation isn't required, and using the water data was just not sufficient.

MR. STEIN: Did you also try using the simple homogeneous model to bring together the pressure drop?

MR. H. W. HOFFMAN: No. The pressure-drop data, because of the location of our pressure taps, are somewhat uncertain. It has only been recently that we have started analyzing this data.

MR. STEIN: If I may make a suggestion of two kinds, with the critical heat-flux data, I think, if possible, it would be better to take the simplest approach first. Maybe the critical heat flux is a function only of local conditions in terms of G, quality, and pressure. And so it would be nice if you could look at the data in this way.

And then for the pressure drop, again maybe we should look at the simplest situation first. Maybe the homogeneous model does predict it with sufficient accuracy, and it is certainly much easier to use, and much more consistent, from a theoretical point of view, than the Lockhart-Martinelli type of correlation.

MR. BERENSON: One additional observation: In Fig. 2 where you plot heat flux versus temperature, with the exception of the data above a temperature difference of 100°, all the data appear to reduce to a constant Nusselt number of plus or minus 20%. I get that impression, looking at the slope of one and the diameter variation that is reported.

MR. H. W. HOFFMAN: Yes.

BOILING STUDIES WITH POTASSIUM

by

Richard E. Balzhiser
Associate Professor of Chemical Engineering
The University of Michigan

Introduction

Liquid metal boiling studies were initiated at The University of Michigan in June 1961 with support from Aeronautical Systems Division. Analytical and experimental investigations were planned to yield a better understanding of the phenomena which characterize boiling liquid metal heat transfer in all regimes. Potassium was chosen as the experimental fluid for all initial phases of the study except the agravic program. The selection was based on its appropriateness with respect to the space energy conversion interests of ASD as well as the similarity of certain of its physical properties with respect to water in the temperature range of interest.

The program is composed of four experimental phases: two pool boiling studies, one in the high flux nucleate regime and the second encompassing the entire boiling range with special emphasis on transitional and film boiling; a forced circulation study which is intended to produce local heat transfer coefficients and two-phase pressure drop and void fraction data; and a study of the effects of acceleration on the boiling process. The latter study employs mercury as the test fluid; all other phases will employ potassium initially with later work to include sodium and rubidium where appropriate. Substantial progress has been achieved in each of these phases during the past year with three of the studies having yielded some data. Significant equipment modifications have been and are still being made in most of the phases as experience is accumulated.

Analytical studies have been concentrated on the transitional and film boiling processes and on the effect of wetting on the heat transfer characteristics of metallic fluids. Analyses of the behavior in other regimes will be accelerated as experimental demands are lessened and data becomes available to suggest rewarding courses of action.

High Flux Nucleate Boiling

This phase of the program constitutes the thesis research of Mr. C. Phillip Colver and the studies with potassium have been essentially completed. The program was designed to yield burnout data for saturated potassium boiling from the surface of a 3/8-in bayonet tube at pressures in excess of one atmosphere.

The results of Noyes (1) have suggested that burnout correlations based on hydrodynamic theory may not be adequate in explaining burnout behavior for metallic fluids. His burnout data for sodium was confined to a very small pressure range, .5 psia to 1.5 psia, and hence couldn't be expected to provide any check on the predictions of existing correlations for pressure variations. His correlation which essentially added a Pr number correction to the Zuber-Tribus equation succeeded in reconciling his data with the existing data for a variety of fluids. Its inability to predict the sulfur results of Sawle (2) suggests that proper recognition of controlling parameters has not yet evolved.

Inasmuch as the physical properties of potassium differ significantly from water only in respect to thermal conductivity and wettability, neither of which would be significant according to hydrodynamic theories, it was anticipated that potassium burnout data might provide considerable insight into the controlling phenomena.

The design of the apparatus is shown in Figure 1. Boiling occurred from the outer surface of a 3/8-in diameter bayonet tube which protruded $1\frac{1}{4}$-inches

into the pool. The boiling vessel consisted of a 2.15-in OD by 1.36-in ID Haynes-25 tube, 24-in long. The upper portion of the system served as a condenser with water as the coolant. Potassium was charged to a desired depth through the charging line at the bottom of the tube. The boiling tube assembly screwed into a threaded 3/8-in diameter hole, centered $2\frac{1}{2}$-inches above the bottom of the boiling chamber.

Guard heaters surrounded the liquid-containing portion of the boiling chamber. They were used to bring the system to test temperature and reduce heat losses during boiling runs.

The boiling tube, shown in Figure 2, consisted of a graphite core surrounded by a thin insulating sleeve of boron nitride inside the Haynes-25 boiling tube. Dimensions are shown in the figure. Thermocouples were embedded in grooves located 90° apart in the tube surface. Nicrobraze was used to fill the grooves after thermocouple installation. The thermocouple assembly consisted of a .0205-in diameter swaged chromel-alumel couple within a .035-in OD by .022-in ID stainless steel hypodermic tube. The later underwent the brazing operation after which the thermocouple was inserted.

Direct current was supplied from a Udylite rectifier rated at 12 KW. The current was introduced to the bayonet tube through a spring-loaded molybdenum rod. The current passed from the molybdenum to the graphite core of the boiling tube. The graphite comprised approximately 90 per cent of the total boiling circuit resistance. The circuit was completed through the Haynes-25 tube in parallel with the potassium pool and then through the vessel wall. Heat flux was determined by measuring I^2R dissipation in the graphite resistor and allowing for reasonable end losses. An analysis of end effects at both ends indicated that the heat flux over the central portion of the tube should be greater than 95 per cent of the measured value.

Temperatures were measured and recorded at 12, 3, and 6 o'clock at the center of the boiling tube. A sliding thermocouple extending from the top of the condenser was used to measure and record pool temperatures at different depths. A single tube with thermocouples located at different longitudinal positions was used to verify the analytical evaluation of axial temperature gradients in the tube.

Water was boiled in preliminary runs to check the apparatus and substantiate the system geometry as being reasonably representative. Results agreed well with Lyon's (3) data from a 3/8-in OD tube by 5-in long, considering the inherent uncertainty in estimating surface temperatures under these conditions. Burnout data for water was not obtained in the original tests but consideration is being given to obtaining such data before charging sodium for further studies. These results contrasted with liquid metal results should prove extremely revealing.

Burnout data for potassium were obtained on four different tubes over the pressure range 0.15 psia to 22 psia and are shown in Figure 3. Two of the tubes experienced destructive burnout, one melting near the center while the other developed a longitudinal crack along one thermocouple groove. This latter tube also developed a hole in the Haynes-25 at the free end of the tube. Either of the above failures would have led to the shorting of the graphite resistor.

Burnout was approached in most cases by fixing the heat flux and gradually decreasing pressure. At burnout, temperatures measured by the three tube thermocouples would simultaneously soar off the recorder scale. Immediate power cutoff to the boiling tube prevented damage to the surface. Several runs were made by increasing flux at constant pressure until burnout was achieved. These runs confirmed the points obtained by the constant flux technique.

Figure 4 contrasts the burnout results with the predictions of Noyes, Addoms, Zuber and Tribus, Rohsenow and Griffith, and Kutateladze. None of these satisfactorily predict the bahavior observed over the pressure range studied. The slope of the data is as significant as the magnitude in that it suggests that functional relationship between pressure dependent properties and burnout flux may need reevaluation.

Interestingly enough the theory of Zuber and Tribus for subcooling corrections to the saturated burnout flux predicts values slightly in excess of those obtained in this study for 10°F subcooling. The slope also approximates that exhibited by the present data.

Pool temperature measurements were made at various depths for a series of fluxes. These measurements indicated temperatures at or above saturation from the liquid free surface to two inches below the tube. From this point the temperature decreased to 4°F below saturation at the base of the pool for nearly all fluxes studied. The subcooling at the bottom of the pool was attributed to conduction losses through the charging line. It seems doubtful that it could have accounted for the differences observed.

The temperature traverse of the pool also revealed superheat at considerable distances from the tube. This behavior tends to support other observations made during nucleate boiling runs and re-enforces certain ideas advanced during the analytical portion of our investigations.

Extrapolation of tube thermocouple readings to the surface produced some insight as to the nature of the nucleate boiling process. Uncertainty in the exact sensing position of the thermocouple junction and the effective conductivity of the Haynes alloy-braze combination made precise determination of surface temperatures difficult. The band of data obtained seemed to fall uniformly around the data of Bonilla (4) and suggests that wall superheats of 20°F at high fluxes are experienced at atmospheric pressure.

Fluctuations in tube temperatures of up to 150°F were observed at lower fluxes. They were characterized by a gradual build up to peak values followed by a sudden drop to near saturation temperature. The tube thermocouples, which were located at the top, bottom and side of the tube, fluctuated in phase at low fluxes suggesting that the cause of the fluctuations affected all simultaneously. The simultaneous drop in tube thermocouple readings was accompanied by an audible "bump." Pressure fluctuations were also observed to occur at the same time. As the flux was increased the frequency increased substantially and the amplitude appeared to decrease. Further study of this is underway and a more complete discussion will be published later.

These observations tend to support the behavior to be anticipated with wetting, metallic fluids. The combination of good wetting and low thermal conductivity makes it difficult to concentrate sufficient energy at the interface to nucleate vapor. Unlike water and organics the superheated region may extend well into the bulk fluid. When nucleation occurs at one point on the surface the flushing operation proceeds along the entire surface until liquid superheat is consumed as latent heat. Evidently seed vapor nuclei do not remain behind on the surface to enhance nucleation of subsequent cycles. The observation that system superheat existed well into the bulk was further evidence of this type of behavior. The scatter in nucleate boiling data can also be explained in part by these fluctuation temperatures.

Film Boiling

An experimental study with film boiling potassium was initiated by Andrew Padilla as a second phase of this project. The purpose was to determine the characteristics of potassium in the transitional and film boiling regimes. The nature of the apparatus is such that it should also yield data at low fluxes in the nucleate boiling regime.

Potassium will be boiled in the upper compartment of a "double boiler" by condensing sodium on the bottom side of the plate (see Figure 5). The sodium will be boiled by radiantly heating the Cb-1Zr tubes which makes up the vessel. Potassium will be condensed by radiating heat from the top of Cb-1Zr tube to its environmental chamber walls.

The boiling plate was machined from Cb-1Zr (see Figure 6) and heliarc welded to the upper and lower pieces of Cb-1Zr tube. The boiling surface is 0.98-inches in diameter by .1065-inches thick. It contains eight .021-in diameter holes drilled to various depths at three longitudinal positions. The heat flux and surface temperatures will be determined by establishing the temperature profile through the plate and extrapolating to the surfaces. The profile will be determined at two radii to check for radial variations in flux.

Heat is supplied to the potassium by passing DC current through a graphite cloth which encircles the sodium pool. Preliminary trials have proven the feasibility of such an approach. Guard heaters and radiation shields are used to minimize heat losses from the sodium boiler and to reduce heat flux distortions in the region of the boiling surface.

The entire boiling tube assembly is contained within an environmental chamber in which a vacuum is maintained to minimize oxidation of the tube and radiant heater. The fluids are charged through the lines shown schematically in Figure 5. A water cooled trap at the top of the vessel serves to condense traces of potassium from inert gas being pumped from the system.

Preliminary operation to date has yielded nucleate boiling data with temperature fluctuations similar to those obtained in the high flux pool boiler. Bumping again characterizes the boiling process but the presence of two boiling pools creates some uncertainty as to the source of the noise. Stable operation has not yet been obtained in the film boiling regime.

Two methods seem feasible for achieving film boiling. The first involves a reduction of system pressure such that the critical heat flux might be exceeded. Transitional boiling is expected to result in a system of this type where surface temperature is an indpendent variable. At higher energy inputs to the sodium the wall superheat at the upper disc surface should increase and stable film boiling should eventually result. This method depends on the capability of the system to produce fluxes in excess of the "burnout flux," which according to Colver's results discussed earlier, is 400,000 Btu/(hr)(sq ft) at 1 psia. This value is greater than anticipated and if the change with pressure is as slight as our earlier data suggests, some difficulty might be encountered with this approach.

The second approach involves charging the potassium slowly to a system which has been preheated so that the surface is above the minimum temperature required to sustain film boiling. Westwater and Hosler employed this technique in their studies. The equipment is operating at the present time and additional data should be forthcoming in the near future.

Inasmuch as the diameter of the surface is the same order of magnitude as the wavelength of the surface waves predicted for potassium, it is planned to duplicate the geometry with a water boiler and determine the significance of edge effects.

Considerable effort has been devoted to an analytical examination of the film boiling regime. The studies of Zuber (5), Berensen (6), Rankin (7) and others have been examined. An explanation for phenomena observed in the transitional and stable film regimes has been advanced and efforts to complete the analysis are currently in progress.

Forced Circulation Studies

A liquid metal circulating facility was installed earlier this year which

is designed to obtain high temperature, high flux two-phase heat transfer and fluid flow data for metallic fluids. The effects of mass velocity, quality, subcooling and pressure on boiling will be examined. Pressure drop and void fraction determinations will also be obtained for various combinations of the above parameters. Prediction of the conditions which lead to sudden depressions in the heat transfer coefficient within the quality region represents a primary goal of the study.

Figure 7 is a schematic diagram of the facility. Initially it is planned to circulate potassium in the primary loop. Heating of potassium in the test section will be accomplished by condensing sodium circulated in a natural convection loop. The test section consists of a 2-in length of 10 mill wall, .355-in ID Haynes tubing. Potassium circulated inside the tube with sodium condensing on the outer surface. The system is designed to achieve fluxes of up to 10^6 Btu/(hr)(sq ft) with the potassium operating at 1800°F. Flow rates of 0 - 4.5 GPM and qualities up to 100 per cent can be obtained at the test section inlet.

Heat transfer measurements will be made by first determining sodium condensing coefficients with the potassium in single phase flow. Temperature measurements in and out of the test section will yield the flux and a suitable bulk potassium temperature. Measurement of the condensing temperature of sodium permits evaluation of an overall coefficient from which the condensing coefficient can be estimated for known values of the tube wall and potassium film resistances.

When boiling coefficients are to be measured, a similar procedure is followed and the boiling coefficient is extracted from a measured overall coefficient. No surface temperatures are involved in these determinations for two reasons. The attainment of high fluxes necessitated using a thin walled tube in which it was virtually impossible to obtain temperature

measurements, and secondly, the accuracy associated with making and extrapolating thermocouple readings at high fluxes to obtain surface temperatures is questionable. Thin film techniques may eventually provide an answer to this problem but the technology was not considered well enough advanced to use in this study.

Two-phase flow studies will include pressure drop readings across a horizontal 3-ft length of 5/8-in OD by .065-in wall tube. These readings will be obtained from a Taylor differential pressure gage. Void fraction measurements will be made by gamma ray attenuation techniques using a thulium-170 source. The results will be used to test the applicability of existing pressure drop correlations to metallic systems.

Operation to date has been concerned with calibration of instrumentation and elimination of plugging difficulties in the potassium loop. Initial attempts to circulate potassium resulted in oxide plugging in the pumping section which necessitated removal and cleaning. Sodium contamination of the potassium likely accentuated the difficulties and a higher grade potassium was therefore used in subsequent charges. A stainless frit filter bypass was inserted in the cooler portion of the loop to remove gross oxide contamination. Circulation through these filters followed by zirconium hot trapping eliminated the plugging difficulties.

More recently attention has been focused on the sodium loop. Nucleating difficulties, not uncommon in liquid metal systems, were initially experienced. Then a leakage of potassium into the sodium system prevented proper operation of the sodium loop.

Two-phase flow data will be obtained while difficulties with the sodium loop are being resolved. The instrumentation has undergone preliminary checkout and data should be forthcoming soon.

Future Efforts

Each of these phases will be continued during the coming year. Pool boiling studies will be extended to sodium and rubidium upon completion of the potassium programs. It is also intended to study sodium in forced convection at a later stage in the program. The effect of swirl flow on heat transfer behavior in the test section will be explored during the final stages of the project.

REFERENCES

1. Noyes, R. C., "An Experimental Study of Sodium Pool Boiling Heat Transfer," ASME Paper No. 62-HT-24, 1962 (also NAA-SR-6769).

2. Sawle, D. R., "Sulfur-Cooled Power Reactor Study," Aerojet-General, Report No. AGN-8015, December, 1960.

3. Lyon, R. E., A. S. Foust, and D. L. Katz, "Boiling Heat Transfer with Liquid Metals," CEP Symposium Series No. 17, 51, 1955, pp. 41-47 (also Ph.D. Thesis, University of Michigan, 1953).

4. Bonilla, C. F., and co-workers, "Alkali Metals Boiling and Condensing Investigations," General Electric Report No. ONE under NASA Contract NAS3-2528, September, 1962.

5. Zuber, N., "Hydrodynamic Aspects of Boiling Heat Transfer," AEC Report No. AECU-4439, June, 1959.

6. Berensen, P. J., "Transition Boiling Heat Transfer from a Horizontal Surface," Report No. NP-8415, M.I.T. Heat Transfer Laboratory, March 1, 1960.

7. Rankin, S., "Forced Convection Film Boiling Inside of Vertical Pipes," Thesis, University of Delaware, September 1, 1960.

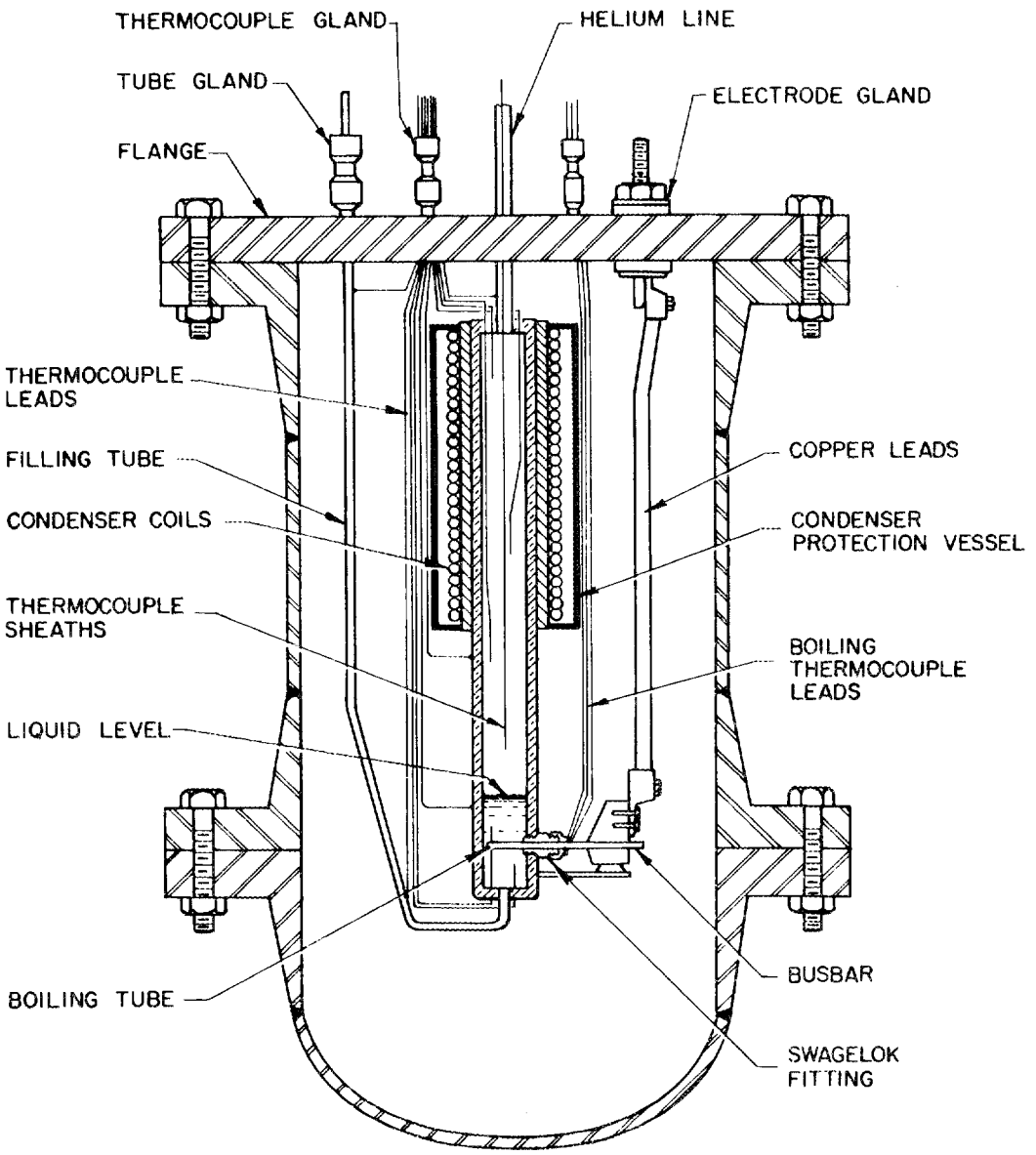

Figure 1 Sectional Drawing of Experimental Apparatus.

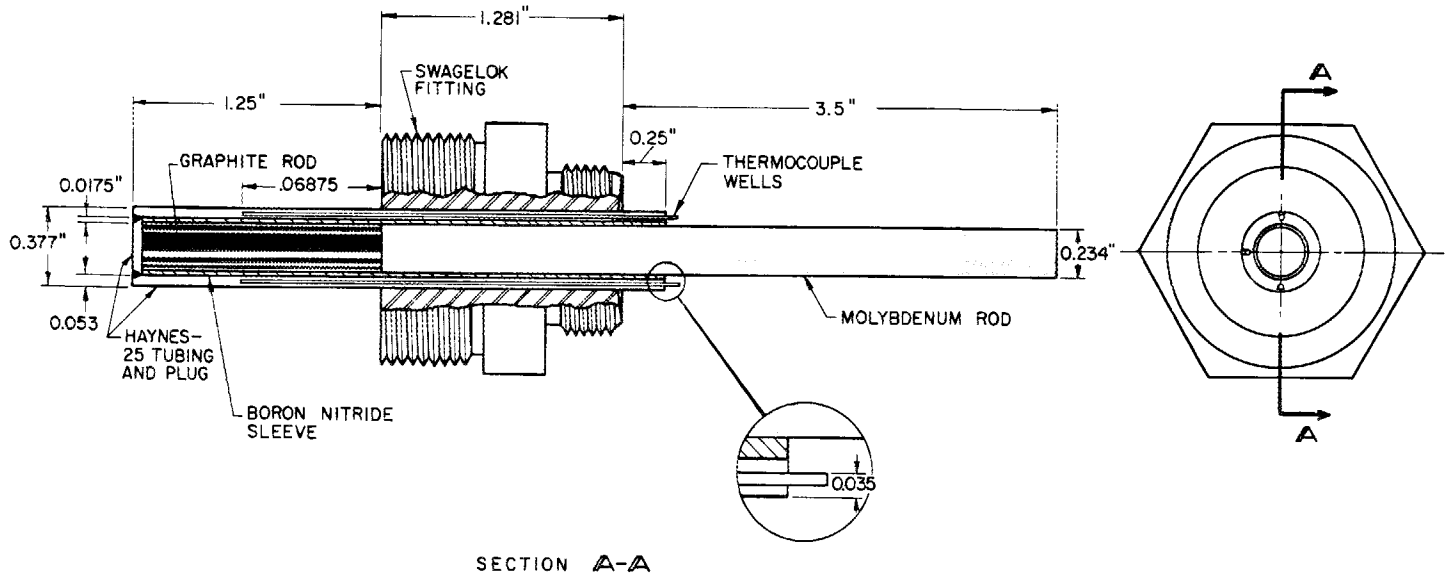

Figure 2 Cross Sectional Drawing of Boiling Tube Assembly.

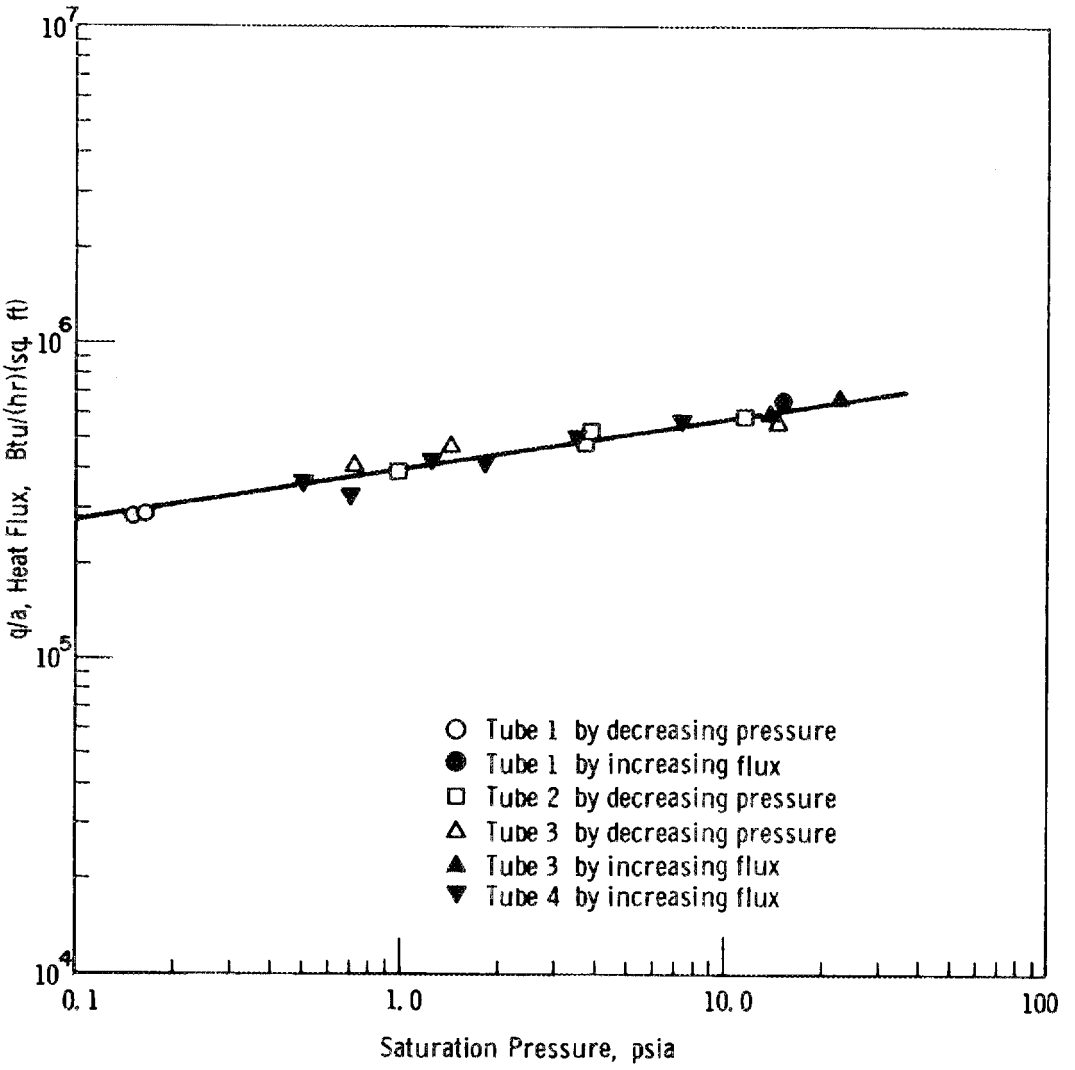

Figure 3 Burnout Heat Flux Versus Saturation Pressure for Saturated Pool Boiling Potassium.

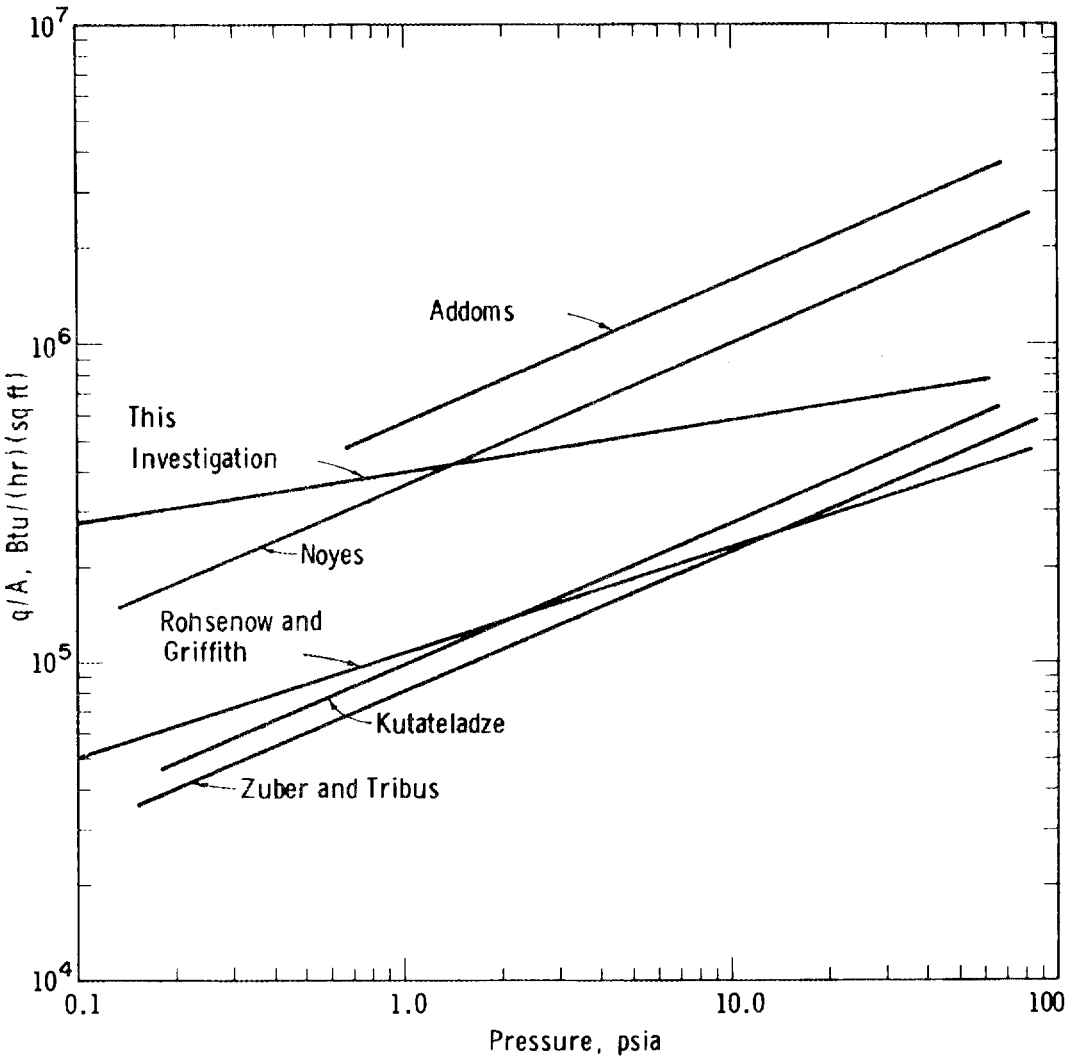

Figure 4 Comparison of Saturated Pool Boiling Potassium Burnout Data with Burnout Correlations.

FILM BOILING SCHEMATIC

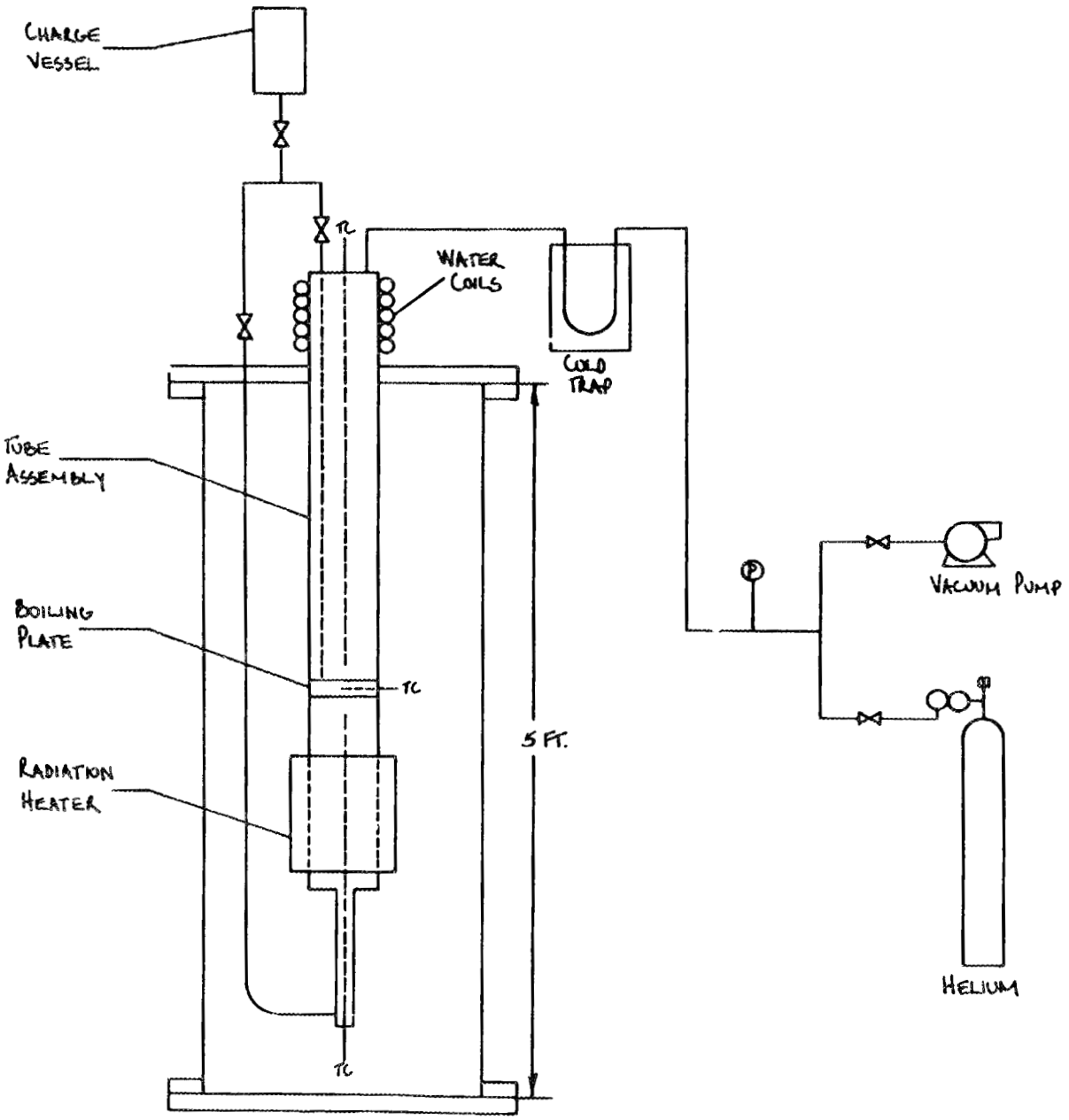

Fig. 5

CB-1ZR BOILING PLATE

THERMOCOUPLE HOLE DIAMETER .021"

RADIAL DEPTH OF THERMOCOUPLE HOLES

1	.250"
2	.450"
2A	.450"
3	.250"
4	.450"
5	.280"
5A	.250"
6	.450"

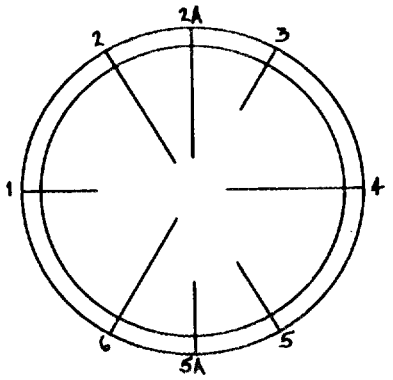

INNER THERMOCOUPLE HOLES - 120° APART

OUTER THERMOCOUPLE HOLES - 120° APART

#2A HOLE - 30° FROM #2

#5A HOLE - 30° FROM #5

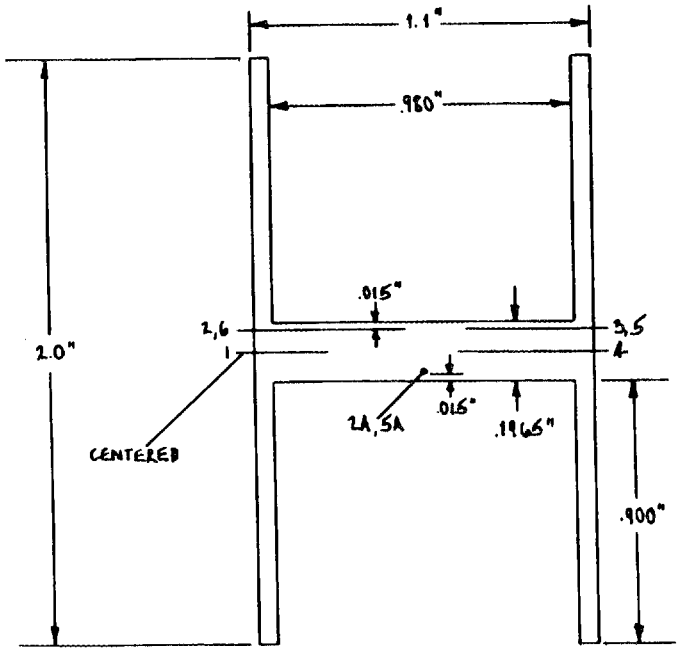

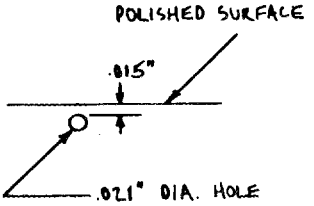

Fig. 6

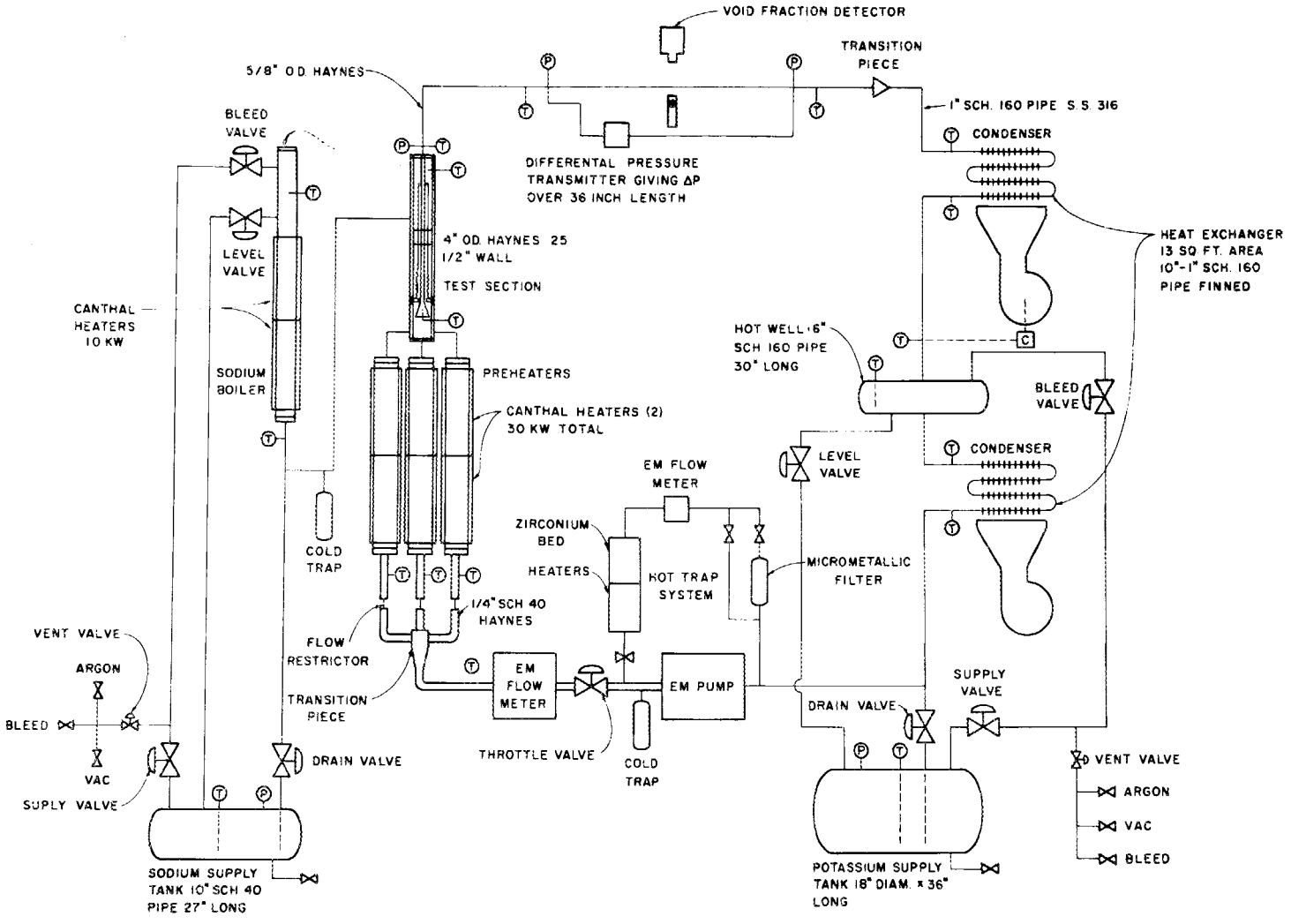

FLOW SCHEMATIC-BOILING LIQUID METAL SYSTEM

Fig. 7

DISCUSSION

MR. BONILLA: I was wondering how certain you are of the state of 10° super-heat that you reported for the pool? What was the technique of measuring that, or estimating it?

MR. BALZHISER: The 10° super-heat? Did I report it here now?

MR. BONILLA: Yes.

MR. BALZHISER: We did have a thermocouple which extended down into the pool. We started at the surface and measured the pool temperature relative to the surface temperature at all depths.

The pool temperature increased as much as 20°F (at a flux of 228,000 Btu/hr·ft^2) as the tube was approached. This increase began to occur just below the surface and increased about 16°F in the 2 in. just above the tube. It then proceeded to decrease at depths below the tube. Near the base of the pool the temperature at the above flux was approximately 4°F below the potassium surface temperature. At lower fluxes the pool super-heat observed within an inch of the boiling tube was less than 20°F and more subcooling was observed at the base of the pool. By the way, there were significant fluctuations in these temperatures, as you would expect. We experienced super-heating well out into the liquid region; a simultaneous flashing seemed to occur periodically which caused all tube thermocouples to drop simultaneously.

There were a couple of errors I had wanted to correct in the paper. I had "flushing" for "flashing", although it seems to me it might be just as descriptive. More important, on page 6, second paragraph, "The combination of good wetting and low thermal conductivity,--" be sure to change that word "low" to "high". It should be "--high thermal conductivity".

MR. BONILLA: You probably had a very uncertain flow regime in that little apparatus.

MR. BALZHISER: I wouldn't want to describe it.

MR. BROOKS: Dick, did you correct for the heat that comes out the end of the tube? Did you have a way to measure that?

MR. BALZHISER: Through molybdenum?

MR. BROOKS: Yes.

MR. BALZHISER: No. I believe the values charted here are essentially the values we computed by assuming uniform dissipation and transfer radially. As I mentioned, our analysis indicated the loss to be almost negligible at the center of the tube so that the actual value should be 95% or more of the theoretical flux over the central portion. We feel that we were within 10% of the correct value. It is small relative to the difference between our results and hydrodynamic equation.

ORNL-3605
UC-33 – Propulsion Systems and
Energy Conversion
TID-4500 (34th ed.)

INTERNAL DISTRIBUTION

1. L. G. Alexander
2. R. A. Armistead, Jr.
3. S. E. Beall
4. C. A. Brandon
5. R. B. Briggs
6. R. D. Bundy
7. J. W. Cooke
8. C. W. Cunningham
9. J. H. DeVan
10. A. P. Fraas
11. W. R. Gambill
12. G. Goldberg
13. A. G. Grindell
14-16. H. W. Hoffman
17. J. J. Keyes, Jr.
18. G. J. Kidd, Jr.
19. A. I. Krakoviak
20. C. E. Larson
21. D. B. Lloyd
22. R. N. Lyon
23. A. J. Miller
24. H. G. MacPherson
25. R. E. MacPherson
26. M. W. Rosenthal
27. G. Samuels
28. W. K. Sartory
29. H. W. Savage
30. M. J. Skinner
31. I. Spiewak
32. J. A. Swartout
33. D. G. Thomas
34. W. C. Thurber
35. A. M. Weinberg
36. R. P. Wichner
37. M. M. Yarosh
38. Gale Young
39-41. Central Research Library
42-43. ORNL – Y-12 Technical Library
Document Reference Section
44-73. Laboratory Records Department
74. Laboratory Records, ORNL R.C.
75. Reactor Division Library

EXTERNAL DISTRIBUTION

76. P. Y. Achemer, Aerojet-General Nucleonics, P.O. Box 77, San Ramon, California 94583
77. C. H. Armbruster, USAF, Aero Propulsion Laboratory (ASRPP-10), Wright-Patterson AFB, Ohio
78. R. E. Balzhiser, Department of Chemical and Metallurgical Engineering, University of Michigan, Ann Arbor, Michigan
79. J. Batch, General Electric Company, Hanford Atomic Products Operation, Richland, Washington
80. P. G. Berenson, AiResearch Manufacturing Company, 9851-9951 Sepulveda, Los Angeles 9, California
81. L. Berkowitz, United Nuclear Corporation, 5 New Street, White Plains, New York 10601
82. H. Bilfinger, c/o Professor C. F. Bonilla, Columbia University, Department of Chemical Engineering, New York 27, New York
83. S. S. Bleckermann, Pratt and Whitney Aircraft Company, CANEL, Middletown, Connecticut
84. C. F. Bonilla, Columbia University, Department of Chemical Engineering, New York 27, New York
85. A. F. Brinsmade, Allegany Ballistics Laboratory, P.O. Box 210, Cumberland, Maryland

86. R. D. Brooks, General Electric Company, Space Power and Propulsion Section, Cincinnati, Ohio
87. M. W. Carbon, University of Wisconsin, College of Engineering, 1513 University Avenue, Madison, Wisconsin
88. J. Carlino, Sunstrand Aviation Corporation, 2480 W. 70th Avenue, Denver, Colorado
89. J. C. Chen, Brookhaven National Laboratory, Building 815, Upton, Long Island, New York
90. R. R. Conrad, Sunstrand Aviation Corporation, 2480 W. 70th Avenue, Denver, Colorado
91. T. A. Coultas, Rocketdyne, 6633 Canoga Avenue, Canoga Park, California
92. J. P. Davis, Jet Propulsion Laboratory, 4800 Oak Grove Drive, Pasadena, California
93. H. W. Deem, Battelle Memorial Institute, 505 King Avenue, Columbus, Ohio
94. C. L. Delaney, USAF, Aero Propulsion Laboratory (ASRDP-10), Wright-Patterson AFB, Ohio
95. L. G. Desmon, Allegany Ballistics Laboratory, P. O. Box 210, Cumberland, Maryland
96. H. T. Drue, c/o Professor C. F. Bonilla, Columbia University, Department of Chemical Engineering, New York, New York
97. J. E. Duval, Chief, Nuclear Power Division, Headquarters USAF (AFRNE-B), Washington, D.C.
98. O. E. Dwyer, Brookhaven National Laboratory, Building 815, Upton, Long Island, New York
99. J. A. Edwards, North Carolina State College, Engineering Mechanics Department, Raleigh, North Carolina
100. R. Egli, USAEC, CANEL Office, Middletown, Connecticut
101. D. G. Elliott, Jet Propulsion Laboratory, 4800 Oak Grove Drive, Pasadena, California
102. C. T. Ewing, U.S. Naval Research Laboratory, Chemistry Division, Code 6130, Washington, D.C.
103. H. B. Finger, NASA, Director Office of Nuclear Systems, Washington, D.C.
104. C. R. Fisher, Aerojet-General Nucleonics, P. O. Box 77, San Ramon, California 94583
105. D. V. Foster, Westinghouse Astronuclear, Pittsburgh, Pennsylvania
106. K. Goldmann, United Nuclear Corporation, 5 New Street, White Plains, New York 10601
107. N. D. Greene, Geoscience Ltd., 410 S. Cedros Avenue, Solana Beach, California 92075

108-109. N. Grossman, USAEC, Division of Reactor Development, Engineering Development Branch, Washington, D.C.

110. M. Gutstein, NASA, Lewis Research Center (SEPO 86-5), 21000 Brookpark Road, Cleveland, Ohio
111. J. B. Heineman, Argonne National Laboratory, 9700 South Cass Avenue, Argonne, Illinois 60440
112. E. B. Hall, Battelle Memorial Institute, 505 King Avenue, Columbus, Ohio

113. B. Hoffman, General Electric Company, Missile and Space Division, P. O. Box 8555, Philadelphia, Pennsylvania
114. E. E. Hoffman, General Electric Company, Space Power and Propulsion Section, Cincinnati, Ohio
115. P. Holstead, USAEC, Richland Operations Office, Richland, Washington
116. J. J. Horan, Pratt and Whitney Aircraft Company, CANEL, Middletown, Connecticut
117. W. Jens, Atomic Power Development Associates, Detroit, Michigan
118. J. C. Jones, Deputy for Development, Office of the Assistant Secretary of the Air Force for Research and Development, Department of Defense, Washington, D.C.
119. R. W. Kelly, Pratt and Whitney Aircraft Company, CANEL, Middletown, Connecticut
120. G. M. Kikin, Jet Propulsion Laboratory, 4800 Oak Grove Drive, Pasadena, California
121. A. Koestal, Thompson Ramo Wooldridge, Inc., 7209 Platt Avenue, Cleveland, Ohio
122. R. R. Kyi, c/o Professor C. F. Bonilla, Columbia University, Department of Chemical Engineering, New York, New York
123. Lamprey Program, Director, Los Alamos Scientific Laboratory, Los Alamos, New Mexico
124. D-I. Lee, c/o Professor C. F. Bonilla, Columbia University, Department of Chemical Engineering, New York, New York
125. G. S. Leighton, USAEC, SNAP 50/SPUR Office, Washington, D.C.
126. A. W. Lemmon, Jr., Battelle Memorial Institute, 505 King Avenue, Columbus, Ohio
127. S. Levy, General Electric Company, Atomic Power Equipment Department, San Jose, California
128. J. P. Lewis, NASA, Lewis Research Center, 21000 Brookpark Road, Cleveland, Ohio
129. S. Lieblein, NASA, Lewis Research Center, 21000 Brookpark Road, Cleveland, Ohio
130. J. Longo, Jr., General Electric Company, Space Power and Propulsion Section, Cincinnati, Ohio
131. W. H. Lowdermilk, NASA, Lewis Research Center, 21000 Brookpark Road, Cleveland, Ohio
132. B. Lubarsky, NASA, Lewis Research Center, 21000 Brookpark Road, Cleveland, Ohio

133-134. J. J. Lynch, NASA, Office of Nuclear Systems, Washington, D.C.

135. G. Malmstrom, USAEC, Canoga Park Area Office, Canoga Park, California
136. P. J. Marto, c/o Professor W. M. Rohsenow, Department of Mechanical Engineering, Massachusetts Institute of Technology, Cambridge, Massachusetts
137. G. Mattingley, USAEC, Chicago Operation Office, Argonne, Illinois
138. T. C. Min, Department of Engineering Mechanics, University of Tennessee, Knoxville, Tennessee
139. A. Murchison, MSA Research Corporation, Callery, Pennsylvania 16024
140. S. G. Nordlinger, USAEC Scientific Representative, United States Embassy, London, England

141. R. C. Noyes, Atomics International, P. O. Box 309, Canoga Park, California
142. W. H. Nurick, Rocketdyne, 6633 Canoga Avenue, Canoga Park, California
143. K. O. Parker, AiResearch Manufacturing Company, 9851-9951 Sepulveda, Los Angeles, California
144. R. L. Phillippone, USAEC, Oak Ridge Operations Office, Oak Ridge, Tennessee
145. W. M. Phillips, Jet Propulsion Laboratory, 4800 Oak Grove Drive, Pasadena, California
146. J. Pidkowicz, USAEC, Oak Ridge Operations Office, Oak Ridge, Tennessee
147. H. F. Poppendiek, Geoscience Ltd., 410 S. Cedros Avenue, Solana Beach, California 92075
148. J. Radcliff, USAEC, San Francisco Operations Office, Berkeley, California
149. D. G. Randall, Pratt and Whitney Aircraft Company, CANEL, Middletown, Connecticut
150. F. Roehlich, MSA Research Corporation, Callery, Pennsylvania 16024
151. W. M. Rohsenow, Department of Mechanical Engineering, Massachusetts Institute of Technology, Cambridge, Massachusetts
152. L. Rosenblum, NASA, Lewis Research Center, 21000 Brookpark Road, Cleveland, Ohio
153. P. T. Rose, Allison Division of General Motors Corporation, P. O. Box 894, Indianapolis, Indiana
154. E. W. Salmi, Los Alamos Scientific Laboratory, Los Alamos, New Mexico
155. W. A. Samuel, MSA Research Corporation, Callery, Pennsylvania 16024

156-157. R. M. Scroggins, USAEC, Division of Reactor Development, Engineering Development Branch, Washington, D.C.

158. J. D. Seador, Rocketdyne, 6633 Canoga Avenue, Canoga Park, California
159. R. J. Self, USAF, Aero Propulsion Laboratory (ASRPP-10), Wright-Patterson AFB, Ohio
160. F. Shair, General Electric Company, Missile and Space Division, P. O. Box 8555, Philadelphia, Pennsylvania
161. D. E. Sill, Thompson Ramo Wooldridge, Inc., 7209 Platt Avenue, Cleveland, Ohio
162. E. M. Simons, Battelle Memorial Institute, 505 King Avenue, Columbus, Ohio
163. H. O. Sloan, NASA, Lewis Research Center (SEPO), 21000 Brookpark Road, Cleveland, Ohio
164. C. R. Smith, Allison Division of General Motors Corporation, P. O. Box 894, Indianapolis, Indiana
165. F. W. Staub, General Electric Company, Advanced Technology Laboratory, Schenectady, New York
166. R. P. Stein, Argonne National Laboratory, 9700 South Cass Avenue, Argonne, Illinois 60440
167. B. Sternlicht, Mechanical Technology, Inc., Latham, New York

168. D. H. Stewart, USAEC, Division of Reactor Development, Program Evaluations, Washington, D.C.
169. S. P. Sukhatme, c/o Professor W. M. Rohsenow, Department of Mechanical Engineering, Massachusetts Institute of Technology, Cambridge, Massachusetts
170. H. Swenson, Babcock and Wilcox Company, Alliance Research Center, Alliance, Ohio
171. Y. S. Tang, Allison Division of General Motors Corporation, P. O. Box 894, Indianapolis, Indiana
172. F. Tepper, MSA Research Corporation, Callery, Pennsylvania 16024
173. D. T. Traitel, Electro-Optical Systems, Inc., 300 N. Halstead Street, Pasadena, California
174-175. U.S. Atomic Energy Commission, Reactor Division, Oak Ridge Operations Office, Oak Ridge, Tennessee
176. U.S. Atomic Energy Commission, Research and Development Division, Oak Ridge Operations Office, Oak Ridge, Tennessee
177. U.S. Atomic Energy Commission, Technical Evaluations Branch, Office of Army Reactors, DRD, Washington, D.C.
178. U.S. Atomic Energy Commission, Reports and Statistics Branch, DRD, Washington, D.C.
179. U.S. Atomic Energy Commission, Reactor Experiments Branch, DRD, Washington, D.C.
180. U.S. Atomic Energy Commission, Space Nuclear Power Office, DRD, Washington, D.C.
181. U.S. Atomic Energy Commission, Military Compact Reactors Branch, Office of Army Reactors, DRD, Washington, D.C.
182. U.S. Atomic Energy Commission, Liquid Metal Reactors Branch, DRD, Washington, D.C.
183. U.S. Atomic Energy Commission, SNAP Reactors Branch, DRD, Washington, D.C.
184. U.S. Atomic Energy Commission, Director, Division of Intelligence, Washington, D.C.
185. U.S. Atomic Energy Commission, Division of Technical Information, Washington, D.C.
186. T. J. Vild, Thompson Ramo Wooldridge, Inc., 7209 Platt Avenue, Cleveland, Ohio
187. R. T. Wainwright, NASA, Lewis Research Center (SEPO 86-5), 21000 Brookpark Road, Cleveland, Ohio
188. C. L. Walker, Allison Division of General Motors Corporation, P. O. Box 894, Indianapolis, Indiana
189. J. F. Walling, Battelle Memorial Institute, 505 King Avenue, Columbus, Ohio
190-191. R. Weltmann, NASA, Lewis Research Center (SEPO), 21000 Brookpark Road, Cleveland, Ohio
192. M. M. Wiener, c/o Professor C. F. Bonilla, Department of Chemical Engineering, Columbia University, New York, New York
193. L. S. Wolfson, Jet Propulsion Laboratory, 4800 Oak Grove Drive, Pasadena, California
194. J. Zelenak, MSA Research Corporation, Callery, Pennsylvania 16024

195-196. N. Zuber, General Electric Company, Advanced Technology Laboratory, Schenectady, New York

197-820. Given distribution as shown in TID-4500 (34th ed.) under Propulsion Systems and Energy Conversion category (75 copies – CFSTI)